# Printing processes dedicated for the mass production of ceramic based microelectronic devices

Rita Faddoul


## To cite this version:

Rita Faddoul. Printing processes dedicated for the mass production of ceramic based microelectronic devices. Fluid mechanics [physics.class-ph]. Institut National Polytechnique de Grenoble - INPG, 2012. English. NNT : . tel-00825123

HAL Id: tel-00825123
https://theses.hal.science/tel-00825123

Submitted on 23 May 2013

**HAL** is a multi-disciplinary open access archive for the deposit and dissemination of scientific research documents, whether they are published or not. The documents may come from teaching and research institutions in France or abroad, or from public or private research centers.

L'archive ouverte pluridisciplinaire **HAL**, est destinée au dépôt et à la diffusion de documents scientifiques de niveau recherche, publiés ou non, émanant des établissements d'enseignement et de recherche français ou étrangers, des laboratoires publics ou privés.

UNIVERSITÉ DE GRENOBLE

# THÈSE

Pour obtenir le grade de

## DOCTEUR DE L'UNIVERSITÉ DE GRENOBLE

Spécialité : **MECANIQUES DES FLUIDES, PROCEDES, ENERGETIQUES**

Arrêté ministériel : 7 août 2006

Présentée par


**Rita FADDOUL**

Thèse dirigée par **Anne BLAYO** et
codirigée par **Nadège REVERDY-BRUAS**

préparée au sein du **Laboratoire de Génie des Procédés Papetiers (LGP2)**
dans **l'École Doctorale IMEP2 : Ingénierie – Matériaux Mécanique Energétique Environnement Procédés Production**


# Procédés d'impression dédiés à la production de masse de microcomposants électroniques à base de céramique

Thèse soutenue publiquement le « **03 Mai 2012** »,
devant le jury composé de :

**M. Didier CHAUSSY**
Professeur - Grenoble INP – LGP2 (Président)
**Mme Martine LEJEUNE**
Professeur Université de Limoges (Rapporteur)
**M. Arnaud MAGREZ**
Docteur – Ecole Polytechnique Fédérale de Lausanne (Rapporteur)
**M. Leszek GOLONKA**
Professeur – Wroclow University of Technology (Examinateur)
**M. Stéphane BREDEAU**
Docteur – Commissariat à l'Energie Atomique et aux Energies Alternatives (Invité)
**Mme Anne BLAYO**
Docteur Ingénieur - Grenoble INP - Pagora (Directrice de thèse)
**Mme Nadège REVERDY-BRUAS**
Docteur - Grenoble INP - Pagora (Co-directrice de thèse)

# *Remerciements*

Je commencerai par remercier le doyen de l'Université Libanaise Dr. Ali Mneimneh ainsi que Dr. Youssef Diab, responsable du département chimie à la Faculté des Sciences - section 2, de m'avoir donné l'opportunité de poursuivre mes études en France.

Je remercie également le président de mon jury, Didier Chaussy qui, en delà de son rôle de chef de l'équipe "Science et Techniques Graphiques", était toujours présent par son soutien moral et humain. Je n'oublie pas de remercier les rapporteurs de cette thèse, Mme Martine Lejeune et M. Arnaud Magrez pour l'intérêt qu'ils ont porté à mon travail. Merci aussi pour les examinateurs qui ont accepté de juger mon travail, Professeur Leszek Golonka et Dr Stéphane Bredeau, également membres du projet européen. Je n'oublie pas de remercier tous les autres membres du projet européen avec lesquels nous avons partagé des résultats, des échantillons mais surtout de bons moments pendant les "meetings" du projet et les essais réalisés au LGP2. Je tiens surtout à citer Stéphane, Mathieu, Mathilde, Johannah, Christian, Thomas, Ola, Bernt et Maelenn.

Evidemment, je remercie mes directrices de thèse, Anne et Nadège, pour leur présence à mes côtés aussi bien d'un point de vue professionnel que personnel. Et quand je parle de "personnel", je sous-entends toutes les difficultés qu'on a rencontrées au niveau administratif, mais aussi tous les moments sympas et de folie qu'on a passés ensemble. Merci à Anne de m'avoir transmis ses connaissances sur les procédés d'impression et à Nadège d'avoir partagé mes premiers coups de raclette sur la presse sérigraphique ! Je n'oublie pas non plus les discussions scientifiques animées suite auxquelles je justifiais à Nadège, à coup d'e-mail avec références biblio, ce que j'avais dit auparavant (car il faut être précis!). Je me souviendrai aussi toujours de tous les voyages et restaurants qu'on a faits, de toutes les folies qu'on a partagées. Enfin, je n'oublierai pas tous les points communs que l'on s'est trouvés, Nadège et moi. Je garde secrets ces petits moments où l'on a trinqué aux quatre coins de l'Europe en découvrant les coutumes locales (la bière en Allemagne, les p'tits dej salés un peu partout...) !!

Je remercie aussi toutes les personnes qui m'ont aidée pour réaliser cette thèse surtout Bertine avec laquelle j'ai passé des centaines d'heures au MEB. Je n'oublie pas de remercier Anne-Marie pour tous les voyages organisés à la dernière minute et toutes les matières premières commandées. Je remercie aussi, Naceur Belgacem et Raphael Passas pour leurs conseils, Jean-Luc, Cécile, Mikael et tout le service technique.

Je tiens aussi à remercier Joséphine avec laquelle j'ai travaillé pendant cinq mois et qui m'a aidée à découvrir mes talents de chef. C'est grâce à son travail qu'on a fait notre première publication.

Je remercie tous les doctorants. Merci pour tous ceux qui ont occupé et continuent à occuper le bureau B117, Jérémie, Ramzi, Soussou, Zied, Fred et Alexandre. Je remercie Fred et Alexandre pour leur patience qui leur a permis de me supporter pendant les mois de rédaction et Jérémie et Ramzi d'avoir supporté les longues discussions de filles entre Soussou et moi. Je remercie aussi les doctorants et autres membres "de la pause-café" et des "jeudis soirs", je sais, je n'y étais pas souvent : Lucie, Bertine, Aurore, Marion, David, Déborah, Elsa, Lara, Karim, Bertrand, Oussama, Sébastien, Jean-Baptiste, Chloé, Nathalie et tous les autres.
Je remercie aussi Robin, Satyajit et Imtiaz qui ne faisaient pas souvent la pause mais avec qui j'ai apprécié de discuter.
Merci aussi à Bertrand pour tous les essais sur le testeur hélio et tous les conseils "Alicona".
Merci à ma nouvelle grande sœur, Lucie, qui a su toujours être là pour moi pour faire un Mc Do mais aussi pour me conseiller et surtout me "casser" afin de m'aider à m'améliorer.

Je n'oublie pas de remercier mes amis au Liban, Lara, Nadine, Thérèse et Jean. Merci pour les longues soirées passées ensemble sur internet pour me motiver, pour rigoler et aussi pour râler.

Finalement, je remercie ma famille, mon papa, ma maman, ma petite sœrette et Rami. C'est grâce à leur simple présence que je me sentais toujours plus forte et capable d'atteindre mes buts.

# Contents

**Abbreviations** 11

**Symbols** 13

**List of papers** 15

**General introduction** 17

**Summary of the original work** 25

Specifications book and challenges . . . 25
Methodology . . . 26
Key findings and main results . . . 30
Main conclusions . . . 43

**I Literature review** 45

**Introduction** 47

**1 Substrates for electronic applications** 49

1.1 Substrates types . . . 49
1.1.1 Ceramic substrates . . . 49
1.1.2 Glass and silica substrates . . . 55
1.1.3 Polymer substrates . . . 56
1.2 Substrates sintering process - ceramics and glasses . . . 56
1.2.1 Sintering methods . . . 56
1.2.2 Sintering stages . . . 57
1.2.3 Other sintering properties . . . 59
1.2.4 Sintering conditions examples . . . 60
1.3 Substrates properties . . . 60
1.3.1 Substrates mechanical properties . . . 60
1.3.2 Thermal properties - Thermal expansion coefficient . . . 61
1.3.3 Wettability of substrates . . . 62

**2 Printed electronics and processes** 63

2.1 Introduction . . . 63
2.2 Lithography methods . . . 64
2.2.1 Soft lithography . . . 64
2.2.2 Other lithography methods . . . 66
2.2.3 Advantages and applications . . . 67
2.3 Offset printing . . . 68

2.3.1 Process description . . . 68
2.3.2 Offset requirements . . . 69
2.3.3 Advantages and applications . . . 69
2.4 Screen printing . . . 69
2.4.1 Process description . . . 69
2.4.2 Screen printing parameters . . . 70
2.4.3 Advantages and applications . . . 73
2.4.4 Limits and printing defects . . . 73
2.4.5 Screen printing inks . . . 74
2.5 Flexography . . . 75
2.5.1 Process description . . . 75
2.5.2 Flexography parameters . . . 76
2.5.3 Advantages and applications . . . 76
2.5.4 Limits and printing defects . . . 77
2.5.5 Flexography inks . . . 77
2.6 Rotogravure printing . . . 78
2.6.1 Process description . . . 78
2.6.2 Rotogravure printing parameters . . . 78
2.6.3 Advantages and applications . . . 79
2.6.4 Limits and printing defects . . . 80
2.6.5 Gravure printing inks . . . 80
2.7 Inkjet printing . . . 81
2.7.1 Inkjet printing methods . . . 81
2.7.2 Advantages and applications . . . 82
2.7.3 Limits and printing defects . . . 83
2.7.4 Inkjet printing inks . . . 84
2.8 Synthesis of lithography and printing processes characteristics . . . 85

**3 Inks** **87**
3.1 Conductive inks formulation . . . 87
3.1.1 Conductive particles . . . 87
3.1.2 Inorganic binder . . . 93
3.1.3 Ink vehicle . . . 96
3.2 Inks properties . . . 97
3.2.1 Surface tension . . . 97
3.2.2 Rheological behaviour of printing inks . . . 98
3.3 Conductive inks processing . . . 100
3.3.1 Formulation . . . 100
3.3.2 Sintering . . . 103
3.4 Examples of conductive inks . . . 105
3.5 Printed conductive lines characteristics . . . 106
3.5.1 Electrical resistivity . . . 106
3.5.2 Sheet resistance . . . 107
3.5.3 The scattering hypothesis . . . 108

**4 Applications within the MULTILAYER project** **109**
4.1 Radio frequency applications - Microwave circuits . . . 109
4.1.1 Overview . . . 109
4.1.2 Examples of applications . . . 109

4.2 Thermoelectric modules . . . 110
4.2.1 Overview . . . 110
4.2.2 Examples of applications . . . 111
4.3 Automotive applications . . . 112
4.3.1 Overview . . . 112
4.3.2 Examples of applications . . . 112
4.4 Medical applications . . . 112
4.4.1 Overview . . . 112
4.4.2 Examples of applications . . . 113

**Conclusion** **115**

**II Experimental** **117**

**Introduction** **119**

**5 Substrates** **121**
5.1 Substrates description and composition . . . 121
5.2 Powders . . . 121
5.3 Energy Dispersive X-ray analysis (EDS) and tapes main components . . . 122
5.3.1 High temperature co-fired ceramics . . . 122
5.3.2 Low temperature co-fired ceramics . . . 123
5.4 Tapes - SEM, pore and particle sizes . . . 123
5.4.1 Green tapes . . . 124
5.4.2 Microstructure evolution after sintering . . . 127
5.5 Other properties . . . 129
5.5.1 Thickness . . . 129
5.5.2 Roughness . . . 130
5.5.3 Surface energy . . . 132
5.6 Conclusion . . . 134

**6 Screen printing** **137**
6.1 Inks . . . 138
6.1.1 Pastes formulation . . . 138
6.1.2 Rheological properties . . . 140
6.2 Printing . . . 142
6.2.1 Printing patterns . . . 143
6.2.2 The screen mesh . . . 143
6.2.3 The squeegee . . . 144
6.2.4 The screen printing press . . . 144
6.3 Sintering . . . 145
6.4 Results and encountered problems . . . 145
6.4.1 Mesh clogging . . . 145
6.4.2 Smudging . . . 146
6.4.3 Non homogeneity . . . 146
6.4.4 Reproducibility . . . 147
6.4.5 Adhesion to substrate . . . 148
6.5 Conclusions and perspectives . . . 149
6.5.1 Main results . . . 149

6.5.2 Perspectives . . . 150
6.6 Paper 1: Silver content effect on rheological and electrical properties of silver pastes . . . 153
6.7 Paper 2: Formulation and screen printing of water based conductive flake silver pastes onto green ceramic tapes for electronic applications . . . 155
6.8 Paper 3: Printing force effect on conductive silver tracks - Geometrical, surface and electrical properties . . . 157

**7 Flexography printing 159**
7.1 Inks . . . 160
7.1.1 Ink optimisation . . . 161
7.1.2 Rheological properties . . . 161
7.1.3 Surface tension . . . 162
7.2 Printing . . . 162
7.2.1 Printing patterns . . . 162
7.2.2 The anilox . . . 163
7.2.3 The flexography printing tester . . . 164
7.3 Sintering . . . 165
7.4 First results and encountered problems . . . 165
7.4.1 Encountered problems . . . 165
7.4.2 Printing direction and resolution effects . . . 167
7.5 Conclusions and perspectives . . . 169
7.5.1 Main results . . . 169
7.5.2 Perspectives . . . 169
7.6 Paper 4: Ink optimisation for an alternative way to print on ceramic substrates . . . 171
7.7 Paper 5: Optimisation of silver paste for flexography printing on LTCC substrate . . . 173
7.8 Paper 6: Flexography printing of silver tracks on LTCC tapes – Effect of printing direction on line properties . . . 175

**8 Rotogravure and inkjet printing 177**
8.1 Rotogravure printing of silver inks onto green ceramic tapes . . . 177
8.1.1 Inks . . . 178
8.1.2 Printing . . . 178
8.1.3 Conclusions and perspectives . . . 179
8.1.4 Paper 7: Formulation of water-based silver inks adapted for rotogravure printing on ceramic green tapes . . . 183
8.2 Inkjet printing of silver inks onto sintered alumina substrates . . . 185
8.2.1 Inks . . . 185
8.2.2 The Dimatix inkjet printer . . . 186
8.2.3 Encountered problems . . . 186
8.2.4 Conclusions and perspectives . . . 186
8.2.5 Paper 8: Inkjet printing of silver nano-suspensions on ceramic substrates – Sintering temperature effect on electrical properties . . . 187

**General conclusion 189**

**Bibliography 193**

**Annexes** **210**

**Résumé** **227**

# Abbreviations

- $\mu$CP Micro Contact Printing
- $\mu$FN Micro Fluidic Network
- AP Acrylic Polymer
- AFM Atomic Force Microscopy
- BSE Back Scattering Electron
- CB Carbon Black
- CIJ Continuous InkJet
- CNT Carbon Nano Tube
- DOD Drop On Demand
- DTA Differential Thermal Analysis
- ESEM Environmental Scanning Electron Microscope
- FAST Field Activated Sintering Technique
- FEG Field Emission Gun
- FET Field Effect Transistor
- FTO Fluorine doped Tin Oxide
- GP Gravure Printing
- GO Glucose Oxide
- GOP Gravure Offset Printing
- HIP Hot Isostatic Process
- HTCC High Temperature Co-fired Ceramic
- IC Integrated Circuit
- IDE Inter Digitated Electrode
- IJP InkJet Printing
- ITO Indium Tin Oxide
- LED Light Emitting Diode
- LTCC Low Temperature Co-fired Ceramic
- MEK Methyl Ethyl Ketone
- MEMs MicroElectro Mechanical Systems
- MWCNT Multi Wall Carbon Nano Tube
- NIL Nano-Imprint Lithography
- OLED Organic Light Emitting Diode
- OTFT Organic Thin Film Transistors
- P3HT Poly(3-HexylThiophene)
- PANI Poly Aniline
- PC PolyCarbonate
- PCB Printed Circuit Board
- PDMS PolyDimethyl Siloxane
- PEN PolyEthyl Naphtalate

- PES PolyEthyl Sulfonate
- PET PolyEthyl Terephtalate
- PEDOT Poly(3,4-Ethylene DiOxyThiophene)
- PHT PolyHexyl Thiophene
- PI PolyImide
- PMMA PolyMethyl MethAcryalate
- PP PolyPropylene
- PPD Plasma Pannel Displays
- PPy Polypyrolle
- PtBA PolyTerButyl Acrylate
- PSS Poly Styrene Sulfonate
- PVC PolyVinyl Chloride
- PVP PolyVinyl Pyrolidone
- R2R Roll-to-Roll
- RF Radio Frequency
- RFID Radio Frequency IDentification
- SAM Self-Assembled Monolayer
- SAP Styrene Acrylic Polymer
- SEM Scanning Electron Microscope
- SL Soft Lithography
- SWCNT Single Wall Carbon Nano Tube
- TFA TriFluoretic Acid
- TFT Thick Film Transistor
- TGA Thermo Gravimetric Analysis
- TG-DTA Thermo Gravimetric Analysis coupled to Differential Thermal Analysis
- UV Ultra-Violet

# Symbols

- $\Delta P$ Power loss (W)
- $\Pi_{ab}$ Peltier effect (J.A.C$^{-1}$)
- $\dot{\gamma}$ Shear rate (s$^{-1}$)
- $\gamma_l$ Total surface tension (mN.m$^{-1}$)
- $\gamma_l^d$ Dispersive surface tension (mN.m$^{-1}$)
- $\gamma_l^p$ Polar surface tension (mN.m$^{-1}$)
- $\gamma_s$ Total surface energy (mJ.m$^{-2}$)
- $\gamma_s^d$ Dispersive surface energy (mJ.m$^{-2}$)
- $\gamma_s^p$ Polar surface energy (mJ.m$^{-2}$)
- $\epsilon$ Strain
- $\varepsilon$ Dielectric permittivity (F.m$^{-1}$)
- $\varepsilon_0$ Vacuum permittivity = 8.85.10$^{-12}$ F.m$^{-1}$
- $\varepsilon_r$ Relative permittivity
- $\eta$ Viscosity (Pa.s)
- $\theta$ Contact angle (rad)
- $\kappa$ Thermal conductance (W.K$^{-1}$.m$^{-1}$)
- $\xi$ Energy (eV)
- $\rho$ Electrical resistivity (Ohm.m)
- $\tau$ Shear stress (Pa)
- $\tau_0$ Yield stress (Pa)
- $A$ Cross-section area (m$^2$)
- $a$ Acceleration (m.s$^{-2}$)
- $B$ Inductance (Wb.A$^{-1}$)
- $C$ Capacitance (F - Farad)
- $c$ Conductivity (S.m$^{-1}$)
- $e$ Electron electrical charge = 1.6.10$^{-19}$ C
- $E_a$ Hoping activation energy (eV)
- $E_{field}$ Electrical field (V.m$^{-1}$)
- $E_n$ Electron energy (eV)
- $f$ Frequency (Hz)
- $G$ Conductance (S, Ohm$^{-1}$)
- $g$ Thermal conduction (W.K$^{-1}$)
- $h$, $k$ Constant coefficients
- $HTC$ Heat Transfer Coefficient (W.K$^{-1}$m$^{-2}$)
- $I$ Current (A)
- $K$ Consistency
- $L$, $L_0$ Length (m)
- $m_0$ Mass of electron = 9.038.10$^{-28}$ g

- $M$ Magnetic flow (Wb)
- $n$ Grain growth exponent
- $N$ Number of wires turns
- $N_e$ Electron density
- $n_i$ Chemical composition
- $p$ Power loss exponent
- $P$, $P_0$ Porosity
- $q$ Charge (C - Coulomb)
- $Q$ Electrical circuit quality factor
- $R_a$ Radius (m)
- $R_s$ Sheet resistivity (Ohm/square)
- $S$ Seebeck effect (V.K$^{-1}$)
- $T$ Temperature (K, °C)
- $TC$ Thermal Conductivity (W.m$^{-1}$.K$^{-1}$)
- $TEC$ Thermal expansion coefficient (K$^{-1}$)
- $t$ Time (s)
- $th$ Thickness (m)
- $U$ Voltage (V)
- $v$ Velocity, speed (m.s$^{-1}$)
- $v_d$ Drift velocity (m.s$^{-1}$)
- $v_s$ System volume (L)
- $W$ System energy (N.m$^{-1}$)
- $w$ Width ($\mu$m)
- $x$ Number of squares
- $Z \cdot T$ Efficiency of thermodielectric devices material (K)

# List of papers

1. Rita Faddoul, Nadège Reverdy-Bruas and Joséphine Bourel **Silver content effect on rheological and electrical properties of silver pastes** Journal of Materials Science: Materials in electronics - 23(7) – 1415-1426 – 2012
2. Rita Faddoul, Nadège Reverdy-Bruas and Anne Blayo **Formulation and screen printing of water based conductive flake silver pastes onto green ceramic tapes for electronic applications** Journal of Materials Science and Engineering B – 177 – 1054-1066 – 2012
3. Rita Faddoul, Nadège Reverdy-Bruas and Anne Blayo **Printing force effect on conductive silver tracks - Geometrical, surface and electrical properties** Journal of Materials Engineering and performance - 22(2) - 640-649 - 2013
4. Rita Faddoul, Nadège Reverdy-Bruas, Anne Blayo and Bertine Khelifi **Ink optimization for an alternative way to print on ceramic substrates** Proceedings of the $8^{th}$ International Conference on Multi-Material Micro Manufacture - 260-263 - 2011
5. Rita Faddoul, Nadège Reverdy-Bruas, Anne Blayo, Thomas Haas and Christian Zeilmann **Optimisation of silver paste for flexography printing on LTCC substrate** Microelectronics Reliability – 52(7) – 1483–1491 – 2012
6. Rita Faddoul, Nadège Reverdy-Bruas and Anne Blayo **Flexography printing of silver tracks on LTCC tapes – Effect of Printing Direction on Line Properties** Proceedings of Ceramic Interconnect and Ceramic Microsystems Technologies Conference - 314-321 - 2012
7. Rita Faddoul, Anne Blayo and Nadège Reverdy-Bruas **Formulation of water based silver inks adapted for rotogravure printing on ceramic green tapes** Journal of Print and Media Technology Research – 1(2) – 103–112 – 2012
8. Rita Faddoul, Nadège Reverdy-Bruas, Anne Blayo and Bertine Khelifi **Inkjet printing of silver nano-suspensions on ceramic substrates – Sintering temperature effect on electrical properties** - Microelectronic Engineering - 105 – 31-39 – 2013

# General introduction

## Background

Printed electronics is an emerging domain allowing to reduce micro-electronic devices cost, increase their production rate and moderate their environmental impact. The history of printed electronics started with the printed circuit boards - PCBs.
In 1904, Frank Sprague proposed to his mentor Thomas Edison the idea of manufacturing PCBs and suggested printing of graphite on linen papers.
In 1924, Charles Ducas deposited a patent application concerning conductive metal deposition onto insulating material. This was considered as the first significant contribution in PCBs area.
In the 1940's, Paul Eisler was the first to manufacture radios in which PCBs were integrated. He suggested a method that allows overlaying of printed resist layers onto copper coatings. He also proposed the establishment of electrical connections on each side of the copper layer. His technology was considered as the base of multi-layered circuit boards.
During the World War II, the United States National Bureau of Standards, installed a mass production method of the army's rocket fuses. This method, associated to present hybrid electronics technology, was based on screen printing of silver pastes onto ceramic substrates.
The commercialisation of PCBs started in 1953 - 1955. Indeed, Motorola developed a mass manufacturing process based on the creation of copper interconnections between two sides of a board [1][2].
Since then, printed electronics domain is continuously in growth and is expected to reach 9.4 billion dollars by 2012. 30% of manufactured devices are mainly printed and flexible substrates constitute only 6% of printed tapes [3]. With the evolution of the printed electronics, attention was especially focused on the development of flexible thin films by flexography and inkjet printing. Organic thin films are of high interest because of their low temperature processing. Thus, polymers were investigated as substrates and/or conductive materials for different domains such as photovoltaïcs, solar cells, displays, batteries and radio frequency identification tags (RFID) [4].

Today, various emerging markets in the field of multimaterial micro-devices offer a huge potential for commercialisation in the near future. However, solutions for mass production for most of them have still to be developed.
Classical processes such as micro injection and hot embossing of polymer materials are nowadays used for the manufacturing of mass-marketed non-silicone micro-devices. The additional steps from material to product, namely patterning, functionalisation, assembly and quality control are performed independently along the process chain. These processes do not offer possibilities to build very complex multi functional 3D parts and are not suitable for inorganic materials (ceramics, metals).
A relevant solution consists in structuring and patterning different layers and then in as-

sembling them. The main advantages of such technology are miniaturisation, preparation of complex parts and the possibility to carry out quality control tests on each layer of the device. This is the aim of the "multilayered technologies" for the fabrication of micro-devices to be developed within the MULTILAYER project. Thus, a set of solutions for large scale production of micro-devices based on a technology called "rolled multi material layered 3D shaping technology" and using the concept of tape casting and advanced printing techniques could be created. This technology would enable manufacturing of complex multifunctional 3D-microparts with a layer by layer manner. Ceramic, silica or glasses are the base material of the manufactured devices. The base substrate will be structured by channels and cavities and will be printed by inkjet, screen printing, rotogravure and flexography.

## Project concept

Nineteen European partners have been working on the MULTILAYER project from October 2008 to October 2012. It is divided into nine sub-projects. Each partner had different milestones and objectives to achieve. Management of the project was taken in charge by the CEA (Commissariat à l'Énergie Atomique et aux Énergies Alternatives).
Figure 1 shows the Multilayer project concept.

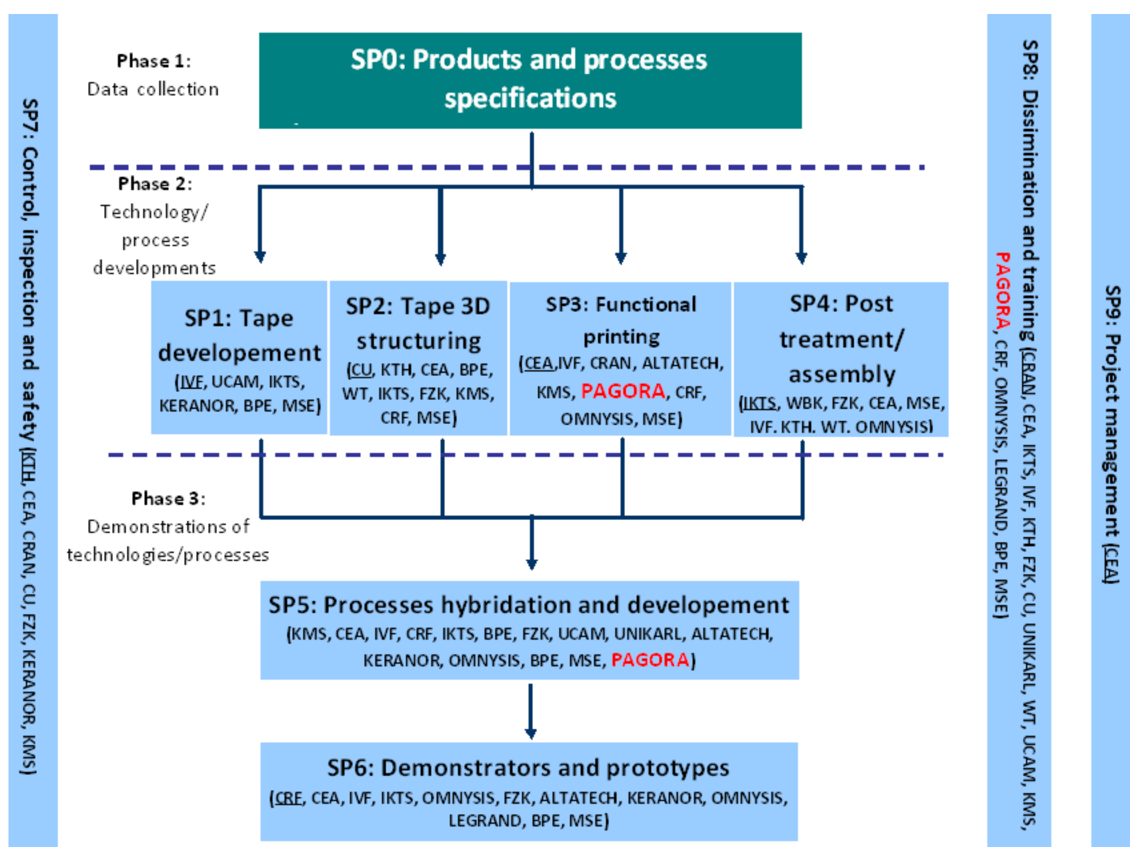


Figure 1: Articulation of MULTILAYER subprojects [5]

Grenoble INP-Pagora and the LGP2 (Laboratory of Pulp and Paper Processes and Graphic Arts) were involved on the third sub-project concerning printing processes and ink formulation (SP3 - functional printing). They were also work package (WP) leader for WP3.2 - Screen printing and WP3.3 - High definition printing.

Regarding results obtained in SP3, a new task was attributed to the laboratory within SP5 - Process hybridation and development. The aim of this sub-project is to up-scale promising experiments obtained in SP3.

After formulation and dispersion of new powders, tapes were cast by partners and ready to be printed with different printing processes. Printing techniques were investigated and adapted to reach multilayer system requirements: mainly, withstanding sintering conditions and depositing conductive tracks with resistivities lower than $1.10^{-6}$ Ohm.m. Substrate structuring could be performed before or after printing.
This stage was followed by lamination and dicing in order to obtain the desired form and dimensions of chip conductors, inductors, sensors or others. Afterwards, sintering and co-firing were performed.
Electroding and demonstrators manufacturing is the project final step and is now in progress.
Control, inspection and safety of processes and materials were guaranteed by the seventh sub-project. Besides, the eight sub-project was implemented for dissemination training and workshops.
Figure 2 shows the techniques used in order to reach the objectives fixed by the specification book.

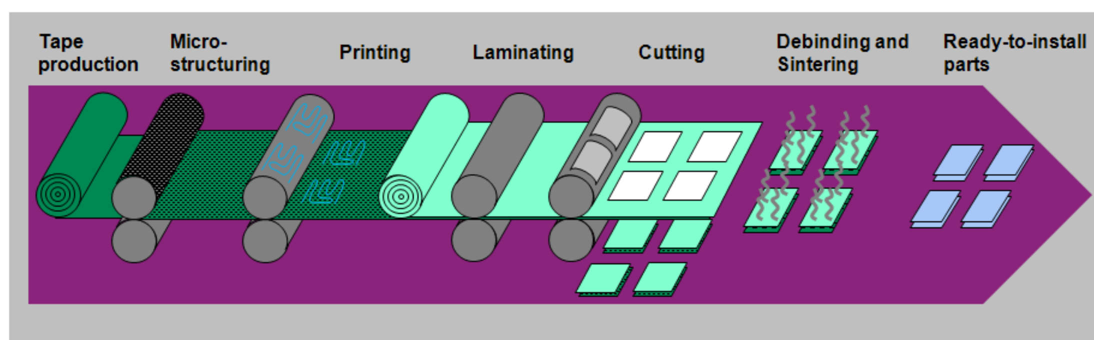


Figure 2: Online successive process steps of the MULTILAYER project [6]

## Demonstrators

Six demonstrators, shown on figure 3, will be manufactured at the end of the MULTILAYER project (SP6).

- Demo 1: Microwave components for terahertz application. The outcome from this project promises to reduce risk, time and cost for development of new sensors. Methods for integration of waveguides in ceramic systems are developed.

- Demo 2: Thermoelectric device for domestic application. The aim of this demonstrator is the development of processes allowing the mass production of a thermoelectric devices. These components are designed to allow powering of wireless sensors and user commands by push button or switch.

- Demo 3: Cooler for automotive lighting system. High flux LEDs (Light Emitting Diodes) lighting systems are based on mounting substrate and metallic heat sink. The objective is to develop low cost manufacturing processes and integrate new high thermally conductive substrates.

- Demo 4: Microfluidic device for micro reactors, fuel cells or medical device. Ceramic micro fluidic devices are produced at lab scale or in small series by ceramic injection moulding, wet shaping techniques or dry-pressing with subsequent laser structuring. Within the MULTILAYER project, the aims of this demonstrator were to develop large scale, non-expensive manufacturing technologies and to realise smaller micro channel geometries ($< 50$ $\mu$m) by cold embossing technique.

- Demo 5: Ceramic embossing tool insert for micro optical structures. This demonstrator objective was to develop a new ceramic tool to replace metallic tools generally used for polymer foils embossing.

- Demo 6: Fluidic based sensor for medical applications. The aim was to optimise printing techniques in order to realise sharp lines patterns on Low Temperature Co-fired Ceramics tapes. Usually, the screen printing technique is used. In this project, inkjet, rotogravure and flexography will also be tested.

Printing techniques are only used for demonstrators 1, 2, 3 and 6.

Figure 3: Demonstrators of MULTILAYER project [5]

# Objectives

## MULTILAYER project objectives and advantages

The project had three main objectives defined below:

- to develop a set of solutions for the large-scale production of micro-devices using the concept of tape casting and advanced printing techniques,

- to develop and adapt individual technologies considered as promising methods for the mass-manufacturing of multi-layered materials,

- to demonstrate the capability of producing high added value micro-devices with advanced functionalities by designing six demonstrators.

The MULTILAYER project had several advantages in many domains such as production, manufacturing and innovation. Techniques and processes employed to build up the demonstrators during the project are promising because:

- they are efficient mass production methods allowing fabrication series able to reach over a million units,
- they offer a good flexibility for a wide variety of possible components designs,
- they allow the integration of different materials as different layers enabling manufacturing of multilayered packages with a high degree of integration,
- they are reliable techniques and processes; indeed, every single layer can be inspected and controlled during the manufacturing process.

## Thesis statement

The originality of this work was to adapt printing processes to the manufacturing of multilayer devices made of ceramic tapes. To this aim, several steps were accomplished:

- ceramic tapes were studied in order to determine their surface properties,
- conductive inks were formulated and adapted for each printing process. These inks withstood temperatures as high as 800 - 900°C,
- printing processes were used in order to achieve smooth narrow lines and thick enough to allow current conduction,
- four printing processes were tested: screen printing, flexography, inkjet and rotogravure.

The aim of the functional printing subproject was to investigate the possibility of adapting printing processes usually used for thin film production - flexography (roll to roll), rotogravure, inkjet - for printing on flexible and/or rigid ceramic substrate. Screen printing is already an established process for ceramic electronic applications. With this process, the challenge was to develop new water-based printing inks with similar and even better electrical properties than commercial solvent-based pastes. Silver was selected as conductive material due to its high conductivity and thermal stability.

The present manuscript is therefore organised in two major parts (figure 4):

- a literature review that describes substrates for electronic applications, printing processes and their input in electronics, conductive inks and the main applications in printed electronics field,
- an experimental part that details the main objectives and key findings of the thesis. Eight publications, numbered ***Paper 1*** to ***Paper 8***, were written during this thesis. This part is divided into four chapters describing the following points:
    * characterisation and investigation of different tapes - ceramic, silica, glass - to determine the main properties of the inks adapted for the substrates,

* formulation of water-based screen printing silver pastes adapted for green and sintered ceramic tapes ***(Papers 1, 2 and 3)***,
* flexography printing of optimised silver inks on green ceramic tapes and investigation of sintering conditions ***(Papers 4, 5 and 6)***,
* investigation of rotogravure printing potential for printing onto flexible green ceramic tapes ***(Paper 7)*** and inkjet printing of silver ink on sintered ceramic tapes ***(Paper 8)***.

- a conclusion that summarises the main results and exposes the perspectives and the future works on this project.

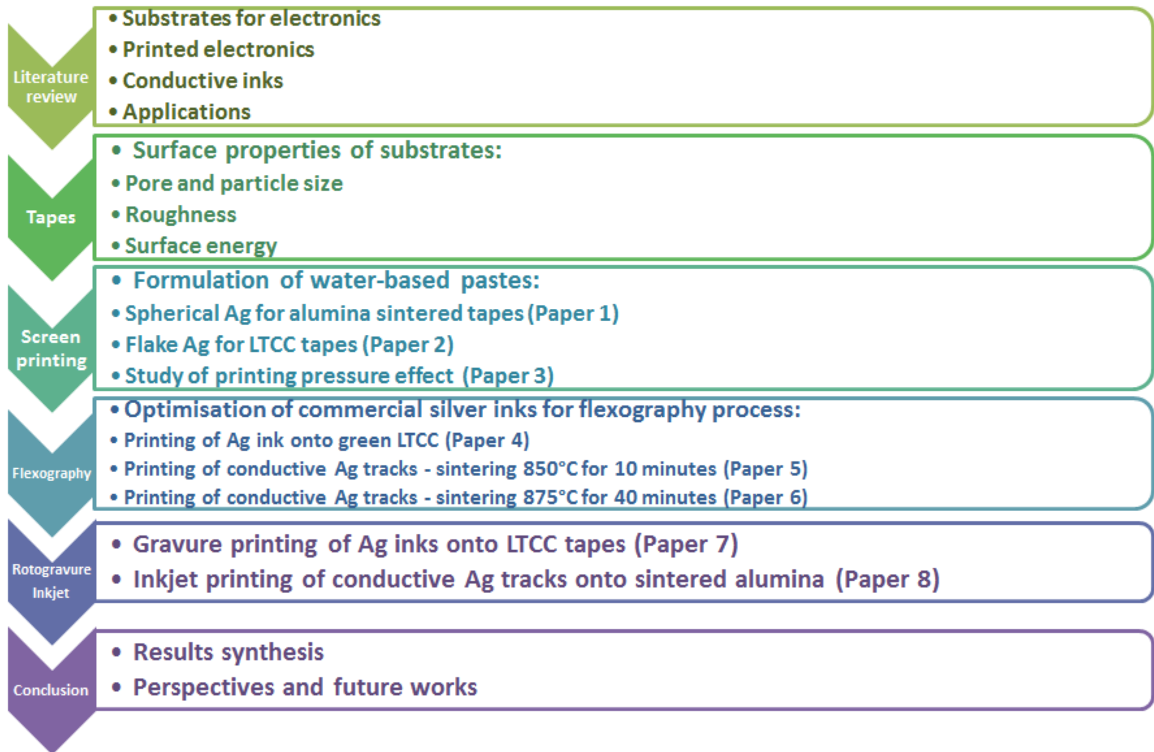


Figure 4: Manuscript general organisation

# References of the general introduction

1. R.S. Khandpur. *Printed Circuits Boards - Design, Fabrication and Assembly.* Mc Graw-Hill - Electronic Enginnering, 2005.

2. P. Ritamaki. Modern radio pioneers: John Sargrove and Paul Eisler. The automatic radio factory and first printed circuits. http://ww.qsl.net - accessed on March $8^{th}$ 2012.

3. R. Das. Printed and potentially printed electronics reach 9.4 billion dollars in 2012. Printed Electronics World, 2012.

4. D. Savastano. Printed electronics: the year in review. Printed Electronics Now, 2011.

5. Grant agreement MULTILAYER project - FP7-NMP-2007 - Annexe I Description of work. MULTILAYER e-doc - internal report, 2008.

6. MULTILAYER standard presentation. MULTILAYER e-doc - internal report, 2010.

# Summary of the original work

## Specifications book and challenges

The main objective of this work was to develop conductive environmentally friendly inks adapted for printing onto ceramic tapes and able to withstand ceramics sintering conditions.

The specification book and scientific challenges of this study are :

- to study different types of ceramic substrates in order to select the most appropriate tape for printing and water-based ink systems,

- to formulate new inks and optimise already existing pastes compatible with the selected substrates,

- to optimise and formulate inks according to the requirements of printing processes (particle and aggregate size, surface tension, rheology),

- to prepare inks able to withstand temperatures as high as 700 to 900°C for 10 to 60 minutes,

- to select a conductive material with high conductivity, relatively low cost compared to gold, resistant to oxidation and handling high temperatures,

- to print uniform well defined lines with sharp edges,

- to reach very low resistivity values, $< 10^{-6}$ Ohm.m, after sintering,

- to test four printing processes:

  * **Screen printing:** the aim of the work was to formulate environmentally friendly water-based conductive pastes. These inks should replace solvent-based inks usually used for screen printing inks formulation. Low evaporation rates solvents are usually used to decrease drying rate of the ink, prevent mesh blocking and enhance ink levelling after deposition on substrate. Typical screen printing solvents such as toluene and terpineol are known for their irritant and toxic character.

  * **Flexography:** the objective was to optimise already existing screen printing paste in order to reduce viscosity and allow printing at laboratory scale.
    The main challenge with flexography inks is the use of particles in sub-micrometer range leading to deposition of very thin layers. As a result, deposited patterns are usually unable to withstand sintering temperatures of green ceramics. Thus, sintering in different atmospheres according to different profiles (temperature, duration) was tested and optimised.

Furthermore, flexography is considered as an innovative method allowing deposition of narrow lines (< 100 $\mu$m). Thus, deposition of different line widths, from 40 $\mu$m to 600 $\mu$m was also investigated.
Finally, in flexography a scale up stage will be performed in the near future. Indeed, this roll to roll process is considered as a high throughput method allowing mass production of printed electronic pieces.

* **Rotogravure:** the objective was to deposit thick enough layers able to form a continuous conductive network after sintering. This process is always in investigation stage. The aim will be to deposit thick ($\sim$ 10 $\mu$m before sintering), narrow (< 100 $\mu$m) and conductive tracks ($\rho < 1.10^{-6}$ Ohm.m).

* **Inkjet:** the objective was to obtain a stable conductive nano-suspension. Furthermore, in order to allow adhesion of inkjet printed lines on ceramic tapes, nano-metric adherence agent should be used. The challenge was to deposit conductive lines by overlaying few layers compared to already published works in which more than 10 layers of metallic inks were deposited to reach low electrical resistivity.

# Methodology

A literature review was completed, in order to understand ceramics formation and behaviour during sintering and then select an adapted conductive material. Printing processes were also investigated in order to determine their typical properties and those of their related inks. Main previous works on printed electronics were also investigated.
The literature review allowed:

- to select silver conductive material due to its high conductivity ($6.10^7$ S.m$^{-1}$), its thermal and chemical stability compared to copper and nickel and its relatively low cost compared to gold,

- to print alumina tapes after sintering: alumina is sintered at temperatures higher than 1600°C. Silver is not able to withstand such high temperatures,

- to print Low Temperature Co-fired Ceramic (LTCC) tapes at green stage. LTCC are sintered at relatively low temperatures (< 900°C) that silver particles could withstand.

This study also revealed that:

- metallic screen printing pastes are usually solvent-based. The vehicle is composed of low evaporation rate solvents such as terpineol and toluene known for their toxicity and their irritant character. The challenge of this study was then to formulate water-based environmentally friendly silver pastes with low evaporation rate adapted to screen printing. The prepared inks should also allow deposition of conductive tracks after sintering at temperatures as high as 875°C. Thus, particles with diameters larger than 1 $\mu$m were selected due to their higher thermal stability. Indeed, smaller particles (< 1 $\mu$m) melt and oxidise at lower temperatures,

- flexography of conductive metallic inks onto ceramic green substrates was not tested yet. This study is then innovative because flexography of silver inks onto LTCC was tested for the first time in this work.

An experimental part based on acquired knowledge was therefore performed:

- ceramic tapes supplied by partners were characterised with the techniques usually used to test the printability of paper substrates. Thus, their surface properties - surface energy, roughness, pore and particle size - were determined before and after sintering in order to select the appropriate inks for these tapes,

- new inks were formulated and commercial inks optimised and adapted for different printing processes,

- ink characterisation was performed to investigate their rheological properties and measure their surface tension,

- printing of new formulated, optimised and commercial inks was performed by screen printing, flexography, rotogravure and inkjet printing,

- deposited lines were then characterised before and after sintering. Their thickness, width, roughness and electrical properties were determined and their microstructure investigated,

- when printing and/or electrical results were not satisfactory, ink formulae, printing parameters and sintering conditions were optimised.

Figure 5 is a schematic of the methodology adopted in this work.

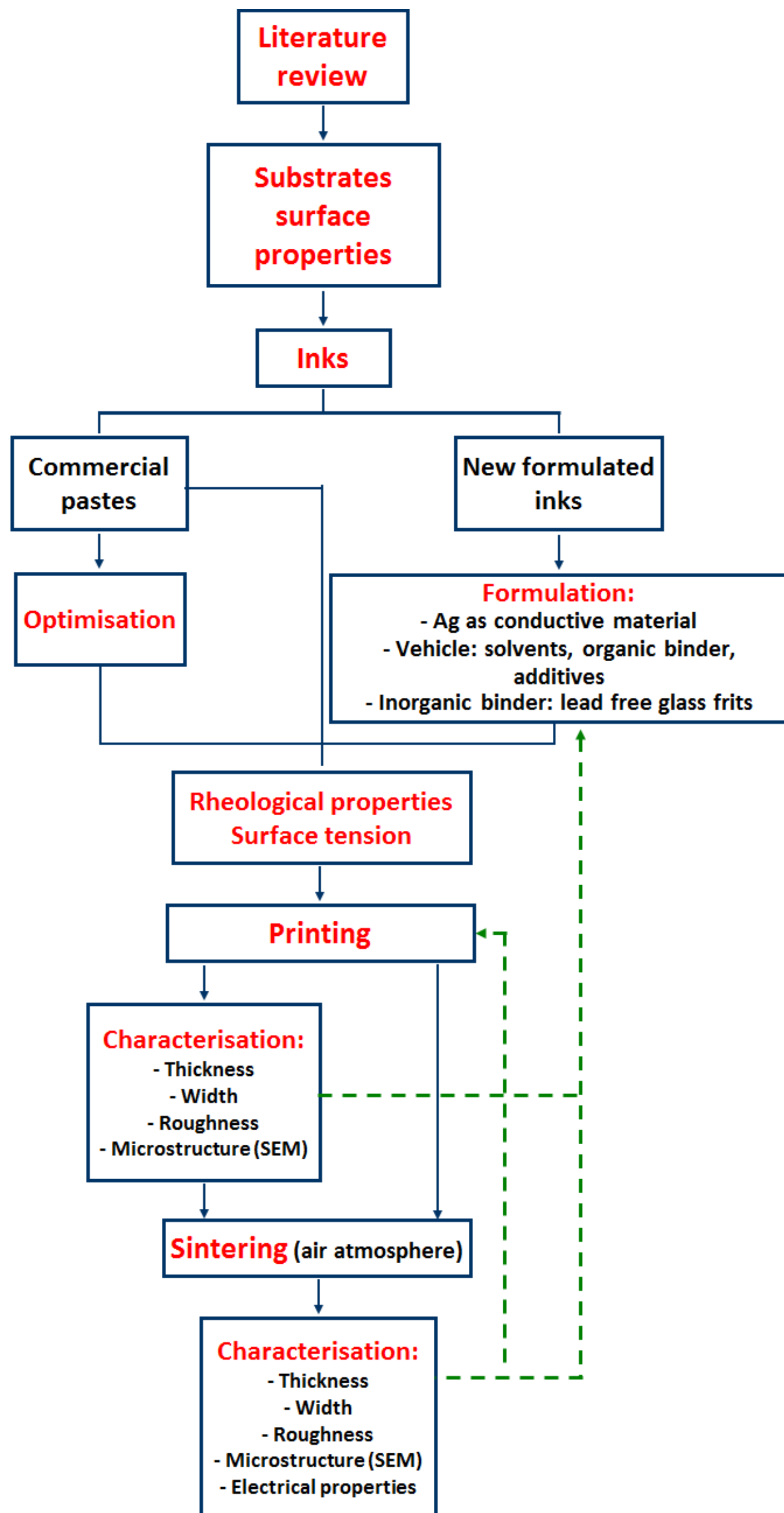


Figure 5: Scheme of the methodology

In order to achieve this methodology skills in different techniques were acquired:

- investigation on Scanning Electron Microscopy (SEM) micrographs allowing to study substrates and lines microstructures (Environmental SEM Quanta 200),
- surface topography measurement allowing to determine the deposited lines thick-

ness, width and roughness (Alicona 3D profilometer),

- optical microscopy to observe definition of deposited lines (Carl Zeiss optical microscope),

- contact angles measurement in order to determine the surface energy (Owens, Wendt, Rabel and Kaelble - OWRK method) and pendant drop method to determine inks surface tension (OCA system),

- conductive inks formulation by mechanical dispersion (Dispermat) and three roll-mill grinding (EXAKT 50),

- rheological behaviour characterisation and models studying in shear mode (Newton, Bingham, Hershel-Bulkley, Casson) and oscillatory rheology investigation (Anton Paar rheometer),

- printing with four processes:

  * screen printing: full automatic DEK Horizon 03i printing press,
  * flexography: laboratory tester Flexiproof 100,
  * rotogravure: laboratory tester IGT 3H,
  * inkjet: drop on demand printer Fujifilm - Dimatix DMP2831,

- sintering in traditional furnace under normal atmosphere (Statop Nagat furnace),

- Thermo Gravimetric Analysis (TGA) in order to understand the silver ink behaviour at high sintering temperatures (Perkin Elmer DT-TGA),

- measurement of the current conduction and calculation of resistivity and sheet resistance (with respectively a 2 probes Jandel apparatus and a 4 probes Jandel apparatus).

# Key findings and main results

In order to overcome the challenges fixed by the specifications book, substrates were first characterised in order to select the appropriate ink particle size and solvents. Water-based inks were formulated and optimised in order to meet printing processes requirements. Then, printed tapes were sintered. Deposited lines were afterwards characterised before and after sintering in order to determine their geometrical and electrical properties. Finally, conclusions were drawn to point out the key findings and original results.

***In this manuscript, all silver and glass powders quantities are given in weight percentage.***

## Substrates study

Two types of substrates, selected to perform printing tests, were investigated: alumina High Temperature Co-fired ceramic (HTCC) and Low Temperature Co-fired Ceramics (LTCC). Their microstructure was investigated before and after sintering.

Their surface properties - pore and particle sizes, roughness and surface energy - were specified. These properties allowed selection of ink particle size able to remain on the surface, to set up the ink formulation and pick up the solvent.
Comparison between green and sintered tapes was also established.

According to pore size and roughness values, green LTCC tapes were printed with inks containing particles with a diameter smaller than 5 $\mu$m. Sintered alumina, with a high smoothness and no visible pores, were printed with inks containing variable particle size - diameter varying from 0.015 $\mu$m to 3 $\mu$m.

Tapes surface energy varied from 30 to 60 mJ.m$^{-2}$ depending on their stage (green or sintered) and initial composition. Thus, in order to adapt water-based inks to low surface energy substrates, surfactant was added.

Tapes roughness depended on the size of powders used to prepare the initial slurries. Thus, when the majority of particles were smaller than 0.4 $\mu$m, the measured roughness was equal to 0.03 $\mu$m. However, when the majority of particles was smaller than 2.0 $\mu$m, roughness varied from 0.22 $\mu$m to 0.27 $\mu$m.

After sintering, substrate pores were closed, their particle size and their surface energy increased. This was attributed on one hand to organic binder and solvent burn out and, on the other hand, to ceramics powders melting. Figure 6 illustrates SEM microstructure of an LTCC tape showing the porous surface before sintering (a) and the closed pores after sintering (b).

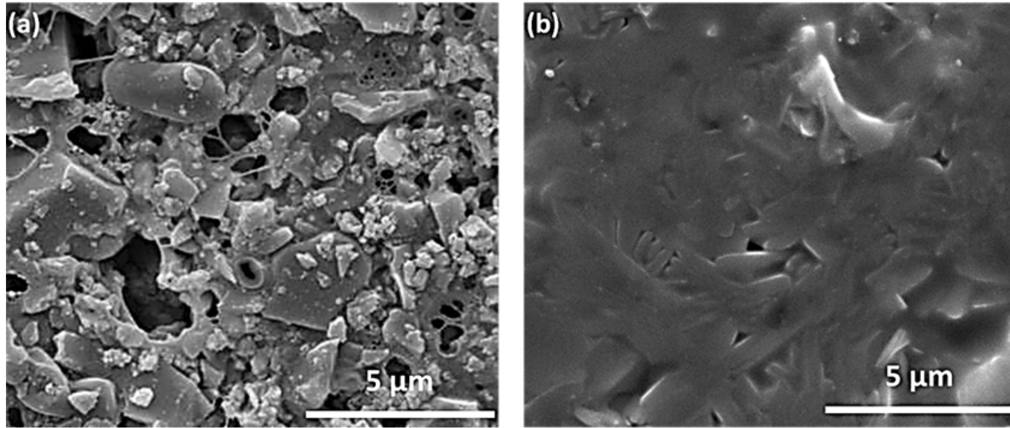


Figure 6: LTCC tape SEM microstructure before (a) and after (b) sintering

## Screen printing onto ceramic tapes

Water-based screen printing pastes were formulated with different types and sizes of silver particles. Mixture of water/ethylene glycol/glycerol was used as a solvent in order to reduce water evaporation rate. Silver particles with 1 to 5 $\mu$m diameter adapted to the process and the tapes and able to withstand 900°C temperatures were selected. Tests were performed on a DEK Horizon 03i full-automatic printing press.

All pastes had a thixotropic behaviour. Viscosity decreased when shear rate increased and was then enhanced after stopping or decreasing shear rate. Pastes also had a yield stress, minimum shear stress below which a material cannot flow. An example of thixotropic behaviour, characterised by hysteresis loop, is shown on figure 7.

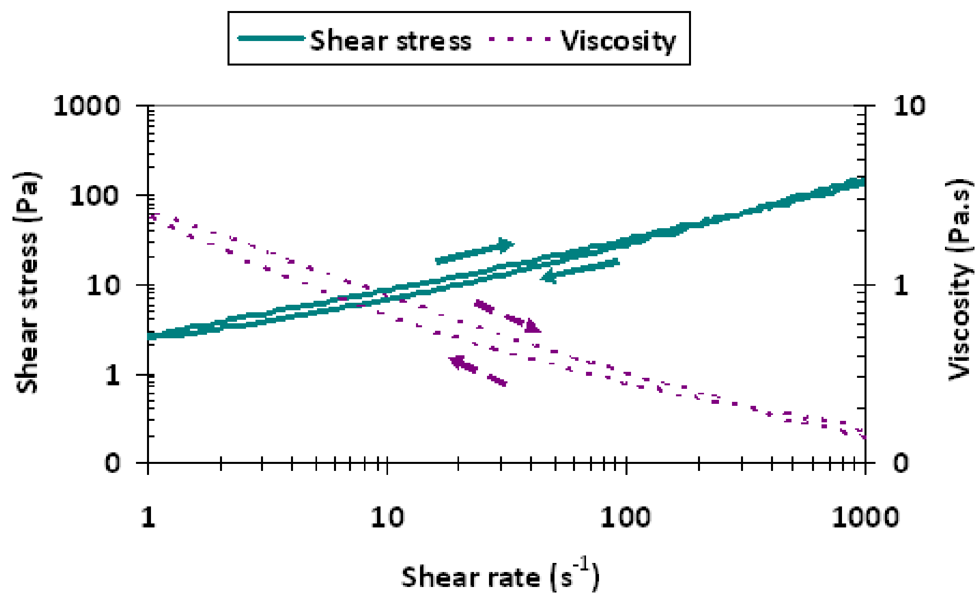


Figure 7: Rheological behaviour of a silver paste containing 45% Ag particles and 10% glass powders as a function of shear rate

Spherical particles were used to formulate pastes containing 70 to 80% silver. Printing

was performed onto sintered alumina tapes ***(Paper 1)***.
Silver content effect on rheological and line properties was investigated. Narrower and thicker lines were obtained with higher solid content and viscosity inks. Resistivity decreased when silver content increased due to the network compactness enhancement when more particles were added.
Temperature effect on electrical properties was also determined. Electrical properties of printed lines were enhanced when temperature increased from 500 to 900°C. It was demonstrated that after sintering a continuous conductive silver network was created. Figure 8 shows the microstructure of a 75% silver ink sintered at 700°C for 15 minutes.

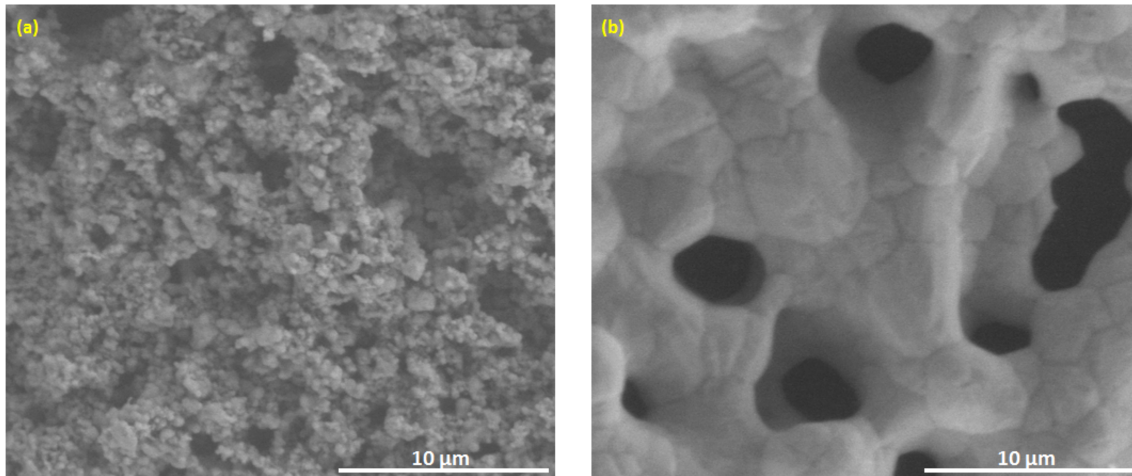


Figure 8: 75% Ag paste on sintered alumina tape before sintering (a) and after sintering at 700° (b): a continuous silver network is formed after sintering (SEM)

Even though, pores were visible after sintering, deposited lines were continuous and exhibited $3.5.10^{-8}$ Ohm.m resistivity. Line resistivity as small as $2.3.10^{-8}$ Ohm.m was achieved after sintering at 900°C for 10 minutes.

Mixture of flake and spherical silver particles was also employed as conductive material for the preparation of environmentally friendly screen printing pastes ***(Paper 2)***.
Printing was performed onto green LTCC tapes. Lines with sharp edges were successfully deposited (figure 9).

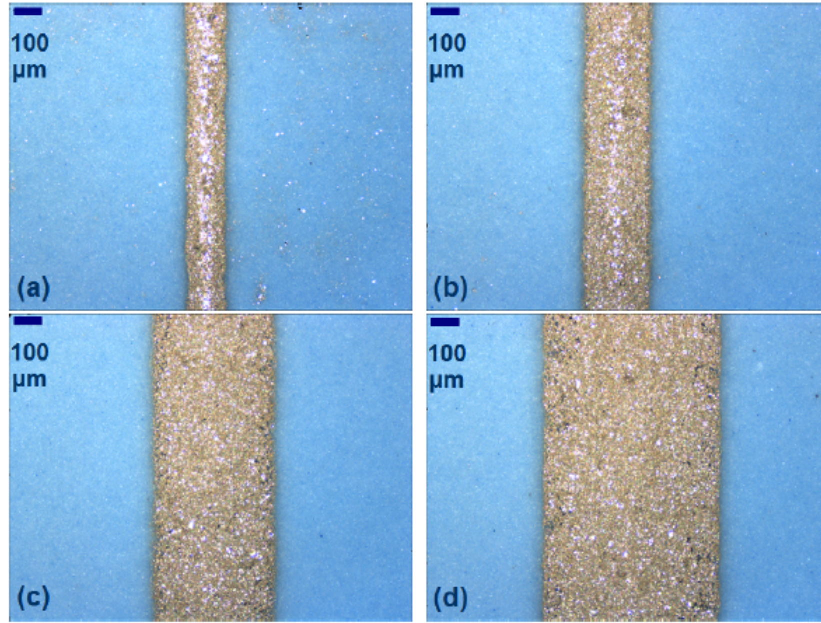


Figure 9: Optical microscope images of green lines printed by 72% Ag ink onto LTCC tape: 100 $\mu$m (a), 200 $\mu$m (b), 400 $\mu$m (c), 600 $\mu$m (d)

Inks rheological behaviour was studied in ***Paper 2***. Elastic and loss modulus were calculated to determine the relationship between inks behaviour and their transfer through the screen mesh. It was demonstrated that high solid content inks had high elastic modulus compared to loss modulus. These inks were very tacky and their release through the screen mesh was disturbed. If viscosity was very low, inks would have low elastic moduli and they would flow easily through the screen opening. Lines with poor definition would be deposited. This case was not observed in this study. Inks containing a minimum 67% silver with a minimum 7 Pa.s viscosity at 0.1 $s^{-1}$ were formulated. The variation of $G''/G'$ ratio traducing the visco-elastic behaviour of materials is shown on figure 10 as a function of the shear stress for 67, 72 and 75% silver pastes. When $G''/G'$ ratio decreased, the elastic behaviour of the material is enhanced and its flowing through the screen mesh is disturbed.

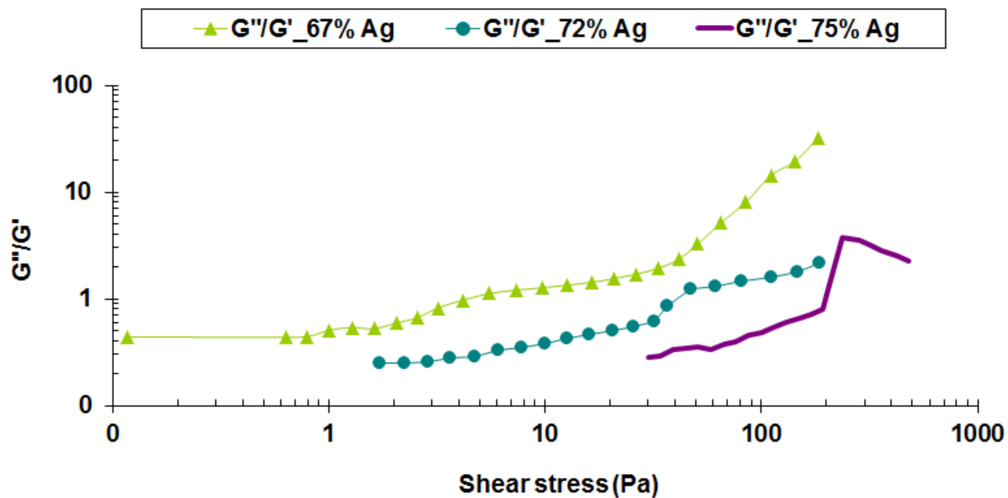


Figure 10: Evolution of $G''/G'$ as a function of shear stress and silver quantity

The printed lines were conductive even at green stage. After sintering, line width and thickness decreased. A conductive line with a minimum width of 60 $\mu$m was achieved after sintering. Resistivity varied from 2 to $4.10^{-8}$ Ohm.m.

Study of screen printing force effect on printed lines and their electrical properties was studied for 75% silver ink because of the non-homogeneous lines deposited in previous study. Force effect on line definition was investigated in ***Paper 3***. A 75% Ag silver paste was screen printed at different printing loads (3 to 12 kg). It was demonstrated that more silver was transferred on the printed lines when higher loads were applied because more solid particles were allowed to pass through the screen mesh (figure 11).

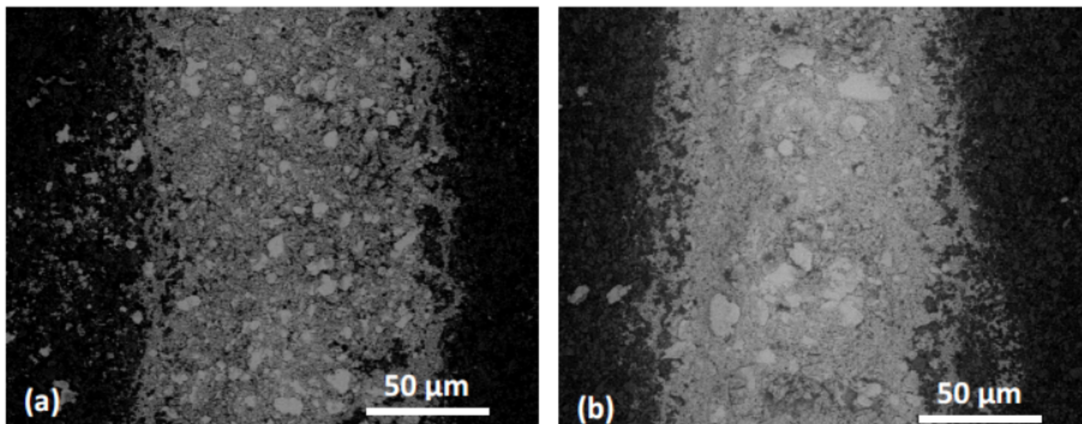


Figure 11: Backscattering SEM surface micrographs of a silver ink printed on LTCC tape before sintering: (a) 3 kg (b) 5 kg

This was explained by the rheological behaviour of the ink and mainly the yield stress. An optimum printing force of 5 kg was obtained. This force allowed deposition of maximum line thickness (14 $\mu$m) and narrower width (114 $\mu$m). At higher loads ($>$ 7 kg), quantity of transferred material was decreased. This was related to the visco-elsatic behaviour of the inks. Indeed, it was demonstrated that at high shear stress ($>$ 150 Pa), 75% paste had a tendency to recover its elastic state. This was related to a slight decrease (from 3.1 to 1.8) of $G''/G'$ shown on figure 12.

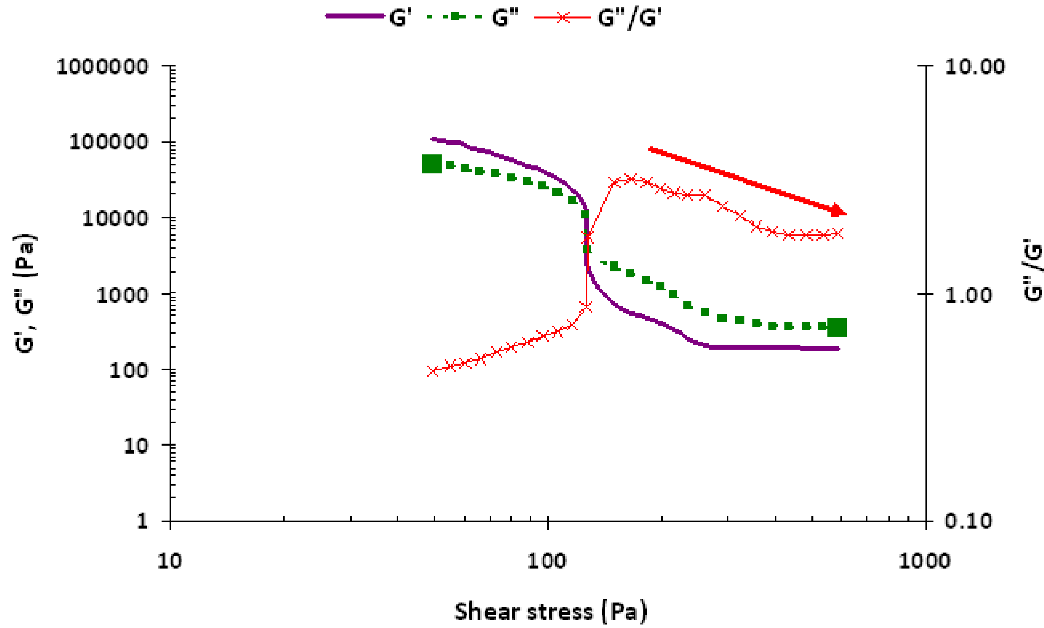


Figure 12: $G'$, $G''$ and $G''/G'$ of 75% silver inks at shear stress higher than 50 Pa

In conclusion, the results obtained meet the specifications book requirements:

- formulation of water-based environmentally friendly screen printing pastes was achieved. These pastes can replace commercial conductive inks containing irritant solvents such as terpineol, toluene, phtalates and others,
- resistivities as low as $2.10^{-8}$ Ohm.m were reached which are better than published and commercial values,
- such inks are able to withstand hard sintering conditions, 875°C for 1 hour, and thus can be integrated in multilayer systems.

Ink formulation (silver quantity and paste viscosity), dispersion (three roll-mill), printing parameters (speed, pressure, off-contact distance, mesh) and sintering conditions could be adjusted to allow optimum ink transfer and maximum conductivity.

## Flexography printing onto LTCC green tapes

A screen printing paste containing 65% flake silver was diluted with distilled water to reach flexographic inks requirements. Particles of 0.4 $\mu$m mean diameter were selected to prevent anilox cells blocking. Inks with viscosities in the same order of magnitude as flexographic inks were prepared. Viscosity was decreased from 28 Pa.s to 3 Pa.s when silver weight decreased from 65 to 40% (figure 13).

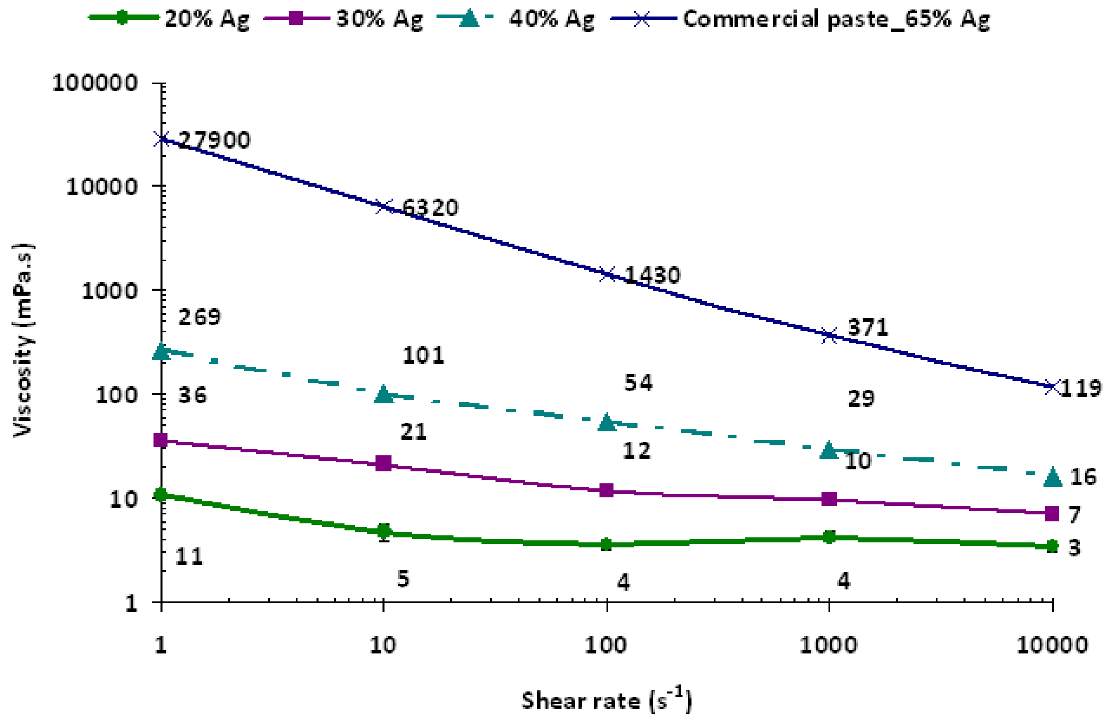


Figure 13: Rheological behaviour of optimised inks - 20%, 30% and 40% Ag - and commercial paste containing 65% Ag

Printing direction was investigated and it was demonstrated that lines oriented in the printing direction allowed deposition of narrower tracks with sharp edges (figure 14).

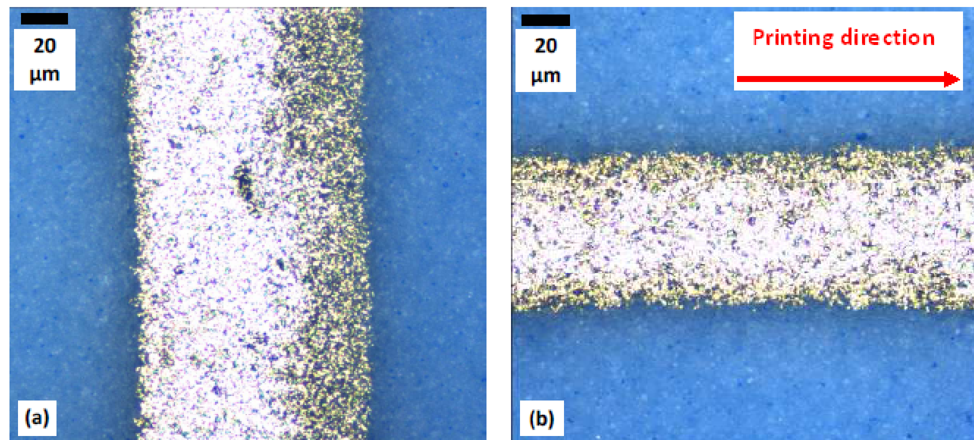


Figure 14: Lines perpendicular (a) and parallel (b) to printing direction - 30% Ag on LTCC tape (Alicona)

An anilox with two different rulings was used in order to perform printing tests:

- 180 lines.cm$^{-1}$ resolution and 5 cm$^3$.m$^{-2}$ volume,
- 100 lines.cm$^{-1}$ and 10 cm$^3$.m$^{-2}$ volume.

Ink transfer is dependent on anilox volume and ruling. On one hand, well defined narrow lines (82 - 92 $\mu$m) were deposited with a high resolution anilox compared to lower reso-

lution one (92 - 105 $\mu$m). On the other hand, thicker lines (0.70 $\mu$m) were printed with high volume anilox compared to low volume one (0.55 $\mu$m) which was expected.

Printing of 20% and 30% silver ink onto green LTCC (Low Temperature Co-fired Ceramics) tape was succussfully carried out ***(Paper 4)***.
Number of layers effect on lines properties was studied. A minimum of three layers was required to allow deposition of more than 1 $\mu$m thickness. High thicknesses were desired to allow better particles connections and more cohesive silver network after sintering. This was attributed to the small ink particle size compared to tape surface pores. Inks with sub-micrometer particles were selected to prevent anilox cells blocking. Thus, in order to cover substrates roughness and pores, minimum three printing passes were required (figure 15).

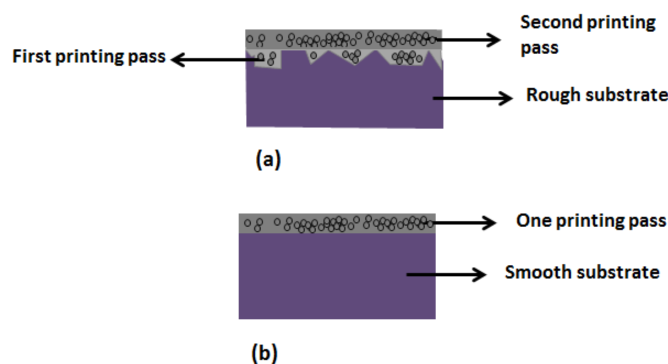


Figure 15: Schematic representation of particles settling on substrates: (a) rough substrates with surface pores larger than ink particle size - particles go into pores, (b) smooth substrate - particles stay at surface

Flexography printing of conductive silver tracks onto ceramic tapes was achieved for the first time in this study ***(Paper 5)***.
Three to five layers of 30% silver ink were overlaid onto green LTCC. Sintering was then performed under normal atmosphere at 850°C for 10 minutes. Line with $3.10^{-8}$ Ohm.m resistivity, close to that of bulk silver, was achieved. It was shown that silver behaviour is dependent on sintering conditions (temperature and duration). Deposited lines were not able to withstand classical multilayer LTCC systems sintering conditions. For this reason, they were sintered at lower temperature and for a shorter time (figure 16).

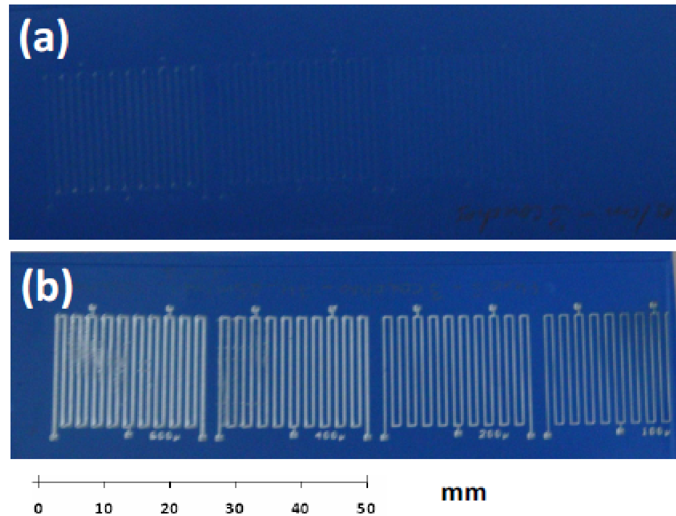


Figure 16: 5 layers 30% Ag ink sintered in normal atmosphere at 875°C for 60 minutes (a) and at 850°C for 10 minutes (b)

In order to increase deposited ink thickness and then allow preparation of conductive tracks withstanding higher temperatures for longer times, 40% silver ink was prepared and printed by flexography ***(Paper 6)***. Multilayer LTCC systems are conventionnaly co-fired for more than 30 minutes.
Thermal behaviour of the optimised ink was analysed by Thermo Gravimetric Analysis coupled to a Differential Thermal Analysis (TG-DTA)(figure 17).

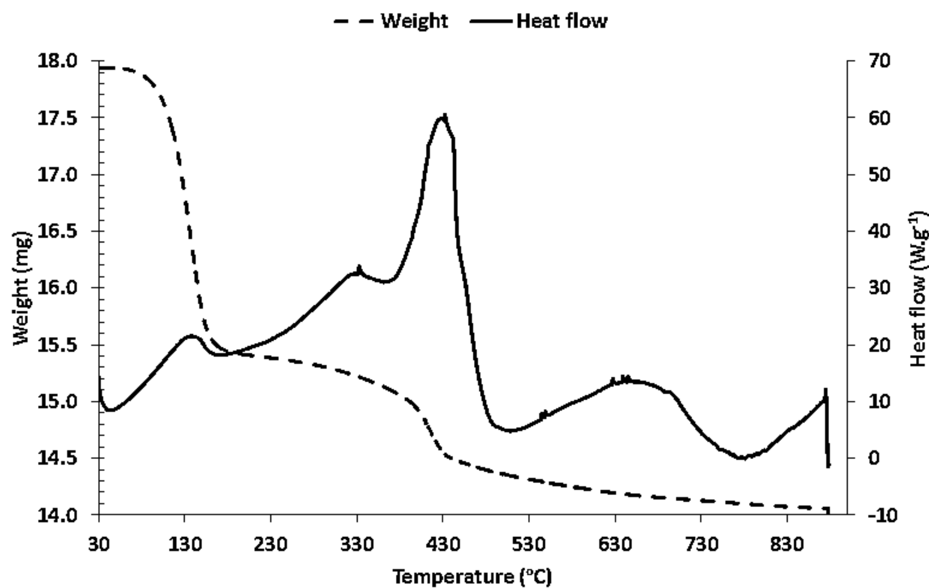


Figure 17: TG-DTA of 40% Ag ink

An endothermic peak related to a weight loss was observed at temperatures higher than 600°C. Thus, it was supposed that 0.4 $\mu$m silver decomposition occurs at high temperatures. If sintering is performed for a long duration and if there is not enough silver to withstand decomposition, no more particles will be left to allow conductive network

creation.
In this work, 5 layers of 40% silver ink were able to withstand hard sintering conditions: 875°C for 40 minutes (figure 18).

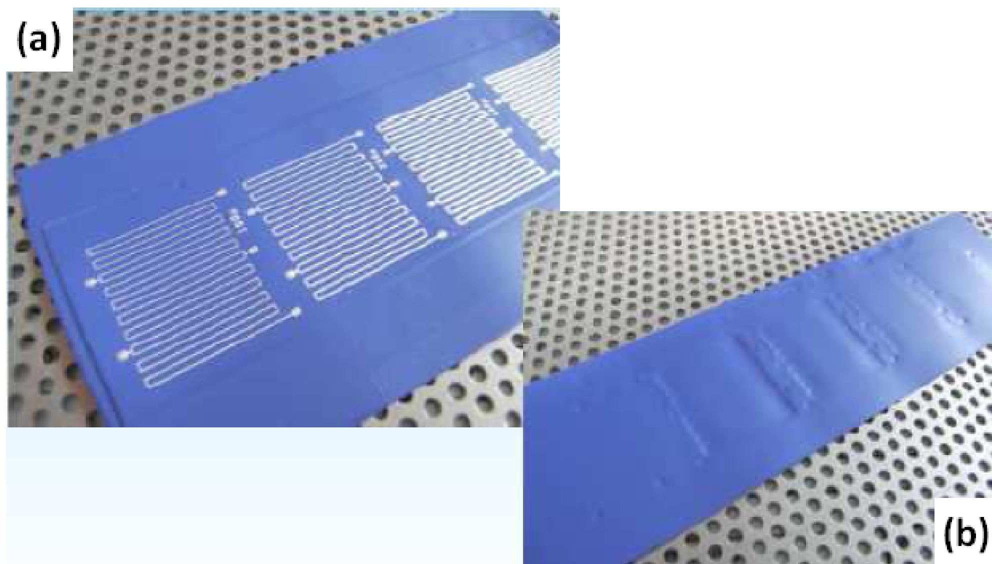


Figure 18: 5 layers of 40% Ag ink sintered at 875°C for 40 minutes - (a) printed side, (b) reverse side (MSE presentation for 30M MULTILAYER meeting)

Conductive lines with 9 to 21.10$^{-8}$ Ohm.m resistivity were obtained after sintering.

In conclusion, obtained results fulfill the specifications book objectives:

- flexography printing of conductive silver metallic tracks onto green ceramic tapes was successfully achieved,
- printed lines withstood even very hard sintering conditions: 875°C for 40 minutes. This promising result is a first step in the development of flexography printing process for printed ceramic multilayer applications. This study demonstrates the huge potential of flexography printing for LTCC multilayer systems,

Printing of conductive metallic tracks onto ceramic tapes by flexography is an innovative study and was successfully carried out for the first time in this work.

## Potential applications of rotogravure and inkjet

Other printing processes such as rotogravure and inkjet methods were investigated to study their potential in ceramic printed electronics.

### Rotogravure printing onto green LTCC tapes

Rotogravure printing of silver tracks onto green LTCC tapes was investigated ***(Paper 7)***.
Water-based inks containing 35 to 55% spherical silver particles with a mean diameter of 2 to 3 $\mu$m were formulated. These inks were printed on different LTCC tapes with variable properties (pore size and surface energy). An intaglio engraved cylinder was used.

Channels of 46 $\mu$m height and 136, 222, 414 and 605 $\mu$m width allowed ink transfer to the substrates. Only inks printed with 136 $\mu$m width channels were continuously printed and exploitable (figure 19).

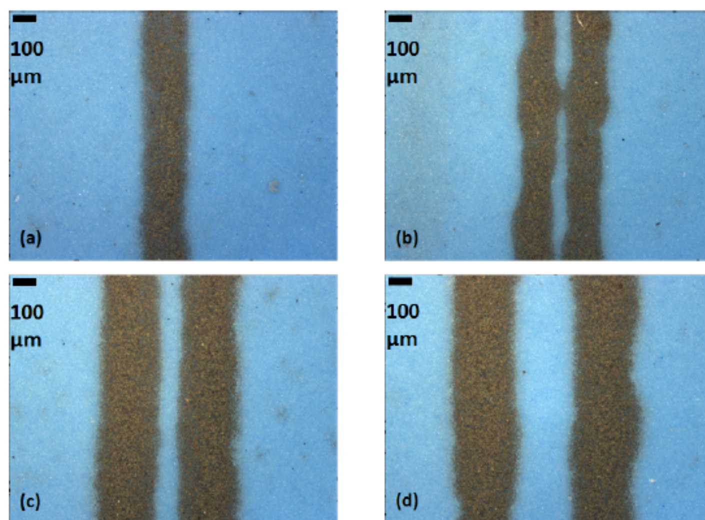


Figure 19: Silver line printed by rotogravure with a 136 $\mu$m (a), 222 $\mu$m (b), 414 $\mu$m (c) and 605 $\mu$m (d) engraved cylinder channels width (Optical microscopy - Alicona)

Relationship between substrates properties (pore size, roughness, surface energy), ink characteristics (viscosity, surface tension) and ink transfer (width, thickness) was established.
Highest thicknesses (5.5 $\mu$m) were deposited with high silver content inks (50 and 55% silver).
The narrowest lines (172 $\mu$m) were printed on the substrate with the lowest dispersive component to total surface energy ratio ($\gamma_s^d/\gamma_s = 0.38$). Indeed, formulated inks exhibited low surface tensions (12 to 16 mN.m$^{-1}$) with a dispersive tendency due to the silicone based surfactant added to ink formulae. Thus, inks were not compatible with the high surface energy tape having a high polar component (36 mJ.m$^{-2}$) compared to the dispersive one (22 mJ.m$^{-2}$). Consequently, dispersive ink spreading on this tape was limited.

Transferred silver did not whithstand sintering at 800°C for 10 minutes. There was not enough particles after sintering to allow conductive network formation (figure 20).

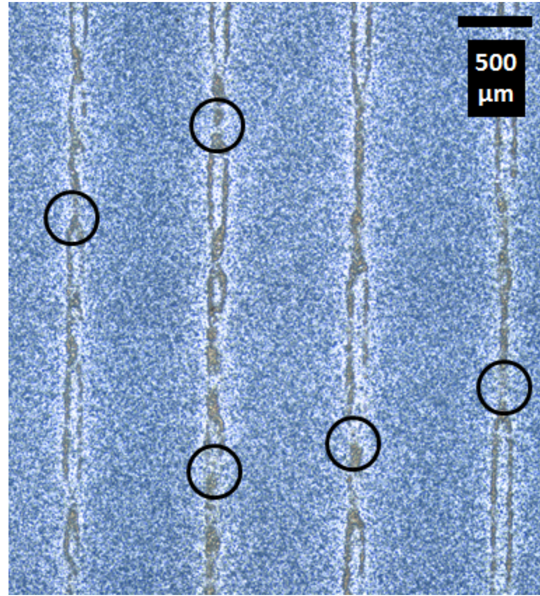


Figure 20: 100 $\mu$m nominal width silver lines printed by rotogravure on LTCC tape after sintering at 800°C for 10 minutes under normal atmosphere (Alicona)

In order to deposit thick films able to handle high ceramics sintering temperatures, cylinder engraved with higher volume cells (100 $\mu$m) would be tested. Futhermore, flake silver particles might be also used, given their higher surface contact.

### Inkjet printing onto alumina sintered substrates

Inkjet printing onto sintered alumina tapes was also studied (***Paper 8***). The main limitation in inkjet printing is the jetting nozzle diameter (10 to 100 $\mu$m). Indeed, to allow metallic ink adhesion to ceramic substrates, usually glass powders are added. Commercial powders are in micro-meter range and cannot pass through inkjet printing nozzles. Futhermore, typical thicknesses deposited by this process are lower than 1 $\mu$m. For this reason, many layers are required to allow conductive lines printing (3 to 60 layers).

A commercial ink with 42% of 15 nm mean diameter silver particles was optimised to obtain 21% silver ink (wt %). 100 nm silica and potassium based powders were added by the manufacturer as adhesion agent. After dilution, viscosity was decreased from 12 to 4 mPa.s and surface tension increased from 40 to 51 mN.m$^{-1}$. Three printed layers were required to allow ejected drops merging and continuous line formation (figure 21).

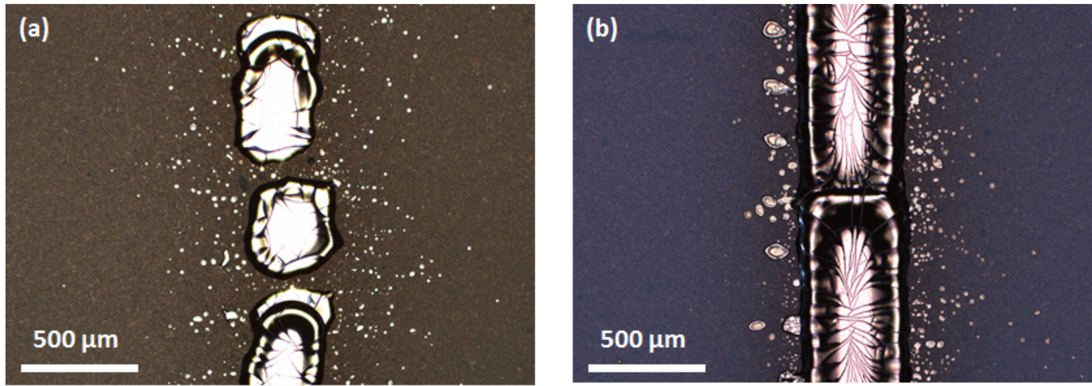


Figure 21: Silver ink printed by inkjet onto alumina sintered tape: (a) one layer, (b) three layers (Optical microscope)

A 700°C optimal sintering temperature allowed silver particles and adhesion promoter softening (figure 22).

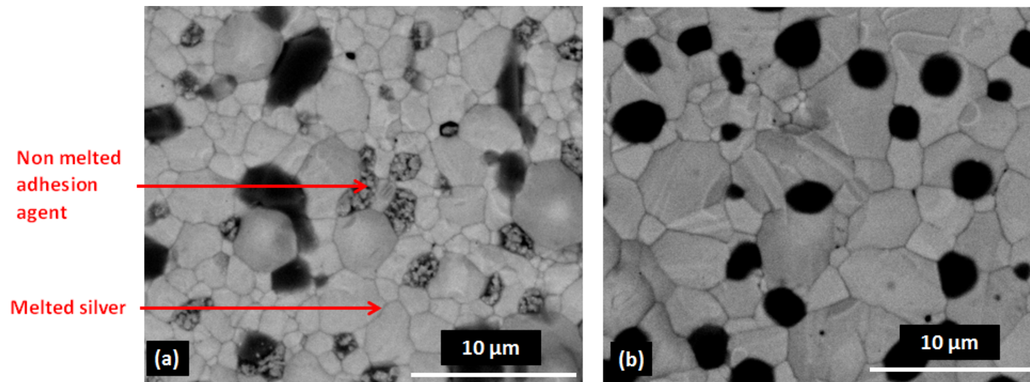


Figure 22: Microstructure of sintered silver line printed by inkjet onto sintered alumina tapes: (a) 500°C, (b) 700°C (SEM)

Electrical resistivity increased at 800°C ($11.10^{-8}$ Ohm.m). This was attributed to silver nano-particles decomposition at high temperature. At 900°C, printed lines were not continuous and were not able to form a continuous conductive network.
In conclusion, a continuous conductive network was created with only three layers and a $2.10^{-8}$ Ohm.m resistivity was measured. This value is very close to that of bulk silver and is one of the lowest resitivities achieved by inkjet printing of conductive inks.
In order to deposit conductive lines by printing only one layer, silver content could be increased and printing parameters optimised (drop spacing, printing speed, frequency, voltage).

# Main conclusions and perspectives

Printing processes are low cost, relatively simple methods and environmentally friendly techniques that allow manufacturing of electronic devices:

Screen printing is a well established process allowing deposition of a thick conductive layer with only one printing pass. The possibility to formulate non hazardous water-based screen printing pastes was shown in this study. These inks could replace commercial solvent-based non ecological inks.
Future works could be performed to optimise and more investigate screen printing for electronic applications:

- screen printing pastes could be optimised by performing the three-roll mill grinding in order to homogenise deposited lines,
- thermoelectric inks would be screen printed onto alumina sintered taped in order to fill 300 $\mu$m height and 0.5 mm diameter holes. This task would be performed with the collaboration of the CEA,
- screen printed tracks potential in radio-frequency transmission is under investigation with the collaboration of Swerea IVF and Omnysis.

It was also shown that flexography that offers a huge potential for the mass-production may be employed for ceramic/metallic electronic devices manufacturing. The ability of flexography printed conductive lines to withstand ceramic sintering temperatures was demonstrated for the first time in this work.
In the near future, pilot tests would be performed on a semi-industrial flexography press in collaboration with the CEA and KMS automation GmbH. Printing of silver inks would be performed onto green LTCC and alumina tapes.

Lines deposited by rotogravure were not able to withstand ceramics sintering conditions. Higher thicknesses should be deposited in order to form continuous silver networks. In order to reach these thicknesses, a new cylinder was engraved with 100 $\mu$m height cells. Thus, higher viscosities and silver content inks could be formulated and tested.

Regarding inkjet printing onto ceramic tapes, the objective was to add nano-sized adhesion promoters able to flow through the inkjet nozzle and which allow ink film adhesion to substrate after sintering. A non-optimised commercial ink containing adhesion promoters was adapted to the Dimatix printer. Three layers were printed by inkjet. They adhered to substrate and had very low resitivity, $1.7.10^{-8}$ Ohm.m. An optimum sintering temperature of 700°C was determined. Ink formulation could be optimised to enhance printing resolution and ink stability during time.

This work highlights the huge capability of printing techniques in ceramic micro-electronic devices manufacturing and opens perspectives for industrialisation and commercialisation of very high conductivity electronics.

# Part I

# Literature review

# Introduction

Different subjects related to printed microelectronics and connected with the MULTI-LAYER project are treated in this part

- In the first chapter, substrates used for electronic devices manufacturing are studied. Ceramics, glass, silicone and polymer substrates are described. Some substrate properties such as mechanical behaviour, thermal characteristics and wettability are highlighted.

- In the second chapter, lithography methods are described and compared to printing processes. The advantages, printing defects and related inks of these processes are exposed.

- In the third chapter, ink formulation and inks major properties are presented. Thus, the subject of conductive materials, inks and previous works concerning conductive inks applications in electronics are drawn out. Sintering process of conductive materials will also be explained.

- Finally, some applications related to printed microelectronics are shown.

The schematic shown in figure i will be followed and detailed in this part.

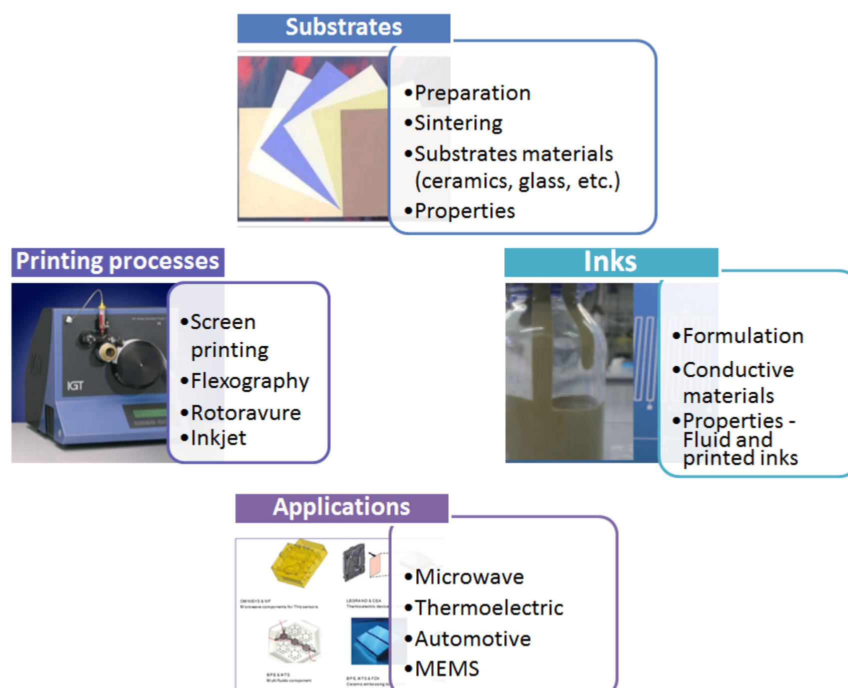


Figure i: Literature review outline

# Chapter 1

# Substrates for electronic applications

Substrates used for electronic applications should have high resistivity to provide adequate insulation of the circuit elements. They must be chemically inert and have good mechanical properties. Their surface must be plane, even and smooth. Glass, ceramics, plastic materials and paper are already used as substrates for printed electronics.

## 1.1 Substrates types

### 1.1.1 Ceramic substrates

*Ceramics* is a general term used to describe mineral oxide materials such as aluminium, barium, magnesium and other mineral oxides.

They are mainly composed of mineral oxides, nitrides or carbides as functional phase and organic binders necessary for inorganic particles dispersion and tape casting. Besides, some additives are added to supply appropriate rheological behaviour, dispersibility and stability.

Ceramics have wide applications domains because of their electrical properties. Indeed, they can be insulators, conductors (metals or superconductors) and also allows ions conduction. Ceramics conductivity varies from $10^{-18}$ to $10^{6}$ S.cm$^{-1}$ [7].
Ceramics are therefore used in high-tech electronics requiring precision, accuracy and high conductivities. Piezoelectric ceramics are especially used for motors and vibration suppressors manufacturing. They are employed as substrates in lasers, cameras, semiconductor chips manufacturing, and other electronic applications.

Ceramics forming starts by powders preparation followed by tape casting. The sintering process is then performed. Ceramics are, thus, influenced by many factors at each stage:

- powders are influenced by particle size distribution, particle morphology, and surface chemistry,
- compaction is related to powders packing density,
- casting is affected by slurry rheological behaviour, dispersibility and stability,
- sintering is influenced by temperature, gas atmosphere and pressure.

### Ceramic preparation process

#### Powders preparation

Powders can be prepared by mechanical stirring of a stoechiometrical mixture of inorganic elements required to manufacture the final ceramics with additives essential to improve grindability and sintering. The objective is to have the minimal possible sintering temperature.
When the size distribution is uniform, green body density is higher, consequently, total contact area increases and also lattice imperfections. This last factor is considered by *Kuang et al., 1997* [8] as the second drive force in the sintering process. Actually, mechanical action exposes imperfections and brings them to the surface of the material. As a result, the solid breaks into particles [8][9].
Grinding aids are added in small percentage, approximately 0.1% by weight, in order to improve grindability by preventing reagglomeration, simplifying dispersion, controlling the slurry rheology and reducing the breakage energy. Sintering additives are also added in a weight percentage ranging from 0.005% to 0.1%. These aids are used in order to inhibit the grain size growth and lower the sintering temperature. For example, *Liu et al., 2011* [10] demonstrated that adding magnesium oxide or silica powders during alumina powders preparation inhibits $Al_2O_3$ grain growth.

Other methods are also used to prepare ceramic powders such as sputtering [11], plasma discharge [12], gas condensation techniques [13] and wet chemical methods [14][15][16].

#### Tapes preparation

**Tape casting** Ceramics are mainly manufactured by tape casting method. This technique allows forming of thin, thick and flexible tapes. Ceramic tapes fabrication is composed of different steps [17]:

- the slurry preparation: mineral ceramic powders are dispersed in solvent such as water. Then, organic binder such as acrylic and modified cellulose are added. Afterwards, additives are introduced to supply appropriate properties for tape casting, drying, etc.

- after mixing, dispersing and homogenisation, the next step is the pumping of the suspension directly to a tape-casting machine through a vessel or a slurry container. At this stage, viscosity and pressure are controlled. Vacuum de-airing is then performed before casting. This allows deposition of uniform slurry with no air bubbles. Thickness is regulated by a doctor blade system allowing spreading of the prepared slurry on the carrier film,

- the drying of the ceramic film is then carried out by heat lamp or heated air or resistance heaters to allow solvent evaporation,

- finally, storage of ceramic roll, as prepared or diced in different shapes and sizes, is realised. Additional processes such as hole punching, firing, metallisation are performed later.

Ceramic tapes casting is shown on figure 1.1.

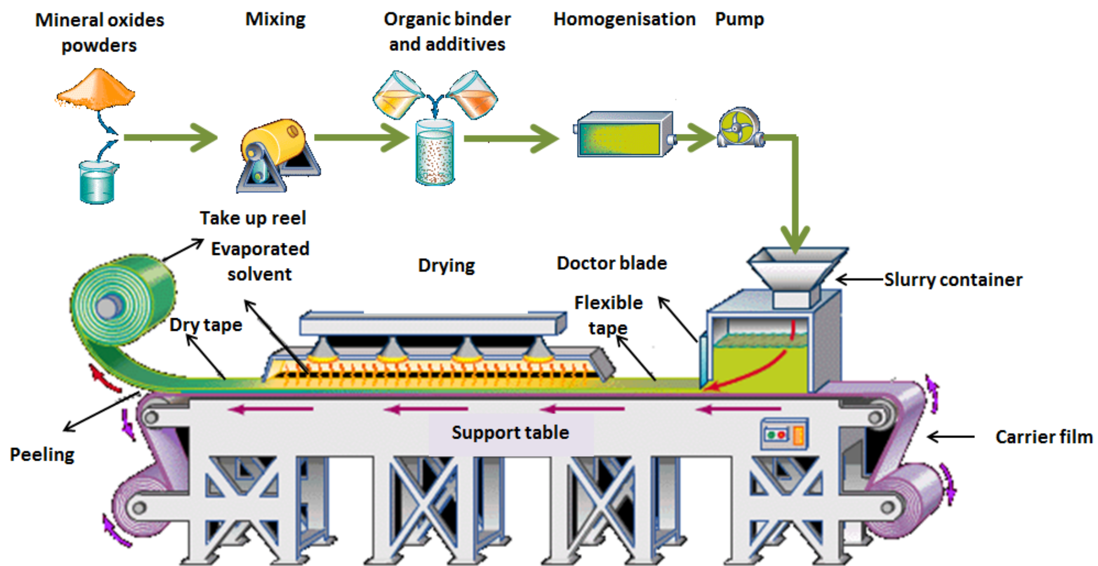


Figure 1.1: Ceramic preparation technique: tape casting (reproduced from [18])

**Tape calendering** Ceramic tapes are also prepared by calendering, a roll to roll method. Same steps as tape casting are performed with this technique. However, casting with a doctor blade is replaced by two rolls fixing the thickness of the tape. Once the substrate is calendered, drying, cutting, sintering and packing steps are realised.
*Nhuapeng et al., 2002* [19] prepared lead zirconate titanate ceramic tapes by calendering. Polyethylene and polyester resins were used as binders.
*Thorstensen et al., 2011* [20] explained that tape calendering is an advantageous method because it allows:

- tapes continuous production process,
- tapes structuring during the production process,
- calendering of tapes with thicknesses varying from some hundred micrometers to more than 1 mm.

### Multilayer systems manufacturing

After tape casting or calendering, ceramic sheets are patterned at green stage with thick-film techniques such as screen printing in order to create conductive, resistive and dielectric lines.
Via holes are perforated by mechanical punching or laser micromachining. Afterwards, they are filled by screen printing, injection or photopatterned. Then, sheets are assembled and laminated by thermo-compression. Laminated tapes are then co-fired at temperatures lower than 400°C to allow solvent and binder burnout. Then temperature is raised up to 850°C to allow inorganic materials densification [21][22][23]. A schematic of the LTCC process is shown in figure 1.2.

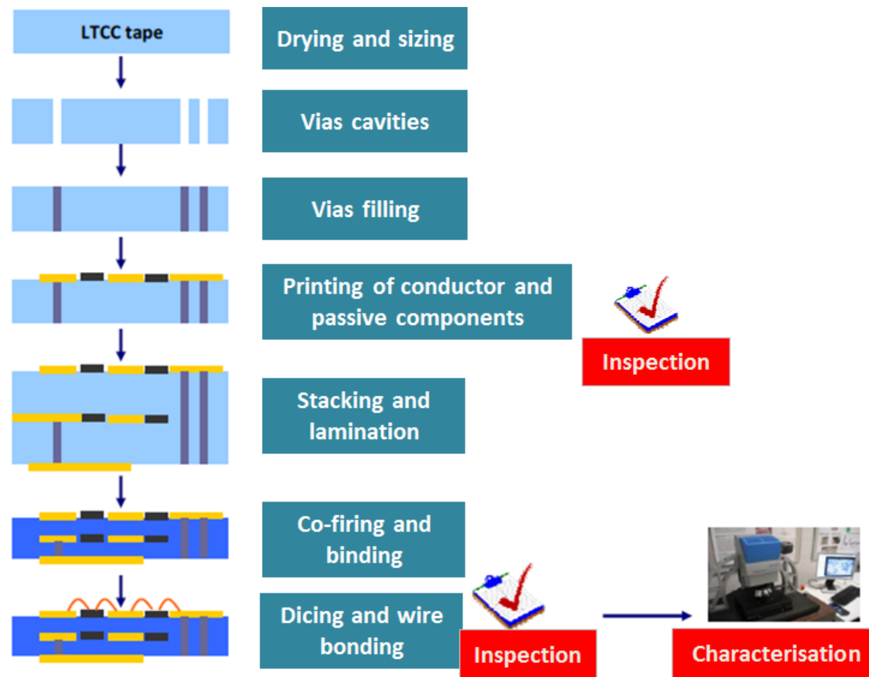


Figure 1.2: LTCC process

### Some ceramic materials

Ceramics are used in several applications. They are employed in electronic domain for the manufacturing of plasma panel displays (PPD), solar cells, ceramic micro-electro mechanical systems (MEMS) and sensors manufacturing. They are also used for microelectronic packaging [24].
Aluminium oxide ($Al_2O_3$), magnesium oxide (MgO), aluminium nitride (AlN), yttria stabilised zirconia (YSZ), strontium titanate ($SrTiO-3$) and ferrites ($Fe_2O_3XO$) are considered as High Temperature Co-fired Ceramics (HTCC) sintered at temperatures higher than 1200°C.
Low Temperature Co-fired Ceramics (LTCC) are ceramics sintered at temperatures lower than 900°C.

In this report, only alumina (HTCC) and different kinds of LTCC are studied.

### High Temperature Co-fired Ceramic (HTCC) - Aluminium oxide

Aluminium oxide($Al_2O_3$) also known as alumina, is one of the most used ceramic materials.

**Preparation** Alumina is generally prepared from bauxite ($Al_2O_3.nH_2O$) by the Bayer process. This process consists in leaching bauxite with sodium hydroxide solution above its boiling point in a pressure reactor. After separating the insoluble material, the pure crystalline aluminium hydroxide is precipitated. The precipitate is then filtered, washed, dried, and calcined into pure $Al_2O_3$ [25].
Alumina tapes are generally prepared by tape casting. Control of grain growth and porosity is performed by preparing water-based slurries of controlled granulometry powders [26].
Alumina is usually sintered at 1600°C.

**Physical properties** Alumina has a density varying from 2.4 to 4.0 g.cm$^{-3}$ depending on its form (corundum, activated or hydrated). Hydrated forms have the lowest densities. Its melting point ranges from 2005°C to 2072°C [27].
Alumina is a stable chemically resistant material.
Alumina properties and structure can be changed by adding sintering additives. Most commonly used additives are mineral oxides such as magnesium, silicone and titanium oxides. For example, silica can be added in order to allow rapid growth of alumina grains and enhance the sintering process speed [26].

**Applications** Alumina most significant use is in the production of aluminium metal. It is also used as abrasive due to its hardness and as a refractory material due to its high melting point. It can be employed as a catalyst for chemical reaction activation such as desulfurising. It is also added as a filler for plastic manufacturing or cosmetic formulae. Alumina tapes are used for high temperatures applications - such as temperature sensors manufacturing - due to their insulating properties maintained even at high temperature (> 800°C) [28]. Alumina substrates are, therefore, widely used for electronic and printed microelectronic applications requiring thermal stability. Some examples are shown in table 1.1.

| Reference | Application | Ink | Substrate | Printing process |
|---|---|---|---|---|
| *Wang and Kumar, 2004* [29] | HCl sensors | Neodymium doped strontium cerate + painted platinum electrodes | 96% alumina | Screen printing |
| *Birdsell et al., 2004* [28] | Temperature sensor | Platinum ink | 99.6% green alumina tape (3 layers) | Screen printing |
| *Mis et al., 2007* [30] | Micro-varistors | ZnO and $Bi_2O_3$ → varistor ink<br>PdAg or Pt or Au → electrodes ink | Sintered alumina | Screen printing |
| *Loffredo et al., 2007* [31] | Ammonia gas sensor | Polyaniline | Alumina tape with gold contacts | Inkjet printing |

Table 1.1: Alumina tapes in printed electronics applications

**Low temperature cofired ceramics (LTCC)**
LTCC are ceramics sintered at low temperatures (800 - 900°C) compared to HTCC. They are composed of a mixture of mineral oxides, carbonates, nitrates allowing softening and melting temperatures decrease. LTCC technology can be defined as a way to produce multilayer circuits with the help of single tapes on which conductive, dielectric and/or

resistive pastes are applied. These single sheets are laminated together and fired in one step. This saves time, money and decreases circuits dimensions.

**Advantages** LTCC tapes are chemically inactive and non permeable. They have high efficiency, low dielectric constant and loss and low thermal expansion coefficient. They are also used for their flexibility allowing the manufacturing of three dimensional structures [32].

LTCC substrates, sintered at low temperatures, allow using of silver, palladium, and gold as conductive materials with low melting temperature ($< 1000°C$) compared to other conductive materials such as tungsten used with HTCC. Tungsten melts at 3422°C and its conductivity , $9.10^6$ $S.m^{-1}$, is lower than that of silver ($6.10^7$ $S.m^{-1}$). Thus, when cofired with silver, copper, palladium or gold, LTCC systems exhibit high conductivity [33][34].

One of the great advantages of multilayer LTCC technique is that every single layer can be checked individually. This prevents the need of manufacturing a whole new circuit in case of problem or malfunctioning.
Furthermore, the LTCC technology allows deposition of different kinds of materials in a sheet shape. Thus, materials with different properties (electrical conductivity, dielectric constant, etc.) can be introduced on different or same sheets and then compose a multilayer stacked system. An LTCC module may be composed of surface or embedded capacitors (silicates or titanates), resistors (ruthenium $RuO_2$, iridium oxide $IrO_2$) and inductors (conductors such as silver and gold) [35][36]. A schematic of an LTCC module is shown in figure 1.3.

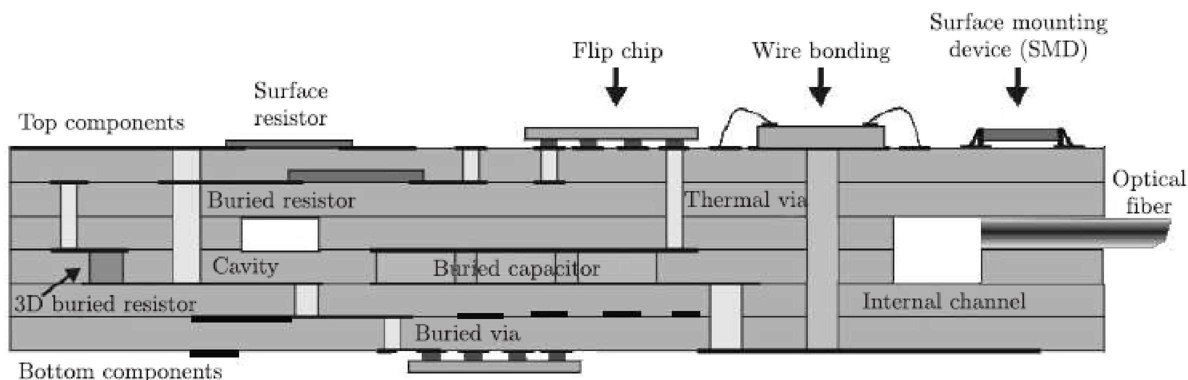


Figure 1.3: Schematic of an LTCC module [36]

**Applications** LTCC technology is nowadays used in many applications. LTCC tapes are, for example, used to manufacture micro-channels for gas and fluid, high voltage electrodes, capacitors, amplifiers, transducers, sensors, actuators, cooling and heating systems [22]. Some examples of LTCC modules are given in table 1.2.

| Reference | Application | Number of layers | Components | Lamination |
|---|---|---|---|---|
| *Golonka et al., 2005* [37] | Microfluidic system | 6 LTCC | AgPd → heater → screen printed<br>Pt → temperature sensor → screen printed<br>Optical fibre → optical detector → glued | Isostatic press |
| *Martínez-Cisneros et al., 2007* [38] | Analysis system | 6 LTCC | AgPd → electronic connections → screen printed<br>conventional thick film paste → conductor → screen printed<br>Ag → vias filler<br>Miniaturised chloride ion analyser<br>Potentiometer | 21 MPa, 100°C |
| *Nowak et al., 2009* [39] | Gas sensor | 4 LTCC | AgPd → heater, conductor → screen printed<br>AgPd , vias filler | Isostatic press (20 MPa, 70°C) |

Table 1.2: Examples of LTCC applications - All modules are sintered at temperatures varying from 800 to 900°C

### 1.1.2 Glass and silica substrates

Silica ($SiO_2$) or silicon dioxide is one of the forms of silicon. Glass substrates are generally cast from a mixture of silica powders and other inorganic oxides, carbonates and nitrates.

#### Physical properties

Silicon dioxide density is about 2.65 g.cm$^{-3}$ and its melting temperature ranges from 1600 to 1725 °C. Its electrical resistivity is equal to 0.10 Ohm.m. It is considered as a semi-conductor. Silicon is thermally stable, highly pure and have low toxicity.

#### Applications

Silicon dioxide (silica) is the main constituent of ceramics and glasses. It has good piezoelectric properties. Thus, it is used in semi-conductors devices manufacturing and computer chips. Electronic components (conductors, resistors, etc.) can be deposited onto silicone surfaces. In order to avoid mechanical shocks and electrical shorting, they can be embedded in silicon multilayer modules.
Silica is relatively expensive and can be attacked by solvents. It easily migrates in either liquid or vapour state into other components of an electronic system. Electrical switch contacts contamination by silicon leads to failures and causes an increase in contact resistance [27][40][41].
Examples of silica and glass substrates in printed electronics are shown in table 1.3.

| Reference | Application | Ink | Substrate | Process | Sintering |
|---|---|---|---|---|---|
| *Quian et al., 2009* [42] | Field emission cathode | Graphene + ethylene cellulose | Glass coated with Ag | Screen printing | 350°C - 20 minutes |
| *Ma et al., 2009* [43] | Electrodes for solar cells | TiO2 | ITO doped glass | Screen printing | 450°C - 60 minutes |
| *Tellier et al., 2011* [44] | Optical applications | $In_2O_3$/ZnO + 1,3 propanediol | Soda-lime glass and $SiO_x$/Si | Inkjet | 450°C - 30 minutes |

Table 1.3: Silica and glass as substrates in printed electronics

### 1.1.3 Polymer substrates

Polymers, such as polyethylene terephtalate (PET) and polyethylene naphtalate (PEN) are used as substrates in printed electronics. They are known for their flexibility and good mechanical properties [45].
Polymer substrates cannot withstand very high temperatures because of their low melting points. For example, PET melts at 260°C.

**In this study, only alumina and LTCC, were used as substrates for conductive inks deposition**.

## 1.2 Substrates sintering process - ceramics and glasses

Sintering is a heating process aiming to bond particles by means of molecular or atomic interactions at solid state [9]. Material sintering is performed to develop high quality final products of either metals or ceramics. During sintering, materials become stronger and more compact because of the micro-pores elimination. Sintering process is realised at high temperatures (500°C to 2000°C) depending on the components used. Mechanisms that take place during sintering are mainly plastic deformation mechanisms and diffusion mechanisms [9].

### 1.2.1 Sintering methods

Sintering process can be performed by conventional and non conventional methods.

#### Conventional sintering

Conventional sintering is based on external heating and thermal diffusion to provide particles bonding [9].
In order to reduce sintering temperature, hot pressing method was investigated. *Kuang et al., 1997* reported that alumina can be sintered within minutes to approximately non porous body at 150 to 200 atmospheres pressure and a 1800°C temperature [8].
Chemical additives can also be added to enhance sintering properties. They allow lower sintering temperatures and decrease sintering duration.
In addition, rapid sintering occurs in presence of a liquid phase. Indeed, as a result of

heating, materials melt leading to a liquid phase that allows quick materials diffusion and, consequently, rapid sintering [9].

**Novel sintering methods**

New sintering methods were recently investigated such as plasma, laser and microwave sintering. They allow faster sintering and provide uniform heating rates. In addition, they ensure time and energy saving and enhance mechanical properties [9].

- The Hot Isostatic Process (HIP) was investigated in recent years. Sintering is performed till the closed-pores stage at the first phase. Then, material is placed in hot chamber under helium gas pressure (several thousands Pa) [8].

- Field Activated Sintering Technique (FAST) is also a non-conventional method allowing material sintering. In this technique, electrical current and discharge allow removal of impurities and activation of particles surface. As a result, powder bonding becomes easier.
  *Scarlat et al., 2004* reported FAST method of tin oxide ($SnO_2$) ceramics. No pores were observed at the end of the sintering process. 99.06% of the theoretical density was achieved and 1 $\mu$m grain size was reached. This method was better than conventional sintering requiring three hours heating at 1100°C and leading to a sintered ceramic with 65% of material bulk density and 8.45% porosity [46].

### 1.2.2 Sintering stages

Sintering process is realised in three stages [8][47]. Figure 1.4 shows a schematic of particles behaviour during these stages.

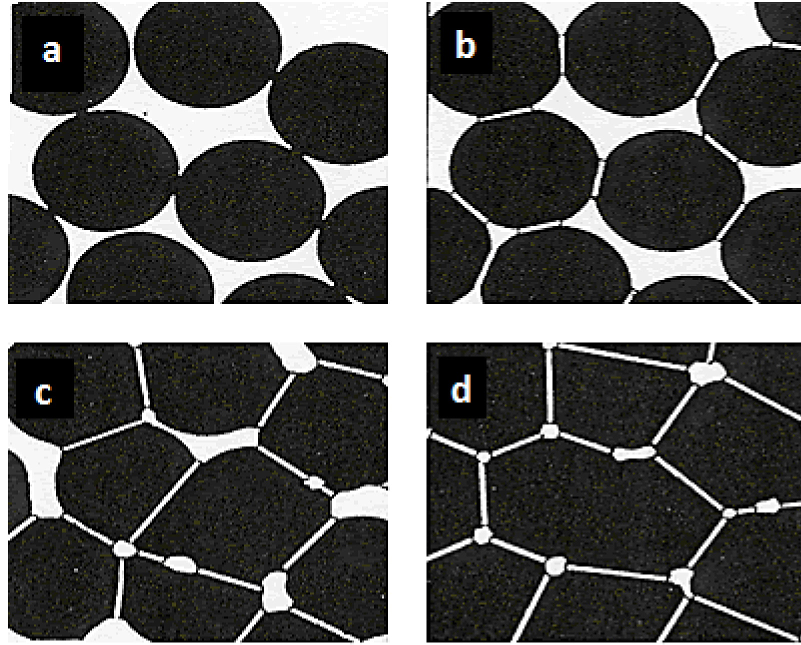


Figure 1.4: Different sintering stages: a and b - Early stage, c -Intermediate stage d - Final stage [48]

### Early sintering stage - a and b

At this stage, process temperature reaches the quarter of the melting point of the material. Neither material densification nor shrinkage happens during this phase. Grains approach each other without growing up. This stage is characterised by plastic deformation of the material.

### Intermediate or middle sintering stage - c

Sintering temperature ranges from 1/4 to 3/4 of melting point of the heated material. During this phase, particles start to adhere to each others leading to material densification. Thus, materials migration starts between grains and particle size increases.
This stage is characterised by diffusion. At this stage, grain growth as a function of time can be expressed by equation 1.1.

$$R_a = k \cdot t^n \tag{1.1}$$

Where:

- $R_a$ (m) is the mean grain radius,
- $k$ is a constant,
- $t$ (s) is the time,
- and $n$ is the grain growth exponent varying from 0.25 to 0.50 [47].

**Final sintering stage - d**

Diffusion also characterises this stage. This is the end of the densification process, pores are isolated and sphere shaped. In some cases, pores are completely blocked. Thus, the sintering process is completed.

### 1.2.3 Other sintering properties

**Porosity**

After sintering, porosity is reduced and in case of complete sintering process, no more pores are observed after the final sintering stage. Porosity evolution is related to densification mechanism and sintering kinetics. During sintering, pore size decreases. Pore shrinkage is considered as a process of materials transferring into the voids leading to open spaces blocking. It has a decisive influence on the microstructure development and influences mechanical, electrical and optical properties of final material. An optimised sintering process is obtained when zero porosity is reached at the end.
*Kuczynski, 1949* proposed an equation (equation 1.2) relating the initial porosity ($P_0$) to the porosity ($P$) at a time $t$ (s) [49].

$$\frac{P}{P_0} = (1 + h \cdot t)^{-b} \tag{1.2}$$

Where:

- $P$ (%) is porosity at a time $t$,
- $P_0$ (%) is the initial porosity,
- $h$ and $b$ are two constant coefficients

**Shrinkage**

Shrinkage occurs in $x$, $y$ and $z$ directions. It is due to solvent evaporation. Its impact is more important when the slurry suspension is water-based because of the high drying rate of water.
Shrinkage is influenced by green tape composition, heating rate, sintering temperature and substrate geometry. It may causes material cracking and fracturing. Besides, mismatch between deposited ink and substrate may be observed. Average x - y shrinkage is estimated to 15% in LTCC tapes. z shrinkage may reach 30%.

Some studies on ceramics shrinkage are reported here after:

- *Zaharescu et al., 1991* showed that 95% $SnO_2$ and 5% CuO sample shrinkage increases from 5.8% at 900°C to 11.9% at 1000°C [50].
- Tape transfer technology is a solution allowing sintering of LTCC tapes without x - y shrinkage. In this method, LTCC is sintered individually on ceramic sintered tape (aluminium nitride, for example) [36].
- *Yang, 2001* managed to prepare silicon nitride ceramics with very low shrinkage value. This was possible because carbon powders were added to the initial ceramic paste. 1% by volume carbon added allows shrinkage reduction from 13% to 2% [51].

**Sintering additives**

As reported before, sintering aids provide better sintering capabilities (lower temperature, shorter time), decrease porosity and increase density. Some powders such as $Bi_2O_3$, $BaTiO_3$, CaO, $SiO_2$, $Sb_2O_3$ are added as sintering additives to improve sintering by providing higher densification degrees at lower temperature, less porosity and smaller grain size [46].
*Jaiban et al., 2011* [52] added 2 to 6% of $Bi_2O_3$ powders to BNZ ($Bi_{0.5}Na_{0.5}ZrO_{0.5}$) ceramics in order to allow sintering at 900°C. It was observed that when only 2% of $Bi_2O_3$ were added pore size decreases from 0.82 to 0.30 $\mu$m compared to particles sintered without additives.

### 1.2.4 Sintering conditions examples

Table 1.4 shows some ceramics sintering examples.

| Reported by | Material | Additives | Sintering process | Temperature |
|---|---|---|---|---|
| *Park et al., 1984* [53] | Tin oxide $SnO_2$ | None | HIP (150 MPa) | 1400°C |
| *Zaharescu et al., 1991* [50] | Tin oxide $SnO_2$ | 20% CuO | Conventional sintering | 1000°C |
| *Zaharescu et al., 1991* [50] | Tin oxide $SnO_2$ | 10% $Sb_2O_3$ | Conventional sintering | 1200°C |
| *Kanade and Puri, 2008* [54] | Manganese (Mn), Cobalt (Co), Nickel (Ni) + inorganic binder (Lead oxide PbO + Bismuth oxide $Bi_2O_3$) | Ethyl cellulose + 2-(2-butoxy-ethoxy-ethyl) acetate | Conventional sintering | 1000°C |

Table 1.4: Examples of different conditions of ceramics sintering

## 1.3 Substrates properties

### 1.3.1 Substrates mechanical properties

A solid is an arrangement of atoms. These atoms are linked together by electromagnetic forces between near electrons. The minimum energy required to assemble atoms depends on thermal activation of the material [55].
Polymers are composed of molecular chains. They are amorphous. Polymerised chains generate crystallites under controlled thermo-mechanical conditions. $T_g$, glass transition temperature, is the temperature at which a material state changes from amorphous to crystal and vice versa.

Ceramics, glass or LTCC substrates are sintered before the final microelectronic device manufacturing. Before sintering, mechanical properties depends on the polymer and/or the plasticiser and the ceramic powders used for the formulation of the green substrate. After sintering, only ceramic powders provide the mechanical properties of the substrate. In some cases, pores are formed during tapes manufacturing. Porosity causes the elastic modulus decrease. Indeed, the stress is concentrated near the pores because of materials area decrease.
During sintering, materials become continuous and then the degree of densification in the material increases because the porosity decreases. Thus, the body stiffness increases and mechanical properties are enhanced. Microcracks can be considered as small fractions of porosity which decrease the elastic modulus. Thermal expansion of substrate may lead to residual stress in ceramic and then generate localised microcracks [56].

### 1.3.2 Thermal properties - Thermal expansion coefficient

Substrates are characterised by their $TEC$ (Thermal Expansion Coefficient, $K^{-1}$) [40].

After heating a body to increase its temperature by $\Delta T$ (K), its dimension changes by $\Delta L$ (equation 1.3). Supposing that the material has an original length equal to $L_0$, the thermal expansion coefficient $TEC$ ($K^{-1}$) can be given by equation 1.3.

$$TEC = \frac{\Delta L}{L_0 \cdot \Delta T} \tag{1.3}$$

Where:

- $TEC$ ($K^{-1}$) is the thermal expansion coefficient,
- $\Delta L$ (m) is the material length variation,
- $L_0$ (m) is the initial length,
- $\Delta T$ (K) is the temperature increase.

The same equation can be written as explained by *Green, 1998* [56] where the strain $\epsilon$ (%) is considered as the response of the material heating (equation 1.4).

$$\epsilon = TEC \cdot \Delta T \cdot 100 \tag{1.4}$$

When a polycrystalline ceramic material is heated, adjacent crystals are pushed or pulled to each other and a residual strain, remaining even when heating is stopped, is generated. In the case of brittle materials, residual stresses could be very high. That may cause cracking and disintegration. This occurs when material is directly and quickly cooled after fabrication process at high temperature. Indeed, during sintering, material flows and stress relaxes. However, if the system is cooled immediately to a temperature lower than the relaxation temperature of the material, residual strain increases and lead to cracks formation after cooling [56].

### 1.3.3 Wettability of substrates

Wettability is the tendency of a liquid to spread onto a solid substrate. It is characterized by two main parameters:

- the wetting degree defined by measuring the contact angle. It depends on the surface and interfacial energies present at the solid/liquid interface,

- the wetting time indicating how fast the liquid spread onto the solid surface.

Surface properties of solids are characterised by the surface energy, $\gamma_s$ (mJ.m$^{-2}$). It is the sum of several terms such as dispersive, polar, covalent and ionic fractions. Substrate wettability by solvent can be studied by calculating the contact angle formed between the fluid and the solid.
A solid can be wet by a liquid when its surface energy is higher than the surface tension of the liquid. Wetting and spreading are related to flow properties of a liquid on the substrate. Flow can be affected by many properties related to the substrate and/or the fluid such as surface roughness and composition, temperature, chemical reaction between the substrate and the solvent and liquid properties such as viscosity, surface tension and density [57].

*For more details about substrates properties, see Annexe 1.*

# Chapter 2

# Printed electronics and processes

## 2.1 Introduction

Printing techniques are used to manufacture electronic devices. Conducting, semi-conducting or electroluminescent materials are employed in order to manufacture resistors and transistors. Screen printing, flexography, rotogravure and inkjet replace conventional methods based on silicon chip manufacturing.
On the one hand, the conventional methods are complicated, high cost, require huge investments and production on large scale to be cost effective. In addition, silicon chips are fragile and rigid.
On the other hand, printing techniques are low cost, allow small quantities fabrication as well as mass production. Besides, they are environmentally friendly methods allowing printing on flexible and rigid substrates [58].

Because of all these advantages, printing techniques are nowadays used in many electronic applications, such as: display pannels, printed circuit boards (PCB) [59], radio frequency identification (RFID) tags [60][61], microwave transmission devices [62][63][64], sensors [65][66], micro-electro mechanical systems (MEMS) [67][68] and Light Emitting Diodes [69][70].

Table 2.1 is a comparison between conventional methods for microelectronic applications and new printed electronics.

| Conventional electronics | New printed electronics |
|---|---|
| Well established techniques and processes for electronic component manufacturing | Screen printing known since the 1950's for electronic applications. Processes optimisation for electronics is still in progress, especially for organic electronics known since the late 1990's |
| Silicon chip and lithography based on silicon micro-machining | Printing processes, especially screen printing and inkjet printing |
| Many steps (spin coating, photo-exposure, etching, baking, etc.) | One step required after preparing the printing form |
| High cost | Relatively low cost |
| Only large scale production to allow cost effective production | Possibility of high and low volume production |
| Time consuming | Quick cycle and turnaround time |
| Limited by tape size | Small and large area capability |
| Use of dangerous solvents and wastes generation after etching | Environmentally friendly processes allowing deposition of conductive elements only where they are needed |

Table 2.1: Conventional methods for manufacturing electronic components versus new printed electronics [58][71][72][73][74]

Different printing processes are nowadays used for electronic components manufacturing. At the beginning of this chapter, photolithography process is described. Then, printing processes - offset lithography, screen printing, flexography, rotogravure and inkjet - are detailed.

## 2.2 Lithography methods

### 2.2.1 Soft lithography

Techniques based on ink transfer from a structured elastomeric stamp are known as soft lithography (SL) methods: microcontact printing ($\mu$CP), microfluidic network ($\mu$FN) and laminar flow patterning [75].

#### Micro-contact printing - $\mu$CP

In this technique, an elastomeric polymer such as PDMS (PolyDiMethyl Siloxane) is used to prepare the stamp by photolithography. First of all, a photoresist is deposited on silicon substrate. Then a master form is prepared by UV exposure. Afterwards, PDMS polymer is cast on the master material and PDMS stamp is generated. In a second step, the stamp is inked - with alkanethiol for example. Then, it is brought to contact with

the substrate (for example, silver or gold coated on silicon or glass) in order to allow ink transfer. Thus, a Self-Assembled Monolayer (SAM) is formed on the contact region between ink and substrate. Consequently, a wet-etching step is performed in order to remove excess material. As a result, only the part of the tape protected by transferred ink is kept. Finally, a metal electroplating step is achieved. $\mu$CP is used in medical applications for which small length in sub-micrometer scale are required [76]. Resolution as high as 15 to 100 nm can be reached with this mehod. Figure 2.1 shows an overview of mask and stamp preparation by lithography and ink deposition by micro-contact printing.

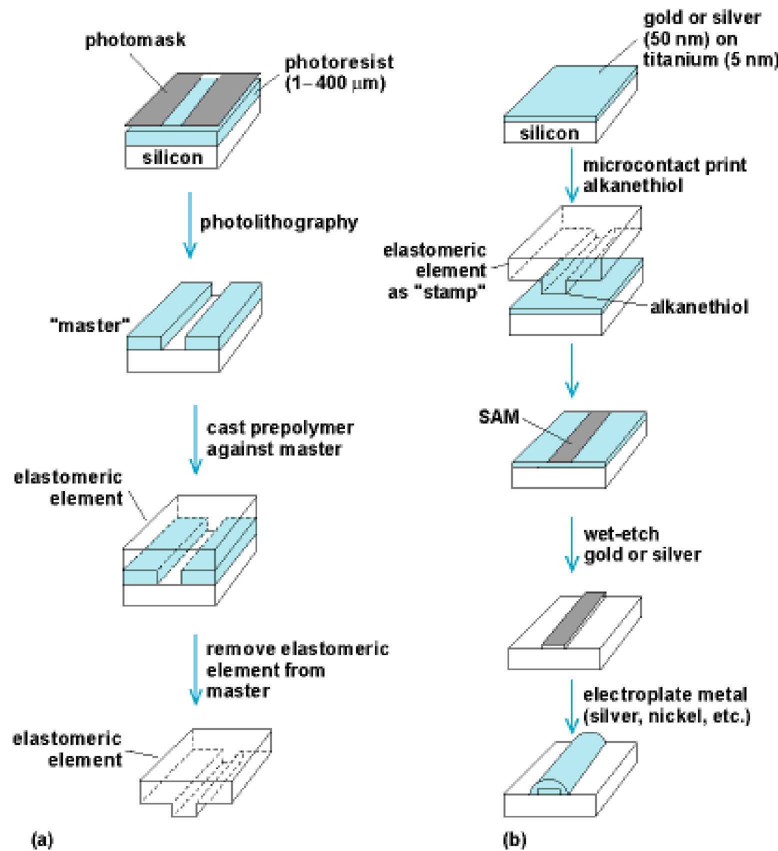


Figure 2.1: Elastomeric element as formed for soft lithography (a) and as used for $\mu$CP (b) [77]

Metal transfer technique is another micro-contact method. However, in this process the PDMS stamp is coated with metal layer which is transferred to a polymeric surface under heating and low pressure. This method is advantageous because it is a fast technique (30 s) allowing patterning of large areas in a single pass. Besides, it can be used for multilayered metallic structures manufacturing [75][78].

### Microfluidic network and laminar flow patterning

In these methods, after preparing stamp by photolithography, stamp is brought to contact with substrate in order to form micro-channels. Channels, of 3 to 200 $\mu$m diameter, deliver ink to defined areas creating microfluidic networks [75].

### 2.2.2 Other lithography methods

#### Nanoimprint lithography

Nanoimprint lithography (NIL) is similar to $\mu$CP. However, it allows better resolutions, $\sim$ 10 nm or less and printing of functional materials structures on different types of polymers. This leads to a wide range of applications in electronics, photonics, data storage, and biotechnology.
NIL was proposed since 1995. It consists in preparing a hard mould with a defined pattern. Afterwards, this mould is applied to polymeric elastic surface under heat and pressure. A thickness difference is created on the polymer surface. By this way, the device structure is transferred to the substrate after mould removal [79]. A schematic of NIL method is shown on figure 2.2.

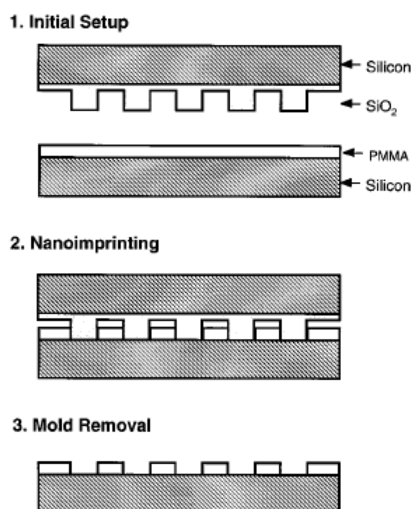


Figure 2.2: Schematic of the nanoimprint lithography process [80]

Mould material is made of silicon, silica, silicon carbide, silicon nitride, metals, sapphire or diamond film. Materials are chosen for their hardness and durability compatible with NIL technologies. To prepare the mould template, UV photolithography, electron beam lithography or nanotransfer lithography are used. The material resist can be a thermal plastic polymer or a UV curable material. Nowadays, new resists materials are developed such as PDMS, PEDOT (Poly(3,4-ethylenedioxythiophene)), olefin copolymers, etc. The resist material should have a Young modulus lower than that of the mould material during patterning in order to allow design transfer. Different families of NIL have been established such as reverse NIL, hot embossing NIL, roller NIL and NI combined to photolithography [79][81].

#### Dip-pen lithography

This method was introduced by *Piner et al., 1999* [82]. Then, it was studied and applied by several researchers in order to deposit graphene oxide patterns on $Si/SiO_2$ substrates [83], to print 30 to 50 nm line width collagen on gold layers [84] and to manufacture 50 nm gold dots by depositing 16-mercaptohexadecanoic acid on $Au/Ti/SiO_x/Si$ substrate [85]. This method is also called atomic force microscopy (AFM) nanolithography because it uses AFM tip chemically modified and patterned with chemical reagent in order to pattern the substrate (see figure 2.3). The chemical material is transferred by capillary

action [75].

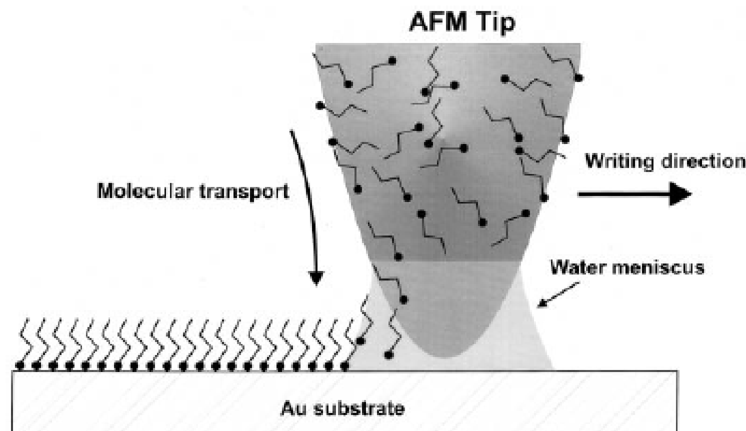


Figure 2.3: Principle of dip-pen lithography [82]

Other lithography methods such as extreme UV lithography [86], X-ray lithography [87] and electron beam lithography [88] were also studied and are promising methods for achieving resolutions of sub 50 nm scale.

### 2.2.3 Advantages and applications

Despite the fact that lithography methods are composed of many steps and are high cost techniques, they allow resolution in sub-100 nm scale and less. These techniques are largely used for microelectronic devices patterning because they allow size miniaturisation. Substrates should be smooth and not embossed. Materials used in each phase should be, compatible with the method and the materials employed at the other stages in order to allow high resolution with clean edge definition. For this reason, materials properties such as elastic, mechanical and rheological behaviour should be investigated in order to realise process goals [75][79][89].
Lithography is used in many fields such as medical and biological for proteins and cells deposition [84][90][91]. Besides, it is also used for transistors and OLED (Organic Light Emitting Diode) manufacturing and other electronic applications. Some examples of lithography uses in electronics are shown in table 2.2. But this technique does not fall into the scopes of this study.

| Reference | Application | Functional material | Substrate | Dimensions | Properties |
|---|---|---|---|---|---|
| *Loo et al., 2002* [78] | Transistors | Au/Ti | PDMS | Thickness $< 50$ nm, Width = 10.0 $\mu$m | $\mu = 0.1$ cm$^2$.V$^{-1}$.cm$^{-1}$, ON/OFF current = $10^4$ |
| *Austin and Choo, 2002* [92] | OTFT | Gold (NIL) + P3HT semi-conductive polymer | n-type silicon | Lenght = 70 nm, Width = 4.0 $\mu$m | ON/OFF current = $10^4$ |
| *Sun and Forrest, 2006* [93] | OLED | PMMA | Glass | Diameter = 6.6 $\mu$m, Height = 2.2 $\mu$m | Quantum efficiency = 21.6% at 220 cd.cm$^{-2}$ luminance |

Table 2.2: Lithography applications in electronic field - *Materials electrical properties are reported in Chapter 3 and Annexe 2*

## 2.3 Offset printing

### 2.3.1 Process description

The schematic of offset printing process is shown on figure 2.4.

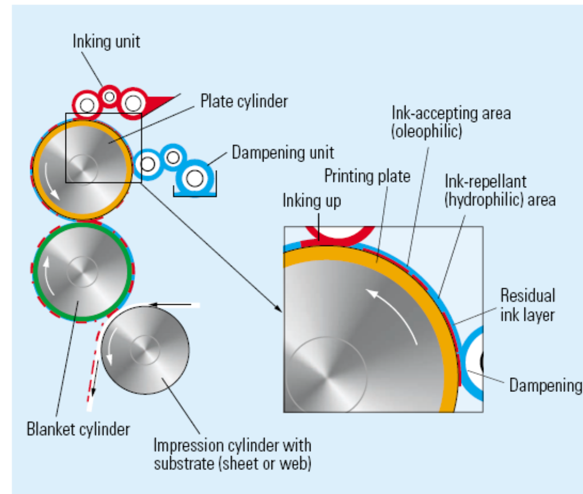


Figure 2.4: Offset printing (components of a printing unit and basic principle) [94]

In this printing process, the image and the non-image areas are in the same plane on the printing image carrier, the plate. The plate is usually made of flexible aluminium. It is covered with a photosensitive emulsion. The image is developed after exposure to UV

light.
For negative working, emulsion becomes insoluble during exposure to light and bonds with the plate base. The unexposed areas (non-image) are then removed chemically using a developing solvent. For positive working, emulsion becomes soluble during the exposure to UV light and is removed during subsequent development.
Afterwards, the plate is fixed to a roll; the non-image areas of the plate are wetted by a water-based solution. Then the inker rollers depose the oil-based ink on the hydrophobic image areas.
With this process, the inked image is not printed directly onto the substrate but it is first offset onto a rubber blanket and then transferred to paper [71][95].

### 2.3.2 Offset requirements

Offset process requires rigorous ink rheology control. Inks should have high viscosity (40 - 100 Pa.s). Furthermore, ink drying speed and water balance controls must be optimised [71].

### 2.3.3 Advantages and applications

This technique has an excellent control of registration and resolution. It allows resolution smaller than 15 $\mu$m. Offset is also a high speed technique. It allows 6000 to 10000 printings per hour depending on the press type, sheet-fed or web-fed [71][96]. Besides, it can be used in electronic applications such as integrated circuits, transistors manufacturing, radio frequency circulator patterning, etc. Two examples of electronic devices manufactured by offset lithography are shown on table 2.3.

| Reference | Application | Functional material | Substrate | Thickness | Properties |
|---|---|---|---|---|---|
| *Harry et al., 1999* [89] | Capacitors | $TiO_2$ ink | PET | 20 $\mu$m | C = 0.65 nF |
| *Evans et al., 1999* [97] | Radio frequency circulator | Ag ink | PET | 3 $\mu$m | $\rho = 1.10^{-7}$ Ohm.m |

Table 2.3: Offset applications in electronic - *Materials electrical properties are reported in Chapter 3 and Annexe 2*

This process was not investigated in this study.

## 2.4 Screen printing

### 2.4.1 Process description

Figure 2.5 shows a schematic of screen printing process.

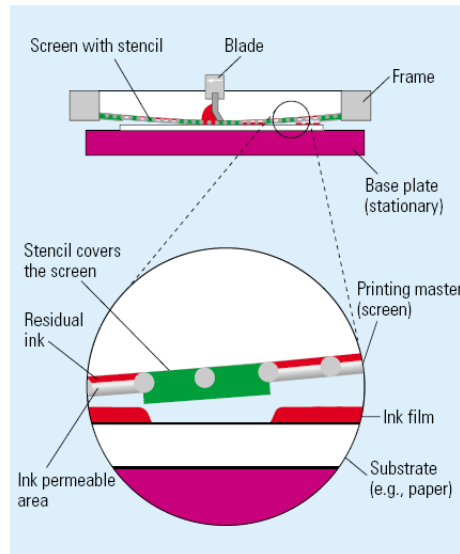


Figure 2.5: Principle of screen printing [94]

In this printing process, ink is transferred to the substrate through a stencil or a textile mesh supported by synthetic fibres or metal stretched tightly on a frame. The pores of the mesh are blocked-up in the non image area with a polymer based emulsion and left open in the image area. The image carrier is called the screen. The screen mesh is supplied with ink. A squeegee is then drawn across it, forcing the ink through the open pores of the screen. The substrate is held in contact with the screen and the ink is transferred to it [95].

### 2.4.2 Screen printing parameters

#### The mesh

Screen printing is influenced by mesh material, count, thread diameter and openings. Stainless steel meshes are especially used for high accuracy patterning such as electronic applications and ceramic transfer printing. Stainless steel is known for its ability to resist corrosion, its durability and relatively low cost. Mesh can be also made of polyester. This type is used especially for commercial graphics and decorative works. Different varieties of polyester meshes can be found such as nickel metallised polyester able to replace stainless steel and antistatic polyester especially conceived to reduce static electricity problems when printing plastic tapes. Nylon screen meshes, largely used in fabric decoration, also exist [98][99]. A schematic of a screen mesh is shown in figure 2.6.

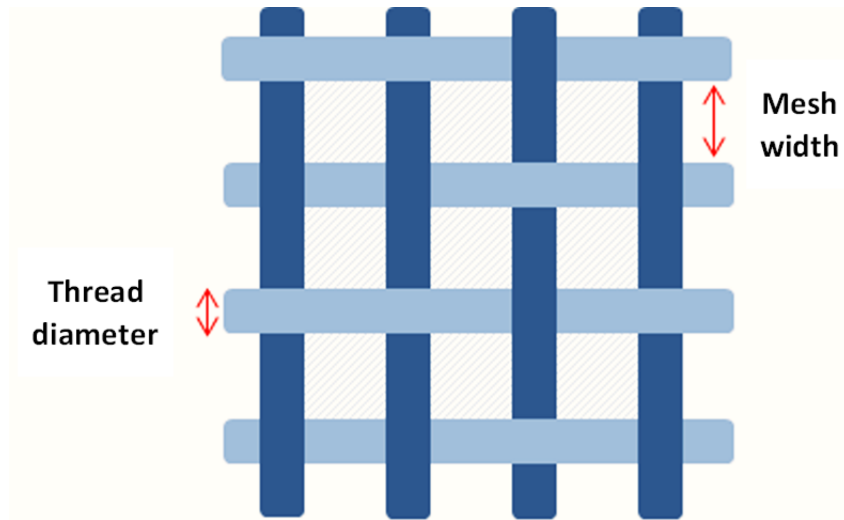


Figure 2.6: Schematic of a screen mesh [98]

The mesh count is the number of threads per unit length. Mesh opening or mesh diameter is the open area allowing ink flowing through the mesh. According to the application, it is important to define the mesh count and the wire or thread diameter (mm). Knowing these two parameters, it is possible to calculate the opening size (equation 2.1) and the open area percentage (equation 2.2).

$$Openingsize = \frac{1}{Meshcount} - Threaddiameter \tag{2.1}$$

$$Openareapercentage = (Openingsize \cdot Meshcount)^2 \cdot 100 \tag{2.2}$$

Where:

- the *opening size* is given in mm,
- the *mesh count* is given in mesh per mm,
- the *thread diameter* is given in mm,
- and the *open area percentage* is given in %.

When the mesh count increases, the opening size decreases. This factor has an important effect on paste separation and flowing quality. The open area percentage affects the flowing of the material through the screen mesh. When it increases, paste flows easily through the mesh and the screen capability is enhanced [100].
Three mesh grades can be roughly defined according to the thread diameter, S for fine, T for medium diameter and HD for heavy duty.
It was explained by *Appleton, 1997* [98] that when the thread diameter increases, the ratio of thread diameter to mesh opening increases, thus leading to higher deposited thickness. Indeed, deposited film thickness is dependant on the theoretical volume of the screen opening. For example, if the open mesh volume is equal to 20 $cm^3.m^{-2}$, the theoretical film thickness is estimated to 20 $\mu$m.
When the mesh count increases, for the same thread diameter, line thickness decreases as well.

Furthermore, mesh count affects printed lines edge definition and also electrical properties. It was demonstrated by *Yin et al., 2008* [101] that when mesh counts increased from 200 to 400 mesh, edges sharpness was enhanced and better silver tracks electrical properties were measured.
Table 2.4 shows an example focusing on mesh parameters effect on printed film thickness.

| Reference | Functional material | Mesh count | Printed film thickness |
|---|---|---|---|
| *Wright and Yeomans, 2008* [102] | Zirconia | 80 mesh | 17 $\mu$m |
| *Wright and Yeomans, 2008* [102] | Zirconia | 325 mesh | 3 $\mu$m |

Table 2.4: Mesh count effect on screen printed film thickness (sintered films)

### The emulsion

Emulsion is a polymeric material coated onto the screen to create the non image areas in order to avoid excessive ink flowing. Line height is enhanced when the emulsion thickness increases. Table 2.5 shows emulsion thickness effect on printed film thickness.

| Reference | Functional material | Emulsion thickness | Printed film thickness |
|---|---|---|---|
| *Lee et al., 2010* [103] | Ag | 5 $\mu$m | 65 nm |
| *Buzby and Dobie, 2011* [104] | Ag | 10 $\mu$m | 7 $\mu$m |
| *Buzby and Dobie, 2011* [104] | Ag | 22 - 25 $\mu$m | 8 $\mu$m |

Table 2.5: Emulsion thickness effect on screen printed film thickness

### Printing speed

Squeegee speed effect on printing resolution is also an important factor to be studied. It was demonstrated by *Pan et al., 1999* [105] that when printing speed increased widths increased. Narrower lines were better defined at lower speeds.
*Shapee et al., 2010* [106] studied printing speed effect on the surface roughness of gold films. They noticed that when squeegee speed increased from 75 mm.s$^{-1}$ to 125 mm.s$^{-1}$, roughness value decreased from 0.9 to 0.8 $\mu$m. They explained this result by the fact that when speed increases, ink is more fluid and flows easily through the screen mesh openings.

Other printing parameters such as printing pressure and off-contact distance, between the substrate and the screen, are also important factors affecting printing resolution.

### 2.4.3 Advantages and applications

Screen printing is a simple, low cost printing technique which can be adapted to different fabrication processes. It allows printing of a wide variety of materials on a large range of substrates (papers, plastic, etc.). It can be used for office equipment, road signs, textiles, vehicle instrumentation, electronic circuits, manufacturing of fully robust chemical sensor, heating elements and fuel cells printing. *Baudry, 1990* [107] reported in a review the screen printing use for the manufacturing of piezoelectric transducers such as lead zirconate titanate deposited between two Ag/Pd layers on alumina substrates. Besides, manufacturing of infra-red, temperature and humidity sensors on ceramic tapes by screen printing was mentioned in this review.
Screen printing use was also reported for organic thin film transistors manufacturing [101][108][109][110]. Other examples of screen printing applications are shown in table 2.6.

| Reference | Application | Ink | Substrate | Dimensions | Properties |
|---|---|---|---|---|---|
| *Bao et al., 1997* [111] | Plastic transistor | Polyimide semi-conductor and Ag electrodes | ITO coated PET film | Electrode thickness = 10 $\mu$m<br>0.5 mm x 4.0 mm<br>100 $\mu$m gap | C = 20 $nF.cm^{-2}$<br>$\mu$ = 0.01 - 0.03 $cm^2.V^{-1}.cm^{-1}$ |
| *Reicher et al., 2001* [112] | Power electronic | AgCuTi | Aluminium nitride ceramic | Thickness = 15 $\mu$m | Power density = $203.10^6$ $W.m^{-2}$ |
| *Wang et al., 2011* [113] | Electronic circuits | Ag/Ni/ MWCNT* | PET | Thickness = 30 $\mu$m<br>Width = 0.2 mm | $c$ = 78 Ohm.cm |

Table 2.6: Other screen printing electronic applications - *Multi-Wall Carbon NanoTubes - *Materials electrical properties are reported in Chapter 3 and Annexe 2*

Screen printing allows deposits of a wide range of thicknesses from 10 $\mu$m to several hundreds of micrometers.

### 2.4.4 Limits and printing defects

The screen printing process has some limitations such as line width (minimum achieved 100 $\mu$m) and speed (30 $m.min^{-1}$) [96][114].
Furthermore, screen printing inks drying is slow depending on the ink type and thickness. If ink is highly loaded, flow is not optimised and mesh marks appear on substrate. This

can be solved by decreasing ink viscosity, for example by adding resin or solvent which can be detrimental for printing sharpness [95]. Figure 2.7 shows a scanning electron micrograph (SEM) of a 84% solid content screen printed paste. Ink viscosity is equal to 60 Pa.s at 0.1 $s^{-1}$ shear rate at 25°C. This defect can be also related to a low printing pressure and to a high off-contact.

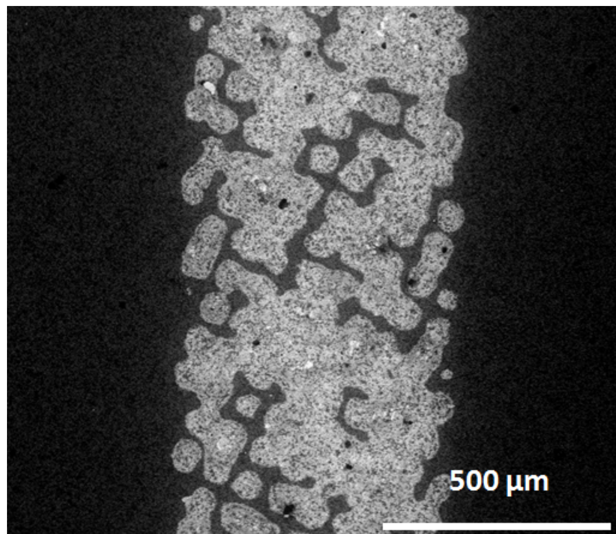


Figure 2.7: Silver screen printed line with a 84% solid content paste - SEM image - Grenoble INP - Pagora

### 2.4.5 Screen printing inks

Screen printing inks are complex systems with flow properties closely related to ink composition. These inks are water or solvent-based [115]. Terpineol, ethyl cellulose, butanol, ethylene glycol and other heavy solvents are used for screen printing pastes formulation. Besides, UV curable screen printing inks can also be prepared. In this case, drying is performed by UV lights [113].

Screen printing inks are highly viscous. An optimised screen printing ink viscosity is close to 120 Pa.s, and can allow a resolution of 100 $\mu$m. Viscosity decreases when shear rate increases. This allows ink flowing through the meshes and removing mesh marks and surface imperfections before recovering a more viscous state.
Indeed, after stopping the shear, viscosity increases preventing ink bleeding and line width expansion. Homogeneous narrow lines can therefore be defined. Viscosity raise should not be very quick. It should remain low for short duration of time. This will allow film levelling and filling the irregularities and voids.
*Neidert et al., 2008* proposed a model to study the screen printing inks rheological behaviour [116]. This model is shown on figure 2.8. Viscosity can be controlled by adjusting particle size and shape [34][109][117][118].

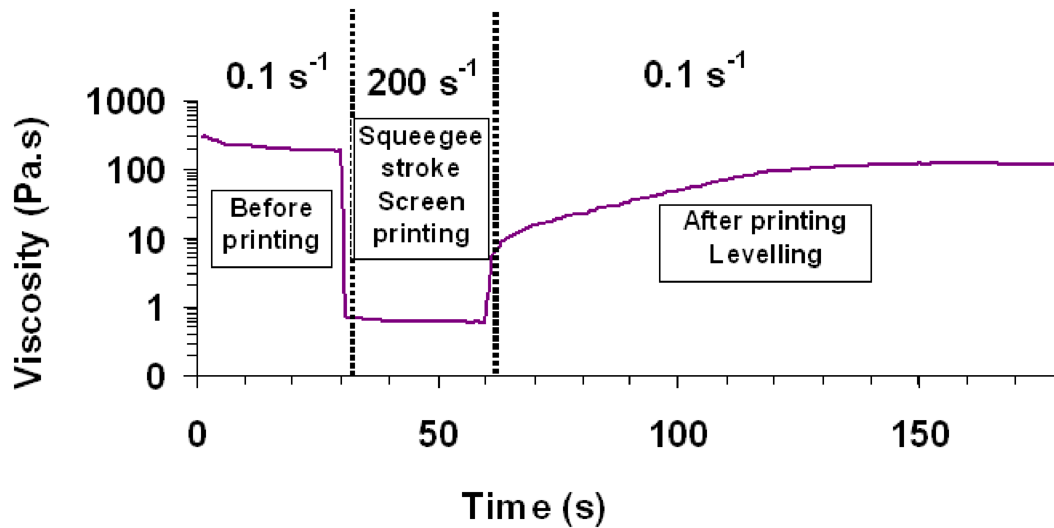


Figure 2.8: Thixotropic behaviour of screen printing inks - test realised on 67% Ag paste at the LGP2 - Inspired from *Niedert et al., 2008* [116]

The particle size in conductive screen printing inks varies from 1 $\mu$m to 20 $\mu$m. The particles have classically flake or spherical shape [119]. Flake silver particles have larger surface contacts and allow better conduction properties. Thickness of screen printing ink film varies from 8 $\mu$m to 30 $\mu$m. An example of formulation of screen printing inks is shown in table 2.7.

| Constituent | Exemple | Weight percentage (%) |
|---|---|---|
| Pigment | Functional phase (color, conductivity, luminescence, etc.) | 50 - 80 |
| Resin | Oil-based, acrylic, etc. | 9 - 11 |
| Solvent | Ethyl cellulose, butyl carbitol acetate, paraffinic solvent, White spirit, toluene, terpineol, etc. | 10 - 45 |
| Additives | surfactants, rheology modifiers, etc., | $\sim 2$ |

Table 2.7: Screen printing ink formulation - Synthesized from [115][120][121]

## 2.5 Flexography

### 2.5.1 Process description

Figure 2.9 shows an overview of the flexography printing process.

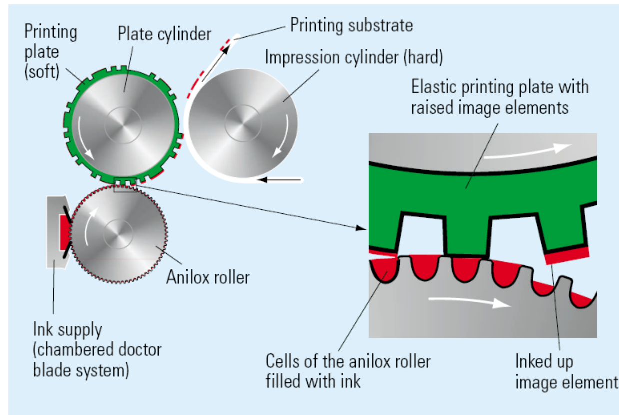


Figure 2.9: Schematic of flexography printing process [94]

In this process, the printing image is in relief on a printing plate made of rubber or plastic. Photopolymers are commonly used in order to increase the printing resolution. The anilox is an inking roller engraved with small cells. Anilox is supplied by ink which is transferred to the printing plate and then to the substrate. A doctor blade is used to remove the excess of ink on the anilox before printing. Pressure exerted by the impression cylinder on the substrate allows the image transfer onto the tape [71][95]. Printing can be performed on rigid and flexible substrate with roll to plate process and only on flexible substrate by roll to roll mode.

### 2.5.2 Flexography parameters

Flexography printed lines and films properties depends on anilox cells shape, depth and width. Line ruling given in lines per cm influences printed lines resolution. When higher anilox line ruling is used, spaces between dots are narrower and smaller dot size is obtained. Thus, higher image quality is achieved.
When the printing plate is strained under pressure, unstable dot structures are formed and larger lines are printed [122].
Printing resolution is also affected by printing pressure. *Yusof et al., 2007* demonstrated that when distance between substrate and printing plate decreased from 0.127 to 0.076 mm, i.e. when printing pressure increased, ink spreading was increased and larger lines were printed [123].

### 2.5.3 Advantages and applications

Flexography is a “simple” and reliable process. It is used to print many types of substrates such as plastics, papers, compressible surfaces such as cardboard packaging and corrugated boards.
Flexography is known for its high throughput. It is a high speed process allowing mass production of printed pieces. Besides, flexography allows high lateral resolution, about 40 $\mu$m. Deposited film thickness varies from 0.8 to 2.5 $\mu$m and may be higher [96].
Flexography process is employed in many applications such as food packaging and decorating. Recently, flexography use was published for high volume production of polymeric electronic structures [96] and for flexible electrical interconnets [124]. Some electronic applications made by flexography are shown in table 2.8.

| Reference | Application | Functional material | Substrate | Dimensions | Properties |
|---|---|---|---|---|---|
| *Kattumenu, 2008* [125] | RFID | Ag | Paper | Thickness = 2.11 $\mu$m Width = 1.20 mm | $R_s$ = 0.35 Ohm/square |
| *Unander and Nilsson, 2009* [126] | Moisture sensors | Carbon | Plastic sheets | Width = 300 $\mu$m | $R_s$ = 13.10 Ohm/square $C$ = 9.8 pF |
| *Deganello et al., 2010* [127] | Conductive tracks | Ag | PET | Thickness = 0.74 $\mu$m; Width = 75 $\mu$m | $R_s$ = 1.26 Ohm/square |

Table 2.8: Some flexography applications in electronic domain- *Materials electrical properties are reported in Chapter 3 and Annexe 2*

### 2.5.4 Limits and printing defects

Ink spreading outside of the image area, also called dot gain, is encountered with the flexography process. This causes registration troubles. Dot gain is mainly due to printing plate deformation, printing pressure and to ink properties (viscosity and surface tension). All these parameters lead to ink spreading and thus line widening.
The halo effect also a flexography defect is related to printing plate deformation and to incomplete ink transfer to substrate. Halo effect and spreading cause limited resolution and heterogeneity of the ink film which can be detrimental for electrical properties [71][122].

### 2.5.5 Flexography inks

Flexography inks have low viscosity, 0.05 to 0.5 Pa.s [96]. Viscosity may be higher for UV inks. They are water or solvent-based or 100% solid content. Solvents used can be alcohols, ethers, cellulosic esters. Besides, vinylic or acrylic binders and additives such as surfactant, dispersing and rheological agent are added [128]. Example of flexography ink formulation is shown in table 2.9.

| Constituent | Exemple | Weight percentage (%) |
|---|---|---|
| Pigment | Functional phase (color, conductivity, luminescence, etc.) | 3 - 31 |
| Resin | Oil-based, nitrocellulose, acrylic, etc. | 22 - 45 |
| Solvent | Water, ethyl acetate, methyl acetate, ethanol, methanol, isopropanol, carbitol, butyl acetate or phtalate, etc. | 46 - 55 |
| Additives | Waxes, stabilisers, etc. | 2 - 3 |

Table 2.9: Flexography ink formulation - Synthesized from [120][121]

## 2.6 Rotogravure printing

### 2.6.1 Process description

Rotogravure printing process consists in transferring ink from the engraved cylinder to the substrate. The cells are chemically or mechanically etched in the metallic surface of cylinder. It can be made of ceramic, copper or stainless steel. Ink is directly transferred onto the substrate and the image is then printed. A doctor blade allows ink excess removing [95]. Figure 2.10 shows a schematic view of the rotogravure printing process.

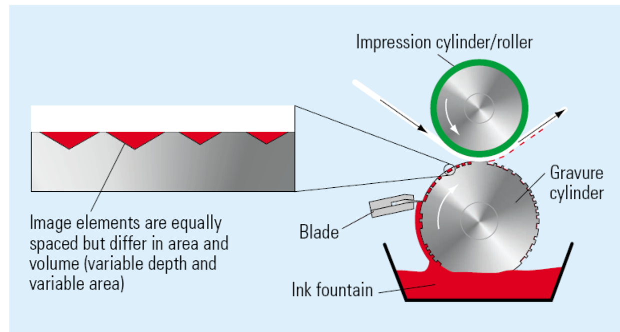


Figure 2.10: Schematic of gravure printing process [94]

### 2.6.2 Rotogravure printing parameters

Ink pick-up is dependent on ink doctoring, printing parameters, substrates and ink characteristics such as surface tension and viscosity [114]. Cell emptying is schematically presented in figure 2.11.

Figure 2.11: Gravure cells emptying [129]

Engraved cell emptying depends on cell characteristics (width and height), printing speed, ink properties and substrate surface energy.
Cells are brought to contact with the substrate, then ink is pulled out of the cells and deposited onto the substrate. Resultant drop spreads and printed width is larger than the cell width. Line thickness and width are dependent on cell height to width ratio. When cell width is too small compared to cell height, less ink is supplied to the substrate because cells have larger surface area compared to volume. Thus, greater adhesive forces are generated and ink cannot be easily pushed out of the cells.
*Sung et al., 2010* demonstrated that when cells with height to width ratio of 2.5/30.0 were engraved, it was not possible to deposit complete dot. But, when cells width was enhanced to 8.0 $\mu$m, complete dots were printed. They showed that a width to height ratio of 7 to 8 was required to print complete dots [129].
Furthermore, printing resolution is also dependent on inks properties which are related to printing parameters. Thickest lines are obtained with more solid content and inks with higher viscosities. However, when viscosity increases excessively, line thickness is decreased because of ink transfer decrease.
Furthermore, *Noh et al., 2010* studied printing viscosity effect on line width and thickness. They demonstrated that when silver content increased from 33% to 50% (viscosity increased), line width decreased from 120 to 100 $\mu$m and line thickness increased from 0.05 to 2.50 $\mu$m. They explained this result by less bleeding at higher viscosities [130].

### 2.6.3 Advantages and applications

Rotogravure printing allows direct patterning of large areas at running speeds of several hundred meters per minute [45]. Furthermore, it allows deposition of very narrow lines ($\sim$ 15 $\mu$m) with sharp edges [96]. Since rotogravure allows high resolution printing, it can be used for photography fine arts reproduction. In industry, it is mainly used for high volume printing (several thousands to millions of printed units).
Recently, rotogravure printing process was introduced as a high volume method for electronic applications and conductive tracks deposition. Thus, production of electronic components (metallic or polymeric) printed on a wide variety of flexible substrates (green ceramics, polymers foils, papers, etc.) by this process was already studied. Some examples are listed in table 2.10.

| Reference | Application | Functional material | Substrate | Dimensions | Properties |
|---|---|---|---|---|---|
| *Pudas et al., 2005* [114] | Conductive tracks | 60 - 70% Ag | PET, PP, PES | Thickness = 4 - 7 $\mu$m Width = 1 mm | $R_s$ = 60 mOhm/square |
| *Puetz and Aegerter, 2008* [45] | OLED | 50 - 60% ITO | PET | Thickness = 0.6 $\mu$m Width = 200 $\mu$m | Optical transmission > 80% $R_s$ = 400 Ohm/square |
| *Jung et al., 2010* [131] | Radio frequency tags | Ag conductor and $BaTiO_3$ dielectric | PET | Ag line width = 200 $\mu$m | $\rho = 20.10^{-8}$ Ohm.m $C = 5$ nF.cm$^{-2}$ |

Table 2.10: Some examples of rotogravure printed electronic applications - *Materials electrical properties are reported in Chapter 3 and Annexe 2*

### 2.6.4 Limits and printing defects

Some defects, related to gravure printing, are listed below [95]:

- streaking appears when the doctor blade fails in properly removing excess ink from gravure cylinder. Streaks generally appear on the unprinted area of the substrate,
- screening appears at the print form edges. It is due to highly viscous inks. In this case further dilution of the ink is required,
- missing dots related to cells poor emptying,
- difficulty to obtain sharp and straight lines due to the gravure with small cells,
- blocking and set-off of the gravure cylinder cells after ink drying.

### 2.6.5 Gravure printing inks

Gravure printing inks can be water or solvent-based. Most used solvent are water, toluene, aliphatic solvents, alcohols and esters. Resins such as cellulosic, vinylic, acrylic, polyamide polymers are added to ensure pigment binding. Finally, additives such as wax, plasticisers, rheological agents and surfactants are added [128]. Rotogravure printing inks have low viscosity, 0.05 - 0.2 Pa.s, and contain small particle size pigments, below 1 $\mu$m to print narrow lines. They dry by solvent evaporation. Slowly drying inks create pick off problems and too fast drying inks cause printability problems [95]. Table 2.11 shows a typical formula of gravure printing ink.

| Constituent | Exemple | Weight percentage (%) |
|---|---|---|
| Pigment | Functional phase (color, conductivity, luminescence, etc.) | 4 - 35 |
| Resin | Ester gum, rosins, acrylic polymers, esterified fumerated resin, etc. | 10 - 60 |
| Solvent | Water, ethylene glycol, propyl alcohol | 18 - 78 |
| Additives | Waxes, plasticizers, stabilisers, etc. | 2 - 10 |

Table 2.11: Typical formula of gravure printing ink - Synthesized from [95][120][121]

## 2.7 Inkjet printing

### 2.7.1 Inkjet printing methods

**Continuous Inkjet System (CIJ)**
Figure 2.12 shows a schematic of CIJ system.

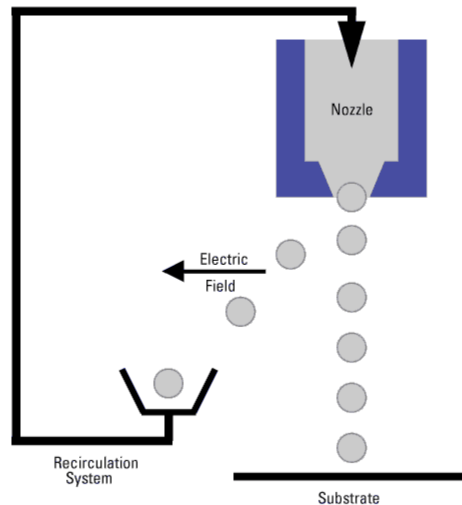


Figure 2.12: Continuous Inkjet System (CIJ) [132]

In this printing system, the ink flows out from a reservoir at a constant pressure through narrow nozzles. Uniformed sized droplets are formed by applying electromechanical stimulation using a piezoelectric or other transducer. The droplets trajectories are controlled by an electrical potential allowing selective charging and droplets deflection. Drop size and speed deposition are related to the orifice size, the fluid properties and the energy supplied to the transducer. This method is advantageous when high-speed coverage of relatively large areas is required.

**Drop On Demand system (DOD)**
In this method, the deflection and recirculation of non-printed droplets is not necessary

because only the needed droplets are produced by applying electrical, thermal or mechanical impulses. This technique is efficient for the deposition of small and controlled ink quantities [133]. In DOD inkjet printing method using piezoelectric head, piezo actuator generates a pressure pulse which induces changes in the fluid volume and causes the drop ejection [134]. Figure 2.13 shows a schematic of DOD inkjet system.

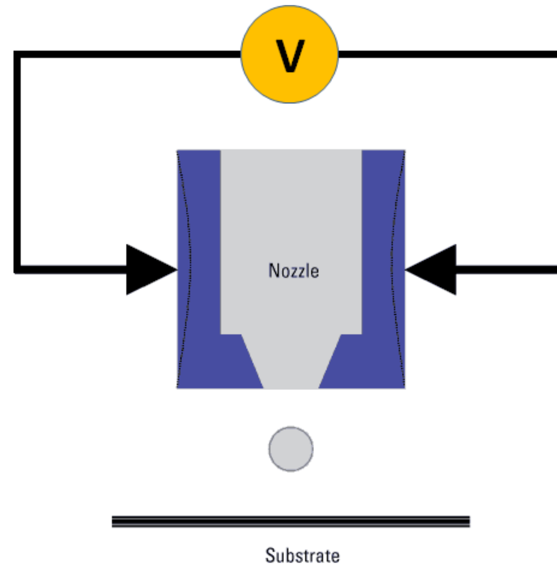


Figure 2.13: Drop On Demand inkjet system - Inspired from [132]

### 2.7.2 Advantages and applications

The ink-jet printing process solves the deformations problems of flexible substrates and improves the accuracy registration performance. This technique is advantageous for many reasons, reported by many researchers such as *Tekin et al., 2008* [135] and *Percin et al., 1998* [136]:

- non contact method (less contamination),
- no printing form manufacturing,
- deposition of picolitres volumes,
- direct writing of micron scale dimensions,
- coating of unusually shaped substrates,
- low cost,
- no wastes,
- computer control,
- rapid drying of inkjet printed droplets providing a fine phase separation and good performances devices with high efficiency.

Inkjet printing process is therefore a promising technique for printed electronics [108]. In a review reported by *Tekin et al., 2008*, inkjet printing is presented as an important technique in many fields such as organic flexible electronics, nanotechnology and tissue engineering [135]. Some applications of inkjet printing in electronic field are cited in table 2.12.

| Reference | Application | Functional material | Substrate | Dimensions | Properties |
|---|---|---|---|---|---|
| *Molesa et al., 2003* [137] | RFID | Gold → conductor PI → dielectric | Polyester | Thickness = 1.6 $\mu$m | $R_s$ = 23 mOhm/square $Q$ factor = 0.5 at 135 kHz |
| *Liu et al., 2005* [138] | Field effect transistors | PEDOT:PSS → gate/drain/source electrodes PVP → insulating polymer, PPy → active layer | Aluminium gate on silica as base substrate | Width PEDOT:PSS = 100 $\mu$m Thickness PVP = 0.59 $\mu$m | ON/OFF current = $2.9.10^3$ $\mu = 0.1$ $cm^2.V^{-1}.cm^{-1}$ |
| *Villani et al., 2009* [139] | OLED | PF6 (blue emitting polymer) in toluene | ITO coated PET | Thickness = 0.57 $\mu$m | Electrical and optical turn on voltage = 8 V |

Table 2.12: Some applications of inkjet printing in electronic domain - *Materials electrical properties are reported in Chapter 3 and Annexe 2*

### 2.7.3 Limits and printing defects

Inkjet printed lines may have some defects [135][137][140]:

- if drop spacing is very large, it is possible to get individual drops. In this case, drop spacing should be decreased (< drop diameter). This problem can be overcome by overlying many printed layers,

- scalloped patterns are obtained when printing is performed at low temperatures and small drop spacing, isolated drops merge but keep individual rounded contact lines. This can be prevented by increasing drop spacing or substrate temperature during printing,

- bulging is observed by increasing width through the line separated by regions of uniform narrow lines. This is attributed to vehicle excess leading to an increase of line width on dried zones. This can be solved by substrate heating or solvent quantity decrease,

- stacked coins effect is noticed when substrate temperature increases too much and leads to single drop dries before the jetting of the following drop. Consequently, each deposited drop will dry alone despite of overlap. This problem is overcome by decreasing temperature or solvent evaporation rate,

- Coffee ring is a well-known inkjet defect. It is caused by the splashing of the droplet on non porous substrates. This phenomenon is due to the higher evaporation rate of a drop at the line edge compared to the center. It can be solved by substrates heating during printing. Thus, evaporation rate is high everywhere on the tape. However, high temperature can cause substrate fast drying and thus jetting nozzle clogging. Indeed, distance between substrate and nozzle is usually less than 2 mm. As a result, before jetting, ink is also heated and evaporates rapidly. For this reason, to reduce coffee ring effect, solvent quantity could be increased or solvent with slower evaporation rate can be used to formulate ink. Coffee ring formation can be also prevented by decreasing the printing speed and increasing the spacing between droplets. This defect is also related to ink/substrate interface properties (surface tension and surface energy).

Figure 2.14 shows examples of inkjet printing defects.

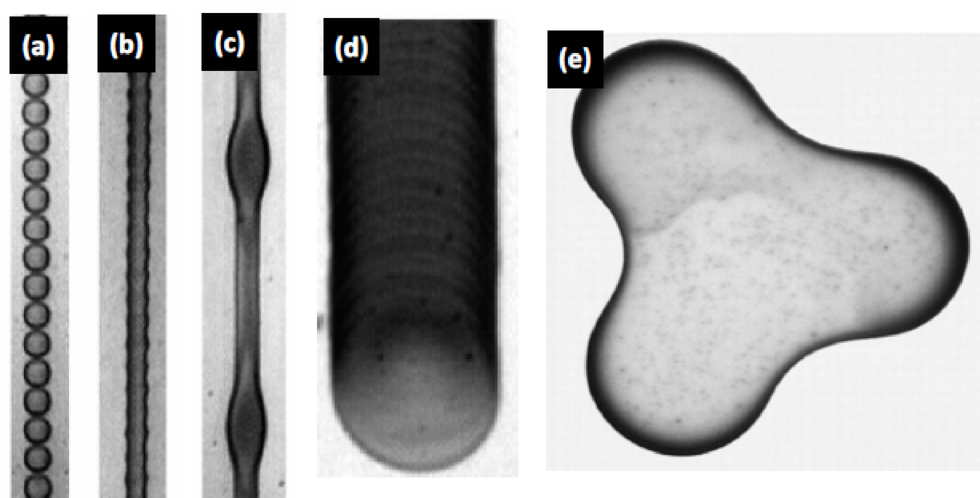


Figure 2.14: Inkjet printing defects: (a) individual drops, (b) scalloped pattern, (c) bulging, (d) stacked coins, (e) coffee ring [140][141]

### 2.7.4 Inkjet printing inks

Inkjet printing inks can be water-based, solvent-based, UV-curable and hot melt. They contain particles in sub-micrometer scale. This is required in order to prevent nozzle blocking and plays an important role in the drop formation.
Viscosity is a limiting factor for the drop formation which is also influenced by the density and the surface tension of the fluid [142]. Example of inkjet printing ink formulation is shown in table 2.13.

| Constituent | Exemple | Weight percentage (%) |
|---|---|---|
| Pigment | Functional phase (color, conductivity, luminescence, etc.) | 3 - 10 |
| Solvent | Water, oil-based, Methyl Ethyl Ketone (MEK), waxes for hot melt and liquid plastics for UV inks | 90 - 95 |
| Additives | Stabilisers, surfactant, dispersing agent, etc. | 1 - 3 |

Table 2.13: Typical formula of inkjet printing ink - Synthesized from [94]

## 2.8 Synthesis of lithography and printing processes characteristics

Table 2.14 shows a synthesis of printing processes properties, minimum line width, average thickness and viscosity of related inks.

| Method | Resolution | Mean thickness | Viscosity | Substrate |
|---|---|---|---|---|
| Soft lithography and NIL techniques | Sub-100 nm | 0.10 - 2.00 $\mu$m | 10 - 100 Pa.s | Rigid |
| Offset | 15 $\mu$m | 0.05 - 2.00 $\mu$m | 10 - 100 Pa.s | Flexible |
| Screen printing | 100 $\mu$m | 3.00 - 20.00 $\mu$m | 1 - 120 Pa.s | Rigid and flexible |
| Flexography | 40 $\mu$m | 0.80 - 2.50 $\mu$m | 0.05 - 0.50 Pa.s | Rigid and flexible |
| Rotogravure | 15 $\mu$m | 0.80 - 8.00 $\mu$m | 0.05 - 0.20 Pa.s | Flexible |
| Inkjet | $\sim$ 10 $\mu$m | $<$ Few $\mu$m (water and solvent based inks), 10.00 - 20.00 $\mu$m (UV and hot melt) | 1 - 50 mPa.s | Rigid and flexible |

Table 2.14: Lithography and printing processes properties [94][96][108][143]

**In this study, only screen printing, flexography, rotogravure and inkjet printing processes were investigated and optimised for ceramic based electronic microdevices manufacturing**.

# Chapter 3

# Inks

## 3.1 Conductive inks formulation

Conductive inks are mixture of three major components, the conductive material, the inorganic binder and the vehicle.

- main raw materials used for conductive inks formulation are nanoparticles or micro particles of noble metals such as gold, silver, platinum and non-noble metal such as copper, nickel, cobalt and iron, or non metallic conductive particles such as carbon, carbon nanotubes and graphite,

- an inorganic binder generally composed of glass powders and other adhesion promoters may be added in some cases,

- a vehicle which is a mixture of organic binder, solvent and additives to promote dispersion stability, adjust rheological behaviour and enhance stability.

### 3.1.1 Conductive particles

Noble metals are used because of their chemical inertness and electrical conductivity [144]. To be used in electronic applications requiring low feature sizes in the sub-micron scale, conductive ink particles should have small diameter ($< 5\ \mu$m). Usually nanoparticles are used [45]. Particles are dispersed in a solvent or a binder sometimes with other fillers and additives.

#### Metal particles generalities

Commercially available conductive inks are dispersion of relatively small conductive particles in a non-conductive resin. Particles can be metallic silver, copper, palladium. Metal particles are used in conductive inks formulae for their high electrical conductivities. Conductive metal particles from group IB of the periodic table of elements such as copper (Cu), silver (Ag) and gold (Au) are among the best conductors and they are used when firing temperature is lower than 1000°C.
Metals such as palladium (Pd), platinum (Pt) and tungsten (W) are also good conductors but they melt at higher temperatures than metals of group IB. For this reason, they are used when higher sintering temperatures are required (> 1200°C).
Nickel can also be used for its good electrical properties. However, nickel oxidises at low temperatures (300°C) in oxygen atmosphere. Thus, reducing atmosphere (oxygen pressure - $P_{O_2} = 10^{-9}$ Pa) should be provided to sinter nickel conductive lines at temperatures

as high as 1100°C [145].
Amounts, shape, conductive particles orientation, particle size distribution have an important effect on ink conductivity. In order to print smooth lines (Ra $< 1$ $\mu$m), in some cases, metal nanopowders are used. These particles have usually a particle size ranging from 1 to 100 nm. They have very low melting points compared to the corresponding bulk materials. Their sintering temperature is close to 300°C. Nanoparticles are dispersed in an organic solvent in order to formulate conductive inks. Nanoparticles of noble metals, such as silver and gold, are used due to their chemical stability, excellent electrical conductivity and catalytic activity [71][119][144][146][147].

### Silver particles

**Physical properties** Silver (Ag) is mainly extracted (80%) from ores such as galena (natural lead sulphide) and copper ores by amalgamation, leaching and cyanidation. Silver nitrate ($AgNO_3$) or silver chloride (AgCl) are used to prepare silver aqueous solutions. Silver nitrate decomposes to silver at temperatures varying from 440°C to 500°C.
Silver is a malleable and ductile metal with 76 GPa elastic modulus. Its melting point is equal to 950 - 960°C. *Yeshchenko et al., 2010* reported that silver melting temperature depends on silver nanoparticles size [148]. Its thermal conductivity is equal to 429 $W.m^{-1}K^{-1}$ at 300°K and its Thermal Expansion Coefficient ($TEC$) equal to $19.2.10^{-6}$ $K^{-1}$. It has low 15.9 nOhm.m electrical resistivity [27][145][149][150].

**Chemical properties** Silver reacts with oxygen under pressure and at high temperature to produce silver oxide $Ag_2O$. Indeed, silver absorbs oxygen at a temperature slightly higher than its melting point. Oxygen absorption is ten times higher than silver volume. This absorption drops drastically at higher temperatures and before solidification, absorbed oxygen is ejected.
Silver is not stable against halides. It also reacts with sulphur and selenium. Nitrogen and phosphor are soluble in hot silver. Carbon is slightly soluble in silver at high temperatures. Silicon and silver are completely miscible. Silver forms alloys with most of the metals and this can be very important technically. Silver is stable against water and acids attacks [27][149].
Silver migration into silica is well known and was studied by different researchers. Many reasons affect silver migration into insulating materials: humid environment, voltage gradient, temperature, conductor composition. Two types of migration can be distinguished: electro-migration involving electron transfer at temperatures higher than 150°C in dry environment and ionic migration occurring at lower temperatures ($<$ 100°C) in high humidity atmosphere. Silver migration is one of the reasons of short circuits. It also generates grain growth and dielectric properties change. To reduce silver migration, silver-palladium alloys are generally used [151][152][153].

**Disadvantages, consequences and solutions for silver as conductive material**
Problems which can be encountered when using silver are listed in table 3.1.

| Problems | Consequences | Solutions |
|---|---|---|
| Ag diffusion in some ceramics pores, especially in calcium titanate ceramics and its relatively high solubility in some glasses compared to other metals (Ag solubility in borosilicate is equal to 0.45% relatively high compared to that of Pd 0.03%) | Loss of silver<br>Ag migration through electrodes to the system edges<br>Microstructures formation<br>Grain growth and densification affected<br>Electrode resistance increase<br>High dissipation factors | Use Ag/Pd alloys with higher melting point than Ag<br>Reduce boron oxide in the substrate because it forms solid solution with Ag<br>Use glass and ceramic materials able to crystallize rapidly when firing |
| Metallic (Ag) - organic (binder) catalysis | Exothermic reaction<br>Hot spots formation<br>Rapid evolution of gases during the binder decomposition<br>Metal-substrate interaction ruptured and adhesion to the substrate weakened | Use large particles with low specific surface area to reduce the metal surface contact with the organic binder<br>Reduce the organic binder amount<br>Sinter at low oxygen pressure and temperatures to limit the catalysis reaction |
| Poor solder leach resistance due to Ag rapid dissolution in tin (Sn) | Swelling and volume increase<br>Pores creation<br>Conductivity decrease | Reduce tin quantity |
| Ag migration between neighbouring conductive lines or between electrode layers in multilayers systems ($Ag^+$ migrates from the cathode to the anode) | Dielectric breakdown<br>Current leakage<br>Failure mechanism<br>Migration through ceramic<br>Short contact | Use Ag/Pd alloys<br>Cover the bottom conductor with a dielectric layer<br>Fire the system to reduce pore size as maximum as possible |
| Wire bonding on the surface of the multilayer system by gold paste | Battery effect between the Ag (cathode) in the inner layers and the Au (anode) on the upper layer<br>Migration of dielectrics from the Ag to the Au<br>Formation of $O_2$ gas at the interface<br>Gases trapped in the multilayer structure<br>Delamination of the thick film | Connect top and inner layers by vias holes |

Table 3.1: Problems encountered with silver when printed onto ceramic and glass for electronic applications, consequences and solutions [145]

**Applications** Silver was essentially valued as a precious metal used to make ornaments and jewellery. It is also used in mirrors fabrications and as catalysis agent in

chemical reactions. Nowadays, silver metal is used as a conductive filler in silver conductive ink manufacturing. Such inks are printed to form electrical contacts, electrodes, conductive tracks. Flake shape metallic particles increase the ink viscosity and also the conductivity, especially at lower temperatures because of their higher surface contact [154].

**In this study, only silver conductive inks are formulated and investigated.**

#### Gold particles

**Physical properties** Gold (Au) is widely distributed in very low concentrations in nature. It is produced from gold ores by combination of different processes such as flotation, amalgamation, treatment with alkaline cyanides, refining, etc.
The melting point of gold is equal to 1063°C. Gold nanoparticles have lower melting points. Its boiling point is equal to 2700°C and its bulk density to 19.3 g.cm$^{-3}$. Gold is also reflective and has low resistivity. Bulk gold has 24.4 nOhm.m electrical resistivity. Its thermal conductivity is equal to 317 W.m$^{-1}$.K$^{-1}$ and its $TEC$ to 14.2.10$^{-6}$ K$^{-1}$ [40][27][150].

**Chemical properties** Gold is chemically inert; it does not combine with oxygen nor dissolve in most acids. It is resistant to oxidation and acids attacks even at high temperatures. It reacts with halogens to form the corresponding halides. Reaction occurs in humid atmosphere or at high temperatures.
Gold allows excellent ohmic contacts [155]. It resists to migration through ceramic multilayers systems and between the conductive lines. Gold cannot withstand tin/lead solder. Platinum or palladium should be added to perform solderability, but the conductivity will decrease [145][27].

**Applications** Gold was known since the ancient times for its precious value. Its main use is for jewellery creation and as monetary standard. Modern industrial uses of gold (Au) include dentistry and electronics. Thus, gold plating or electroplating is employed in order to manufacture electrodes, diodes and printed circuits. Gold powders are used as conductive element in conductive inks manufacturing for printed electronics applications.

#### Copper particles

**Physical properties** Copper (Cu) is a reddish-coloured metallic element, widely used in manufacturing and industry. It is low-cost, possesses high conductivity (6% lower than silver conductivity) corresponding to 17.24 nOhm.m resistivity. It has good solderability. Melting temperature of bulk copper is approximately equal to 1085°C. Melting temperature is dependent on copper particle size. Copper thermal conductivity is equal to 401 W.m$^{-1}$.K$^{-1}$, its $TEC$ to 16.5.10$^{-6}$ K$^{-1}$ and its elastic modulus to 110 GPa [145][148][150].

**Chemical properties** Exposed to air, copper oxidises and loses its electrical properties. To prevent oxidation, it should be sintered in nitrogen or hydrogen atmosphere.

Copper is thermodynamically stable in nitrogen atmosphere when temperature is higher than its melting point (1083°C).

**Applications** Copper is used in several fields such as automotive, energy, construction, transportation and communications. It is used for heat exchanging, electronic interconnections, motor systems and other applications. Copper or copper alloys are used for electrodes, batteries, cables, connectors and air conditioning tubes manufacturing [156].

#### Nickel particles

**Physical properties** Nickel (Ni) is a silvery-white lustrous metal with a slight golden tinge. The natural form of Nickel contains magnesium, sulphides or arsenide. Bulk nickel has a 8.9 g.cm$^{-3}$ density, a 1455°C melting point and a 2900°C boiling temperature.
It is a hard and malleable material with 207 GPa elastic modulus [149]. Nickel is a good conductor with 69 nOhm.m electrical resisitivity [40]. Its thermal conductivity is equal to 91 W.m$^{-1}$.K$^{-1}$ and its $TEC$ to 13.10$^{-6}$ K$^{-1}$.

**Chemical properties** When heated, Ni reacts with hydrogen. A chemisorption reaction occurs leading to $H_2$ dissociation and absorption at the Ni surface. A metal hydride surface layer is then formed.
Nickel surface is oxidised after exposure to air leading to nickel monoxide formation. The nickel oxide can be easily reduced by hydrogen, carbon monoxide and carbon. Nickel oxidation at temperatures ranging from 314°C to 375°C was studied by *Sales and Maple, 1977* [157]. Oxidation rate increases when temperature increases. Nickel oxidation is one of the main reasons for conductivity decrease.
Nickel does not react with water at temperatures lower than 1000°C. It is stable to some acids (chlorhydric acid (HCl) and sulfuric acid ($H_2SO_4$)) attacks. But, it can be oxidised by very strong acids such as $HNO_3$ and $HClO_4$. It can also be attacked by melted sodium and potassium hydroxide and then forms the nickel monoxide (NiO). Nickel is attacked by carbon monoxide at 45°C and produces a volatile carbonyle $Ni(CO)_4$ [149].

**Applications and properties** Nickel is used in many industrial and consumer products, including stainless steel, magnets, rechargeable batteries, electric guitar strings and special alloys [150][158].

#### Palladium and Platinum

**Physical properties** Palladium (Pd) and Platinum (Pt) are transition metals from the platinum group (group VIIIB of the periodic table).
Platinum is malleable and ductile with a 112 GPa elastic modulus. Bulk palladium electrical resistivity is equal to 108 nOhm.m, its $TEC$ to 11.10$^{-6}$ K$^{-1}$ and its thermal conductivity to 72 W.m$^{-1}$.K$^{-1}$. It has high melting temperature (1825°C) and its density is about 12 g.cm$^{-3}$.
Platinum (Pt) is also a transition element from the platinum group. It has 21 g.cm$^{-3}$ density and 2045°C high melting temperature. It has a high electrical resistivity compared to silver and gold (106 nOhm.m). Its $TEC$ is equal to 9.10$^{-6}$ K$^{-1}$ and its thermal conductivity to 72 W.m$^{-1}$.K$^{-1}$. Its elastic modulus is equal to 147 GPa [145].

**Chemical properties** Palladium exhibits more chemical reactivity than other noble metals. It oxidises at 350°C when heated in air atmosphere to form the palladium oxide (PdO). However, at higher temperatures (790°) oxide decomposes to metal form. Palladium reacts with halogens to form halides. It can also be attacked by nitric acid in the presence of nitrogen oxides. It is able to absorb 800 times its volume of hydrogen. Pd reaction with $H_2$ leads to electrical properties degradation [27].
At ordinary temperatures, platinum is considered as an inert material. It oxidises at 500°C to form platinum dioxide ($PtO_2$). At higher temperatures (> 1000°C), it looses its oxide form. It is attacked by alkali, cyanides and nitrates. It absorbs large quantity of hydrogen [27].

**Applications** Platinum, palladium and other platinum group elements (ruthenium, rhodium, iridium, etc.) are used in high quality glass and glass fibres manufacturing because of their high melting temperatures (> 1700°C). They are also used in space technology.
They can be added as additives in conductive pastes in order to provide X-Y shrinkage matching.
On one hand, palladium and/or platinum are added to silver or gold conductive top conductive layers in multilayer systems and in solder pads in order to reduce gold and silver poor solder leach resistance and to inhibit silver migration through the multilayer ceramic system. On the other hand, palladium and platinum are too expensive and reduce electrical conductivity of gold and silver [145][159].

**Metal particles properties** Some of conductive metal particles properties are summarized in table 3.2.

| | Bulk metal melting point (°C) | Nanoparticle melting point (°C) | Resistivity (nOhm.m) | Thermal expansion coefficient ($10^{-6}.K^{-1}$) | Thermal conductivity ($W.m^{-1}.K^{-1}$) |
|---|---|---|---|---|---|
| Silver (Ag) | 961 | 11 nm → 200<br>20 nm → 300<br>30 nm → 350 | 16 | 18.9 | 429 |
| Gold (Au) | 1063 | 5 nm → 500 - 600 | 24 | 14.2 | 317 |
| Copper (Cu) | 1085 | 40 nm → 200<br>50 nm → 400 | 17 | 16.5 | 401 |
| Nickel (Ni) | 1455 | 10 nm – 90 nm → 900 | 69 | 13.4 | 91 |
| Platinum (Pt) | 2045 | | 106 | 9.0 | 72 |
| Palladium (Pd) | 1825 | | 108 | 11.2 | 72 |

Table 3.2: Metal particles properties summary [27][148][160][161]

**Non-metallic conductive particles – Carbon**

Carbon is a non metallic tetravalent chemical element with four electrons available to form covalent chemical bonds. There are several allotropes of carbon. The best known are the crystalline forms, i.e. hexagonal graphite, cubic diamond and amorphous carbon such as carbon black and carbon fibers [162].
All forms of carbon are highly stable, requiring high temperature to react even with oxygen. When heated to 600°C, carbon reacts with oxygen and forms carbon dioxide. If the temperature is higher than 900°C, the reaction is reversed [163].
Carbon is used to provide work function of counter and working electrodes in electrochemical devices. Electrodes can be screen printed by carbon inks [164].

**Graphite** Graphite is considered as a semi-metal. It is a very good conductor. Its structure is composed of hexagonal non packed sheets, graphene. Carbon atoms are highly bonded with covalent bonds but sheets affinity is very weak. Graphite electrical resistivity is equal to 50 $\mu$Ohm.m. For a semi-metal as graphite, there are two kinds of carrier, electrons and holes. Electric properties depend on lattice defects and temperature. Depending on carbon organisation, electrical resistivity can be as low as 1 $\mu$Ohm.m [162].

**Carbon nanotubes** Carbon nanotubes have special structure compared to other carbon composites. They were seen for the first time by Iijima and co-workers in 1993 as a tubular form of carbon. Carbon nanotubes are one dimensional system organised in single or multi wall (SWNT or MWCNT). SWCNT can be represented as a rolled graphene sheet. MWNTs are formed of many stacked tubes of variable diameters. Depending on their arrangement, diameter and helicity of the tubes, nanotubes can be highly conductive and act as metals or as semiconductors [162].

**Non-crystalline carbon – carbon black (CB)** The majority of non-crystalline carbons is obtained after primary carbonisation when condensed poly-aromatic units, called basic structural units (BSU), are formed. During the secondary carbonisation, these units slightly join together forming nanoscales crystallites. A large variety of morphologies is issued from local molecular ordering (LMO) or lamellar arrangements of BSU following either liquid or gaseous phases. Plastic and gaseous phase carbons can be obtained. Different forms and shapes are also obtained:

- planar symmetries - lamellar carbons,
- cylindrical carbons - carbon fibres,
- spherical carbons - carbon black [162].

Carbon black has many properties such as electrical conductivity and ultra violet rays protection. Carbon black is used as reinforcing agent in rubber products, as a black pigment in paints and inks and for manufacturing electrodes or electrical conductors. [162].

### 3.1.2 Inorganic binder

An inorganic binder is generally added in screen printing conductive pastes for thick films applications. Such pastes are especially formulated to print ceramic and glass tapes.
Mineral binders are employed to enhance densification process and provide adhesion of

the metal to the ceramic substrate. Furthermore, they can be added as sintering aids to reduce the sintering temperature of the metal. They also control the shrinkage and thermal expansion coefficients mismatches. Indeed, shrinkage mismatch is due to the metal low densification temperature compared to that of ceramics.
Mineral binder can be precious metal, organo-metallic compound or glass powders added in small quantities compared to the conductive phase.

#### Precious metals

Small quantities of precious metals or their oxides such as nickel, copper oxides or copper/cadmium oxides systems can be added in order to ensure better electrical conductivity and stability. In this case, metal is reactively bonded to the ceramic. Chemical interactions mainly interfere in this bonding process [165]. *Hitch, 1974* added copper oxide particles to screen printing inks, in order to provide adhesion to the substrate. Resistivity close to 34 nOhm.m was measured on printed lines [166]. When metal oxides are added, sintering should be performed in inert atmosphere to prevent oxidation. This increases the process cost and makes it more difficult [145][167].

#### Organo-metallic materials

Organo-metallic compounds such as ruthenium, rhodium, aluminium, platinum with alkyl organic medium can be added to grant highly dense conductive metallic film surface and better shrinkage match between the substrate and the metal powders [145].

#### Glass powders

Glass powders are added in conductive pastes as adhesion promoter. High lead glasses were commonly used because of the low melting temperature of lead (327°C) which helps reducing glass softening point and thus, sintering temperature. Nowadays, the tendency is to reduce lead in glass powders, because of its bad impact on the environment and human health. Thus, glass powders composed of a mixture of magnesium oxide, bismuth oxide, alumina, zinc oxide, sodium and calcium carbonates and others are used.

Figure 3.1 shows the difference between a screen printed silver/glass film on a ceramic substrate before and after sintering at 875°C. On this figure, spherical glass powders are clearly observed. They are larger than silver conductive particles. In addition, some pores are also seen on the non-sintered film. After sintering, both silver and glass powders melt. No more pores are detected and a continuous packed network is formed. However, cracks are observed.

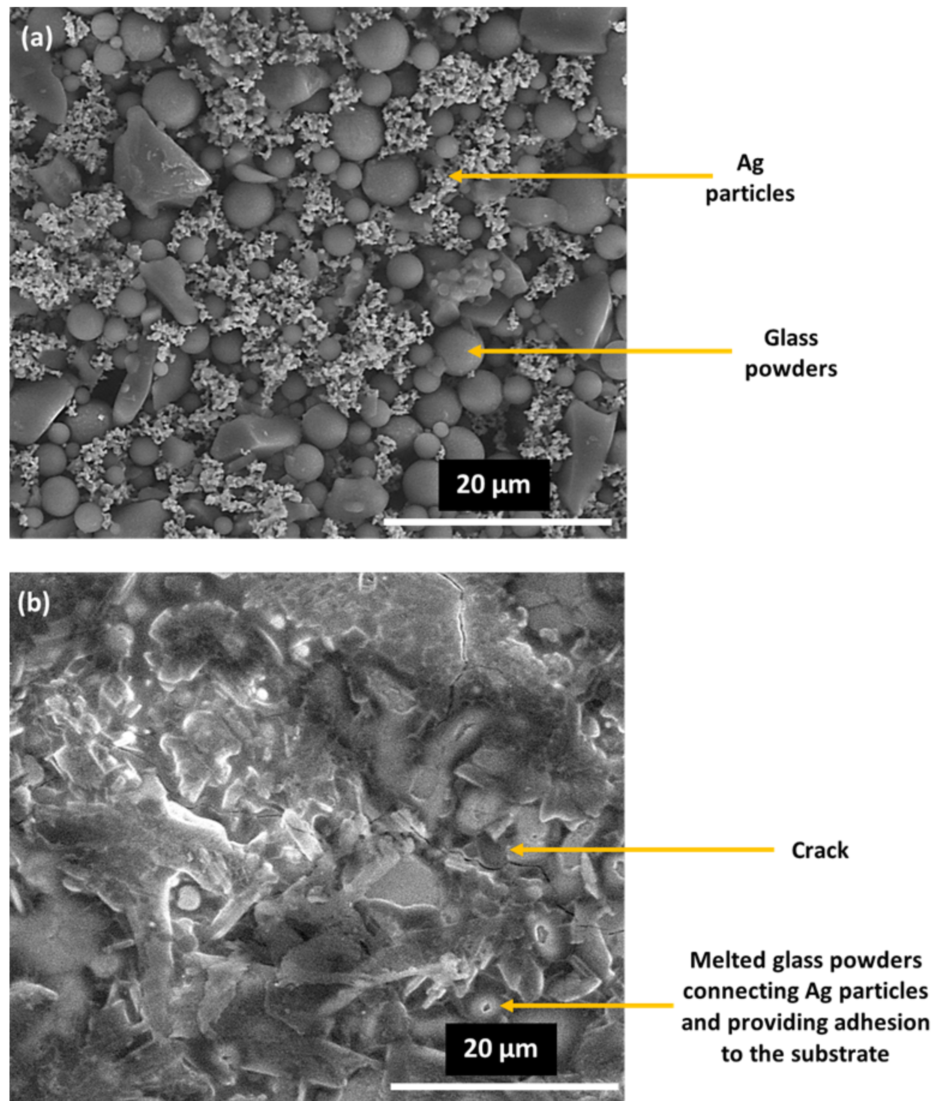


Figure 3.1: Screen printed silver/glass film before (a) and after (b) sintering at 875°C - SEM Grenoble INP - Pagora

During sintering, glass melts and passes to liquid state. This phenomenon allows migration to ceramic – metallic film interface and provide adhesion to the substrate. Migration is performed by capillary effect. Glass with low viscosities and high densities are preferred to enhance the wetting of the particles and aid bonding to the substrate [165][167][168].

Besides, glass provides interconnections between the metallic particles.
It was demonstrated that 5 to 10% of frit contents are enough to provide good adhesion of silver and gold inks to alumina substrates [166].
*Rane et al., 2003* showed that when glass content increased from 4 to 10%, lateral grain growth also increased with simultaneous decrease of pore sizes [118].
*Hitch, 1974* demonstrated that when excessive glass quantity was added to a conductive ink, more pores can be observed in the film, after sintering [166].

At excessively high temperatures, it is possible that glass floats to the conductor surface, thus generating cracks propagation and contacts blocking. Besides, glass floating may result in line spreading and poor resolution.

Furthermore, glass conductivity is very low. Consequently, higher film resistivity can be obtained when glass powders are added to conductive inks.
*Hitch, 1974* showed that when 7.4% of glass powders were added to gold ink suspension, only 16% of gold particles were covered by glass after sintering. But, when 11% of glass powders were added, 26% of gold particles were covered by glass after sintering, at 1000°C [166]. This percentage of glass covering is called “apparent bondability”. Glass covering increase after sintering is a reason for reducing conductive films electrical properties and also increasing porosity percentage in the film. Thus, a compromise should be found between conductive particles adhesion to the substrate and porosity of the printed film, after sintering.

Glass powders are the main component of resistor pastes: about 90% of glass powders are added to reach resistivity values as high as 1 to $10^7$ Ohm.m. Resistors control the electrical current conduction in an electronic circuits. Thus, glass plays different roles, sintering aid, inorganic binder and provide high resistivity phase.
Besides, 60 to 70% of glass powders are added to dielectric pastes. Dielectric provides insulating layers between conductors to avoid current shorting. In this case, glasses stabilise the dielectric structure and stop mobile species migration [165].

**In this work, only glass powders were studied as inorganic binder allowing silver particles adhesion to ceramic substrates.**

### 3.1.3 Ink vehicle

Ink vehicle is a mixture of solvent, polymeric binder and additives. A vehicle is required in a conductive ink formulation:

- to ensure a stable dispersion,
- to confer fluid properties to the ink (viscosity and surface tension) and allow ink transfer from the printing form to the substrate,
- to control the drying rate of the paste at room temperature,
- to control the line thickness and provide an homogeneous thickness.

To grant these properties a vehicle should:

- be chemically non reactive with the substrate and the metal powders in order to avoid the metal-organic catalysis
- be easily removable in the early sintering stage,
- have a combustion temperature lower than the softening point of used mineral binder.

#### Solvent

Solvents with a vaporisation temperature ranging from 200°C to 300°C at pressure atmosphere (1 atm), such as terpineol, ethylene glycol ethers and esters, are generally used to manufacture screen printing conductive pastes. They can be also used as co-solvent with water. For inkjet inks, generally mixture of water/ethylene glycol/ethanol is made in

order to obtain lower viscosities ($< 20$ mPa.s). For flexography and rotogravure printing inks, mixtures of water and high density solvent ($> 1$ g.cm$^{-3}$) are used. Their main role consists in dispersing adequately the metallic and inorganic powder. They also guarantee slow evaporation rate, provide better line resolution and prevent printing elements clogging (screen mesh in screen printing, anilox in flexography, engraved cylinder in rotogravure and jet nozzle in inkjet) [145].

**Organic binder**

The binder maintains mechanical integrity of the film after the solvent evaporation and binds the different powders to each other. It also allows the ink film formation. When low binder quantity is used, burnout is easier thus, less cracking and metal-organic catalysis occurred. Organic binder should be compatible with both the metal and the substrate. For example, terephthalic acids react with bismuth oxides and then paste viscosity enhances during time. Ethyl cellulose, acrylic and styrene acrylic polymers, polyesters and other polymers can be used as binders [145].

**Additives**

Additives such as rheological agents are used to modify viscosity and to guaranty ink specific rheological behaviour such as pseudoplasticity and thixotropy. Besides, surfactants are added to enhance the dispersion stability by creating steric or electrostatic stabilisation to prevent particles agglomeration. Wetting agent can be used in order to adjust the surface tension of the ink and induce substrate wetting. In addition, antifoaming agents can be used in order to avoid foam formation in the water-based inks, because bubble foams generate voids in the conductive lines during printing [145][169].

*Thermoelectric materials are reported in Annexe 3.*

## 3.2 Inks properties

### 3.2.1 Surface tension

The surface tension of a liquid is the reversible work as a result of the creation of a unit specific surface area [170]. The energy ($W$) of a system is related to its volume ($V_s$), its chemical composition ($n_i$) and its interfacial area ($A$). So, when the area $A$ changes, the energy of the system will change according to equation 3.1:

$$dW = \gamma_l \cdot dA \tag{3.1}$$

$$\gamma_l = \frac{dW}{dA} \tag{3.2}$$

Where:

- $\gamma_l$ (N.m$^{-1}$) is the liquid surface tension,

- $W$ (N.m) is the system energy,

- and $A$( m$^2$) is the surface.

Surface tension is the sum of different components depending on the interactions leading to energy variation:

- polar interaction creates the polar fraction of the surface tension, $\gamma_l^p$. It is established due to ions and magnetic dipoles. It is related to polar and hydrogen bonds.

- interaction of dispersion generates the dispersive fraction of the surface tension, $\gamma_l^d$. Dispersion is due to the electrical charges of molecules.

### 3.2.2 Rheological behaviour of printing inks

Rheology is the study of a material flow behaviour and of the resulting deformations when a material is exposed to a force. Flow behaviour is controlled by the intermolecular forces between system constituents. Several ink rheological behaviours are described in the following [95][56][171][172][173].

#### Bingham

A Bingham fluid has a yield stress: the minimum shear stress required to allow material flowing. Rheological behaviour of a Bingham fluid can be modelised according to equation 3.3.

$$\tau = \tau_0 + \eta_\infty \cdot \dot{\gamma} \tag{3.3}$$

Where:

- $\tau$ (Pa) is the shear stress,
- $\tau_0$ (Pa) is the yield stress,
- $\eta_\infty$ (Pa.s) is the viscosity when $\dot{\gamma} \to \infty$,
- $\dot{\gamma}$ (s$^{-1}$) is the shear rate.

Figure 3.2 shows the rheological behaviour of a Bingham fluid.

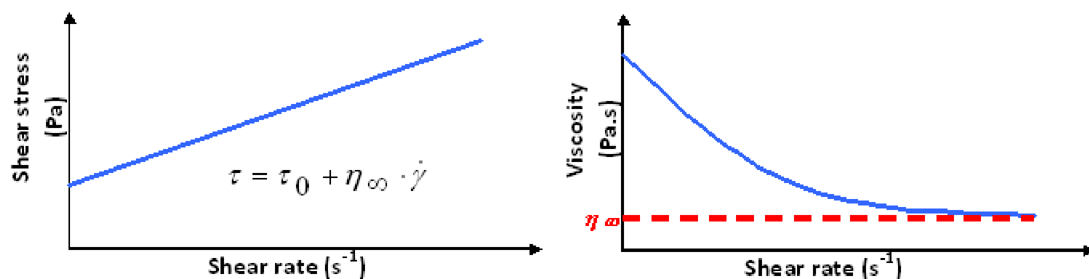


Figure 3.2: Bingham, ideal plastic, behaviour [172]

#### Hershel – Bulkley

A Hershel – Bulkley fluid can be described mathematically by equation 3.4:

$$\tau = \tau_0 + K \cdot \dot{\gamma}^p \tag{3.4}$$

Where:

- $\tau$ (Pa) is the shear stress,

- $\tau_0$ (Pa) is the yield stress,

- $\dot{\gamma}$ ($s^{-1}$) is the shear rate,

- $K$ is the "consistency",

- and $p$ is the power low exponent.

Figure 3.3 shows the variation of shear stress as a function of shear rate of a Hershel-Bulkley fluid.

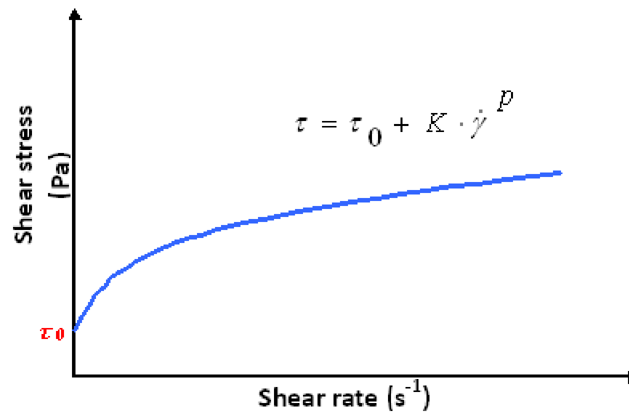


Figure 3.3: Hershel-Bulkley behaviour [172]

### Casson

A Casson fluid is a shear thinning fluid with a solid like behaviour at zero shear rate and a small viscosity ($\eta_\infty$, Pa.s) when shear rate is infinite. The Casson model is an empirical model proposed to describe the rheological behaviour of printing inks and other solid suspensions. Casson mathematical model is given by equation 3.5.

$$\sqrt{\tau} = \sqrt{\tau_0} + \sqrt{\eta_\infty \cdot \dot{\gamma}} \tag{3.5}$$

Where:

- $\tau$ (Pa) is the shear stress,

- $\tau_0$ (Pa) is the yield stress,

- $\eta_\infty$ (Pa.s) is the viscosity when $\dot{\gamma} \to \infty$,

- $\dot{\gamma}$ ($s^{-1}$) is the shear rate.

### Thixotropy

Thixotropy is a time-dependent effect defined by *Barnes et al., 1989* as a decrease of a material apparent viscosity under constant shear stress or rate. A gradual recovery is observed when shear rate or stress is removed [174]. Screen printing inks are thixotropic fluids.

## 3.3 Conductive inks processing

To control the properties of a conductive film, particles, pastes and sintering processing should be understood (figure 3.4).

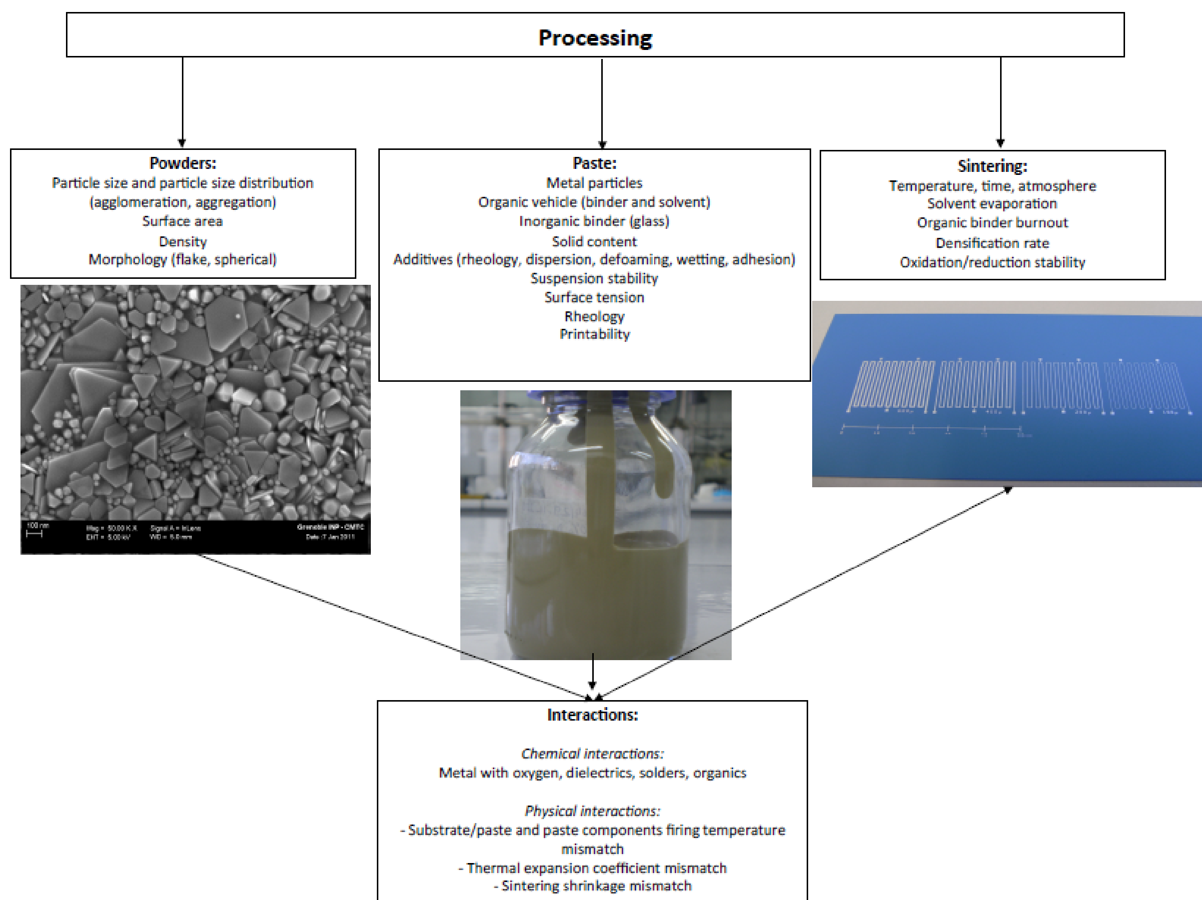


Figure 3.4: Conductive film processing (powders, paste and sintering) reproduced from *Wang et al., 1994* [145]. Powders photograph is a Field Emission Gun – Scanning Electron Microscope photograph of conductive commercial paste (Novacentrix), paste is a screen printing ink formula prepared with 50% of silver, sintered lines are commercial paste printed by screen printing of green LTCC tapes and sintered at 875°C

Pastes and deposited lines processing affects film extrinsic (smoothness, line resolution, continuity, porosity, thickness, width, etc.) and intrinsic properties (electrical and thermal conductivity, density, thermal expansion coefficient, etc). Intrinsic and extrinsic properties are deeply related. Electrical properties can be affected by many factors such as line thickness, edge definition, surface morphology, interfacial properties, curing temperature and duration and impurities modifying the carrier density.

### 3.3.1 Formulation

The ink vehicle is prepared and roughly mixed to homogenise the suspension. Then, powders (conductive and glass) are progressively added. Mechanical mixing is performed in order to ensure powders dispersibility in the vehicle. Suspensions can be roll-milled or sonicated in order to formulate stable suspensions in organic vehicle [175]. In the case of flexography, rotogravure and inkjet inks, the prepared suspension is not three-roll

milled. Mechanical dispersion and sonication are mainly performed for the "liquid inks". A schematic of screen printing pastes formulation is shown on figure 3.5.

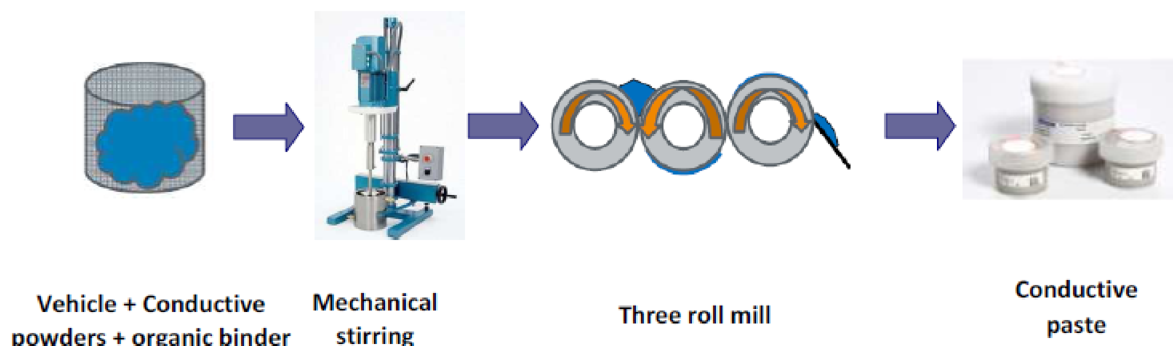


Figure 3.5: Screen printing conductive pastes formulation processing

Ink dispersibility and printed lines properties are dependent on powders properties. When selecting the metal powders to be used for ink formulation, many factors should be considered such as powder morphology; powder specific surface area, particle size and particle size distribution, agglomeration and tap density.

### Morphology

Particles can be spherical, flake, nodular, acicular and dendritic. Usually, flake and spherical powders are used for ink formulation. Flake powders have higher surface contacts which gives inks with higher viscosities. Besides, flake shape powders have higher sintering temperatures than spherical ones [145].

### Specific surface area

Silver particles specific surface areas vary from 0.1 to 15 $m^2.g^{-1}$ depending on manufacturing method. Table 3.3 shows particles specific surface area effect on ink formulation and printed lines properties.

| High specific surface area particles | Low specific surface area particles |
|---|---|
| Small diameter | Larger diameter |
| Need more solvent for wetting → higher solid content after sintering → enhanced conductivity | Require less solvent for wetting → more particles needed to achieve high solid content and good contacts after sintering |
| Sintering at lower temperatures (300°C) | Higher sintering temperatures (> 300°C) |
| Narrow lines definition | Larger lines due to larger diameters |
| Oxidises at relatively low temperatures (< 300°C) | Oxidation at higher temperatures and at a slower rate |
| Low porosity | More numerous and larger pores |

Table 3.3: Particles properties dependent on their specific surface area

### Particle size, particle size distribution and agglomeration

To allow good packing and good film density, particles should not be agglomerated. An optimum specific surface area is defined and multi-modal particle size distribution is preferred in order to allow pores blocking by mixing small particles to larger ones.

When particles are de-agglomerated, better dispersion quality is obtained and smoother films are printed. Thus, higher electrical conductivities are reached.
Besides, when particles are homogeneously dispersed, vehicle and molten glass capillary forces are higher. Consequently, the paste fluidity is enhanced and sintering can happen at lower temperatures.
Aggregated particles have the tendency to enlarge during sintering. Film sintering is then delayed and obtained films have smaller densities [168].

Screen printing inks are generally formulated with particles smaller than 10 $\mu$m in diameter, rotogravure and flexography inks particles are in the sub-micron scale and inkjet printing inks are generally formulated with nanoparticles (< 100 nm).

Particle size determines the ink flow properties. Small particles require more solvent for wetting which increases the viscosity of the suspension.
Small particles densification and sintering start at lower temperature than for larger ones because of their higher specific surface area.

### Tap density

Tap density is the apparent bulk density of material obtained when powders are tapped in order to decrease their volume. When a material tap density increases, densification rate is higher [145]. Tap density is related to particles specific surface area. High density particles have higher specific surface areas.

### 3.3.2 Sintering

After film deposition, levelling takes place which enhances film homogenisation. Then, printed patterns are dried: the organic vehicle is evaporated and/or burnt out. Afterwards, sintering is performed. During sintering, three main steps may happen:

- organic solvent combustion and burn out (low temperatures $< 300°C$),
- possibility of oxidation/reduction of the metallic elements,
- sintering of the conductive metallic elements and inorganic binder in order to ensure conductive film adhesion to the substrate.

The sintering process depends on temperature, process duration and atmosphere (inert, vacuum, oxygen, nitrogen) [145][167]. Sintering process starts by a solid-state diffusion of particles such as silver and finally a conductive network is formed after grain boundaries diffusion. Conductive particles sintering is dependent on vehicle combustion temperature, glass softening point and conductive particles melting temperature.

**Vehicle combustion temperature**

Particles should be sintered at higher temperature than that of organic materials combustion or evaporation. If not, metal particles will be trapped by organics and electrical properties will be deteriorated.
For example, *Lin and Wang, 1996* showed that after infra-red drying of silver particles dispersed in terpineol at 140°C, 13.7 Ohm/square sheet resistance was obtained. This value is very high compared to that of the same film sintered at 800°C, approximately 0.03 Ohm/square. This was explained by the fact that the vehicle, terpineol, has a higher boiling temperature (220°C) than the infra-red drying temperature (140°C). When sintering was performed at 800°C, terpineol burnt out and silver particles was free from organic materials [168].

**Glass softening point**

Glass softening point is an important characteristic. On one hand, glass should have high softening point in order to ensure all organic binder combustion before the starting of glass melting. If not, organic molecules released during the organic binder burn out will be trapped within the system. On the other hand, glass powders with lower melting points allow sintering at lower temperatures and minimize X-Y shrinkage and porosity. For this reason, it is important to use glasses with a softening point between organic binder combustion temperature and sintering temperature.

*Liu and Chung, 2004* demonstrated, that when softening point of glass frits was reached, the sintering process was almost finished. A constant resistivity was observed even after heating at temperatures higher than glass softening point (700°C). When sintering temperature was higher than 700°C, resistivity of a glass containing silver film was equal to $4.10^{-8}$ Ohm.m [167]. Besides, no more changes were observed on SEM (Scanning Electron Microscope) photographs of the films (figure 3.6).

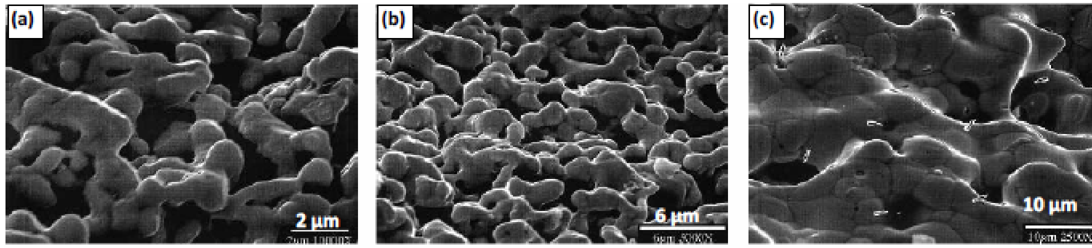


Figure 3.6: Surface morphology of a glass containing conductive paste after sintering at 400°C (a), 450°C( b) and 750°C (c) Reproduced from *Liu and Chung, 2004* [167]

In addition, *Lin and Wang, 1996* showed that when glass softening point was reached, the granular transformation of silver particles was activated, and thus particle size increased. Furthermore, when glass melting point is reached, the granular transformation phenomenon is accelerated [168][167].

### Conductive particle melting point

Conductive particles melting temperature is also an important factor on which depends the sintering process. Sintering temperature should be as close as possible to the melting temperature of conductive particle in order to provide particle adhesion to the substrate [165].
*Hitch, 1974* performed a peeling test on silver ink screen printed on alumina substrates and sintered at 150°C and 955°C. Films heated at lower temperature only withstand force equal to 35 g.mm$^{-1}$ before peeling and those heated at approximately 955°C withstand higher force, 50 mm.g$^{-1}$ [166].
Furthermore, *Liu and Chung, 2004* showed that the resistivity of a conductive silver film decreased from 16.10$^{-8}$ Ohm.m to 4.10$^{-8}$ Ohm.m, when sintering temperature increased from 400°C to 930°C [167].

## 3.4 Examples of conductive inks

Some examples of conductive inks are given in the table 3.4.

| Reference | Conductor | Vehicle Organic binder | Substrate | Printing process | Dimensions | Resistivity (Ohm.m) |
|---|---|---|---|---|---|---|
| *Lahti et al., 2001* [176] | Au | Organic binder and vehicle (commercial ink) | LTCC | SP | $w$ = 0.20 mm $th$ = 2.00 $\mu$m | $2.10^{-8}$ |
| *Molesa et al., 2003* [137] | Au | $\alpha$-terpineol | Polyester | IJP | $th$ = 1.00 $\mu$m | $23.10^{-9}$ |
| *Yin et al., 2008* [101] | Ag | Diethylene glycol, Water | Glass | SP | $w$ = 0.50 mm $th$ = 2.12 $\mu$m | $3.10^{-7}$ |
| *Pudas et al., 2005* [114] | Ag | Organic polymer | Paper | GP | $w$= 0.50 mm $th$ = 4.00 – 7.00 $\mu$m | $3.10^{-7}$ |
| *Jang et al., 2008* [24] | Ag | Ethylene glycol, diethylene glycol, water Glass frit | Glass | IJP | $w$ = 0.15 mm $th$ = 0.50 $\mu$m | $2.10^{-5}$ |
| *Jagtap et al., 2008* [177] | Ag | $\alpha$-terpineol Glass frit/oxides | LTCC | SP | $th$ = 15.00 $\mu$m | $3.10^{-5}$ |
| *Denneulin et al., 2009* [178] | SWCNT-PEG | PEDOT:PSS | PET | IJP | $th$ = 1.00 $\mu$m | $225.10^{-6}$ |
| *Voigt et al., 2010* [179] | Ag | $\alpha$-terpineol | Polyester | GP | $th$ = 0.12 $\mu$m | $5.10^{-8}$ |

Table 3.4: Conductive inks examples (SP - Screen printing; GP - Gravure Printing; IJP - Inkjet printing; $w$ - width; $th$ - thickness)

## 3.5 Printed conductive lines characteristics

Two variables allow the determination of the conductive potential of a material: the electrical resistivity and the sheet resistance.

### 3.5.1 Electrical resistivity

Electrical resistivity, $\rho$ is a measure of the capacity of a material to oppose the flow of electric current. A low resistivity indicates that a material allows the movement of electrical charge. It is also defined as the inverse of the material conductivity [180]. Electrical resistivity is given by equation 3.6:

$$\rho = \frac{1}{c} \tag{3.6}$$

Where:

- $\rho$ (Ohm.m) is the electrical resistivity,
- and $c$ (S.m$^{-1}$) is the conductivity.

In the case of cylindrical conductor (figure 3.7), resistance is defined by equation 3.7 [181].

$$R = \rho \cdot \frac{L}{A} \tag{3.7}$$

Where:

- $R$ (Ohm) is the resistance,
- $L$ (m) is the length,
- and $A$ (m$^2$) is the cross sectional area,

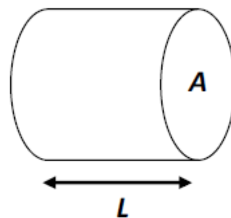


Figure 3.7: Resistivity geometry

The resistance $R$ is calculated by the Ohm's law:

$$U = R \cdot I \tag{3.8}$$

Where:

- $U$ (V) is the voltage,
- $I$ (A) is the current,
- and $R$ (Ohm) is the resistance.

### 3.5.2 Sheet resistance

The sheet resistance is a measure of the resistance of large width films with a uniform thickness. It is commonly used to characterise materials made by semiconductor doping, metal deposition, resistive paste printing, and glass coating. It depends on the number of squares present in the film (equation 3.9).

$$R_s = \frac{R}{x} \tag{3.9}$$

Where:

- $x$ is the number of squares,
- $R$ (Ohm) is the resistance,
- and $R_s$ (Ohm/square) is the sheet resistance [40].

When, a conductive film, deposited on insulator tape, have a large surface compared to its thickness, the $x$ value is estimated to 4.53 [182]. Thus, equation 3.9 can be written as:

$$R_s = R \cdot 4.53 \tag{3.10}$$

In a regular three-dimensional conductor and according to figure 3.8, the resistance can be written as:

$$R = \rho \cdot \frac{L}{A} = \rho \cdot \frac{L}{w.th} \tag{3.11}$$

Where:

- $R$ (Ohm) is the resistance,
- $\rho$ (Ohm.m) is the electrical resistivity,
- $L$ (m) is the length,
- $w$ (m) is the film width,
- and $th$ (m) is the thickness.

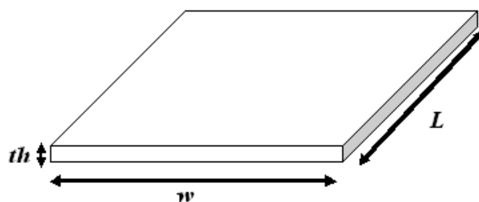


Figure 3.8: Sheet resistance geometry

The sheet resistance is the ratio of the resistivity to the thickness (equation 3.12):

$$R_s = \frac{\rho}{th} \tag{3.12}$$

Thus, according to previous equations, the sheet resistance can be given by equation 3.13:

$$R_s = R \cdot \frac{w}{L} \tag{3.13}$$

The resistance unit is Ohm. Ohms per square (Ohm/sq) is a common unit used for sheet resistance, it is equal to 1 Ohm [183].

### 3.5.3 The scattering hypothesis

Electrical properties of conductive inks are closely related to line and film properties such as porosity, width, thickness and roughness.
The scattering hypothesis is given by equation 3.14. This equation shows that film resistivity depends on grains shape, diameter and type, film surface characteristics and roughness.

$$\rho = \rho_0 + \rho_{GB} + \rho_{SS} + \rho_{SR} \tag{3.14}$$

Where:

- $\rho_0$ (Ohm.m) is the bulk material resistivity,
- $\rho_{GB}$ (Ohm.m) is the grain boundary scattering contribution,
- $\rho_{SS}$ (Ohm.m) is the surface contribution,
- and $\rho_{SR}$ (Ohm.m) is the roughness scattering contribution.

Equations 3.15 to 3.17 give scattering contribution of grain boundary, surface and roughness.

$$\rho_{GB} = \rho_0 \cdot \frac{K_1}{D} \tag{3.15}$$

$$\rho_{SS} = \rho_0 \cdot \frac{K_2}{th} \tag{3.16}$$

$$\rho_{SR} = \rho_0 \cdot \frac{K_2 \cdot B^2}{th^2} \tag{3.17}$$

Where:

- $D$ (m) is the mean crystallite extension,
- $th$ (m) is the film thickness,
- $K_1$ and $K_2$ are two constants proportional to the mean free path of electrons,
- and $B$ is a constant related to asperities [184].

**In this study, only silver conductive inks were printed onto ceramic tapes. Their geometrical and electrical properties were then investigated.**

*Other electrical and thermo-electrical properties of materials are given in Annexe 2.*

# Chapter 4

# Applications within the MULTILAYER project

## 4.1 Radio frequency applications - Microwave circuits

### 4.1.1 Overview

Development in radio frequency field have been progressing from the low frequency applications to the higher frequencies. Nowadays, researches in microwave region for GHz and THz applications are in expansion. The term microwave designates a broad range or radio-frequency spectrum comprising all frequencies greater than 1 GHz. Current and voltage were first considered as the basic entities for microwave transmission. Then, the concept of power transmission by electromagnetic waves through a dielectric material associated with the transmission line was established.
Microwave circuits are generally composed of four units :

- the source or the emitter producing the emission,
- the coupler or duplexer component transferring the emitted energy,
- the receiver generating the signal,
- the antenna conveying radio frequencies into radio frequency voltage.

Dielectric loss is one of the important factors to control in order to allow good response when processing is performed. Indeed, low dielectric loss are seek for high performance devices. At higher frequency, greater losses are registered. Loss is related to radiation or surface wave generation and to the active layer conduction [185][186].

### 4.1.2 Examples of applications

Microwave transmission circuits are used in military applications for radars manufacturing [187]. Navigation and communication applications, such as mobile networks can also be performed with microwave transmission circuits [188].

Printed methods are used in order to prepare microwave transmission circuits. Some examples are given in table 4.1.

| Reference | Application | Functional material | Substrate | Process | Properties |
|---|---|---|---|---|---|
| *Lahti and Lantto, 2001* [176] | RF band-pass filters | Ag | LTCC | Gravure Offset Printing | Dielectric loss = 0.7 $dB.cm^{-1}$ at 1.2 GHz and 7.6 $dB.cm^{-1}$ at 1.8 GHz $\rho = 2.4.10^{-8}$ Ohm.m |
| *Chai et al., 2001* [189] | Resonators | Ag | Alumina | Screen printing | Dielectric loss < 0.12 $dB.cm^{-1}$ at 20 GHz |
| *Shaker et al., 2011* [190] | Ultra wide band antennas | Ag | Paper | Inkjet | $c = 0.9.10^7$ - $1.1.10^7$ $S.m^{-1}$ |

Table 4.1: Some examples of printed microwave applications *Electrical properties of materials are reported in Annexe 2*

# 4.2 Thermoelectric modules

## 4.2.1 Overview

Bases of thermoelectricity have been studied and investigated since the 1820's when the Seebeck, Peltier and Kevin's relations where established. Voltaic thermo cells and thermometry fundamentals were developed at the same time. However, particularly due to environmental reasons concerning refrigerant fluids and cooling electronics, new generation of thermoelectric modules is in expansion phase since the 1990's [191].
Thermoelectric devices combine electrical and thermal currents. They allow power generation from a difference of temperature.
p-type semiconductors are positively doped in order to create “holes” in the material. These holes are able to accept electrons from neighbouring atoms. n-type semiconductors are negatively doped, thus creating an excess of negative charges. A thermomodule is a unit where semiconductors elements (p and n types) are connected in series on ceramic substrates.
When applying current, heat is absorbed from a side and pumped through the other side. Thermoelectric module size generally varies from 10 to 40 $mm^2$ and its thickness from 3 to 6 mm. Figure 4.1 shows a thermoelectric module.

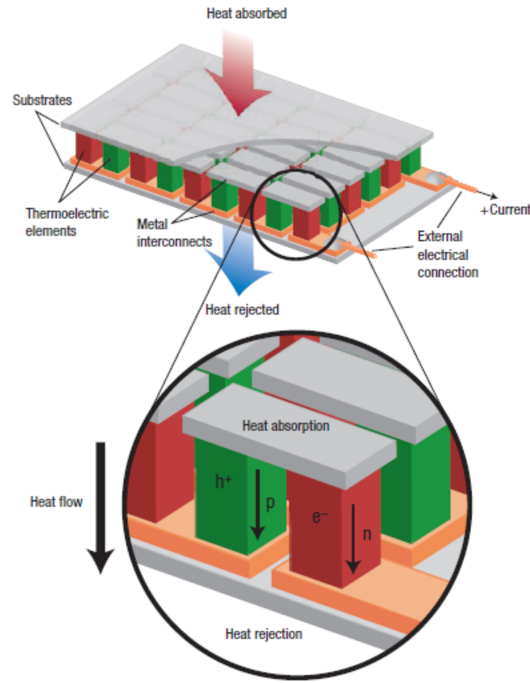


Figure 4.1: Thermoelectric module [192]

### 4.2.2 Examples of applications

Thermo-modules are widely used in cooling and heating domains. They can be found in optical systems requiring temperature control [193]. They are also used for generators manufacturing for cars engines and heat waste recovery in automotive domain [194][195]. Thermoelectrics can be prepared by printing methods. Some examples are shown on table 4.2.

| Reference | Application | Functional material | Substrate | Process | Seebeck coefficient |
|---|---|---|---|---|---|
| *Shin et al., 2003* [196] | $H_2$ sensor | Lithium and sodium doped nickel oxide | Alumina | Screen printing | |
| *Weber et al., 2006* [197] | Power generator | Antimony or Bismuth | Polyimide | Screen printing | 97 $\mu V.K^{-1}$ |
| *Navone et al., 2008* [198] | Thermo modules | $(BiSb)_2(TeSe)_3$ | Polyethylene naphtalate | Screen printing | 160 $\mu V.K^{-1}$ |

Table 4.2: Some examples of printed thermoelectric modules or films - *Thermoelectric materials properties are reported in Annexe 2*

## 4.3 Automotive applications

### 4.3.1 Overview

The automotive industry includes development, design, manufacturing and selling of automobiles parts. Many research studies are performed in this domain in order to develop new components and vehicles achieving relatively low cost and environmental goals. Thus, research works allowing production of flexible, low weight sensors and fuel cells are in expansion. Interest is also focused on hybrid electric low carbon dioxide emission vehicles [199].

### 4.3.2 Examples of applications

Printing methods are used in automotive applications such as interconnections establishment [200], sensors for gas emission control [201], lighting emitting assemblies [202], etc. Other examples are shown on table 4.3.

| Reference | Application | Functional material | Substrate | Process |
|---|---|---|---|---|
| *Kloeser et al., 1998* [203] | Solder and interconnections in flip chips systems | Ni/Au AuSn | Ceramic, FR-4 and wafers | Screen printing |
| *Billi et al., 2002* [204] | CO and $NO_2$ automotive sensors | Au/Pt | $\alpha$-Alumina | Screen printing |
| *Neri et al., 2008* [205] | | $In_2O_3$ - $SnO_2$ | Alumina | Screen printing |

Table 4.3: Some examples of printed electronics for automotive applications

## 4.4 Medical applications

### 4.4.1 Overview

Sensors and microfluidic systems involve printing methods in order to achieve devices used in medical domains. They are employed in different fields such as microbiology, analytical chemistry, pharmaceutical development and chemical synthesis systems.
Biomedical sensors are devices receiving chemical or biochemical signals. These signals are usually substances delivered analysis. Sensor is then able to convert received information into analytical quantitative answer [206]. Generally electrochemical, biochemical and chemical sensors are used for medical applications.
Printing methods are employed to prepare sensors electrodes.

A microfluidic system is a system able to handle small liquid volumes, typically in microlitre and picolitre ranges. Fluids in microsystems have generally a very low flow rate

[207]. Printing methods are used to seal and bond channels in microfluidic systems. They can be also used to fill via holes in microfluidic systems.

### 4.4.2 Examples of applications

Some examples of medical devices prepared by printing methods are shown on table 4.4.

| Reference | Application | Functional material | Substrate | Process | Properties |
|---|---|---|---|---|---|
| *Yussuf et al., 2007* [110] | Sealing of polymeric microfluidic devices | PANI | PMMA or PC | Screen printing | Bond strength = 1.92 N (PMMA) and 1.43 N (PC) |
| *Gill et al., 2009* [208] | pH sensors | Au (IDE) and PANI | Alumina | Screen printing | Response time = 1 - 2 minutes |
| *Wang et al., 2009* [209] | Glucose biosensors | CB electrode and GO | Polyester | Screen printing (CB) Inkjet (GO) | |

Table 4.4: Some examples of medical devices prepared by printing methods (PANI for Polyaniline, PMMA for PolyMethyl MethAcrylate, PC for PolyCarbonate, IDE for Inter Digitated Electrode CB for Carbon Black and GO for Glucose Oxidise)

# Conclusion

Printed electronics is an innovative domain allowing deposition of conductive, resistive, dielectric, thermoelectric materials by relatively simple, non expensive, automatically controlled and high precision methods.

Different types of substrates were already investigated in printed electronic domain. HTCC such as alumina, LTCC, silicon, glass and polymer substrates are employed as carrier for functional printed patterns. Application domains are dependent on mechanical, chemical, dielectric and thermal properties of substrates.

In order to prepare printed electronic devices, several printing processes such as screen printing, inkjet, flexography and rotogravure techniques are investigated. They allow narrow and homogeneous lines patterning of different materials with various properties.

Functional materials such as conductive inks are also studied. Thus, inks based on metal nano- and micro-particles (silver, gold, etc.), non metallic particles such as carbon and conductive polymers (polypyrrole, polyaniline, etc.) are considered as appropriate candidates for electronic applications.

Printing techniques are already used in automotive, medical and biological fields, for RFID tags, lighting systems patterning, inductors and resistors fabrication. Moreover, radio frequency transmission lines and thermoelectric coolers and heaters can also be prepared by printing techniques.

The main objective of the present research is to adapt and optimise printing techniques to microelectronic domain in order to prepare performing devices less expensive, easily manufactured and mass produced.

The literature review revealed that:

- small particles ($< 1$ $\mu$m) thermal behaviour is different from the bulk material. Particles thermal stability decreases when their size decreases. Thus, in order to allow sintering at temperatures higher than 700°C particles larger than 1 $\mu$m should be used.
- solvents of metallic screen printing pastes are based on low evaporation rate solvents such as terpineol and toluene known for their toxicity and their irritant character. The challenge of this study is to formulate water-based environmentally friendly silver pastes with relatively low evaporation rate adapted for screen printing.
- flexography of conductive metallic inks on ceramic green tapes was not tested yet.

The literature review allowed:

- to select silver conductive material due to its high conductivity ($6.10^7$ $S.m^{-1}$), its thermal and chemical stability compared to copper and nickel and its relatively low cost compared to gold,
- to choose conductive particles with diameters larger than 1 $\mu$m, when possible,
- to print alumina tapes after sintering: alumina is sintered at temperatures higher than 1600°C. Silver is not able to withstand such high temperatures,
- to print Low Temperature Co-fired Ceramic (LTCC) tapes at green stage. LTCC are sintered at relatively low temperatures ($< 900$°C) compared to alumina. These temperatures can be withstood by silver particles.

All these research fields are investigated and developed in the following pages.

# Part II

# Experimental

# Introduction

Several steps were applied to reach main project objectives and overcome the scientific challenges, i.e. deposit silver lines onto ceramic tapes and reach high conductivities even at temperatures higher than 800°C.
In this part of the work, steps will be detailed and results will be exposed and discussed.
First of all substrates surface properties were studied, already sintered alumina tapes and three different types of LTCC (Low Temperature Co-fired Ceramics) tapes were selected to perform printing tests.
After that, inks were optimised and adapted for printing processes. Silver was picked up as conductive material due to its low electrical resistivity ($\simeq$ 16 nOhm.m) and its chemical and thermal stability.
Then, four printing techniques were tested. Flexography and rotogravure were only performed on green LTCC tapes. Inkjet printing was used to print sintered alumina tapes. Screen printing was tested on both sintered alumina and green LTCC tapes.
Printed lines were observed and characterised to study printing properties, i.e. thickness, width, roughness and uniformity.
Then, sintering was performed. Different sintering profiles were applied in order to determine the best sintering conditions adapted for tapes and inks.
Finally, characterisation of sintered patterns was realised, i.e. geometrical and electrical properties (see figure i).

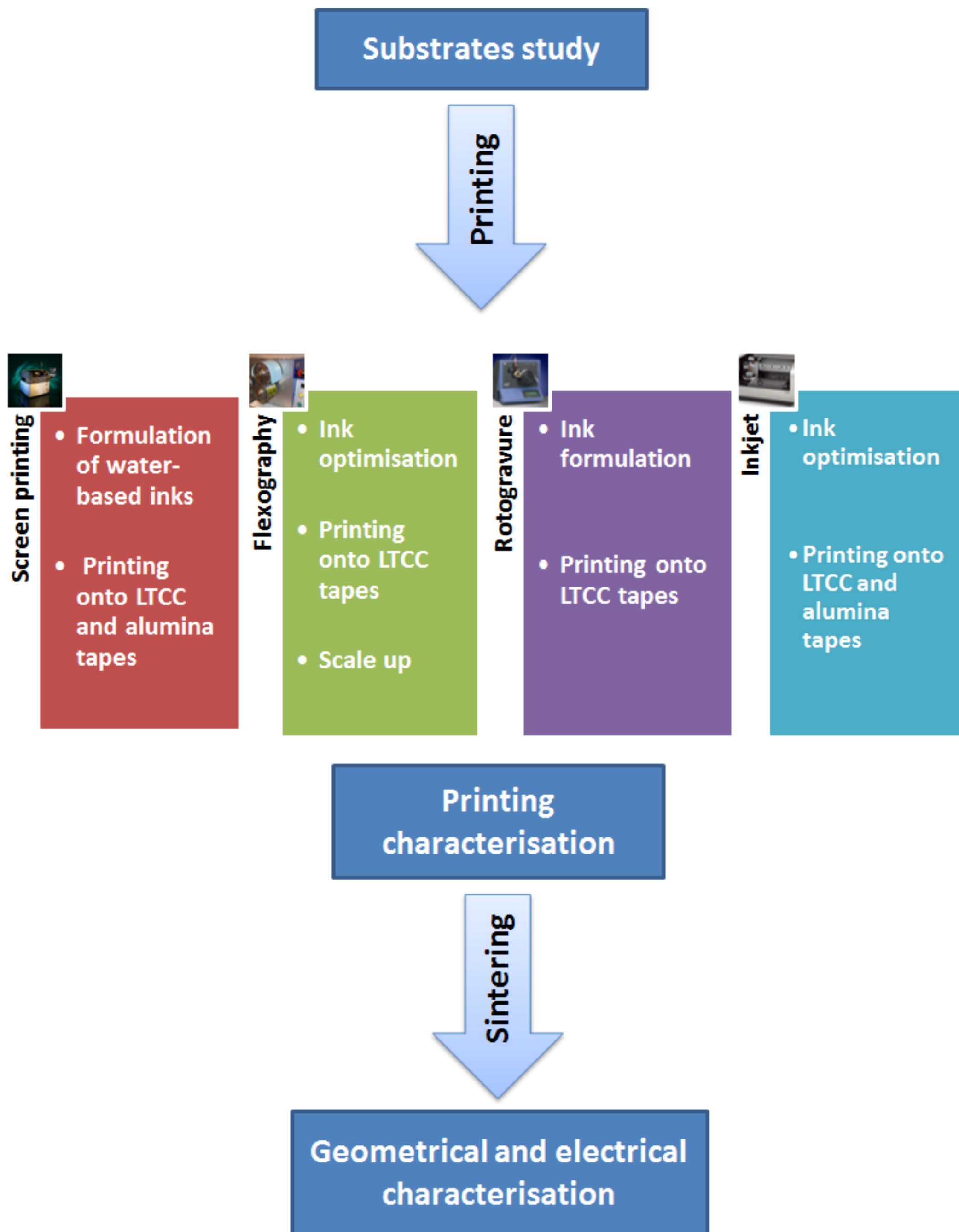


Figure i: Outline of experimental work

# Chapter 5

# Substrates

## 5.1 Substrates description and composition

Different types of substrates were tested within the MULTILAYER project (alumina, zirconia, silica, glass and low temperature co-fired ceramics (LTCC)). In this manuscript, only properties of LTCC and alumina will be reported. These tapes were selected to perform printing due to their smoothness and homogeneous surfaces.

Alumina tapes were provided by Swerea IVF - Sweden (SIVF). Tapes were based on pure alumina ($Al_2O_3$) powder dispersed in 25% per volume of aqueous suspension of styrene acrylic polymer (M400SAP). These tapes are considered as thin film HTCC (High Temperature Co-fired Ceramics). With 400 $\mu$m thickness, these tapes were sintered at 1650°C and characterised before and after sintering.

LTCC (Low Temperature Co-fired Ceramics) substrates (SIVF-LTCC) were manufactured by Swerea IVF with a mixture of alumina and other mineral oxides usually used used for commercial tapes manufacturing. These tapes were water-based and can be sintered at lower temperatures (800 - 900°C).

LTCC commercial tapes were provided by Micro Systems Engineering (MSE) - Germany. DP951 (DuPont - USA) and CT700 (Heraeus - Germany) were sent to the LGP2 in order tp perform their characterisation. These tapes were also sintered at temperatures ranging from 800 to 900°C.

## 5.2 Powders

Only alumina powders used to prepare the HTCC tape were investigated. Powders used to prepare the LTCC were not provided by the partners. A Field Emission Gun coupled to Sanning Electron Microscope (FEG – SEM) apparatus, Zeiss Ultra Column 55 gemini, was used to perform alumina powders micrographs before tape casting and determine particle sizes. The FEG - SEM allows resolutions as low as 0.5 nm. A statistical study, based on 100 to 200 measurements made on microscopic images, allowed the definition of powders particles sizes. Alumina powders FEG - SEM and micrograph is shown on figure 5.1.
Micrograph shows that Swerea IVF alumina powders have slightly a spherical shape. 63% of particles had diameters varying from 0.2 to 0.3 $\mu$m.

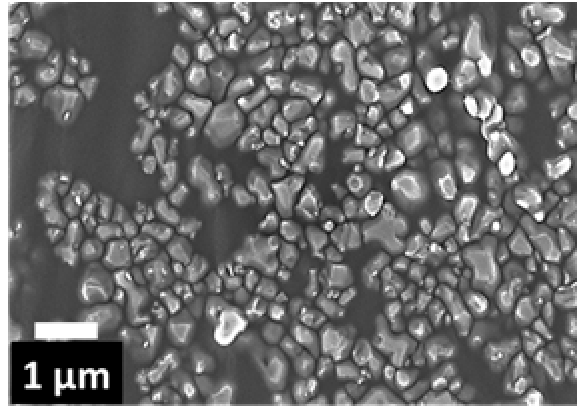


Figure 5.1: Alumina powders observed by FEG - SEM microscope

## 5.3 Energy Dispersive X-ray analysis (EDS) and tapes main components

In order to determine substrates main elements an elementary EDS analysis was performed.

### 5.3.1 High temperature co-fired ceramics

The EDS analysis of HTCC alumina tape is shown on figure 5.2. This tape was composed of pure $Al_2O_3$ powders, aluminium (Al) and oxygen (O) peaks can be observed on the EDS analysis graph. Small quantity of carbon (C) was detected. It was attributed to organic polymer.

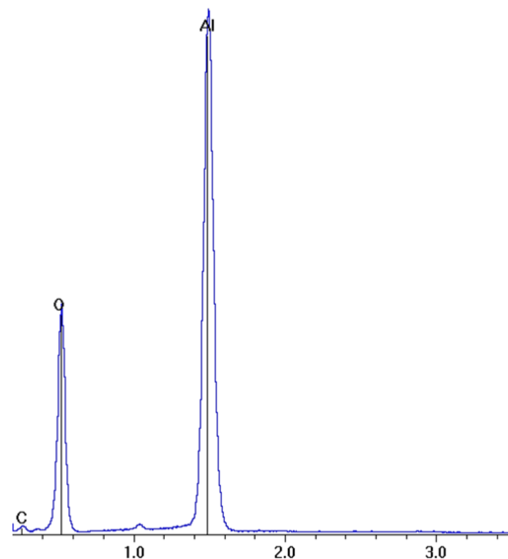


Figure 5.2: EDS analysis of alumina HTCC substrate

### 5.3.2 Low temperature co-fired ceramics

X analyses of LTCC tapes are shown on figure 5.3. CT700, DP951 and SIVF-LTCC were composed of a mixture of different mineral powders such as Al, Si, Sr, Mg, Pb, Zn, Co, Ba, Ca Na. Oxygen and carbon were also detected. These elements demonstrated the presence of mineral oxides. *Jones et al., 2000* demonstrated that CT700 tape contains $\alpha$-$Al_2O_3$, $BaAl_2Si_2O_8$, $SiO_2$ and (Mg, Ca)$SiO_3$. They also showed that DP951 tape contains $\alpha$-$Al_2O_3$ and Ca(Si,Al)$_4O_8$ [210]. Mixture of these inorganic materials are added as sintering aids in order to reduce ceramics sintering temperatures (see paragraphs 1.1.1 and 1.2.3).

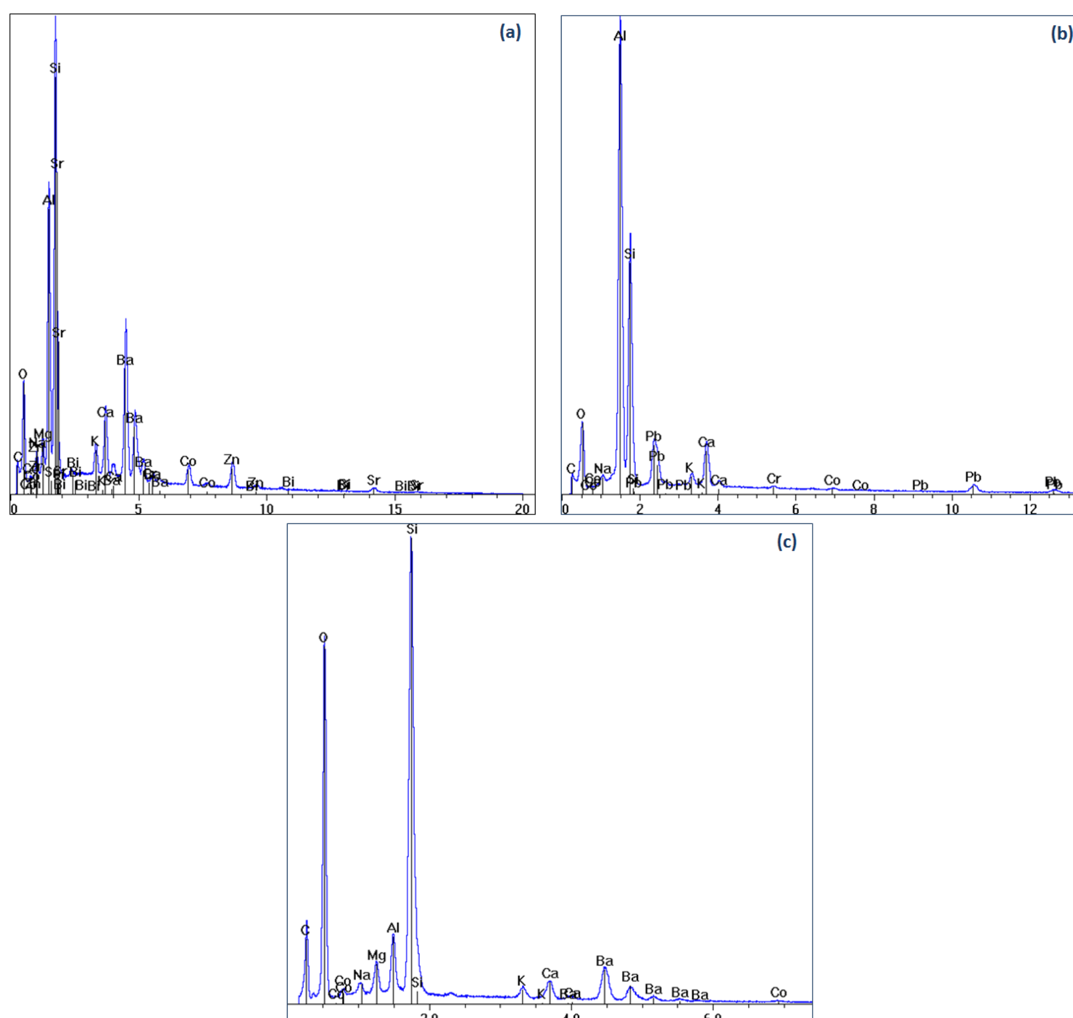


Figure 5.3: X analyses of LTCC and glass tapes: (a) CT700, (b) DP951, (c) LTCC -SIVF

## 5.4 Tapes - SEM, pore and particle sizes

Surface and cross section microstructures and porosities were studied by a Scanning Electron Microscope (SEM) Quanta 200. Surface images allowed to measure the pore and particle sizes. Cross section images enabled determination of substrate thickness. Pore and particle size measurements were realised on a 1.5 $\mu m^2$ samples area.
It is important to determine surface pore size in order to know which size of particle can be suitable for formulating printing inks. Indeed, conductivities are enhanced when particles stay at the surface and do not go into the substrate surface pores.

### 5.4.1 Green tapes

#### Thin HTCC tapes - Swerea IVF

**SEM micrographs** Figure 5.4 shows surface and cross-section SEM micrographs of green alumina. Particles used in this tape formulation were homogeneous. Surface pores were smaller than cross section one.

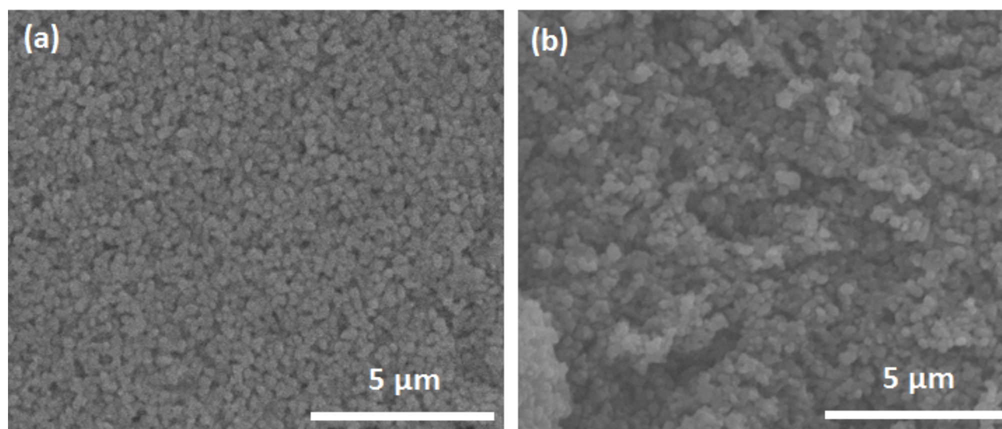


Figure 5.4: ESEM surface (a) and cross section (b) of green alumina tape (Swerea IVF)

**Surface pore and particle size distributions** Small pores were observed at the tapes surface, especially pores which diameters varied from 0.2 to 0.4 $\mu$m. Only 3% of surface pores were larger than 0.8 $\mu$m. Inks suitable to these tapes should contain particles with a diameter larger than 0.8 $\mu$m. Consequently, they will be blocked at the surface of the substrate and do not go in the pores. Surface pore size distribution is shown on figure 5.5.

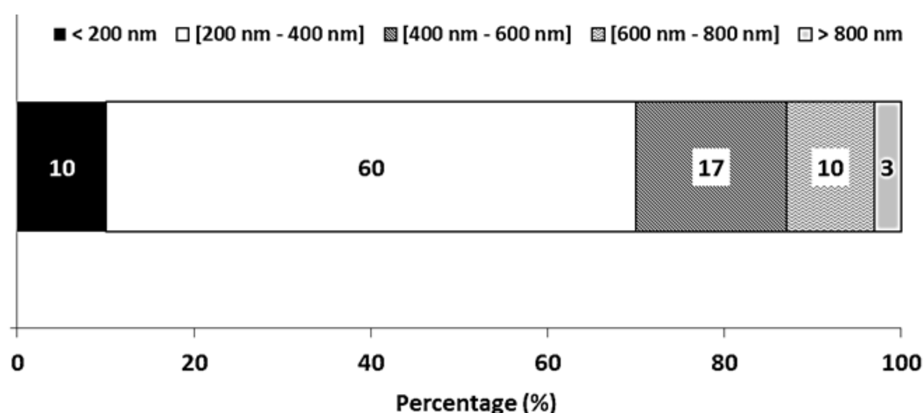


Figure 5.5: Pore size distribution of alumina green tape (Swerea IVF) - Surface analysis

Particle size was homogeneous and few aggregates were observed. 68% of particles had a diameter mainly ranging from 0.2 to 0.4 $\mu$m. Particle size distribution is shown on figure 5.6.

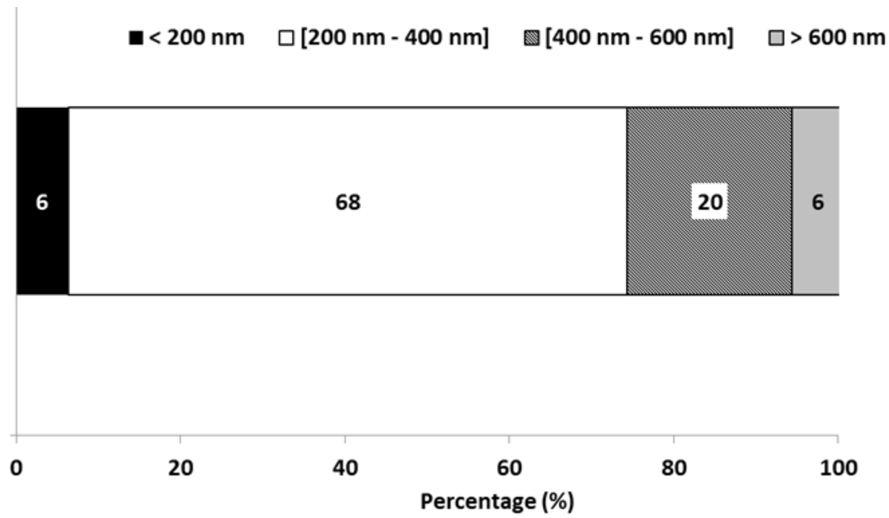


Figure 5.6: Particle and aggregate size distribution of M400SAP alumina green tape (Swerea IVF)

### LTCC films - MSE and Swerea IVF

**SEM micrographs** SEM surfaces LTCC tapes are shown on figure 5.7. Particle size distribution was not homogeneous. This was attributed to the mixture of powders used to prepare the slurry before tape casting.

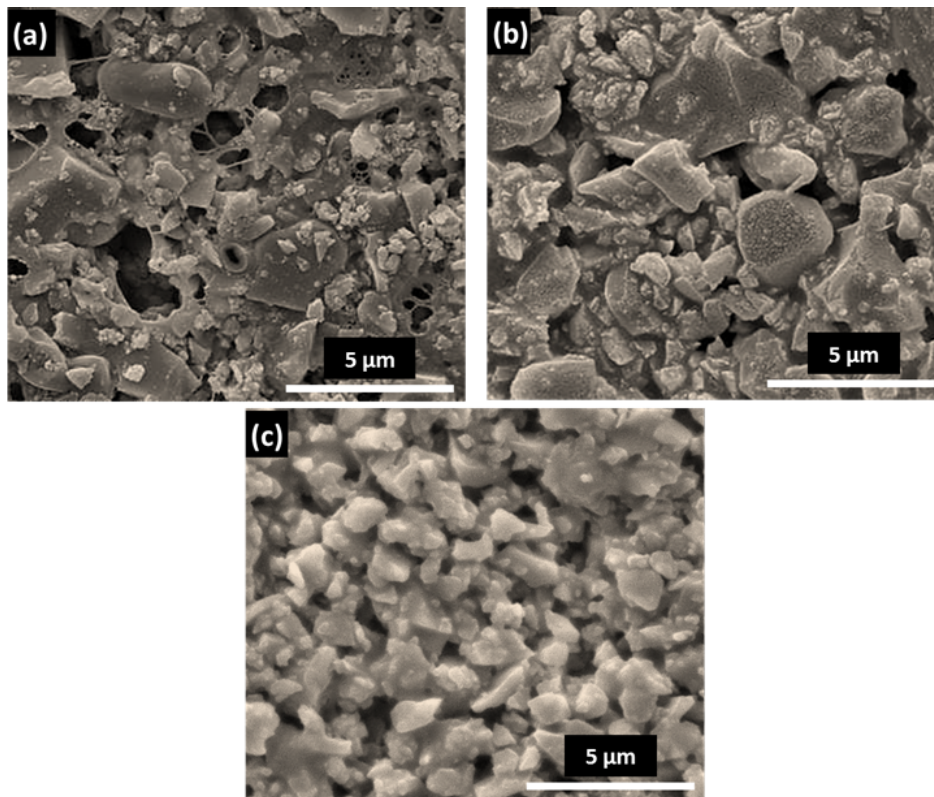


Figure 5.7: SEM surface of commercial green LTCC tapes: (a) CT700, (b) DP951, (c) LTCC-SIVF

More than 50% of measured LTCC pores ranged from 0.5 to 1.5 $\mu$m. Pore diameters

varied from 0.3 $\mu$m to 7.0 $\mu$m maximum (figure 5.8).

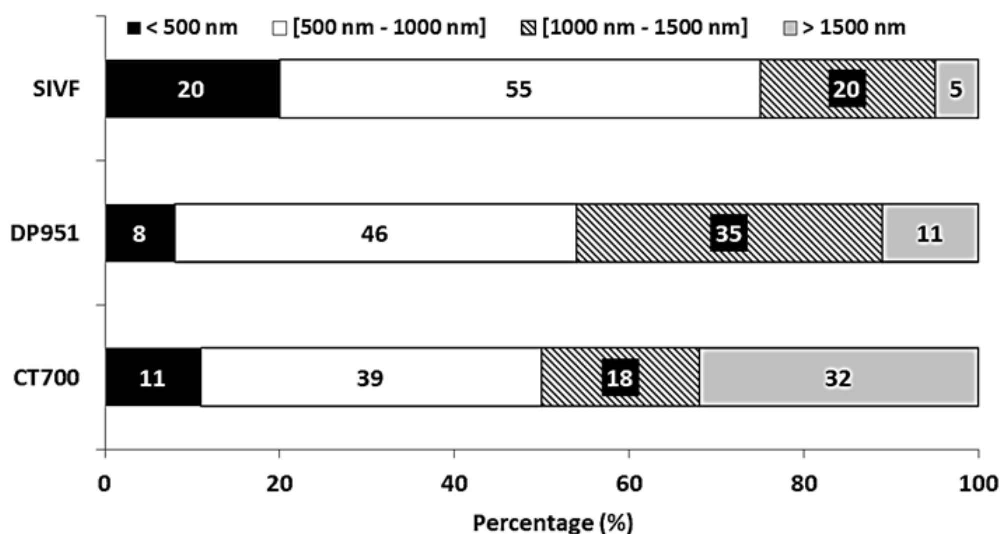


Figure 5.8: Pore size distribution of LTCC tapes - Surface analysis

To print these tapes, inks containing particles with a diameter larger than 1 $\mu$m are preferred. Screen printing process is more appropriate than other techniques to print these tapes, because it allows using relatively large particle size with a diameter larger than 1 $\mu$m without blocking the screen mesh. Engraved cylinder or anilox with cells depth larger than 30 $\mu$m should be manufactured in order to allow rotogravure and flexography printing onto these tapes. If not, small particles ($< 1$ $\mu$m) will diffuse through the substrate and many layers should be performed in order to achieve a convenient thickness. Figure 5.9 shows a representation of small particles diffusion into rough tapes pores.

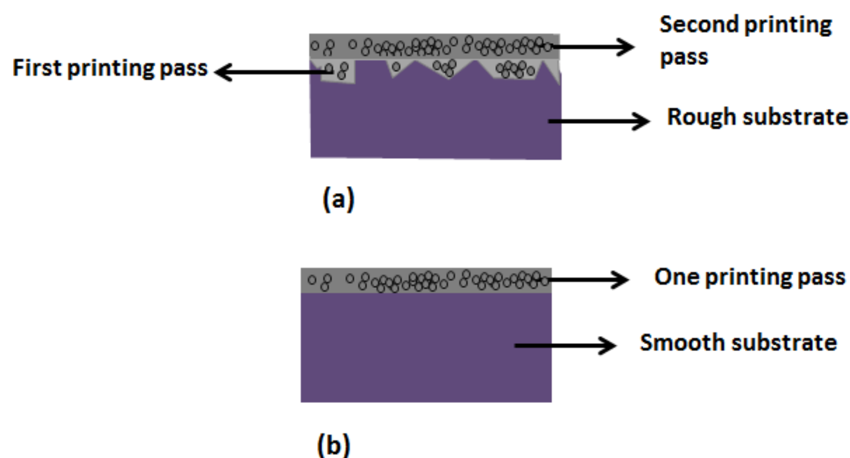


Figure 5.9: Scheme representation of small particles deposit onto substrates surface pores

**Particle size distribution** LTCC tapes powders were not provided by the manufacturer. For this reason, only, particle and aggregates size study was realised on the green substrates. Results are shown on figure 5.10.
63% of CT700 particles were smaller than 1 $\mu$m. DP951 particles were larger, 85% of particle diameters were larger than 1 $\mu$m and reached 6 $\mu$m. 86% of particles were smaller than 2 $\mu$m.

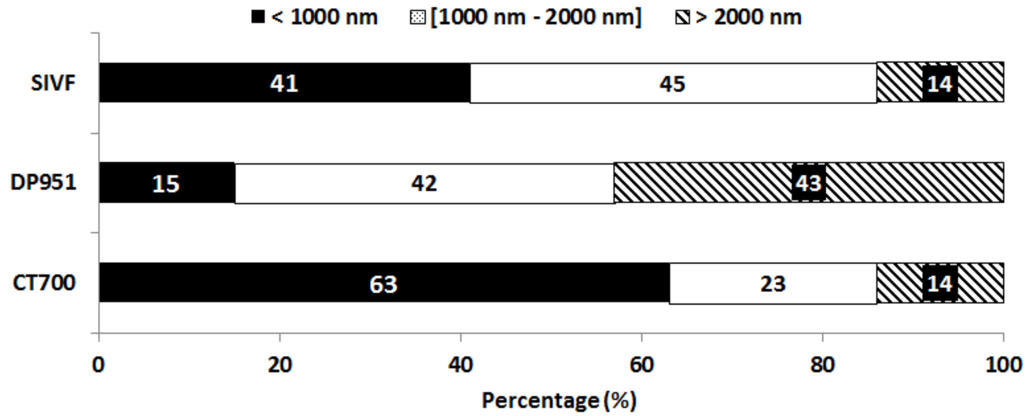


Figure 5.10: Particle and agglomeration size distribution of LTCC tapes

Particle size affects substrates surface topography. When smaller particles are used to prepare the slurry, smoother tapes can be cast.

**Summary of green tapes surface pore size**

Table 5.1 summarises surface pore sizes of studied green tapes and gives an indication about the particle size to use for ink formulation.

| | Surface pore size | Appropriate particle size |
|---|---|---|
| Thin film - Alumina (HTCC) | 60% $\rightarrow$ 0.2 - 0.4 $\mu$m | $\sim$ 0.8 $\mu$m |
| Thin film LTCC | Mainly 0.5 to 1.5 $\mu$m | $\geq$ 1 $\mu$m |

Table 5.1: Summary of substrates pore size and appropriate ink particles

### 5.4.2 Microstructure evolution after sintering

ESEM micrographs of sintered substrates surfaces are shown on figure 5.11.

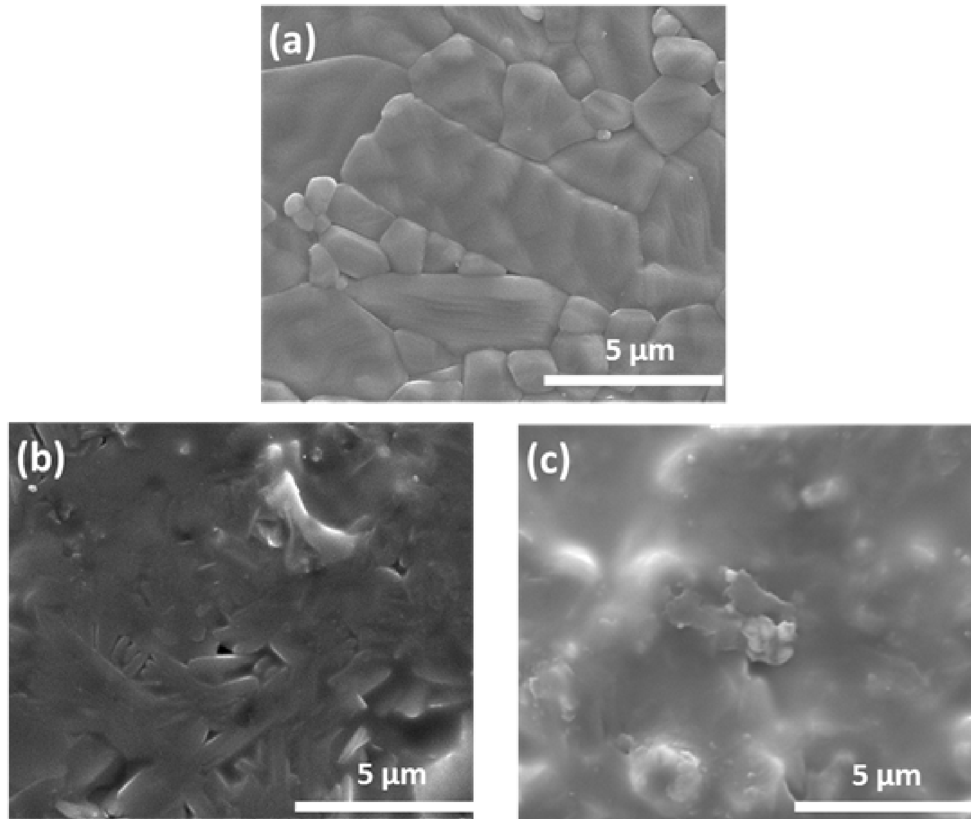


Figure 5.11: ESEM micrographs of some sintered tapes: (a) Alumina SIVF - , (b) CT700, (c) DP951

New LTCC tapes manufactured by Swerea IVF were not sent by partners at sintered stage and thus, were not tested. During sintering, particles melted and at the end of the sintering process a compact particle network was formed (see paragraph 1.2). Porosity decreased after sintering. Alumina tapes manufactured by Swerea IVF and DP951 LTCC substrates had no more pores after sintering. Some pores were observed on CT700 surface. A threshold analyse followed by binarisation was performed on CT700 surface images. 5% of porosity was calculated after this analyse.

A study about particle sizes measurement before and after sintering was also carried out. Figure 5.12 shows the difference between alumina powder sizes before casting and sintered tape particle sizes after sintering.

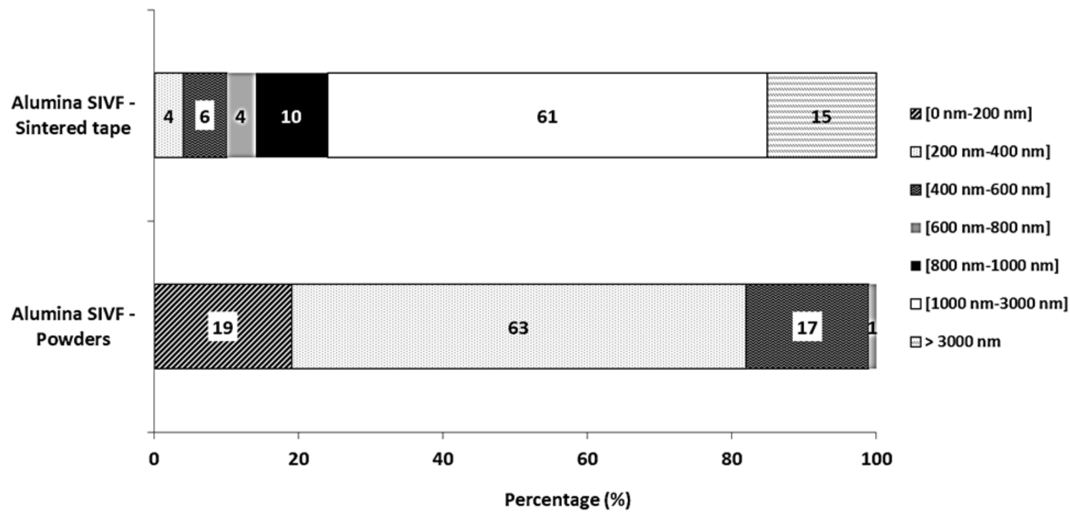


Figure 5.12: Powder size versus sintered tapes particle size distribution

After sintering, larger particles were observed. Indeed, during sintering particles melted together and formed a compact network. LTCC thin tapes particles melted completely and were not separated by boundaries after sintering. Regarding alumina particles (Swerea IVF), about 60% of powders had a diameter varying from 0.2 $\mu$m to 0.4 $\mu$m, before sintering. After sintering, 60% of the particles diameters increased and ranged from 1.0 $\mu$m to 3.0 $\mu$m.

## 5.5 Other properties

### 5.5.1 Thickness

Cross-section micrographs allowed comparison of substrates thicknesses before and after sintering (figure 5.13).

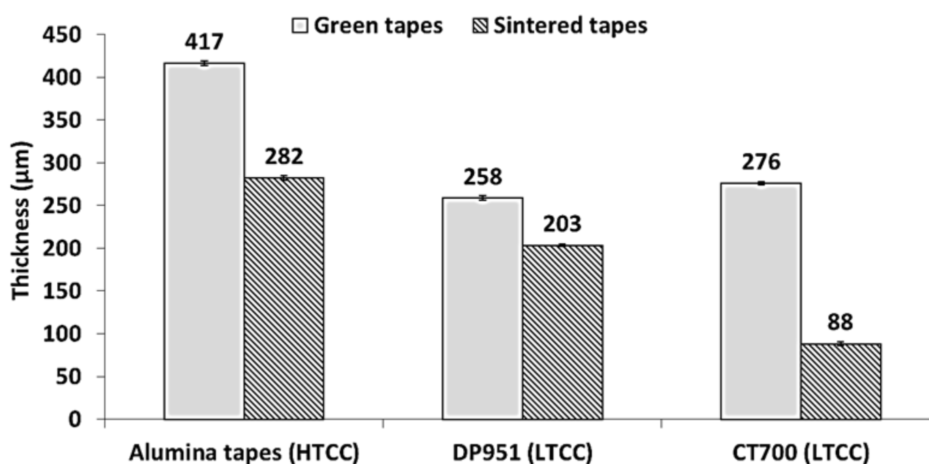


Figure 5.13: Thickness variation before and after sintering

During sintering, organic binder burnt out and particles melted and became closer to each other. A compact network was formed and thickness decreased. Depending on substrate,

after sintering, z shrinkage may be higher than 50%. For example, CT700 thickness was decreased by 68%.

### 5.5.2 Roughness

Substrate roughness was measured by an Alicona infinite focus 3D profilometer. Image 3D reconstruction was realised with x100 magnification allowing 10 nm resolution. Tests were performed according to ISO 4287 and ISO 4288 standards on a minimum 4 mm length profile. Profile roughness was calculated according to equation 5.1.

$$R_a = \frac{1}{l} \cdot \int_0^l |z(x)| dx \tag{5.1}$$

Where:

- $R_a$ is the profile roughness (m),
- $l$ is the base line length (m),
- and $z$ is the distance fixed for 3D reconstruction [211].

Surface roughness determination before printing allows choosing the appropriate particle size for ink formulation. Indeed, all substrates roughness and non homogeneities should be covered by the ink. Thus, if substrate is too rough, many printing layers will be required to obtain connections between silver or other active particles all over the printed film on the substrate surface (see figure 5.9).

#### HTCC - Swerea IVF

Surface topography and roughness, ($R_a$, nm), results of Swerea IVF alumina tapes are shown on figures 5.14.

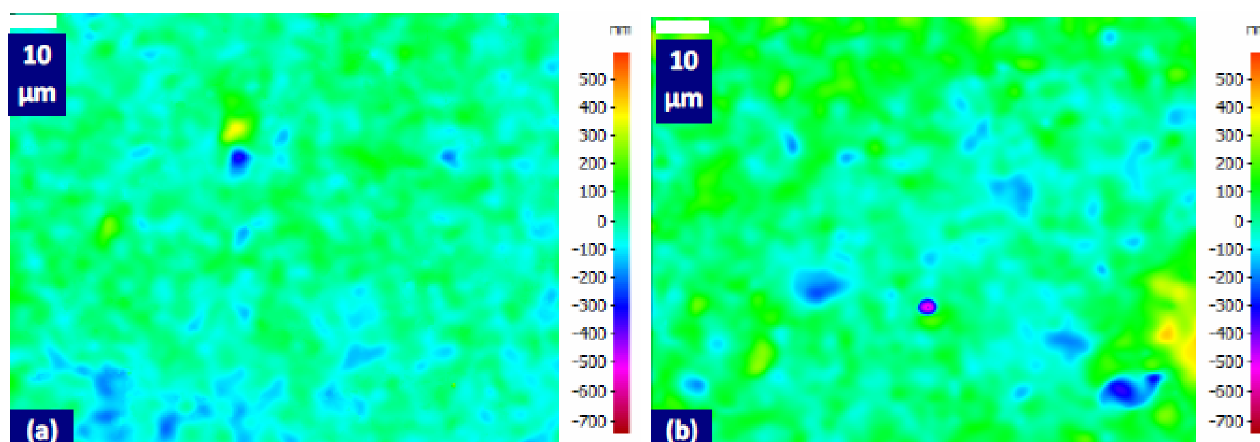


Figure 5.14: Surface topography of Swerea IVF thin HTCC film tape before (a) and after (b) sintering

Before sintering, alumina tape had 36 ± 2 nm (0.04 $\mu$m) surface roughness. After sintering, $R_a$ increases to 55 ± 4 nm (0.06 $\mu$m). Substrates roughness is dependent on alumina powders size. To prepare the slurry from which these ceramics were cast, 0.2 to 0.3 $\mu$m

mean diameter particles were used. This explain the smooth surfaces obtained after casting.
For example, *Hu et al., 2004* showed that when 0.05 to 0.10 $\mu$m barium strontium titanate (BST) particles were used to cast a tape, a 0.15 $\mu$m roughness was measured on the surface. And, when particles with 0.60 to 1.50 $\mu$m diameters were used, a tape with 0.20 $\mu$m roughness was obtained [212].
In addition, *Vozdecky and Roosen, 2010* prepared alumina tapes with nano-sized powders ($\sim$ 0.06 $\mu$m) to get smooth tape surface ($R_a \sim 0.17$ $\mu$m) compared to commercial tapes ($R_a \sim 0.60$ $\mu$m) [213].
Ink particle size should be larger than 0.06 $\mu$m; otherwise more than one layer should be printed in order to cover the substrate surface.
Roughness increase after sintering was attributed to boundaries formation between melted alumina particles.

**LTCC - MSE and Swerea IVF**

Figure 5.15 shows LTCC tapes surface roughness.

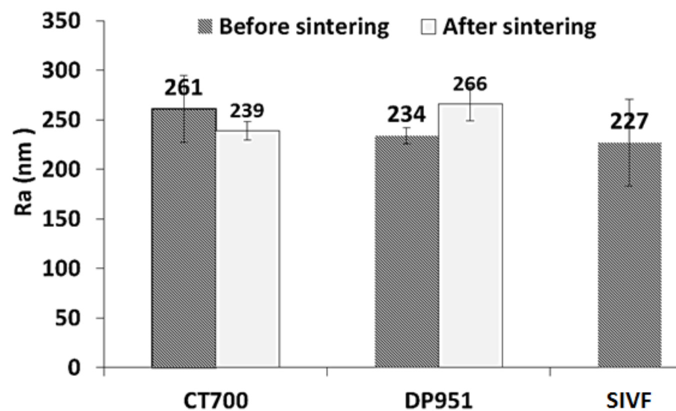


Figure 5.15: LTCC tapes roughness

Green new manufactured tapes and commercial ones roughness values were in the same order of magnitude. CT700 roughness decreased from 0.26 $\mu$m to 0.24 $\mu$m, after sintering. DP951 roughness increased from 0.23 $\mu$m to 0.27 $\mu$m. LTCC substrates could be printed with ink containing particles of 0.5 to 2.0 $\mu$m diameter. Figure 5.16 shows LTCC tapes surface topography.

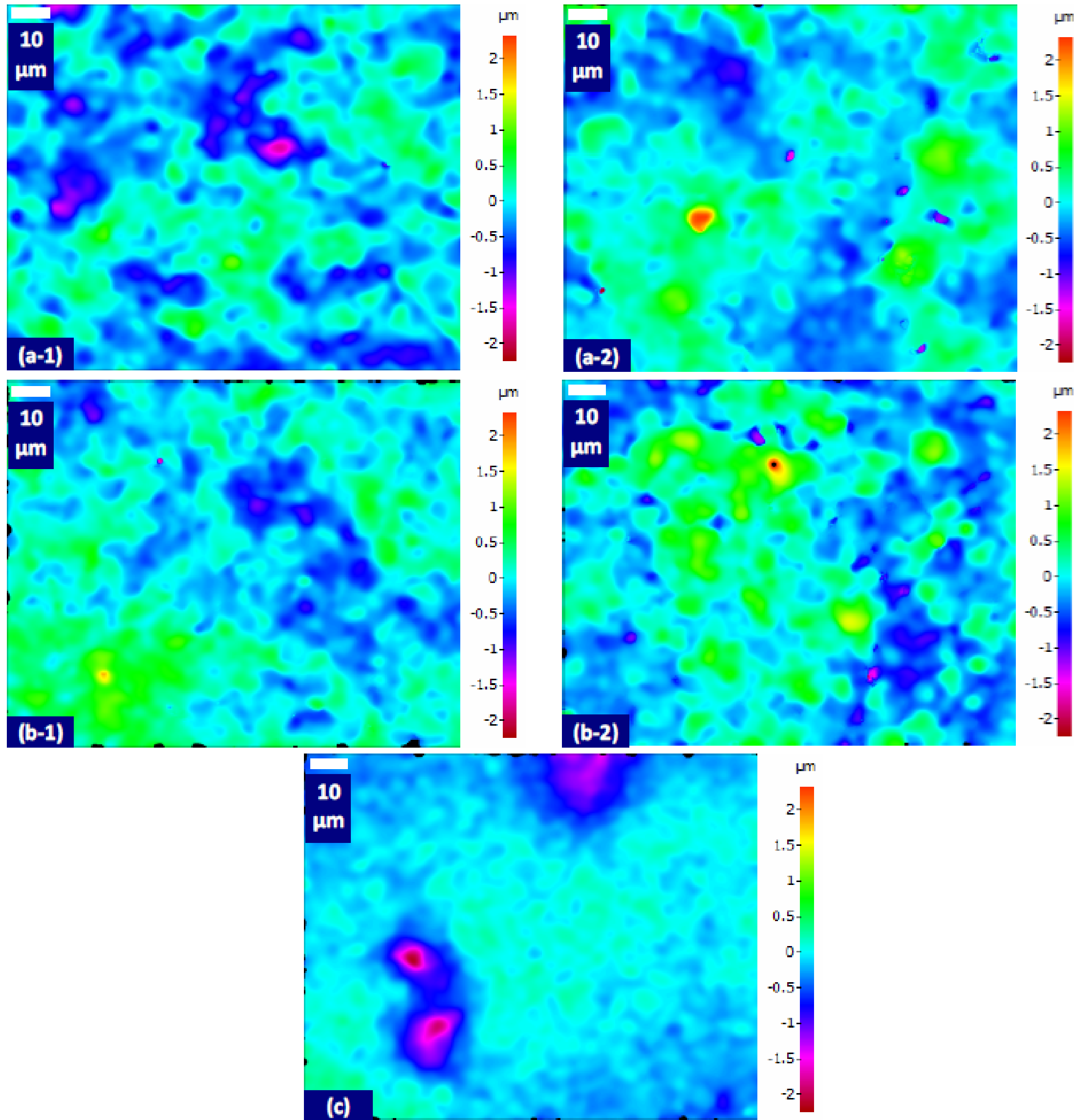


Figure 5.16: Topography of LTCC substrates: CT700 before (a-1) and after (a-2) sintering; DP951 before (b-1) and after (b-2) sintering and green Swerea IVF LTCC tape (c)

### 5.5.3 Surface energy

Study of wettability of substrates by various liquids is important for many industrial processes such as printing. It helps determining the surface energy of the substrate and then the appropriate solvent to be used for the ink formulation.
Substrate surface energy should be higher than that of the solvent to provide a good wetting of the substrate. Dispersive and polar components of surface energy were calculated according to OWRK method. To this aim, a contact angle Dataphysics system was used in sessile drop mode.
For polar liquids Owens, Wendt, Rabel and Kaelble (*Owens and Wendt, 1969*) assumed that the surface energy is composed of polar and dispersive fractions [214].
Contact angles between substrates and minimum five solvents were measured in order to calculate the surface energies of the substrates. Solvents were all purchased from Fischer Scientific and their surface tensions (total ($\gamma_l$), dispersive ($\gamma_l^d$) and polar ($\gamma_l^p$)) are given

in table 5.2.

| Solvent | $\gamma_l$ (mN.m$^{-1}$) | $\gamma_l^d$ (mN.m$^{-1}$) | $\gamma_l^p$ (mN.m$^{-1}$) |
|---|---|---|---|
| Water | 72.8 | 21.8 | 51.0 |
| Formamide | 58.0 | 37.6 | 20.4 |
| Amino Ethanol | 48.9 | 31.5 | 17.4 |
| Ethylene Glycol | 48.2 | 29.3 | 18.9 |
| Diiodomethane | 50.8 | 50.8 | 0.0 |
| $\alpha$-Bromonaphtalene | 44.6 | 44.6 | 0.0 |

Table 5.2: Surface tensions of solvents used for tapes surface energy calculation

### HTCC - Swerea IVF

Surface energies, before and after sintering, of alumina HTCC tape are shown on figure 5.17.

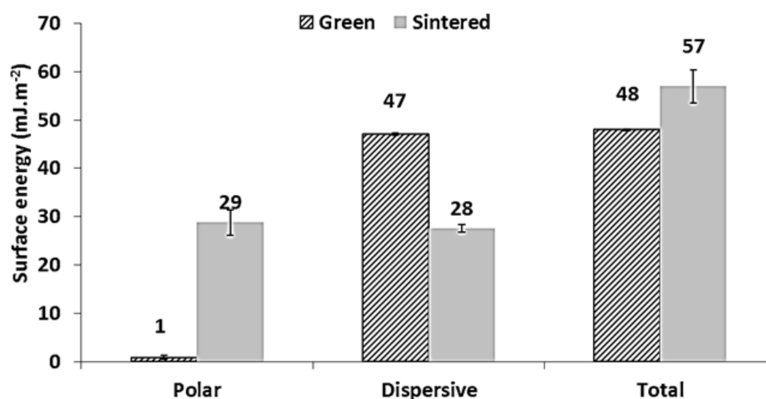


Figure 5.17: Swerea IVF - M400SAP tape surface energies before and after sintering

High surface energy was measured before and after sintering (48 and 57 mJ.m$^{-2}$, respectively). This was attributed to the water-based slurry from which the tapes were cast. Total surface energy increased after sintering. Variation was due to polar component increase, from 1 to 29 mJ.m$^{-2}$. This was related to hydrophobic organic binder, styrene acrylic polymer, burn out. Dispersive component decreased from 47 to 28 mJ.m$^{-2}$. Before sintering these tapes should be printed by solvent-based inks. Water-based formulae could be used if surfactant is added in order to allow ink surface tension decrease. Sintered tapes are compatible with water based inks because of their high surface energy, 56 mJ.m$^{-2}$.

**LTCC - MSE and Swerea IVF**

Surface energies, before and after sintering, of LTCC tapes are shown on figure 5.18.

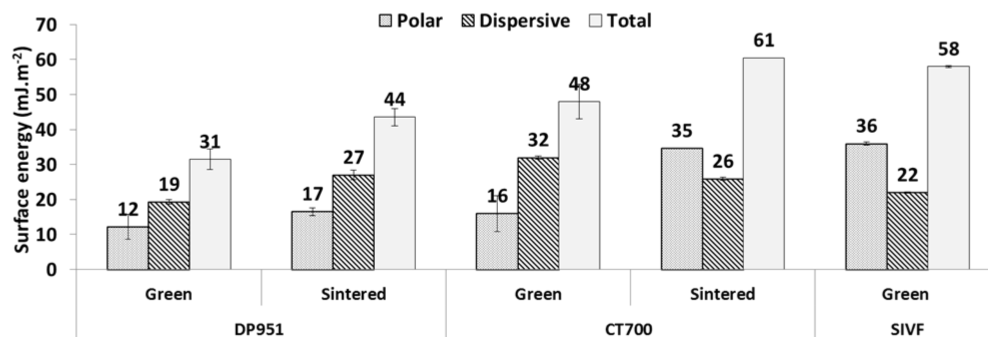


Figure 5.18: LTCC tapes surface energies before and after sintering

Water-based inks have usually a surface tension in the order of magnitude of 40 - 45 mN.m$^{-1}$ with a high polar component. DP951 exhibited the lowest surface energy, 31 mJ.m$^{-2}$, among green LTCC tapes. This tape could be printed with water-based inks only if surfactant was added to the ink. CT700 and Swerea IVF LTCC tape surface energies was respectively equal to 48 and 58 mJ.m$^{-2}$. Commercial tapes had lower surface energies than the new manufactured tapes because they are prepared from solvent-based slurries. To print CT700 tape with water-based ink, surfactant should be added because of its high dispersive component (32 mJ.m$^{2}$). Swerea IVF LTCC could be printed with water-based inks because of its high surface energies.
After sintering, as expected, DP951 and CT700 surface energies increased to 44 and 61 mJ.m$^{-2}$, respectively. These tapes, mainly CT700, could be printed by water based inks. It is preferable to add surfactant to inks formulated to print DP951 sintered tape and green commercial LTCC tapes.

## 5.6 Conclusion

Tapes of different compositions were tested. It was demonstrated that microstructure and surface properties were related to powders nature, polymer used to prepare the green tape and to powders sizes. Properties of sintered tapes also depended on sintering temperature and process. After sintering, the organic binder burnt out, ceramic powders melted and particles aggregates were formed. Thus, porosity decreased and in some cases no more pores were observed especially on tapes surfaces.

These tapes are designed to be printed at the green or the sintered stage depending on the process.

According to pore sizes at the green stage, particles larger than 0.4 $\mu$m and smaller than 1.0 $\mu$m could be used to print alumina tape manufactured by Swerea IVF.
In order to print LTCC tapes, it is better to use larger powders. Conductive particles with a diameter larger than 1 $\mu$m are suitable to print these tapes.
Regarding the ink system to be used for printing, Swerea IVF alumina tape had high surface energies ($> 48$ mJ.m$^{-2}$), water based ink system could be used to print these tapes.

Commercial LTCC tapes were relatively hydrophobic. It is better to use solvent-based inks to print these substrates. It is also possible to add surfactants to water-based ink in order to decrease the ink surface tension and then promote substrate wetting.

The sintered tapes exhibited low roughness with no pores on surface, thus particles with diameters smaller than 1 $\mu$m could be used to print all sintered substrates. In addition, surface energies of all sintered tapes were very high, water-based inks could be employed to print sintered tapes.

After determining properties of sintered and green tapes, suitable inks were formulated and adapted to printing processes by working on rheology, dispersion, surface tension and printing processes.

# Chapter 6

# Screen printing

The screen printing process is used since many years in electronic field for the manufacturing of ceramic, silicon and glass chips, electronic circuits, radio frequency resonators and others.
This process allows printing onto flexible and rigid substrates such as papers, polyethylene, ceramics, glasses, etc.
Screen printing pastes are usually solvent based. Solvent with low evaporation rate, such as terpineol and toluene, are employed to prevent mesh openings from clogging during printing. Metallic powders are especially used as conductive particles. Glass powders are added as adhesion promoters *(see paragraphs 2.4 and 3.1).* In this part, the following steps were performed:

- first of all,water-based silver screen printing pastes were formulated. Formulae with lead free glass frits were also prepared,

- after ink formulation, rheological properties were determined in order to study the thixotropic behaviour of pastes. Furthermore, rheology effect on line properties were determined by oscillatory shear stress study,

- afterwards, screen printing was performed on sintered alumina and green LTCC tapes. Printing parameters were tested, i.e. speed, pressure, off-contact distance,

- characterisation of deposited lines was performed in order to measure lines thickness, width and roughness. Furthermore, line microstructure was observed on ESEM (Environmental Scanning Electron Microscopy) micrographs,

- finally, sintering under normal air atmosphere was performed and followed by characterisation of printed lines dimensions and electrical properties. Thus, comparison of green and sintered lines could be performed.

Figure 6.1 shows a synthesis of the screen printing applications versus the objectives to reach in this work.

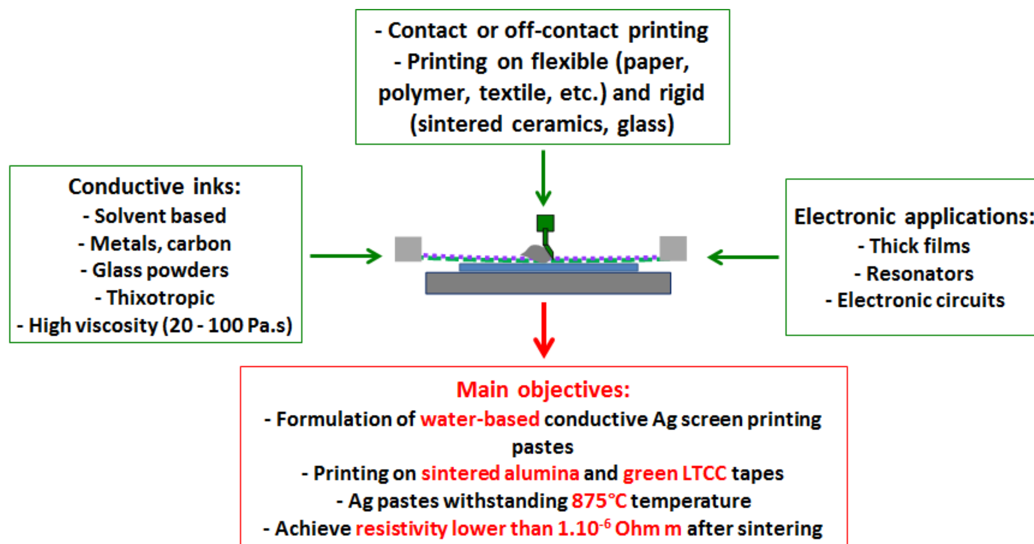


Figure 6.1: Synthesis of screen printing and main objectives

## 6.1 Inks

Environmentally friendly water-based screen printing pastes were formulated. Silver particles were selected as conductive material due to their good electrical properties - resistivity $\sim$ 16 nOhm.m, their relatively low price compared to gold and their chemical and thermal resistance compared to copper and nickel *(see paragraph 3.1.1)*. Spherical and flake particles were tested. Pastes rheological properties - behaviour, viscosity, yield stress, loss and elastic moduli - were also determined.

### 6.1.1 Pastes formulation

#### Silver particles

Silver conductive particles were purchased from Heraeus and Métaux et Chimie (M-C). Particles with different shapes and sizes were tested. Table 6.1 gives some information about silver particles.

| Particle | Supplier | Shape | D50 ($\mu$m) | Tap density (g.cm$^{-3}$) | Surface area (m$^2$.g$^{-1}$) |
|---|---|---|---|---|---|
| Silpowder 188 | M-C | Spherical | 0.6 - 1.1 | | 1.1 - 2.1 |
| Silpowder 222 | M-C | Spherical | 4.0 - 6.0 | 1.7 - 2.5 | |
| Silflake 720 | M-C | Flake | $\sim$ 1.0 | 2.0 - 3.0 | 1.5 - 2.1 |
| Ag 300-02 | Hereaus | Spherical | 2.0 - 3.0 | 1.4 - 1.9 | 2.1 - 2.7 |
| HCF38 | Hereaus | Flake | 1.0 - 2.0 | 2.8 - 3.8 | 1.2 - 1.9 |

Table 6.1: Properties of silver particles used for screen printing formulation

### Glass powders

Glass powders with a 3 $\mu$m mean diameter were provided by Sovitec - France. Glass powders ensured particles cohesion after firing and organic binder burn out. Besides, glass powders act as adhesion promoter *(see paragraph 3.1.2)*.

### Vehicle components

Vehicle main components were:

- solvent with a mixture of water/ethylene glycol/glycerol to allow slower drying rate and better levelling,
- organic binder allowing particle cohesion before sintering,
- additives providing appropriate surface tension, rheological behaviour and ensuring dispersion stability.

Used vehicle components and their functions are shown on table 6.2.

| Raw material | Nature | Function | Manufacturer |
|---|---|---|---|
| Water | Water | Solvent | |
| Ethylene glycol | Ethylene glycol | Solvent | Fisher Scientific |
| Glycerol | Glycerol | Solvent - moisturiser | Fisher Scientific |
| Joncryl 2136 | Water-based acrylic polymer | Organic binder | BASF |
| Joncryl 8055 | Water-based styrene acrylic copolymer | Organic binder | BASF |
| XP53 | Water-based acrylic copolymer | Rheological agent | Coatex |
| Hydropalat 216 | Mixture of ionic and non-ionic surfactants | Dispersing agent | Cognis |
| Foamaster 8304 | Hydrocarbons and non-ionic surfactants | Anti-foaming agent | Cognis |
| Foamaster 361 | Water-based fatty acids emulsion | Anti-foaming agent | Cognis |
| Hydropalat 140 | Modified polysiloxane (silicone based) | Wetting agent | Cognis |

Table 6.2: Screen printing pastes vehicle components

To prepare pastes the following protocol was performed:

- first of all, solvents, dispersive, antifoaming and wetting agents were weighed in a beaker and agitated with a magnetic agitator for 1 minute,
- then, conductive particles and glass powders were added,
- afterwards, binders and rheological agent were added,
- the total mixture was then mechanically dispersed in a Dispermat VMA apparatus for 20 minutes at 2000 rotations per minute. The agitation geometry diameter was approximately equal to the half of the beaker diameter,

To optimise the pastes a three roll mill could be used. It allows ink homogenisation and aggregation breaking. An EXAKT 50i was purchased from Montceram society and will be used to perform milling with chrome plated hardened steel rollers.

### 6.1.2 Rheological properties

Rheological properties of inks were performed with an Anton Paar Physica MCR301 rheometer. Measurements were realised at 25°C. The gap was fixed to 1 mm. A plate -

plate geometry with 2.5 cm diameter was used.
All pastes had a thixotropic shear thinning behaviour. It is a time dependent rheological behaviour characterised by the decrease of material apparent viscosity submitted to constant shear stress or rate. Then, viscosity is progressively recovered when stress or shear is removed [174]. Thixotropy is characterised by an hysteresis loop showing material viscosity and shear stress variation as a function of shear rate (figure 6.2).

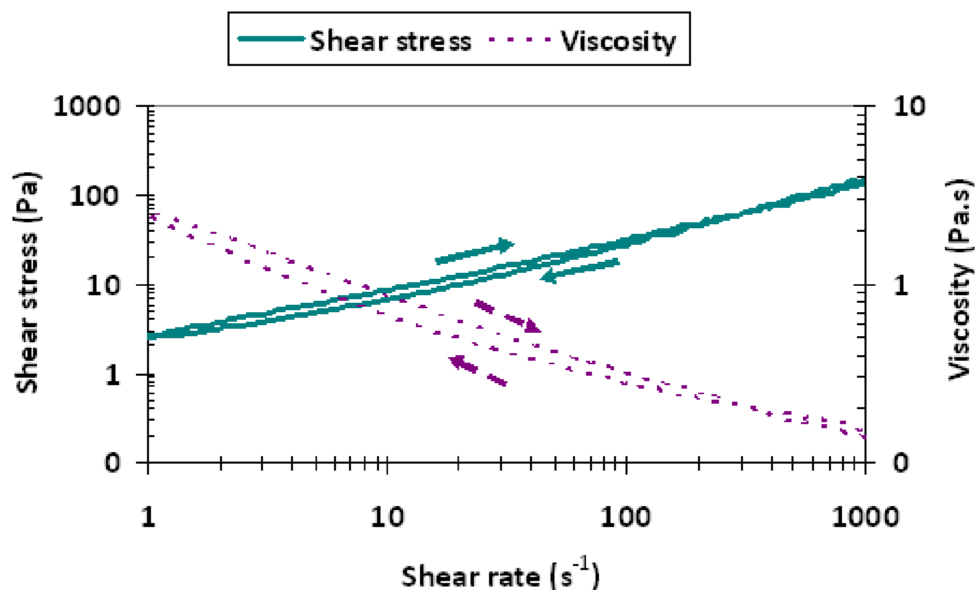


Figure 6.2: Hysteresis loop observed when shearing a screen printing paste - 45% Ag HCF38 and 10% glass

Viscosity variation as a function of silver content was also studied. It increased when silver content increased. This was attributed to interaction improvement between silver powders when more particles were added to the formula. An example is given on figure 6.3. At 1 $s^{-1}$ shear rate, viscosity increased from 51 to 435 Pa.s when silver weight increased from 15 to 60%.

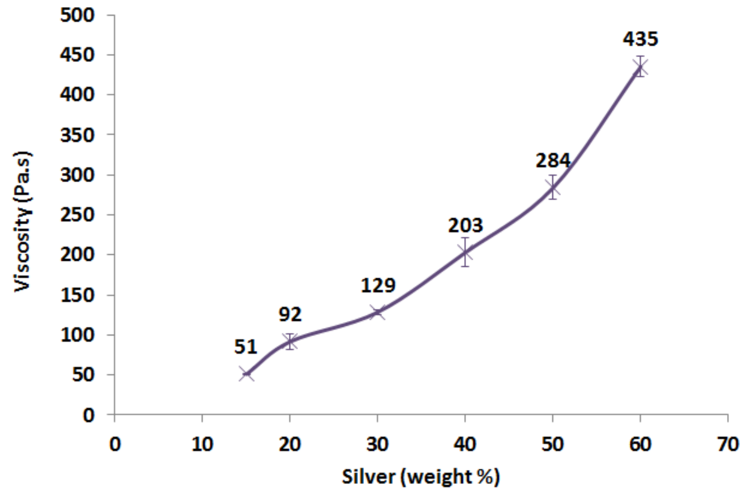


Figure 6.3: Viscosity variation as a function of silver content - 1 $s^{-1}$, 25°C - Flake Ag pastes (Silflake 720)

Furthermore, Hershel-Bulkley model was applied to determine the yield stress value. It is the minimum stress value required in order to allow ink flowing. In the experiment performed with screen printing pastes, it was shown that yield stress increased when silver content increased. An example is given on figure 6.4. Yield stress increased from 47 to 612 Pa when silver content increased from 15 to 60%.

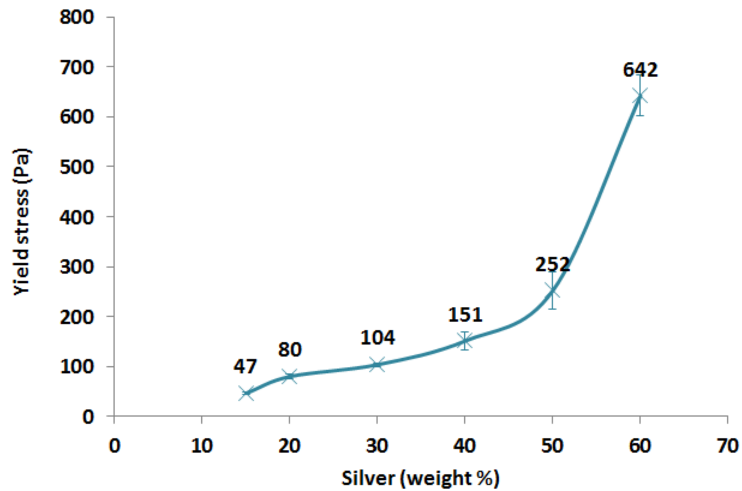


Figure 6.4: Yield stress variation as a function of silver content - 1 $s^{-1}$, 25°C - Flake Ag pastes (Silflake 720)

## 6.2 Printing

Screen printing of silver pastes onto LTCC and sintered alumina tapes was performed. The minimum line width able to be achieved with prepared ink and screen printing process was determined. Furthermore, printing force effect on printed lines properties was also studied.

### 6.2.1 Printing patterns

Two printing patterns were tested.

- the first one was composed of different widths lines - 100, 200, 400 and 600 $\mu$m. It allowed studying of printing resolution and lines continuity (Figure 6.5 - a). This pattern was printed on a commercial low temperature co-fired ceramics, DP951 - DuPont,

- the second was a serpentine line with 300 $\mu$m line width (Figure 6.5 - b). This pattern was conceived for microwave transmission and dielectric properties testing. It was printed on sintered pure alumina tapes manufactured by Swerea IVF.

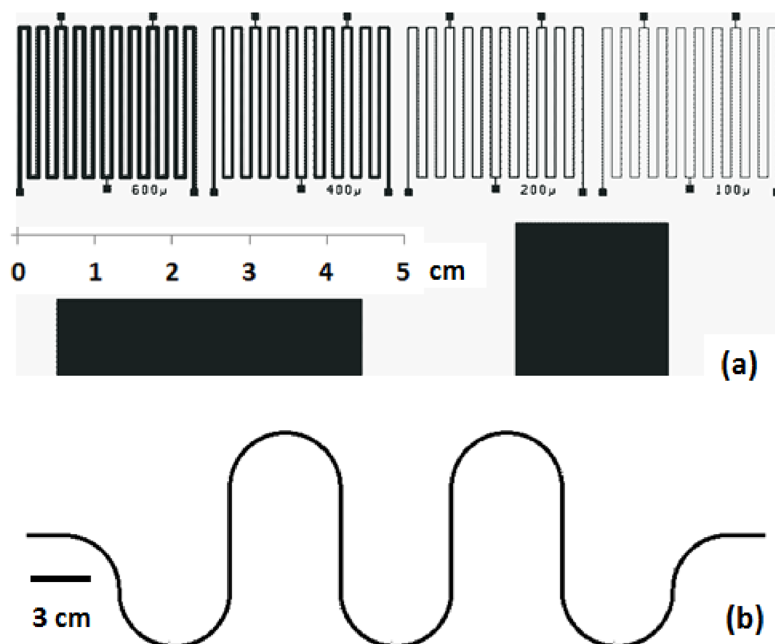


Figure 6.5: Screen printed patterns: (a) different line widths, (b) serpentine line

### 6.2.2 The screen mesh

Two screen meshes were manufactured by KOENEN (different line widths) and DEK (serpentine). Stainless steel was chosen as mesh material because of its ease to clean, its durability and chemical resistance. Printing resolution is dependent on mesh count. Better quality is obtained when mesh count increases. Mesh count varies from 16 to 330 mesh/inch or finer for special applications [215]. Concerning mesh opening, it should be at least 3 times larger than the mean particle size used for ink formulation. In this study, particles with diameters varying from 0.6 to 5.0 $\mu$m were used.
Thread diameter and emulsion thickness affects deposited film thickness. In this work, a minimum line thickness of 15 $\mu$m was aimed. Screens properties are given on table 6.3. An optical microscope image of KOENEN screen is shown on figure 6.6.

| | KOENEN (figure 6.5(a)) | DEK (figure 6.5(b)) |
|---|---|---|
| Printing pattern | Different line widths | Serpentine |
| Mesh material | Stainless steel | Stainless steel |
| Mesh count (threads/inch) | 325 | 325 |
| Mesh opening | 90 $\mu$m | 50 $\mu$m |
| Thread diameter | 24 $\mu$m | 30 $\mu$m |
| Angle | 22.5° | 45.0° |
| Emulsion thickness | 15 $\mu$m | 13 $\pm$ 2 $\mu$m |

Table 6.3: Screen mesh properties

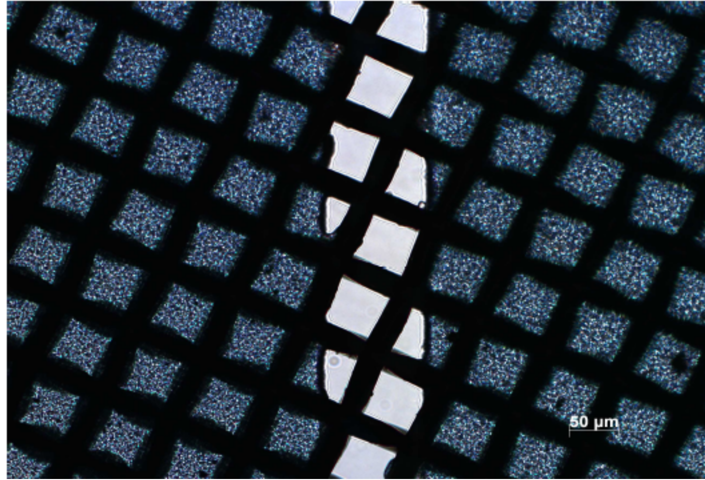


Figure 6.6: KOENEN mesh used to print pattern shown on figure 6.5-a

### 6.2.3 The squeegee

A single-sided bevel squeegee was used. Made of polymer, it has 17 cm length, forms an angle of 60° with the screen and has a hardness of 70 – 75 Shore. Generally, this type of squeegee is used for glass and nameplate printing [215].

### 6.2.4 The screen printing press

Screen printing tests were performed with a DEK Horizon 03i automatic flatbed press. This type of press is conceived for printing on flat flexible or rigid substrates. Off-contact printing allowed sharp printings without smudging. A vacuum base was also used to prevent flexible lightweight tapes from sticking to the screen. After squeegee stroke and impression, a metallic squeegee was used to allow coating of an ink layer on the screen without forcing it through the mesh openings. The DEK Horizon 03i screen printing press is shown on figure 6.7.

Figure 6.7: DEK Horizon 03i screen printing press

## 6.3 Sintering

Sintering was performed under normal air atmosphere in different furnaces. A batch furnace from LINN was used at Micro-System Engineering (MSE - Germany). The sintering profile is shown on figure 6.8. Printed lines were sintered at 875°C for 40 minutes.

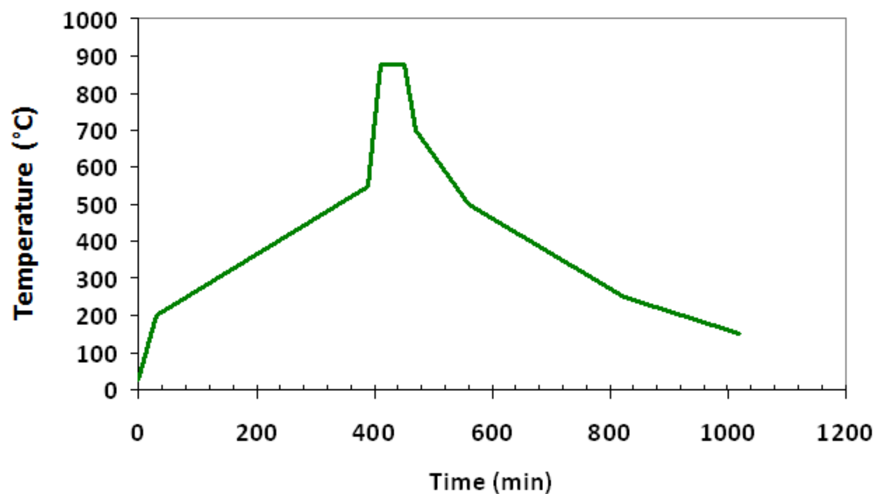


Figure 6.8: Sintering profile (MSE - Germany)

At Grenoble INP - LGP2, a StaTop – Nagat furnace was used. Temperature was increased from ambient to 875°C during 75 minutes. Then, it was maintained at 875°C for 60 minutes. Finally, substrates were left in the furnace for cooling down to 100°C, approximately.

## 6.4 Results and encountered problems

### 6.4.1 Mesh clogging

The earlier prepared formulae contained only water. Thus, solvent evaporated quickly leading to inks drying and then mesh openings blocking. For this reason, new formulae

with mixtures of water/ethylene glycol/glycerol were prepared. Ethylene glycol evaporates slower than water and glycerol is known for its moisturising effect.

### 6.4.2 Smudging

Smudging was observed when on-contact printing was performed (figure 6.9).

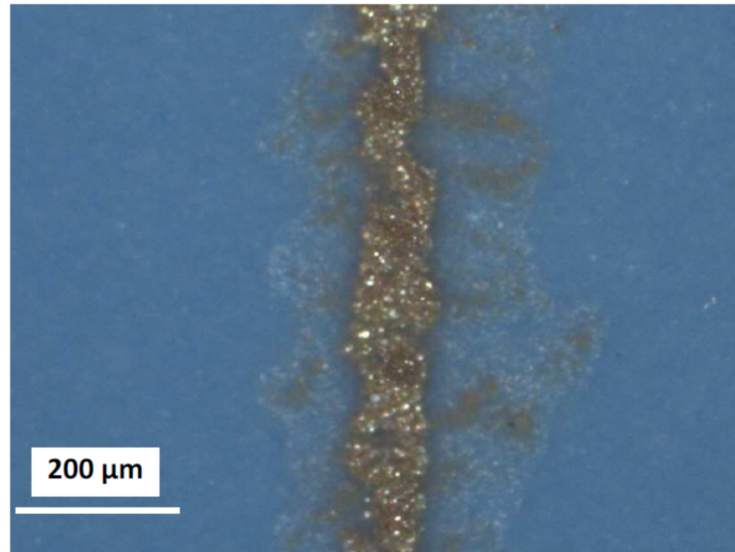


Figure 6.9: Smudging - On-contact printing - 40% Ag Silpowder 188 - 20% glass on DP951 LTCC tape - Before sintering - Optical microscope

Indeed, according to *Magee, 1985* [215], on-contact printing is performed when image sharpness is of little importance. Off-contact printing should be realised in order to allow sharper lines printing by avoiding spreading and smudges.

### 6.4.3 Non homogeneity

Non homogeneous lines with surface pores were deposited. The non homogeneity was attributed to the rheological behaviour of the inks and to poor levelling. This was observed on excessively loaded pastes (figure 6.10).

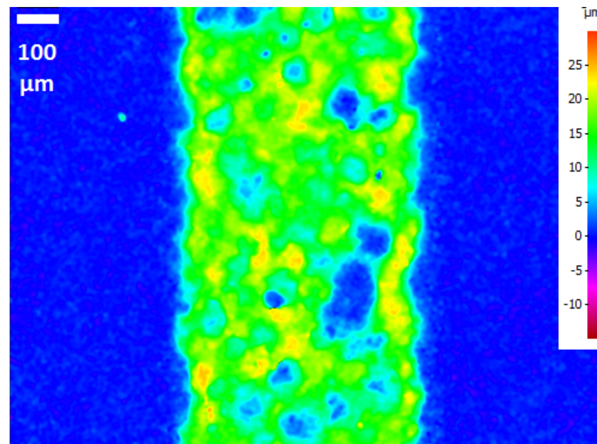


Figure 6.10: Non homogeneous line printed with 75% flake Ag (HCF38) paste printed on DP951 LTCC tape before sintering - Alicona

High viscosity also led to mesh marks observation on printed lines (figure 6.11).

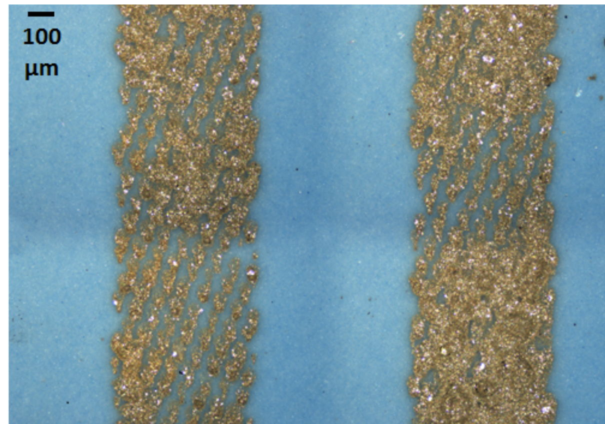


Figure 6.11: Mesh marks observed on 65% silver flake (HCF38) and 13% glass frits paste printed on DP951 LTCC tape before sintering - Alicona 2D image

Furthermore, thickness was not the same all along the lines. Higher thickness values were measured on line center than on edges.
It was explained by *Björninen et al., 2010* [216] that uneven screen printed layer formation is usual because of the pseudoplastic thixotropic ink behaviour and high viscosities.
Non-homogeneity could also be related to aggregation formation. A three roll mill step is required to break aggregations and perform printing of uniform lines.

### 6.4.4 Reproducibility

Reproducibility of line thickness and width was studied on 100 and 600 $\mu$m nominal width lines. Results are shown on figure 6.12. Regarding measured values and standard deviations, line widths were practically reproducible on narrow and large lines. Line thickness could be considered as repeatable on 100 $\mu$m lines. However, 17 to 21% variation was observed on the thickness of 600 $\mu$m line. This thickness variation was attributed to the non-homogeneity of printed lines.

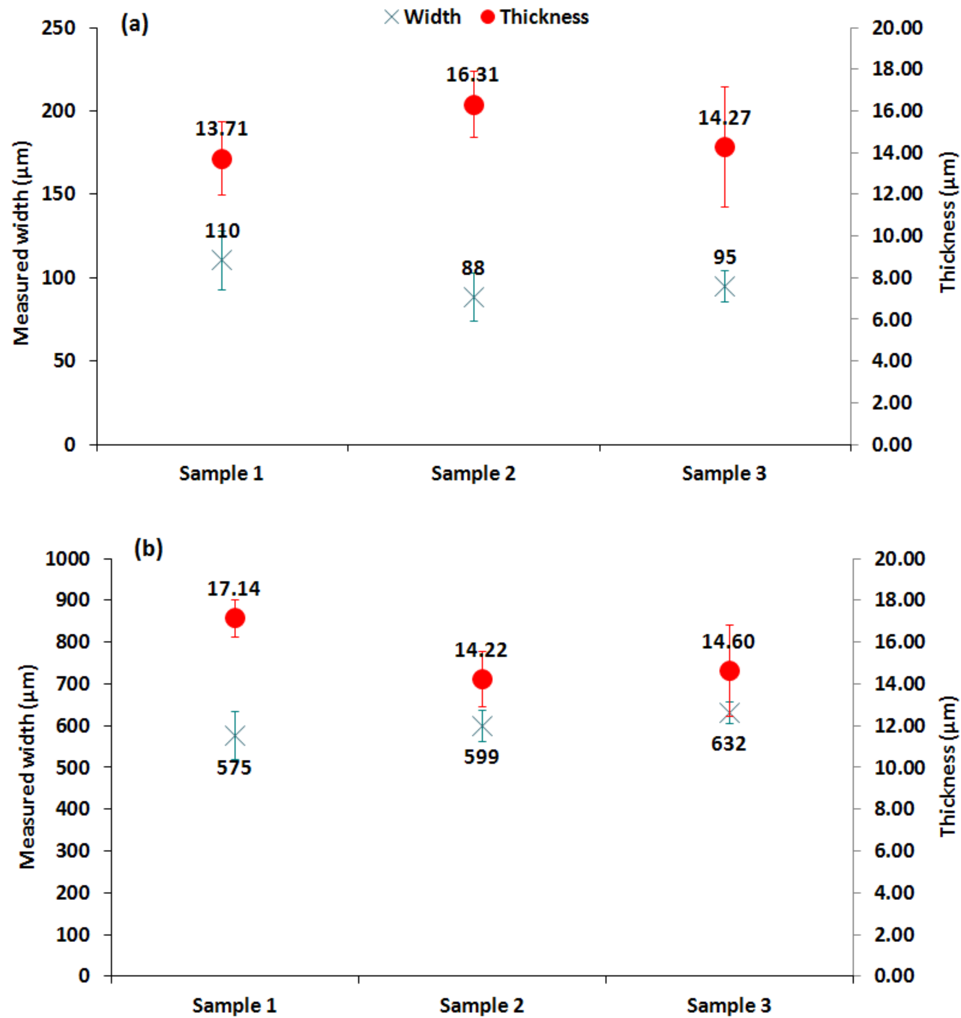


Figure 6.12: Measured width and thickness reproducibility of screen printed lines: (a) 100 $\mu$m (b) 600 $\mu$m nominal widths

### 6.4.5 Adhesion to substrate

A peel test was performed after sintering in order to determine silver paste adhesion to substrate. It was demonstrated that when silver content was lower than 75%, printed films did not resist to peel test and was peeled by the normalised scotch (figure 6.13).

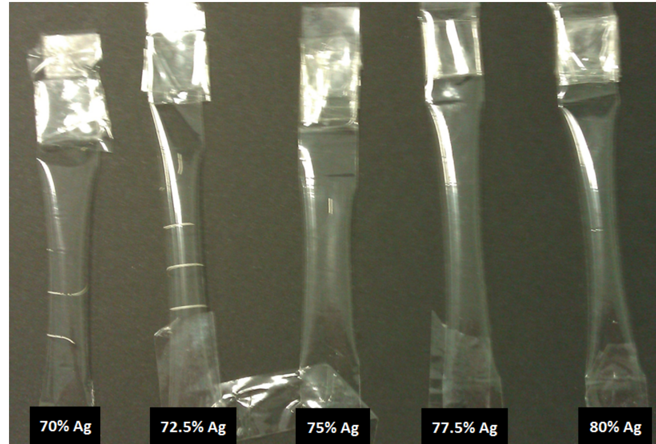


Figure 6.13: Peel test result on screen printed pastes containing 70 to 80% silver weight (Ag300-02)

With a 72.5% silver, good electrical resistivity value was measured - $2.4.10^{-8}$ Ohm.m after sintering at 900°C for 15 minutes. For this reason, 1 to 5% glass powders were added to 72.5% silver paste as adhesion promoter. Glass powders did not deteriorate electrical properties of printed lines and allowed better adhesion to substrate. All lines resisted to the peel test.
Silver pastes adhered very well to LTCC substrate after sintering even without adding glass frits. This was attributed to a possible diffusion of silver particles into silica and vice-versa.

## 6.5 Conclusions and perspectives

### 6.5.1 Main results

Formulation and printing of water-based environmentally friendly screen printing pastes was successfully accomplished. These inks, with equivalent and even better results than commercial solvent-based inks, could replace already commercialised pastes.

All formulated pastes exhibited a shear thinning thixotropic behaviour. They were able to flow over a shear stress value called the yield stress. Viscosity decreased when shear rate increased and ink was able to recover its initial state when shear rate was decreased or stopped. When silver content increased, yield stress, viscosity, elastic and plastic moduli increased. It was demonstrated that line definition was related to ink rheological properties, especially to the elastic behaviour of the pastes. When elastic modulus was too low and plastic modulus high, ink spread excessively and line width was too large. When plastic modulus was too low and elastic modulus too high, ink had a tacky aspect and its release through the screen mesh was disturbed. Thus, printed line properties were dependent on printing speed and force which affected rheological behaviour of inks.
A study based on printing pressure effect on line properties was also performed. It was demonstrated that when printing force increased, more silver particles passed through the screen mesh opening and then thicker and narrower lines with higher electrical resitivities were obtained. However, at excessively high load (> 7 kg), pastes had a tendency to recover their elastic state ($G''/G'$ decreased) and ink flowing through the mesh openings

was disturbed.
It was also shown that electrical resistivity is dependant on sintering temperature. It increased from 2.4 to $7.6.10^{-8}$ Ohm.m when temperature decreased from 900 to 500°C.
Conductive silver lines which withstood hard sintering conditions, 875°C for 1 hour, were achieved. Low electrical resistivity values close to that of bulk silver were measured after sintering, 2 to $4.10^{-8}$ Ohm.m.

### 6.5.2 Perspectives

**Screen printing of thermoelectric inks**

Bismuth telluride pastes were prepared at the CEA (Commissariat à l'Énergie Atomique et aux Énergies Alternatives). These pastes had a thixotropic behaviour with viscosities varying from 30.9 to 0.4 Pa.s for 1 to 1000 $s^{-1}$ shear rate range.
Metallic stencil screen and squeegees were used to print structured alumina tapes provided by Keranor - Norway. Two layers were deposited in order to allow filling of 0.35 or 0.50 mm diameter holes with 0.30 mm height. The holes should be alternatively filled by n and p-type $Bi_2Te_3$ pastes. The first results are shown on figure 6.14.

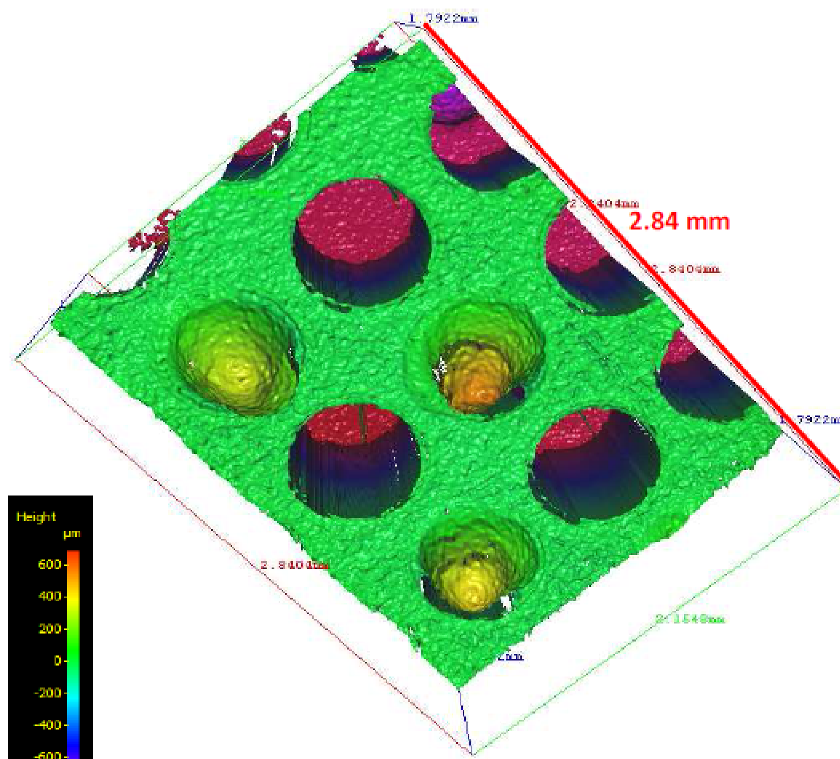


Figure 6.14: First results for p-type $Bi_2Te_3$ screen printed on alumina tape (Alicona)

About 300 $\mu$m paste thickness was deposited. However, inks should be optimised by decreasing viscosity in order to allow easy flowing and holes filling. After p and n-type thermoelectric pastes printing, silver connections will be deposited by screen printing or pulverised by spray method. The aim of this task is to manufacture Demo 2 - thermoelectric device for domestic application *(see Project Concept section)*.

### Investigation of dielectric properties of printed tracks

Dielectric properties of printed lines are under investigation at Swerea IVF and Omnysis (Sweden) in order to determine their ability to be used for microwave systems applications. A 8720D microwave vector network analyser from Agilent Technologies was used to determine the dielectric loss (see annexe 2). It allowed loss measurement between 0.05 and 40 GHz frequency. Substrates were mounted on Universal Test Fixtures 3680 Series. Serpentine lines printed on alumina sintered substrates with 72.5% silver paste with different glass frits content (2 to 4% by weight) were tested. As substrate were cut before test, glass free printed lines were not adhered to the substrate and measurement was not possible. Results were compared to silver commercial paste, Ferro silver paste CN33-79 with 75% solid content (silver and glass frits). Figure 6.15 shows test results.

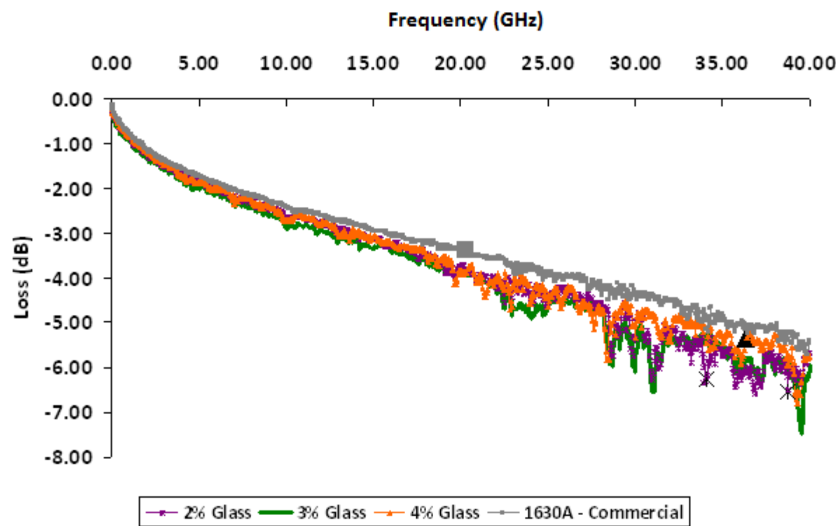


Figure 6.15: Dielectric loss versus frequency - 72.5% silver paste (Ag300 - 02) with different glass content compared to commercial paste

When frequency increased, dielectric loss increased. Furthermore, new formulated paste showed dielectric loss close to that of commercial paste. A loss value approximately equal to 6 dB was registered for new formulated pastes and commercial one. Thus, new pastes can be used for microwave applications.
This task will be continued in order to manufacture a device transmitting the radio and microwave frequencies.

These promising results show that water-based screen printing pastes are suitable for electronic applications. Therefore, they could be integrated in ceramic systems for microelectronic devices manufacturing.

## 6.6 Paper 1: Silver content effect on rheological and electrical properties of silver pastes

**Authors:**
Rita Faddoul, Nadège Reverdy-Bruas and Joséphine Bourel

**Published in:**
Journal of Materials Science: Materials in Electronics - 23(7) – 1415-1426 – 2012

**Introduction:**
This paper is dedicated to the study of spherical silver powders use as conductive particles in screen printing paste. Water-based pastes were formulated and screen printed on sintered alumina substrates.

Rheological properties of the pastes were determined and compared to commercial silver paste manufactured by Heraeus (C1075).

After printing and sintering, dimensions and roughness of deposited lines were studied. Besides, their electrical properties were determined. Line aspect and resistivity were compared to commercial paste.

## 6.7 Paper 2: Formulation and screen printing of water based conductive flake silver pastes onto green ceramic tapes for electronic applications

**Authors:**
Rita Faddoul, Nadège Reverdy-Bruas and Anne Blayo

**Published in:**
Journal of Materials Science and Engineering B - 177 – 1054-1066 – 2012

**Introduction:**
The aim of this work was to formulate water-based conductive screen printing pastes. Mixture of spherical and flake shape particles was used to prepare inks with 67 to 75% silver. Printing was performed onto green LTCC tapes, DP951.

Rheological properties of the paste and their effects on printability were determined. For this reason, viscosity variation as a function of shear rate and Hershel-Bulkley yield stress were measured. Furthermore, simulation of screen printing at 50 mm.s$^{-1}$ evaluated to 200 s$^{-1}$ was performed in order to determine rheological behaviour during printing and observe line levelling. In addition, Oscillatory stress test was applied in order to measure elastic and viscous moduli and study the pastes elasticity.

Finally, lines properties, before and after sintering, were determined. Thus, line and film width, thickness, roughness, sheet resistance and electrical resistivity were calculated.

## 6.8 Paper 3: Printing force effect on conductive silver tracks - Geometrical, surface and electrical properties

**Authors:**
Rita Faddoul, Nadège Reverdy-Bruas and Anne Blayo

**Published in:**
Journal of Materials Engineering and Performance - 22(2) - 640-649 - 2013

**Introduction:**
The aim of this paper was to study screen printing force effect on 75% silver deposited lines.

Different printing forces were applied (3 to 12 kg) to determine their effect on line width, thickness, roughness, microstructure and electrical properties.

# Chapter 7

# Flexography printing

Flexography is nowadays considered as a high-quality printing process. It is also a high speed and throughput technique allowing mass production of printed electronic circuits. With flexography, it is possible to print on a wide variety of flexible substrates in roll-to-roll process. Besides, roll-to-plate flexography can be employed to print on rigid substrates. In this work, only roll-to-roll flexography is treated.
Flexography is used in many printed electronics domains such as RFID tags, batteries, organic circuits, photovoltaics and low-cost lighting *(see paragraph 2.5)* [217].

In this part the following steps were performed:

- first of all, commercial screen printing paste was optimised in order to meet flexographic ink requirements,
- then, rheological properties and surface tensions of optimised inks were determined and compared to original paste,
- afterwards, roll-to-roll flexography printing was performed on green LTCC tapes. One to five printing passes were deposited,
- in addition, different sintering conditions (temperature, duration) were tested in order to optimise the electrical properties,
- finally, characterisation of deposited and sintered lines was performed in order to measure lines thickness, width, roughness and electrical properties. Furthermore, line microstructure was observed on SEM micrographs.

Figure 7.1 shows a synthesis of the flexography printing applications versus the objectives to reach in this work.

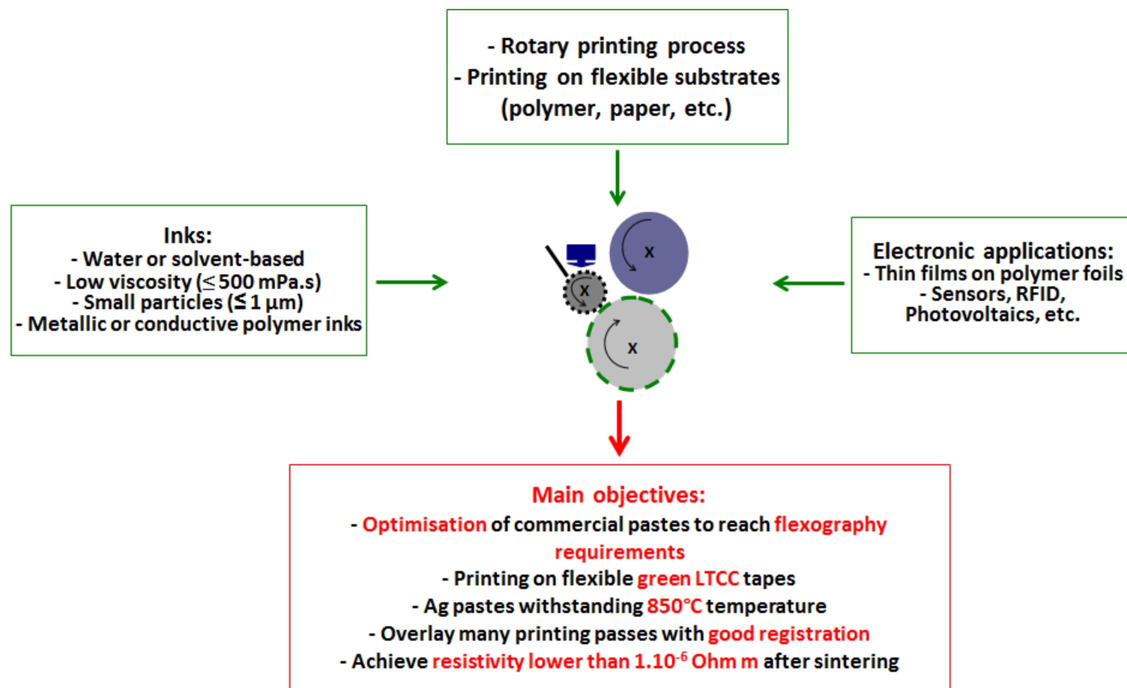


Figure 7.1: Synthesis of flexography printing and main objectives

## 7.1 Inks

Inks with different silver contents were optimised from a screen printing paste purchased from Novacentrix - USA. Original paste, HPS-30, contained 65% silver flakes with a 0.4 $\mu$m mean diameter. Micrographs of this ink was performed by a Field Emission Gun - Scanning Electron Microscope (FEG-SEM) Zeiss Ultra Column 55 Gemini (figure 7.2) allowing nano-scale resolution.

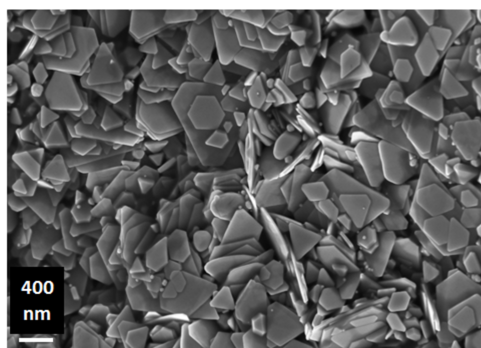


Figure 7.2: FEG-SEM image of silver ink provided by Novacentrix

### 7.1.1 Ink optimisation

Composition of commercial screen printing paste HPS-30 is given on table 7.1.

| Raw material | Weight percentage |
|---|---|
| Silver | 65% |
| Diethylene glycol monobutyl ether | 15% |
| Other | 20% |

Table 7.1: Commercial paste composition - HPS-30 - Novacentrix

Distilled water was added to original paste to allow preparation of silver flexographic inks with 20, 30 and 40% silver by weight (table 7.2).

| | 20% Ag | 30% Ag | 40% Ag |
|---|---|---|---|
| Paste (HPS-30) | 31% | 46% | 62% |
| Distilled water | 69% | 54% | 38% |

Table 7.2: Optimised flexographic inks composition

Dispermat mechanical agitation was, finally, performed for 20 minutes at 1000 rotations per minutes.

### 7.1.2 Rheological properties

A cone-plate geometry with 5 cm diameter allowed studying the rheological behaviour of inks under shear rate ranging from 1 to 10000 $s^{-1}$ with an Anton Paar rheometer. The gap distance was equal to 0.05 mm and measurements were carried out at a constant temperature of 25°C. Figure 7.3 shows the rheological behaviour of commercial paste and optimised flexographic inks.

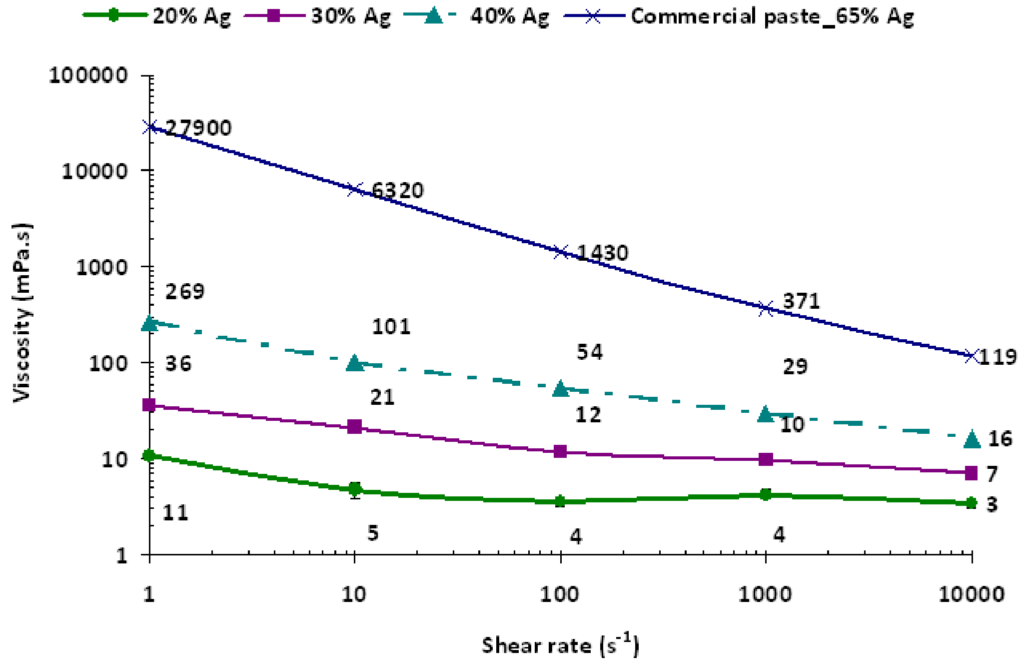


Figure 7.3: Rheological behaviour of HPS-30 commercial paste (65% Ag) and optimised inks (20, 30 and 40% Ag) - 25°C

All inks exhibited shear thinning behaviour: viscosity decreased when shear rate increased. Viscosity also decreased when silver content decreased. This is related to the interactions flagging with fewer particles. All optimised inks had a viscosity lower than 500 mPa.s in the range of flexographic inks requirements (50 - 500 mPa.s) [94].

### 7.1.3 Surface tension

Surface tensions were measured with a contact angle OCA apparatus (Dataphysics) in pendant drop mode. Surface tensions of 20%, 30% and 40% silver inks were respectively equal to $22.4 \pm 2.5$, $20.8 \pm 0.6$ and $18.9 \pm 0.1$ mN.m$^{-1}$. Surface tension decreased when silver content increased. This was attributed to water quantity decrease. These inks can print substrates with surface energies higher than 23 mJ.m$^{-2}$.

## 7.2 Printing

One to five printing passes were deposited on LTCC - CT700 and DP951 - tapes. Number of passes effect on resolution, registration and electrical properties was investigated.

### 7.2.1 Printing patterns

Flexography printing plates are known for their flexibility, their affinity with a large variety of substrates and their relatively low cost [218]. Two designs were patterned on a photopolymer printing plate (figures 7.4 and 7.5).

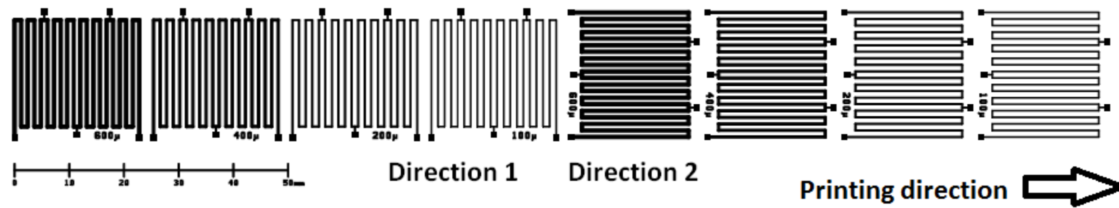


Figure 7.4: Flexography printing pattern: 100 to 600 $\mu$m - Flexiproof 100

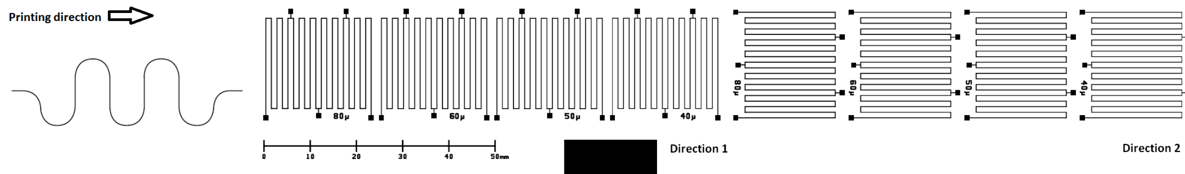


Figure 7.5: Flexography printing pattern: 40 to 80 $\mu$m, serpentine and solid area - Flexiproof 100

The design shown on figure 7.4 allowed:

- testing the possibility to deposit and overlay lines with widths varying from 100 to 600 $\mu$m by flexography,
- compare two printing directions - perpendicular to printing orientation (direction 1) and same direction as printing (direction 2),
- compare geometrical properties of lines deposited by flexography to screen printing,
- compare two different rulings because the pattern was duplicated and printed simultaneously with an anilox engraved with 100 and 180 lines per cm.

Pattern of figure 7.5 was designed to :

- test the possibility of printing narrower lines (40 to 80 $\mu$m),
- print serpentine lines for dielectric properties testing,
- calculate sheet resistivity on solid print area.

### 7.2.2 The anilox

A ceramic anilox was engraved by Bachkine BAT Graphics - France. Two line rulings were performed 100 and 180 lines per cm. When line ruling increases cell volume decreases and patterns with better resolution are defined. Cell characteristics are shown on table 7.3.

| Line ruling (lines per cm) | 100 | 180 |
|---|---|---|
| Cell height ($\mu$m) | 35 ± 1 | 15 ± 1 |
| Cell dimension ($\mu$m) | 91 ± 4 | 49 ± 2 |
| Cell volume ($cm^3.m^{-2}$) | 10 ± 3 | 5 ± 1 |

Table 7.3: Anilox cells characteristics - Alicona measurements

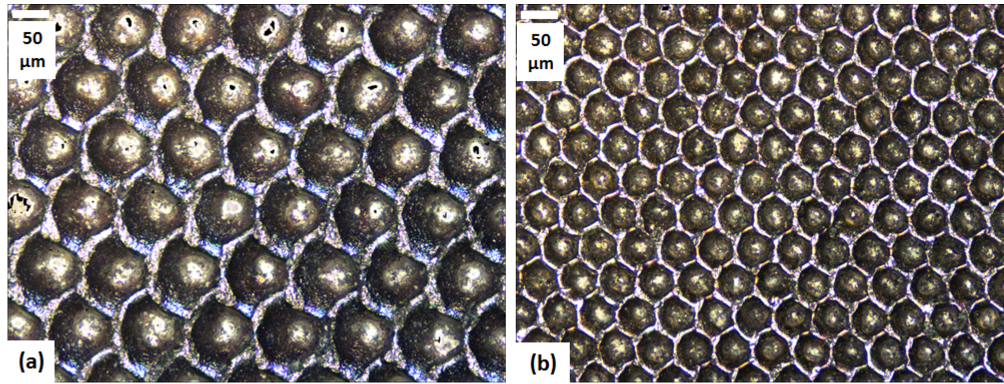


Figure 7.6: Anilox optical images - (a) 100 lines per cm, (b) 180 lines per cm - Alicona

Figure 7.6 shows the anilox cells engraved in the cylinders used in this study.

A de-clogging machine, Recyl Media Clean 800, allowed cleaning of anilox cylinder by plastic powders projection.

### 7.2.3 The flexography printing tester

A Flexiproof 100 (figure 7.7) laboratory printing tester was used to perform printing tests.

Figure 7.7: Flexiproof 100 laboratory printing tester

This apparatus is used in research and development domain to test product viability and commercial feasibility. It allows printing on typical flexible substrates such as plastic foils and papers. Thus, it is suitable for quality and ink properties control and minimises wastes on production printing press.
However, the Flexiproof is not equipped by a registration control system. For this reason, misregistration problem is usually encountered when overlaying many printing passes.
All tests were performed at a printing speed of 25 m.min[1] and an engagement equal to 74 for CT700 tape and to 73.4 for DP951 tape. The printing engagement is related to the distance between printing plate and substrate. When engagement increases, printing pressure decreases.

## 7.3 Sintering

Different sintering profiles were tested. At the LGP2, sintering was performed in a Statop Nagat furnace at 875°C for 1 hour. This profile was used because it corresponds to the one used by industrial partners (MSE - Germany) involved in ceramic micro-components manufacturing. The same furnace was also used to test sintering at different temperatures (700 to 850°C) and different sintering durations (10 to 50 minutes).
Micro System Engineering (MSE) also performed sintering in normal atmosphere at 850°C for 10 minutes and at 875°C for 40 minutes in a batch furnace from LINN.

## 7.4 First results and encountered problems

Effects of printing direction, anilox, number of layers and printing speed were investigated. Some problems such as line widening and misregistration were encountered. Preliminary results are shown hereafter.

### 7.4.1 Encountered problems

#### Line widening

All measured widths were larger than the nominal ones. This was attributed to printing plate deformation under pressure and ink spreading [122]. For example, for 100 $\mu$m nominal width, lines with 150 $\mu$m width were printed (figure 7.8).

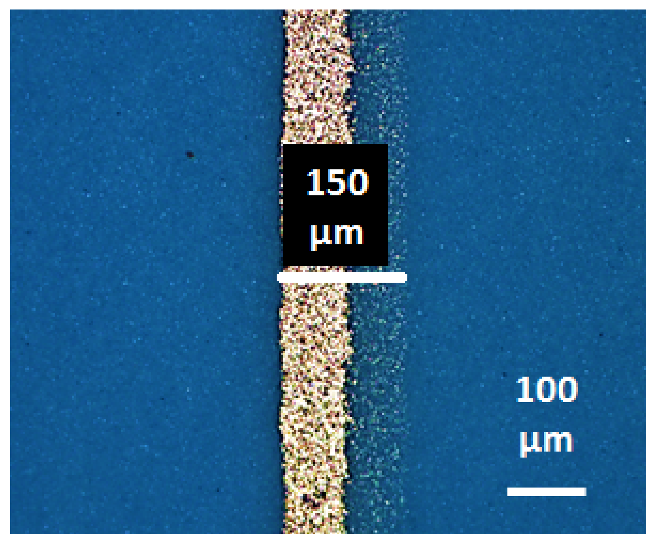


Figure 7.8: Example of line widening - 100 $\mu$m line printed with 20% Ag ink on DP951 LTCC tape (optical microscope)

#### Reproducibility

Thicknesses and widths were measured on three samples in order to study printing reproducibility. When one pass was performed, measured values were reproducible (figure 7.9). Line width varied from 1 to 6%. Line thickness varied from 0.6 to 0.8 $\mu$m. Regarding standard deviation, thickness was considered as reproducible.

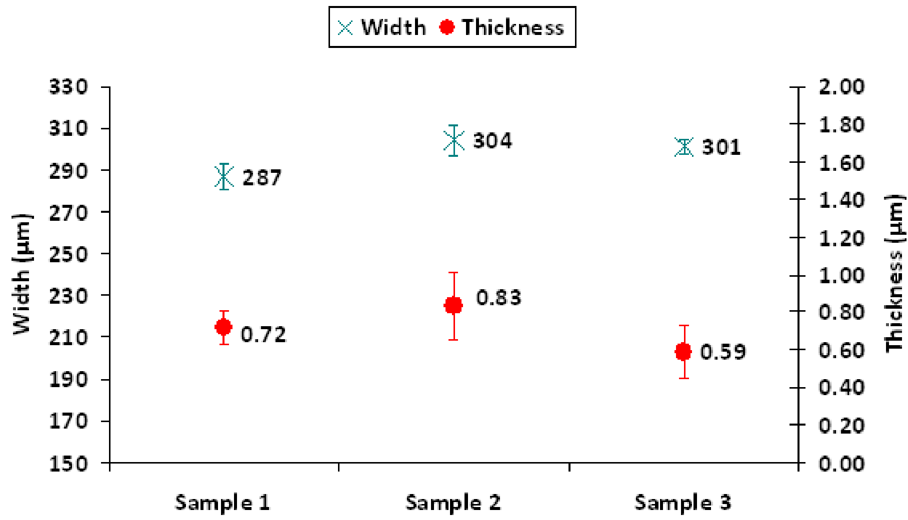


Figure 7.9: Reproducibility investigation - 180 lines per cm - Serpentine - 1 pass

Figure 7.10 shows line widths and thicknesses measured on 3 samples of 4 overlaid printing passes.

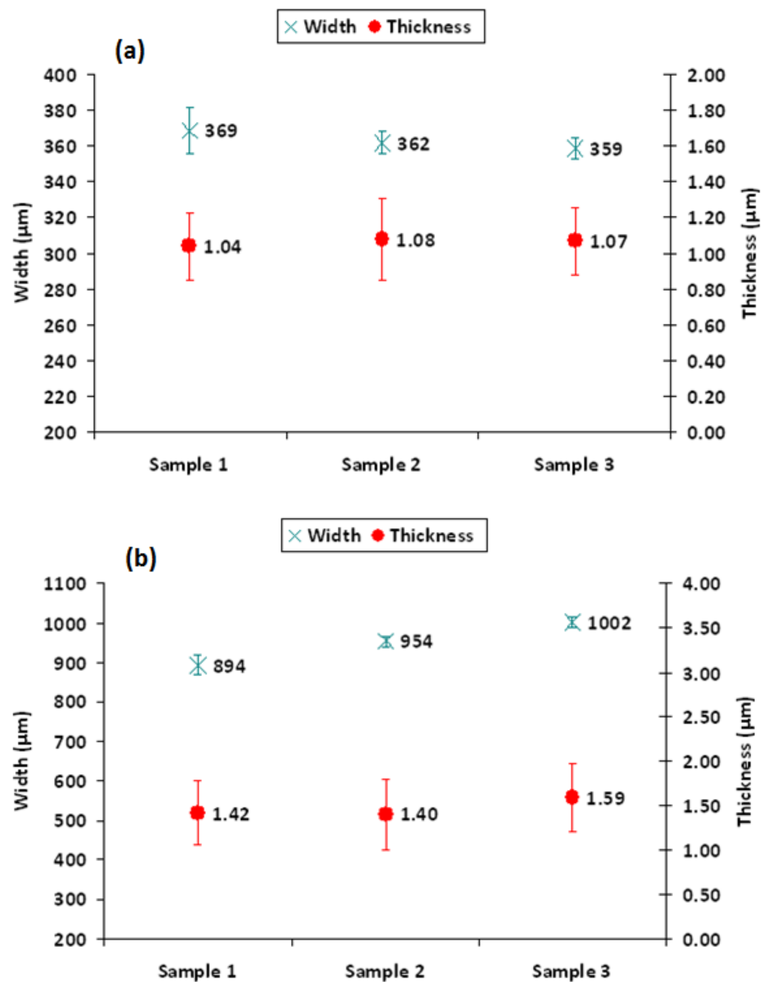


Figure 7.10: Reproducibility investigation - 100 lines per cm - 4 passes - (a) 100 $\mu$m (b) 600 $\mu$m nominal width

When two to five printing passes were overlaid, line thickness and width were reproducible for narrow lines. Line width varied from 359 to 369 $\mu$m and line thickness from 1.04 to 1.08 $\mu$m. For larger lines, line thickness was reproducible (1.4 to 1.6 $\mu$m). However, line width varied from 5% to 12%. This was attributed to the misregistration when several printing passes were performed. Indeed, the Flexiproof 100 laboratory press is not equipped with a registration control system.

### 7.4.2 Printing direction and resolution effects

Printing direction and anilox properties effects on line width and thickness were investigated. Figure 7.11 shows measured widths for 40 $\mu$m nominal width line printed with 100 and 180 lines per cm anilox in directions 1 and 2.

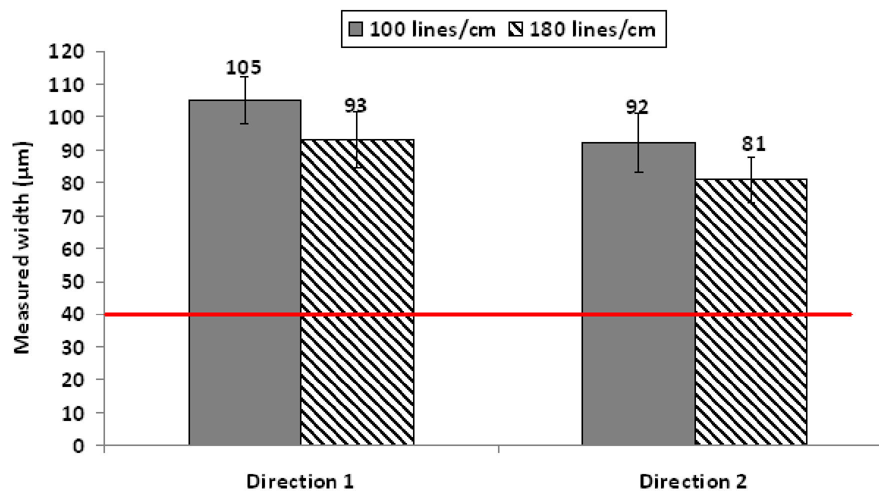


Figure 7.11: Printing direction and resolution effects on line width - 40 $\mu$m nominal width

Narrower lines - 81 and 93 $\mu$m versus 92 and 105 $\mu$m - were printed when line ruling increased. This slight difference was attributed to the higher number of cells and the better resolution of 180 lines per cm anilox compared to 100 lines per cm one. On the other side, ink deposition in printing direction (2) allowed better line definition. This was attributed to more homogeneous ink deposition in printing direction compared to the cross direction (1). Indeed, silver was only deposited on one of the line edges and widening was observed on the other side (figure 7.12).

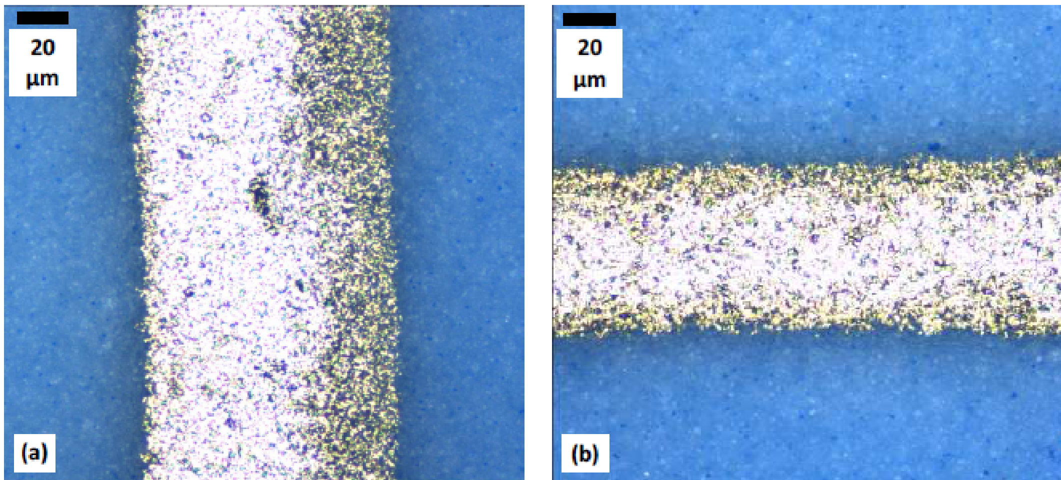


Figure 7.12: Optical microscope images of 40 $\mu$m nominal width line printed with 180 lines per cm anilox (a) Direction 1 (b) Direction 2

A similar result was observed by *Hrehorova et al, 2011* [219] who observed that narrower lines were deposited in printing direction (parallel to sheet movement): 250 $\mu$m lines were printed in printing direction versus 300 $\mu$m for lines perpendicular to printing direction.

Line thickness evolution depending on printing direction and resolution is shown on figure 7.13.

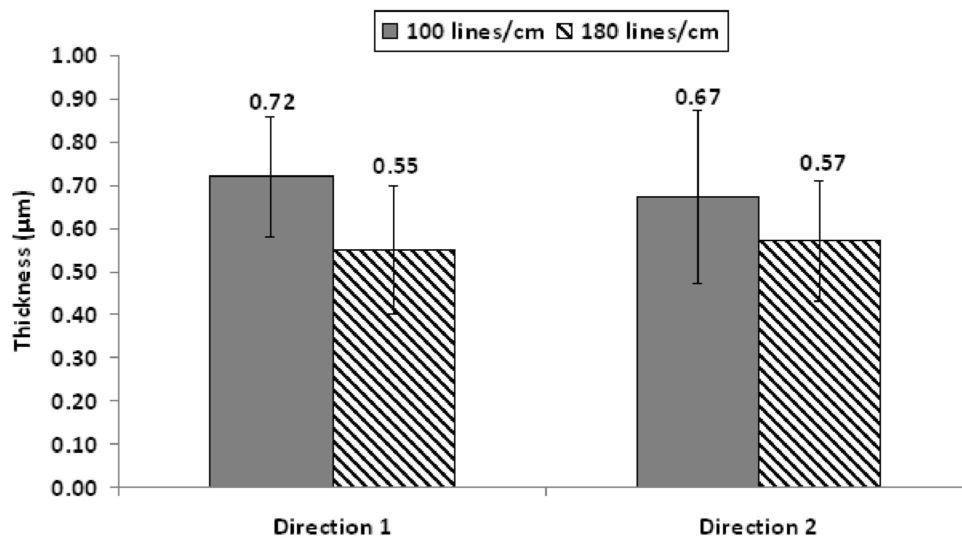


Figure 7.13: Printing direction and resolution effects on line thickness - 40 $\mu$m nominal width

Printing direction had no effect on line thickness. $0.56 \pm 0.19$ $\mu$m thickness was deposited for 180 lines per cm anilox and $0.70 \pm 0.15$ $\mu$m for 100 lines per cm anilox. Slightly higher thickness deposited with lower resolution anilox is related to the greater cells volume (10 $cm^3.m^{-2}$) compared to the higher resolution anilox (5 $cm^3.m^{-2}$).

## 7.5 Conclusions and perspectives

### 7.5.1 Main results

The printability of metallic silver inks onto green ceramic tapes by flexography process was demonstrated. Lines able to withstand 875°C for 40 minutes were deposited.

A commercial screen printing paste with 0.4 $\mu$m mean diameter particles was optimised by adding water in order to meet the flexographic inks requirements (viscosity $\leq$ 500 mPa.s).

Narrow lines were printed in printing direction with a high resolution anilox (180 lines per cm). Higher cell volumes allowed printing of thicker lines. Three minimum printing passes were required to allow deposition of more than 1 $\mu$m thickness.

Decomposition of small silver particles (D50 = 0.4 $\mu$m) started at temperatures higher than 600°C. Thus, high printed thicknesses were required to allow withstanding of LTCC systems sintering conditions (> 875°C for more than 30 minutes). Resistivities after sintering varied from 3 to $21.10^{-8}$ Ohm.m depending on sintering conditions and number of deposited layers.

### 7.5.2 Perspectives

Scalability of flexography printing onto green LTCC and alumina tapes will be studied with the Flexiane pilot press (figure 7.14).

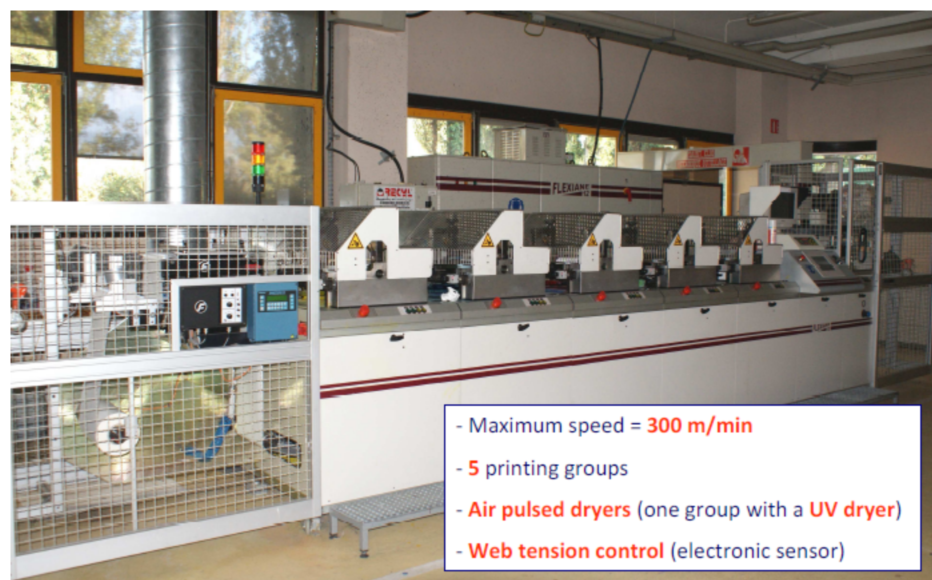


Figure 7.14: The Flexiane printing press and characteristics - Flexography pilot adapted to roll to roll printing

The Flexiane printing press can reach a 300 $m.min^{-1}$ maximum speed, it is equipped by five printing groups which allow printing with registration. An air drying system permits solvent evaporation. Besides, a ultra violet dryer is related to one of the printing groups. Alumina substrates and newly developed LTCC were provided by Swerea IVF. Screen

printing pastes (75% Ag) were purchased from Novacentrix by the CEA and will be optimised to reach flexography requirements (40% - 50% Ag).
Lines with nominal widths varying from 40 to 600 $\mu$m will be deposited in printing direction to study printing resolution. A serpentine line will be also printed to evaluate the dielectric properties (figure 7.15).

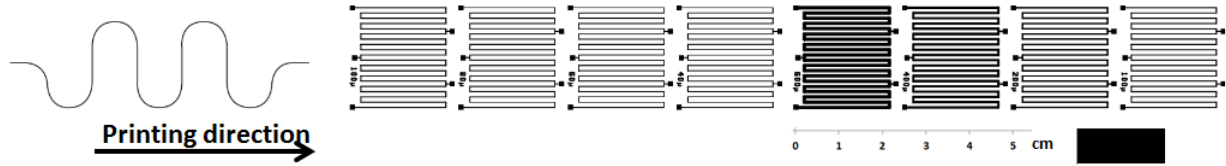


Figure 7.15: Flexography printing pattern: 40 - 600 $\mu$m, serpentine line and solid area - Flexiane

The current study demonstrates the huge potential of flexography printing for the manufacturing of LTCC multilayer systems.

## 7.6 Paper 4: Ink optimisation for an alternative way to print on ceramic substrates

**Authors:**
Rita Faddoul, Nadège Reverdy-Bruas, Anne Blayo and Bertine Khelifi

**Published in:**
Proceedings of the $8^{th}$ International Conference on Multi-Material Micro Manufacture - 260-263 - 2011

**Introduction:**
This paper studied the printability of ceramic green tapes by flexography process. A screen printing paste was optimised and diluted to decrease viscosity and meet flexography requirements.

Two inks with 20 and 30% silver particles were printed, 1 to 3 printing passes. Silver content and number of layers effects on printing properties - thickness and width - were investigated.

Flexography printing of silver metallic inks on ceramic tapes was successfully achieved.

## 7.7 Paper 5: Optimisation of silver paste for flexography printing on LTCC substrate

**Authors:**
Rita Faddoul, Nadège Reverdy-Bruas, Anne Blayo, Thomas Haas and Christian Zeilmann

**Published in:**
Microelectronics Reliability - 52(7) – 1483–1491 – 2012

**Introduction:**
This work consisted in printing by flexography process low resistivity silver tracks on ceramic tapes.

Ink with 30% silver per weight was prepared and printed onto LTCC substrates. Three to five printing passes were overlaid.

The challenge was to deposit silver tracks able to withstand sintering conditions: 850°C under normal air atmosphere for 10 minutes.

Conductive silver lines, with 2.8 to $12.0.10^{-8}$ Ohm.m resistivity, were successfully achieved after sintering.

## 7.8 Paper 6: Flexography printing of silver tracks on LTCC tapes – Effect of printing direction on line properties

**Authors:**

Rita Faddoul, Nadège Reverdy-Bruas, Anne Blayo and Didier Chaussy

**Published in:**

Proceedings of the $8^{th}$ International Conference on Ceramic Interconnect and Ceramic Microsystems Technologies - 314–321 - 2012

**Introduction:**

The objective of this study was to study the possibility to integrate flexography process in LTCC multilayer devices manufacturing. Thus, the challenge was to deposit thick enough silver layer able to whithstand sintering at 875°C for 40 minutes under normal atmosphere.

Ink with 40% silver per weight was prepared and printed onto LTCC substrates. Five printing passes were performed.

Besides, printing direction effect on overlaid line widths and thicknesses was also studied.

Lines conductive along 34 cm length with a resistivity varying from 9 to $21.10^{-8}$ Ohm.m were obtained after sintering.

# Chapter 8

# Rotogravure and inkjet printing

## 8.1 Rotogravure printing of silver inks onto green ceramic tapes

Rotogravure printing is considered as high throughput and speed method able to reach 100 m.min$^{-1}$ [220]. It is conventionally used for packaging, newspaper, PVC (Poly Vinly Chloride) flooring and other applications for which long runs are required [221].
Rotogravure printing for electronic applications is nowadays in quick growth due to the high resolution and the good reproducibility of the process. Besides, it is an economical method for long runs. It is used in many electronic fields such as RFID, photovoltaïcs and OLED.
In this study, rotogravure was studied according to different steps:

- the formulation of water-based inks for rotogravure printing onto ceramic substrates,
- the design of an intaglio engraved impression cylinder allowing deposition of high thickness and handling 2 to 3 $\mu$m diameter particles,
- the study of the printability of ceramic tapes by formulated inks,
- the study of the sinterability of deposited lines,
- the evaluation and the characterisation of deposited lines before and after sintering,
- the investigation of the relationship between substrates properties, ink characteristics and ink transfer.

Figure 8.1 shows a schematic of rotogravure printing main applications and requirements versus the aimed objectives.

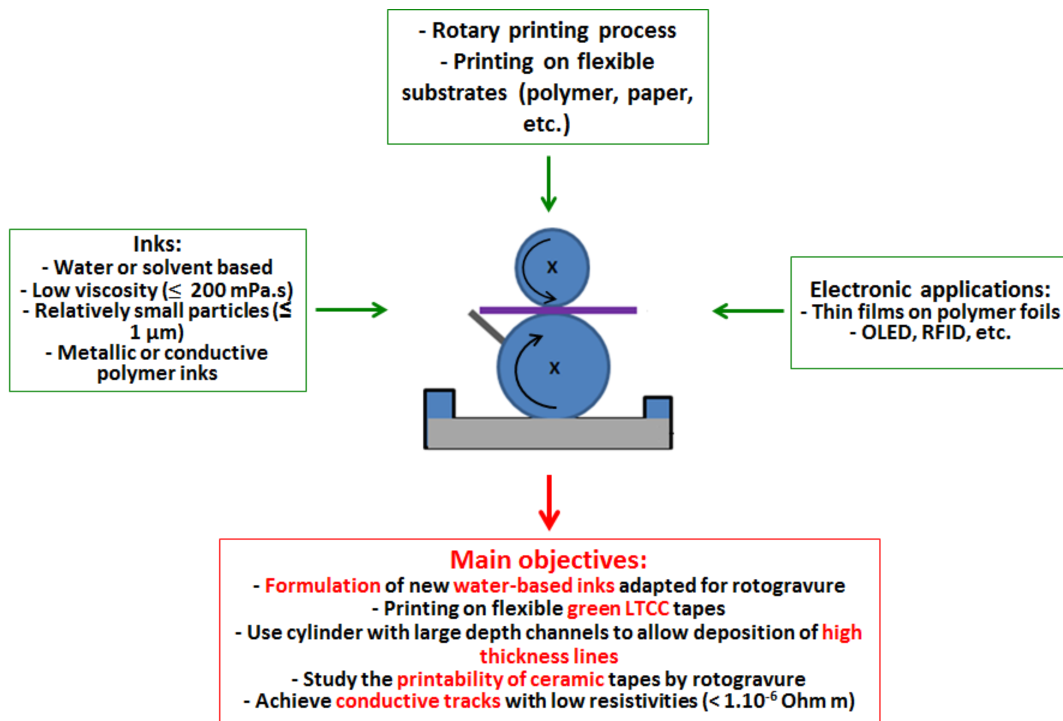


Figure 8.1: Synthesis of rotogravure printing and main objectives

### 8.1.1 Inks

Water-based inks were formulated with 35 to 55% of silver. Silver particles with 2 to 3 $\mu$m mean diameter were purchased from Heraeus - Germany. A mixture of water/ethylene glycol/glycerol (3/6/1) was employed as solvent. Ink surface tensions varied from 12 to 16 mN.m$^{-1}$ depending on silver content. All inks exhibited shear thinning behaviour. Maximum viscosity was equal to 519 mPa.s at 1 s$^{-1}$ shear rate and 25°C.

### 8.1.2 Printing

#### Printing pattern

Lines with 100 to 600 $\mu$m width were printed in printing direction on LTCC tapes. Printing pattern is shown on figure 8.2.

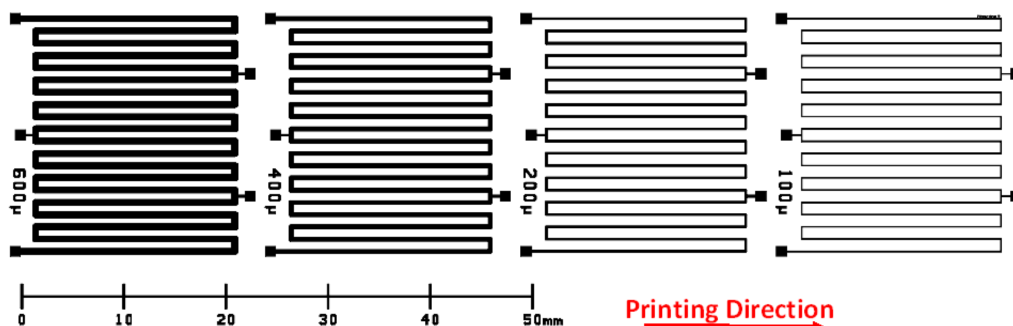


Figure 8.2: Rotogravure printed pattern - intaglio gravure

**The engraved cylinder**

An anilox was engraved in intaglio with variable channel widths: 136, 222, 414 and 605 $\mu$m measured widths for 100, 200, 400 and 600 $\mu$m nominal widths, respectively. Channel depth was equal to 45 $\mu$m. This engraved cylinder was designed in order to allow printing of inks with 2 to 3 $\mu$m diameter without blocking the anilox cells. This anilox is deeply characterised in **Paper 7**.
Printing tests were performed with an IGT 3H Global Standard Tester (figure 8.3).

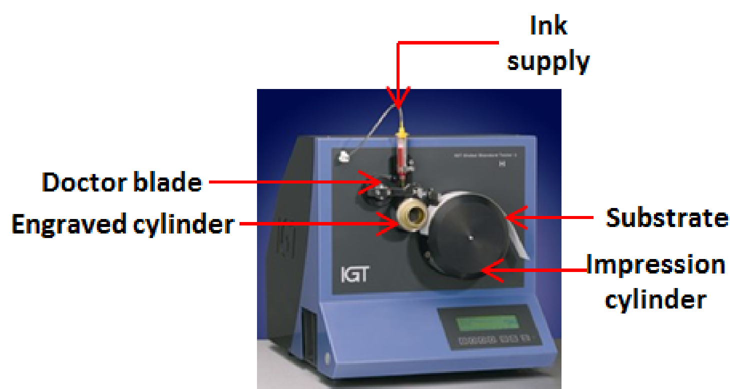


Figure 8.3: The IGT 3H Global Standard Tester

The IGT3H printing tester is not equipped with a registration control system. Thus, it was not possible to overlay several printing passes.

### 8.1.3 Conclusions and perspectives

Rotogravure printing of silver metallic inks onto LTCC tapes was achieved. It was observed than narrower lines were better defined than the larger ones.
Low thicknesses were deposited (3.4 to 5.6 $\mu$m) and silver quantity was not enough to allow continuous conductive network formation after sintering.
To optimise ink transfer from engraved cylinder to substrate, the following steps could be realised:

- increase silver content and then the possibility to have more silver particles transferred to substrates,
- formulate inks with flake shape silver particles having larger surface contacts,
- try a new engraved cylinder with higher volume cells.
  Pattern shown on figure 8.4 was engraved on ceramic impression cylinder with helicoïdal and intaglio channels.

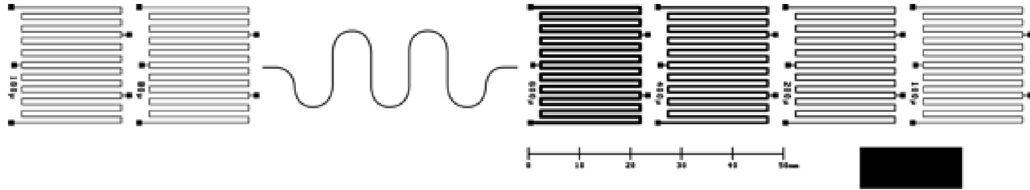

Figure 8.4: New rotogravure printing pattern - on the right: serpentine line and 100 to 600 $\mu$m lines width helicoïdal gravure, on the left: 80 and 100 $\mu$m with intaglio gravure

Characteristics of the intaglio and helicoïdal channels of this cylinder are shown on table 8.1.

| Nominal width ($\mu$m) | Channel | Volume ($cm^3.m^{-2}$) | Height($\mu$m) | Measured width ($\mu$m) |
|---|---|---|---|---|
| 80 | Intaglio | 41 ± 6 | 77 ± 6 | 95 ± 12 |
| 100 | Intaglio | 47 ± 2 | 107 ± 2 | 167 ± 6 |
| 250 - Serpentine | Helicoïdal | 21 ± 1 | 89 ± 5 | 356 ± 8 |
| 100 | Helicoïdal | 23 ± 1 | 100 ± 6 | 236 ± 6 |
| 200 | Helicoïdal | 21 ± 1 | 96 ± 6 | 293 ± 7 |
| 400 | Helicoïdal | 23 ± 2 | 90 ± 5 | 501 ± 16 |
| 600 | Helicoïdal | 24 ± 1 | 93 ± 8 | 694 ± 11 |

Table 8.1: Characteristics of intaglio and helicoïdal channels engraved in impression cylinder

Lines of 80 $\mu$m and 100 $\mu$m width were engraved in intaglio with a cell volume varying from 40 to 50 $cm^3.m^{-2}$. 100 to 600 $\mu$m width and serpentine lines were engraved in helicoïdal form. Cell volume was equal to 20 - 25 $cm^3.m^{-2}$. Engraved channel widths were larger than the nominal ones. Figure 8.5 shows a topographic view of the 100 $\mu$m nominal width channels engraved with helicoïdal form and in intaglio.

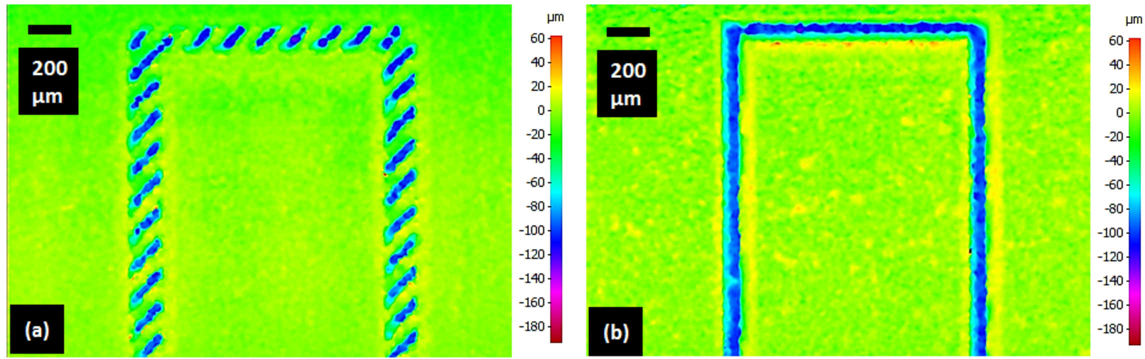


Figure 8.5: Topography of 100 $\mu$m nominal width channels engraved in helicoïdal form (a) and in intaglio (b)

With such high volume and height channels, more viscous with higher solid contents inks are expected to be printed. Therefore, higher silver quantity would be transferred to LTCC substrates and larger thicknesses able to withstand temperatures higher than 800°C could be obtained.

### 8.1.4 Paper 7: Formulation of water-based silver inks adapted for rotogravure printing on ceramic green tapes

**Authors:**
Rita Faddoul, Anne Blayo and Nadège Reverdy-Bruas

**Published in:**
Journal of Print and Media Technology Research - 1(2) - 103-112 – 2012

**Summary:** The main objective of this work was to study the printability of ceramic tapes with a metallic silver ink by rotogravure process.

Water-based inks with 35 to 55% silver were formulated and printed with an impression cylinder engraved in intaglio.

It was demonstrated that thicker lines were obtained when inks with higher solid contents were printed.

Printed lines could not withstand sintering conditions because of the small quantity of silver particles transferred to substrate. A new design is therefore proposed in order to overcome this problem.

## 8.2 Inkjet printing of silver inks onto sintered alumina substrates

Inkjet printing is a digital non-contact method allowing printing of flexible and rigid substrates. Inkjet is a low speed method compared to other printing processes. Printing speed may reach 1 m.s$^{-1}$. Nanoparticles are required in inkjet printing to prevent jet nozzle blocking. Indeed, nozzle diameter generally varies from 10 to 100 $\mu$m. Usually conductive polymers are used for manufacturing electronic pieces by inkjet. Metallic inks formulated with nano-silver, gold, copper or other metals can be also employed for electronic device manufacturing by inkjet printing. This process is used in many electronic applications such as RFID, MEMS, solar cells, chemical and bio-sensors [222].

The aims of this part are:

- optimisation of a silver commercial ink to meet inkjet printing requirements,
- inkjet printing onto sintered alumina tapes,
- determine the optimum sintering temperature allowing to reach the lowest electrical resistivity.

Figure 8.6 shows a synthesis of the inkjet printing applications and the objectives to reach in this work.

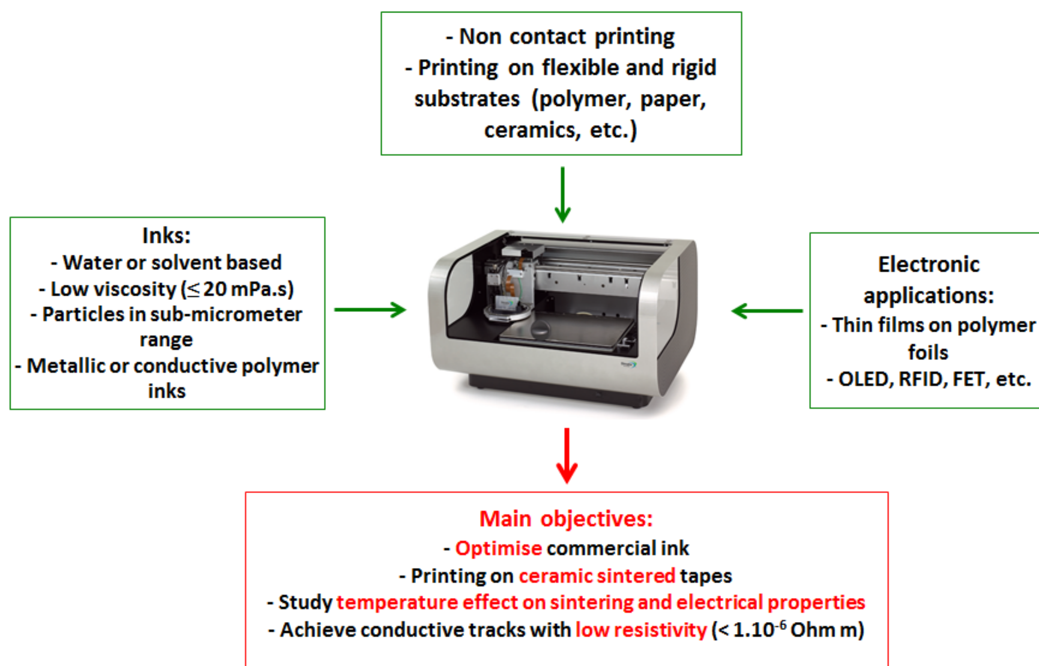


Figure 8.6: Synthesis of inkjet printing and main objectives

### 8.2.1 Inks

A 42% silver nano-suspension with 15 nm mean diameter particles was purchased from Heraeus. This ink was optimised in order to prepare 17 and 21% silver inks. All inks exhibited Newtonian behaviour with viscosities increasing from 2 to 12 mPa.s when silver

content increased from 17 to 42%. Inks surface tension increased from 40 to 54 mN.m$^{-1}$ when silver content decreased from 42 to 17%.

### 8.2.2 The Dimatix inkjet printer

The Fujifilm Dimatix DMP2831 is a laboratory piezoelectric drop on demand inkjet printing with 10 picolitres size cartridge. The nozzle diameter is equal to 21.5 $\mu$m (figure 8.7).

Figure 8.7: The Fujifilm Dimatix DMP2831

### 8.2.3 Encountered problems

The nozzle diameter (21.5 $\mu$m) was too small to allow the commercial nano-suspension (42% silver) printing. When one printing pass was performed, drop spacing was too large to allow particles merging. Thus, three printing layers were required to allow continuous lines printing.

### 8.2.4 Conclusions and perspectives

Inkjet printing of optimised silver ink was performed onto alumina sintered tape. Only three layers were required to reach resistivity value close to that of bulk silver. Adhesion was guaranteed by 100 nm diameter silica and potassium based adhesion agent. An optimum electrical resistivity - 1.7.10$^{-8}$ Ohm.m - was reached at 700°C sintering temperature. At this temperature, adhesion agent was already softened and smooth lines were obtained.

Printing of the same ink could be tested on green LTCC tapes. Sintering should be performed at temperature lower than 800°C for less than 15 minutes. Indeed, 15 nm silver particles decomposition started at temperature higher than 800°C.

Ink viscosity could be decreased to allow easy merging of deposited drops. Printing parameters - voltage, speed, drop spacing - could also be optimised to reach lower resistivity with only one printed layer.

### 8.2.5 Paper 8: Inkjet printing of silver nano-suspensions on ceramic substrates – Sintering temperature effect on electrical properties

**Authors:**
Rita Faddoul, Nadège Reverdy-Bruas, Anne Blayo and Bertine Khelifi

**Published in:**
Microelectronic Engineering - 105 – 31-39 – 2013

**Introduction:** The objective of this study was to investigate the effect of sintering temperature on the electrical properties of silver nanosuspensions printed by inkjet onto sintered alumina tapes. Optimisation of a commercial silver nano-suspension containing 15 nm silver particles was performed by adding water and ethylene glycol to original suspension, in order to reduce viscosity and allow printing through nozzle with small 21.5 $\mu$m diameter.

$1.7.10^{-8}$ Ohm.m minimum resistivity was measured along 14 cm line length after sintering at an optimum temperature of 700°C.

# General conclusion

The present work, which was a part of the European project MULTILAYER, is a contribution to the study of the application of printing techniques to microelectronic devices manufacturing.
The general objectives of the project were to adapt printing processes to the manufacturing of multilayer devices made of ceramic tapes, and more precisely, to develop conductive environmentally friendly inks, adapted for printing onto ceramic tapes and able to withstand ceramics sintering conditions.

While some printing processes, such as screen-printing or inkjet, are already well known for their potential in the context of electronic manufacturing, roll-to-roll techniques have not been systematically tested, yet. In addition, the use of ceramics as printing substrates gives rise to specific printability problems due to the nature of these materials.

One of the main challenges to overcome was to formulate non hazardous ink, made of conductive particles that could withstand high sintering temperature used in sintering process of ceramic microsystems. Another key point was to select conductive particles as well as to fix ink rheology suitable for the four printing processes investigated.

After a characterisation of the ceramics, from a printer's point of view, the present work gave original answers to the challenges proposed by the MULTILAYER project.

The main results are summarised in the following:

**Substrates**

High and low temperature co-fired ceramics were characterised. Their surface properties such as surface energy, pore and particle size were determined in order to select the appropriate ink formulation.
Depending on their composition, tapes exhibited hydrophobic and hydrophilic characters. Thus, to print all the tapes with water-based inks, wetting agents were added to the ink. Green tapes had larger pore sizes than sintered ones. After sintering, tapes had no more pores on surface and it was possible to perform printing with nano-scale particles inks. Inks with larger particles ($> 1\ \mu$m) were preferred to print green tapes.

**Screen printing**

The novelty of this work was the formulation of water-based screen printing pastes. These environmentally friendly inks could replace irritant and toxic solvent-based screen printing commercial pastes.

Rheological behaviour of pastes were studied in order to establish the relationship between tapes rheological properties and line definition. Pastes exhibited shear thinning thixotropic behaviour. A minimum stress value was required to allow ink flowing. Viscosity decreased when shear rate increased. Pastes with very high silver content (75%) exhibited low plastic to elastic modulus ratios. They were very tacky and their flowing through the screen mesh openings was disturbed.

A minimum printing pressure of 5 kg was required to allow maximum silver particles passing through the mesh openings. However, at higher printing loads, plastic to elastic modulus was slightly decreased. This leaded to the material restructuration and consequently to lower deposited thicknesses.

Printing was performed on green LTCC tapes and sintered alumina substrates. Spherical and flake shape particles were tested. It was shown that flake particles allowed to reach lower resistivity values. Furthermore, with flake particles, lines were conductive even before sintering.

Temperature increase leaded to conductivity enhancement. Lines with very low resistivity, 2 to $8.10^{-8}$ Ohm.m, were reached.

**Flexography**

Commercial screen printing paste was optimised in order to meet flexographic inks requirements. Minimum three printing passes were required to reach a minimum line thickness of 1 $\mu$m.

It was shown that with higher silver content and number of deposited layers, lines were able to withstand multilayer LTCC systems sintering conditions, 875°C for 40 minutes. With a fewer number of layers and lower silver content, printed silver lines were conductive after sintering at 850°C for 10 minutes.
Resistivity values as low as 3 to $21.10^{-8}$ Ohm.m were reached.

Flexography printing of metallic inks onto LTCC tapes was tested for the first time in the present study. This promising result shows the huge potential of flexography for the manufacturing of LTCC multilayer systems.

**Rotogravure**

Rotogravure printing potential for ceramic electronic applications was also investigated. Printing of silver inks onto green LTCC substrates was successfully achieved.
It was shown that higher thicknesses were deposited with higher solid contents. Narrower and smoother lines were printed when substrate dispersive to total surface energy ratio decreased. This was attributed to a limited spreading of dispersive low surface tension (12 - 16 $mN.m^{-1}$) inks on these polar substrates.
Maximum deposited line thickness (5.5 $\mu$m) and transferred silver quantity were not enough to allow silver conductive network formation after sintering at 800°C.

**Inkjet**

"Commercial" silver nano-suspension with 15 nm mean diameter particles was optimised for inkjet printing onto sintered alumina tapes. Original paste contained silica and potassium based adhesion agent with 100 nm particle size. Three layers of an ink containing 21% silver were printed.
Temperature effect on electrical properties was studied. An optimum 700°C temperature was required to allow silver and adhesion agent softening. A minimum resistivity of $1.7.10^{-8}$ Ohm.m was reached at this temperature.

Main electrical properties of printed lines are synthesized on table i.

| Process | Substrate | Ink | Sintering | Sintered width | Sintered thickness | Resistivity |
|---|---|---|---|---|---|---|
| Screen printing | Sintered alumina Green LTCC | 70-80% Ag spherical 67-75% Ag flake | 500-900°C - 15 min 875°C - 60 min | 234 to 284 $\mu$m 51 to 493 $\mu$m | 7.7 to 9.9 $\mu$m 1.4 to 6.5 $\mu$m | 2 to $8.10^{-8}$ Ohm.m 2 to $3.10^{-8}$ Ohm.m |
| Flexography | Green LTCC | 30% Ag flake 40% Ag flake | 850°C - 10 min 875°C - 40 min | 156 to 740 $\mu$m 157 to 674 $\mu$m | 1.4 to 3.5 $\mu$m 1.6 to 3.8 $\mu$m | 3 to $12.10^{-8}$ Ohm.m 9 to $21.10^{-8}$ Ohm.m |
| Rotogravure | Green LTCC | 35-55% Ag spherical | 800°C - 10 min | Not continuous | Not continuous | Not conductive |
| Inkjet | Sintered alumina | 21% Ag nano-suspension | 500-900°C - 15 min | 446 to 469 $\mu$m | 0.5 to 1.7 $\mu$m | 2 to $116.10^{-8}$ Ohm.m |

Table i: Synthesis of the most relevant properties of sintered conductive lines

**Suggestions for future work:**

Some questions remained open, and suggestions for future work are proposed:

- thermoelectric inks prepared at CEA (Commissariat à l'Énergie Atomique et aux Énergies Alternatives) will be screen printed in order to fill 300 $\mu$m height and 0.5 mm diameter holes,

- integration of silver tracks screen printed on sintered alumina tapes and allowing radio-frequency transmission is under investigation at Swerea IVF and Omnysis,

- scale up of flexography process onto ceramic tapes will be tested. Silver inks will

be printed onto LTCC and green alumina tapes. This study will be performed in collaboration with KMS and CEA,

- in order to optimise rotogravure printing, larger heights engraved cylinder could be tested in order to allow transferring of higher ink quantity. Flake shape particles could be also used as conductive materials due to their higher surface contact,
- regarding inkjet, ink could be optimised by reducing viscosity and surface tension to allow easy spreading of the ink on the substrate and thus, drop merging even after one layer printing.

This work highlighted the huge potential of printing techniques for the fabrication of micro-electronic devices made of ceramic. It opens perspectives for industrialisation and the mass production of very high conductivity electronics.

# Bibliography


[1] R.S. Khandpur. *Printed Circuit Boards - Design, Fabrication and Assembly.* Mc Graw-Hill - Electronic Engineering, 2005.

[2] P. Ritamaki. Modern radio pioneers: John Sargrove and Paul Eisler. The automatic radio factory and first printed circuits. http://www.qsl.net - accessed on March $8^{th}$ 2012.

[3] R. Das. Printed and potentially printed electronics reach 9.4 billion dollars in 2012. Printed Electronics World - accessed on March $7^{th}$ 2012, 2012.

[4] D. Savastano. Printed electronics: The year in review. Printed Electronics Now - Accessed on March $2^{nd}$ 2012, 2011.

[5] Grant agreement 214122 MULTILAYER project - FP7-NMP-2007 - Annexe I Description of work. MULTILAYER e-doc - internal report, 2008.

[6] MULTILAYER standard presentation. MULTILAYER e-doc - internal report, 2010.

[7] J.-M Haussone. *Céramiques pour l'électronique et l'électrotechnique.* Presses Polytechniques et Universitaires Romandes, 2002.

[8] X. Kuang, G. Carotenuto, and L. Nicolais. A review of ceramic sintering and suggestions on reducing sintering temperatures. *Advanced Performance Materials*, 1997.

[9] G.S. Upadhyaya. Some issues in sintering science and technology. *Materials Chemistry and Physics*, 67:1–5, 2001.

[10] Z. Liu, S. Shao, X. Hu, and X. Wang. Surface modification and microstructure design of alumina ceramics. *Journal of American Ceramic Society*, 94(9):2764 – 2766, 2011.

[11] H. Hahn and R.S. Averback. The production of nanocrystalline powders by magnetron sputtering. *Journal of Applied Physics*, 67:1113 – 1115, 1990.

[12] J.L. Andújar, G. Viera, M.C. Polo, Y. Maniette, and E. Bertran. Synthesis of nanosize Si-C-N powder in low pressure plasmas. *Vacuum*, 52:153 – 156, 1999.

[13] D.-Y. Lee, J.-C. Lee, Y.-S. Shin, S.-E. Park, T.-U. Yu, Y.-J. Kim, and J. Hwang. Structuring of conductive silver line by electrohydrodynamic jet printing and its electrical characterization. *Journal of physics: conference series*, 142, 2008.

[14] T. Kodama, Y. Wada, T. Yamamoto, M. Tsuji, and Y. Tamaura. Synthesis and characterization of ultrafine nickel (II)-bearing ferrites. *Journal of Material Chemistry*, 5:1413–1418, 1995.

[15] Y.-S. Her, E. Matijevi, and M.C. Chon. Preparation of well-defined colloidal barium titanate crystals by the controlled double-jet precipitation. *Materials Research Society*, 17(12):3106 – 3114, 1995.

[16] M. Mott, J.-H. Song, and R.G.J. Evans. Microengineering of ceramics by direct inkjet printing. *Journal of the American Ceramic Society*, 82(7):1653 – 1658, 1999.

[17] J.W. Dennis. Tape casting advanced materials. May 2007.

[18] Encyclopeadia Britannica Online - Accessed on November $20^{th}$ 2011, 1997.

[19] W. Nhuapeng, J. Tontrakoon, and T. Tunkasiri. Distribution of ceramic powder dispersed in 0-3 piezoelectric ceramic–polymer composites and their properties. *CMU Journal*, 1(1):62 – 66, 2002.

[20] B. Thorstensen, M. Le Gall, S. Bredeau, E. Eklund, C. Zeilmann, G. Hagen, and R. Faddoul. High volume production of ceramic thick sheet materials. In *Proceedings of the $8^{th}$ International Conference on Multi-Material Micro Manufacture*, pages 272 – 274, 2011.

[21] M. Lahti, V. Lantto, and S. Leppavuori. Planar inductors on an LTCC substrate realized by the gravure-offset-printing technique. *Components and Packaging Technologies, IEEE Transactions*, 24(4):606 – 610, 2000.

[22] L.J. Golonka. New application of LTCC technology. *$28^{th}$ international spring seminar on electronics technology*, 2005.

[23] Y. Imanaka. *Multilayered Low Temperature Cofired Ceramics (LTCC) Technology.* Springer, 2005.

[24] D. Jang, D. Kim, B. Lee, S. Kim, M. Kang, D. Min, and J. Moon. Nanosized glass frit as an adhesion promoter for ink-jet printed conductive patterns on glass substrates annealed at high temperatures. *Advanced functional materials*, (18):2862–2868, 2008.

[25] F. Habashi. A short history of hydrometallurgy. *Hydrometallurgy*, 79:15 – 22, 2005.

[26] N.P. Bansal. *Handbook of Ceramic Composites.* Kluwer Academic Publishers, 2005.

[27] P. Patnaik. *Handbook of Inorganic Chemicals.* McGraw-Hill, 2002.

[28] E.D. Birdsell, J.-W. Park, and M.G. Allen. Wireless ceramic sensors operating in high temperature environments. Technical report, American Institute of Aeronautics and Astronautics, 2004.

[29] L. Wang and R.V. Kumar. Thick film miniaturized HCl gas sensor. *Sensors and Actuators B*, 98:196 – 203, 2004.

[30] E. Mis, A. Dziedzic, and W. Mielcarek. Thick-film and LTCC microvaristors. In *Electronics Technology, $30^{th}$ International Spring Seminar*, pages 53 – 58, 2007.

[31] F. Loffredo, G. Burrasca, L. Quercia, and D. Della Sala. Gas sensor devices obtained by ink-jet printing of polyaniline suspensions. *Macromolecular Symposia*, 247:357 – 363, 2007.

[32] K. Malecha and L. J. Golonka. Microchannel fabrication process in LTCC ceramics. *Microelectronics Reliability*, 48(6):866 – 871, 2008.

[33] A. Sutono, A.-V.H. Pham, J. Laskar, and W.R. Smith. RF/microwave characterization of multilayer ceramic-based MCM technology. *Advanced Packaging, IEEE Transactions on*, 22(3):326 – 331, 1999.

[34] Y. Wang, G. Zhang, and J. Ma. Research of LTCC/Cu, Ag multilayer substrate in microelectronic packaging. *Materials Science and Engineering B*, 94(1):48 – 53, June 2002.

[35] A.J. Piloto. Integrated passive components: A brief overview of LTCC surface mount and integral options. www.kyocera.com/kai/semiparts/pdfs/imaps99.pdf - accessed on May 2011, 1999.

[36] L.J. Golonka. Technology and applications of low temperature cofired ceramic LTCC based sensors and microsystems. *Bulletin of the Polish Academy of Sciences - Technical Sciences*, 54:221 – 231, 2006.

[37] L.J. Golonka, H. Roguszczak, T. Zawada, J. Radojewski, I. Grabowska, M. Chudy, A. Dybko, Z. Brzozka, and D. Stadnik. LTCC based microfluidic system with optical detection. *Sensors and Actuators B*, 111–112:396 – 402, 2005.

[38] C. S. Martínez-Cisneros, N. Ibánez-García, F. Valdés, , and J. Alonso. Miniaturized total analysis systems: Integration of electronics and fluidics using low-temperature co-fired ceramics. *Analytical Chemistry*, 79(21):8376 – 8380, 2007.

[39] D. Nowak, D. Kulckaz, M. Januskziewicz, and A. Dziezdic. High temperature LTCC package for SiC-based gas sensor. *Optica Applicata*, XXXIX(4):701 – 704, 2009.

[40] M. Massénat. Circuits en couches minces – couches minces traditionnelles. *Techniques de l'Ingénieur*, E3365, 2003.

[41] A.C. Arias, S.E. Ready, R. Lujan, W.S. Wong, K.E. Paul, A. Salleo, M.L. Chabiny, R. Apte, and R.A. Street. All jet-printed polymer thin-film transistor active-matrix backplanes. *Applied Physics Letters*, 85(15):3304 – 3306, 2004.

[42] M. Qian, T. Feng, H. Ding, L. Lin, H. Li, Y. Chen, and Z. Sun. Electron field emission from screen-printed graphene films. *Nanotechnology*, 20:425702 – 6 pp, 2009.

[43] L. Ma, M. Liu, T. Peng, K. Fan, L. Lu, and K. Dai. Fabrication and properties of meso-macroporous electrodes screen-printed from mesoporous titania nanoparticles for dye-sensitized solar cells. *Materials Chemistry and Physics*, 118:477 – 483, 2009.

[44] J. Tellier, B. Malic, D. Kuscer, G.Trefalt, and M. Kosec. Ink-jet printing of $In_2O_3$/ZnO two-dimensional structures from solution. *Journal of American Ceramic Society*, 94(9):2834 – 2840, 2011.

[45] J. Puetz and M.A. Aegerter. Direct gravure printing of indium tin oxide nanoparticle patterns on polymer foils. *Thin Solid Films*, 516(14):4495 – 4501, 2008.

[46] O. Scarlat, S.Mihaiu, Gh. Aldica, J. Groza, and M. Zaharescu. Semiconducting densified $SnO_2$-ceramics obtained by a novel sintering technique. *Journal of the European Ceramic Society*, 24:1049 – 1052, 2004.

[47] F. Xu, X.-F Hu, Y.Niu, J.-H Zhao, and Q.-X. Yuan. In situ observation of grain evolution in ceramic sintering by SR-CT technique. *Transactions of nonferrous metals society of China*, 19:s684 – s688, 2009.

[48] A.M. Guzman, P. Rodriguez, and E. Sereno. Development of AZS refractories for the glass industry. *The AZo Journal of Materials Online*, 2, 2006.

[49] G.C. Kuczynski. Study of the sintering of glass. *Journal of Applied Physics*, 20:1160 – 1163, 1949.

[50] M. Zaharescu, S. Mihaiu, S. Zuca, and K. Matiasovsky. Contribution to the study of $SnO_2$-based ceramics. *Journal of Materials Science*, 26:1666 – 1672, 1991.

[51] J.-F. Yang. Fabrication of low-shrinkage, porous silicon nitride ceramics by addition of a small amount of carbon. *Journal of American Ceramic Society*, 84(7):1639 – 1641, 2001.

[52] P. Jaiban, S. Jiansirisomboon, and A. Watcharapasorn. Densification of $Bi_{0.5}Na_{0.5}ZrO_3$ ceramic using liquid-phase sintering method. *Science Asia*, 37:256 – 261, 2011.

[53] S.J. Park, K. Hirota, and H. Yamamura. Densification of nonadditive $SnO_2$ by hot isostatic pressing. *Ceramic International*, 10(3):115 – 116, 1984.

[54] S.A. Kanade and Vijaya Puri. Electrical properties of thick-film NTC thermistor composed of $Ni_{0.8}Co_{0.2}Mn_2O_4$ ceramic: Effect of inorganic oxide binder. *Materials Research Bulletin*, 43(4):819 – 824, April 2008.

[55] J. Lemaitre and J.-L. Chaboche. *Mécanique des matériaux solides*. Dunod, 2001.

[56] D.J. Green. *An introduction to the mechanical properties of ceramics*. Cambridge University Press, 1998.

[57] G. Kumar and K. N. Prebhu. Review of non-reactive and reactive wetting of liquids on surfaces. *Advances in colloid and interface science*, 133:61 – 89, 2007.

[58] J. Birkenshaw. Printing electronics. In *Pira on printing - England*, 2004.

[59] R. Kisiel, J. Borecki, G. Koziol, and J. Felba. Conductive adhesives for through holes and blind vias metallization. *Microelectronics Reliability*, 45:1935 – 1940, 2005.

[60] M. Allen, C. Lee, B. Ahn, T. Kololuoma, K. Shin, and S. Ko. R2R gravure and inkjet printed RF resonant tag. *Microelectronic engineering*, 88:3293 – 3299, 2011.

[61] H-E. Nilsson, J. Siden, T. Olsson, P. Jonsson, and A. Koptioug. Evaluation of a printed patch antenna for robust microwave RFID tags. *IET Microwaves, Antennas and Propagation*, 1(3):776 – 781, 2007.

[62] R.N. PATEL. Microwave conductivity of thick film conductors. *Electronics Letters*, 6(15):455 – 456, 1970.

[63] R.W. Johnson, P.W. Rich, D.D. Rich, and L.K. Wilson. Advances in thick film conductors for microwave integrated circuits. *Electrocomponent Science and Technology*, 6:215 – 218, 1980.

[64] O. Azucena, J. Kubby, D. Scarbrough, and C. Goldsmith. Inkjet printing of passive microwave circuitry. In *Microwave Symposium Digest IEEE*, pages 1075 – 1078, 2008.

[65] D.J. Adlam and D.E. Woolley. A multiwell electrochemical biosensor for real time monitoring on the behavioural changes of cells in vitro. *Sensors*, 10:3732 – 3740, 2010.

[66] D. Vincenzi, M.A. Butturi, V. Guidi, M.C. Carotta, G. Martinelli, V. Guarnieri, S. Brida, B. Margesin, F. Giacomozzi, M. Zen, G.U. Pignatel, A.A. Vasiliev, and A.P. Pisliakov. Development of a low-power thick-film gas sensor deposited by screen printing technique onto a micromachined hotplate. *Sensors and Actuators B*, 77:95 – 99, 2001.

[67] P. Cooley, D. Wallace, and B. Antohe. Applications of inkjet printing technology to BioMEMS and microfluidic systems. *Journal of the Association for Laboratory Automation*, 7(5):33 – 39, 2002.

[68] C. Liu. Recent developments in polymer MEMS. *Advanced Materials*, 19:3783 – 3790, 2007.

[69] D.A. Pardo, G.E. Jabbour, and N. Peyghambarian. Application of screen printing in the fabrication of organic Light-Emitting devices. *Advanced Materials*, 12(17):1249 – 1252, 2000.

[70] J. Burgin, V. Jubera, H. Debéda, B. Glorieux, A. Garcia, and C. Lucat. Screen-printed phosphor coatings for white led emission. *Journal of Materials Science*, 46:2235 – 2241, 2011.

[71] A. Karwa. *Printing Studies with Conductive Inks and Exploration of New Conducting Polymer Compositions*. PhD thesis, Rochester Institute of Technology , New York, 2006. Master of Science in Materials Science and Engineering.

[72] A. Denneulin. *Inkjet printing of conductive inks for RFID technology: Influence of substrate, ink and process*. PhD thesis, Grenoble INP, 2010.

[73] D. R. Gamota, P. Brazis, K. Kalyanasundaram, and J. Zhang. *Printed organic and molecular electronics*. Kluwer academic publisher, 2004.

[74] J.R. Larry, R.M. Rosenberg, and R.O. Uhler. Thick film technology: An introduction to the materials. In *IEEE transactions on components, hybrids, and manufacturing technology*, volume CHMT - 3(2), page 211 – 225, 1980.

[75] L. Gonzalez-Macia, A. Morrin, M.R. Smyth, and A.J. Killard. Advanced printing and deposition methodologies for the fabrication of biosensors and biodevices - critical review. *The Royal Society of Chemistry - Analyst*, 135:845 – 867, 2010.

[76] C.L. Feng, A. Embrechts, I. Bredebusch, J. Schnekenburger, W. Domschke, G.J. Vancso, and H. Schönherr. Reactive microcontact printing on block copolymer films: Exploiting chemistry in microcontacts for sub-micrometer patterning of biomolecules. *Advanced Materials*, 19:286 – 290, 2007.

[77] R.J. Jackman, S.T. Brittain, and G.M. Whitesides. Microstructures. Access Science - accessed on November $15^{th}$ 2011, 2000.

[78] Y.-L Loo, R.L. Willett, K.W. Baldwin, and J.A. Rogers. Additive, nanoscale patterning of metal films with a stamp and a surface chemistry mediated transfer process: Applications in plastic electronics. *Applied Physics Letters*, 81:562 – 564, 2002.

[79] L.J. Guo. Nanoimprint lithography: Methods and material requirements. *Advanced Materials*, 19:495 – 513, 2007.

[80] S.Y. Chou, P.R. Krauss, and P.J. Renstrom. Imprint of sub-25 nm vias and trenches in polymers. *Applied Physics Letters*, 67:3114 – 3116, 1998.

[81] T. Glinsner, G. Kreindl, and M. Kast. Nanoimprint lithography - The technology makes its mark on CMOS image sensors and in the nano-world. *Optik and Photonik*, 2:42 – 45, 2010.

[82] R.D. Piner, J. Zhu, F. Xu, S. Hong, and C.A. Mirkin. “Dip-pen” nanolithography. *Science*, 283:661 – 663, 1999.

[83] G. Lu, X. Zhou, H. Li, Z. Yin, B. Li, L.Huang, F. Boey, and H. Zhang. Nanolithography of single-layer graphene oxide films by atomic force microscopy. *American Chemical Society*, 26(9):6164 – 6166, 2010.

[84] D.L. Wilson, R. Martin, S. Hong, M. Cronin-Golomb, C.A. Mirkin, , and D.L. Kaplan. Surface organization and nanopatterning of collagen by dip-pen nanolithography. In *Proceedings of the National Academy of Sciences of the United States of America*, volume 98, pages 13660 – 13664, 2001.

[85] H. Zhang, S.-W. Chung, and C.A. Mirkin. Fabrication of sub-50-nm solid-state nanostructures on the basis of dip-pen nanolithography. *Nano Letters*, 3(1):43 – 45, 2003.

[86] J.E. Bjorkholm. EUV lithography — the successor to optical lithography? *Intel Technology Journal*, Q3:1 – 8, 1998.

[87] X.M. Yang, R.D. Peters, T.K. Kim, and P.F. Nealey. Patterning of self-assembled monolayers with lateral dimensions of 0.15 $\mu$m using advanced lithography. *Journal of Vacuum Science Technology B*, 17(6):3203 – 3207, 1999.

[88] L. Pain, B. Icard, S. Manakli, J. Todeschini, B. Minghetti, V. Wang, and D. Henry. Transitioning of direct e-beam write technology from research and development into production flow. *Microelectronic Engineering*, 83:749 – 753, 2006.

[89] P.M. Harrey, P.S.A. Evans, B.J. Ramsey, and D. Harrison. A novel manufacturing process for capacitors using offset lithography. In *Environmentally Conscious Design and Inverse Manufacturing Proceedings*, pages 842 – 846, 1999.

[90] D.T. Chiu, N. Li Jeon, S. Huang, R.S. Kane, C.J. Wargo, I.S. Choi, D.E. Ingber, and G.M. Whitesides. Patterned deposition of cells and proteins onto surfaces by using three-dimensional microfluidic systems. In *Proceedings of the National Academy of Sciences*, volume 97, pages 2408 – 2413, 2000.

[91] A. Ruiz, L. Buzanska, D. Gilliland, H. Rauscher, L. Sirghi, T. Sobanski, M. Zychowicz, L. Ceriotti, F. Bretagnol, S. Coecke, P. Colpo, and F. Rossi. Micro-stamped surfaces for the patterned growth of neural stem cells. *Biomaterials*, 29:4766 – 4774, 2008.

[92] M.D. Austin and S.Y. Chou. Fabrication of 70 nm channel length polymer organic thin-film transistors using nanoimprint lithography. *Applied Physics Letters*, 81(33):4431 – 4433, 2002.

[93] Y. Sun and S.R. Forrest. Organic light emitting devices with enhanced outcoupling via microlenses fabricated by imprint lithography. *Journal of Applied Physics*, 100:073106, 6 pp, 2006.

[94] H. Kipphan. *Handbook of print media.* Springer, 2001.

[95] R.H. Leach and R.J. Pierce. *The ink print manual.* Kluwer Academic Pub, 1993.

[96] A. Huebler, U. Hahn, W. Beier, N. Lasch, and T. Fischer. High volume printing technologies for the production of polymer electronic structures. *IEEE Polytronic Conference*, pages 172 – 176, 2002.

[97] P.S.A. Evans, P.M. Harrey, B.J. Ramsey, and D.J. Harrison. RF circulator structures via offset lithography. *Electronics Letters*, 35(19):1634 – 1636, 1999.

[98] W. Appleton. *Pira reviews of printing - Screen printing.* Pira, 1997.

[99] J. Dierig. Choosing a woven wire screen for top separation performance. Technical report, Powder and bulk engineering, 2006.

[100] J. Stephens. *Screen Printing Process.* BLUEPRINT, $2^{nd}$ edition, 1996.

[101] W. Yin, D.-H. Lee, J. Choi, C. Park, and S. Min Cho. Screen printing of silver nanoparticle suspension for metal interconnects. *Korean journal of chemistry engineering*, 25(6):1358 – 1361, 2008.

[102] G.J. Wright and J.A. Yeomans. The influence of screen-printing parameters on the microstructure and gas permeance of a zirconia electrolyte. *Journal of the European Ceramic Society*, 28:779 – 785, 2008.

[103] M.-Y. Lee, M.-W. Lee, J.-E. Park, J.-S. Park, and C.-K. Song. A printing technology combining screen-printing with a wet-etching process for the gate electrodes of organic thin film transistors on a plastic substrate. *Microelectronic Engineering*, 87:1922 – 1926, 2010.

[104] D. Buzby and A. Dobie. Fine line screen printing of thick film pastes on silicon solar cells. *Hereaus - White Papers*, February 2011.

[105] J. Pan, G.L. Tonkay, and A. Quintero. Screen printing process design of experiments for fine line printing of thick film ceramic substrate. digitalcommons.calpoly.edu - accessed on june 2010, 1999.

[106] S.M. Shapee, R. Alias, A. Ibrahim, Z. Ambak, M.Z.M. Yussof, and M.R. Saad. Screen printing parameters effect on surface roughness measurement of printed gold paste on LTCC tape. *Key Engineering Materials*, 421 - 422:485 – 489, 2010.

[107] H. Baudry. Détecteurs, capteurs et transducteurs céramiques sérigraphiés. *L'industrie Céramique*, 885:834 – 838, 1990.

[108] R. Parashkov, E. Becker, T. Riedl, H.-H. Johannes, and W. Kowalsky. Large area electronics using printing methods. In *Proceedings of the IEEE*, volume 93, pages 1321 – 1329, 2005.

[109] A. Sanson, E. Mercadelli, E. Roncari, R. Licheri, R. Orru, G. Cao, E. Merlone-Borla, D. Marzorati, A. Bonavita, G. Micali, and G. Neri. Influence of processing parameters on the electrical response of screen printed $SrFe_{0.6}Ti_{0.4}O_{3-\delta}$. *Journal of the European Ceramic Society*, 24:1049 – 1052, 2010.

[110] A.A. Yussuf, I. Sbarski, M. Solomon, N. Tran, and J.P. Hayes. Sealing of polymeric-microfluidic devices by using high frequency electromagnetic field and screen printing technique. *Journal of Materials Processing Technology*, 189(1-3):401 – 408, 2007.

[111] Z.Bao, Y. Feng, A. Dodabalapur, V.R. Raju, and A.J. Lovinger. High-performance plastic transistors fabricated by printing techniques. *Chemistry of Materials*, 9:1299 – 1301, 1997.

[112] R. Reicher, W. Smetana, J.C. Schuster, and A. Adla$\beta$nig. A fritless copper conductor system for power electronic applications. *Microelectronics Reliability*, 41(4):491 – 498, 2001.

[113] H. Wang, J. Guo, J. Li, and J. Wei. Fabrication of bimetallic nanoparticles/multi-walled carbon nanotubes composites for microelectronic circuits. *Carbon*, 49:779 – 786, 2011.

[114] M. Pudas, N. Halonen, P. Granat, and J. Vahakangas. Gravure printing of conductive particulate polymer inks on flexible substrates. *Progress in Organic Coatings*, 54(4):310 – 316, 2005.

[115] R.H. Leach. *The ink print manual.* Van Nostrand Reinhold (International), $4^{th}$ edition, 1988.

[116] M. Neidert, W. Zhang, D. Zhang, and A. Kipka. Screen-printing simulation study on solar cell front side silver paste. Conference – PVSC – Hereaus-voltaics.com - accessed on June 2011, 2008.

[117] T.-X. Liang, W.Z. Sun, Y.H. Wang, and H.-D. Li. Effect of surface energies on screen printing resolution. *IEE transactions on components, packaging, and manufacturing technology – Part B*, 19(2):423 – 426, 1996.

[118] S.B. Rane, P.K. Khanna, T. Seth, G.J. Phatak, D.P. Amalnerkar, and B.K. Das. Firing and processing effects on microstructure of fritted silver thick film electrode materials for solar cells. *Materials Chemistry and Physics*, 82(1):237 – 245, 2003.

[119] S. Merilampi, T. Laine-Ma P., and Ruuskanen. The characterization of electrically conductive silver ink patterns on flexible substrates. *Microelectronics reliability*, (49):782 – 790, 2009.

[120] E.A. Apps. *Ink technology for printers and students*. Leonard Hill - London, 1963.

[121] A.M. Wells. *Printing inks - Recent developments*. Noyes Data Corporation, 1976.

[122] D.C. Bould, T.C. Claypole, and M.F.J. Bohan. An investigation into plate deformation in flexographic printing. In *Proceedings of Institution of Mechanical Engineering IMech*, volume 218 - B, pages 1499 – 1511, 2004.

[123] M.S. Yusof, A.M.A. Zaidib, T.C. Claypole, and D.T. Gethin. The effects of printing plate on the reproduction of fine solid line printing in flexography. In *Printing Future Days - 2nd International Student Conference on Print and Media Technology*, pages 214 – 218, 2007.

[124] D. Lochun, E. Zeira, and R. Menize. Reel-to-reel manufacturability of flexible electrical interconnects and radio-frequency identification structures. In *IEEE Proceeding of Electronic Components and Technology Conference*, pages 686 – 689, 2002.

[125] R.C. Kattumenu. *Flexography printing of silver based conductive inks on packaging substrates*. PhD thesis, Faculty of The Graduate College - Department of Paper Engineering, Chemical Engineering and Imaging, 2008.

[126] T. Unander and H.-E. Nilsson. Characterization of printed moisture sensors in packaging surveillance applications. *IEEE Sensors Journal*, 9(8):922 – 928, 2009.

[127] D. Deganello, J.A. Cherry, D.T. Gethin, and T.C. Claypole. Patterning of microscale conductive networks using reel-to-reel flexographic printing. *Thin Solid Films*, 518:6113 – 6116, 2010.

[128] A. Blayo. Formulation des encres pour l'impression. Techniques de l'ingénieur - J2290, 2007.

[129] D. Sung, A. de la FuenteVornbrock, and V. Subramanian. Scaling and optimization of gravure-printed silver nanoparticle lines for printed electronics. In *IEEE Transactions on Components and Packaging Technologies*, volume 33, pages 105 – 114, 2010.

[130] J. Noh, D. Yeom, C. Lim, H. Cha, J. Han, J. Kim, Y. Park, and V. Subramanian. Scalability of roll-to-roll gravure printed electrodes on plastic foils. In *IEEE Transactions on Electronics Packaging Manufacturing*, volume 33, pages 275 – 283, 2010.

[131] M. Jung, J. Kim, J. Noh, N. Lim, C. Lim, G. Lee, J. Kim, H. Kang, K. Jung, A.D. Leonard, J.M. Tour, and G. Cho. All-printed and roll-to-roll-printable 13.56-MHz-operated 1-bit RF tag on plastic foils. In *IEEE Transactions on Electronic Devices*, volume 57, pages 571 – 580, 2010.

[132] J.B. Blum. Ink jet printing for high-frequency electronic applications. Printed circuit design and fab - accessed on february 2011, 2007.

[133] J. Moon, J.E. Grau, V. Knezevic, M.J. Cima, and E.M. Sachs. Inkjet printing of binders for ceramic components. *Journal of the American Ceramic Society*, 85(4):755 – 762, 2002.

[134] R.M. Meixner, D. Cibis, K. Krueger, and H. Goebel. Characterization of polymer inks for drop-on demand printing systems. *Microsystem Technology*, (14):1137 – 1142, 2008.

[135] E. Tekin, P.J. Smith, and U.S. Schubert. Inkjet printing as a deposition and patterning tool for polymers and inorganic particles. *Soft Matter*, 4:703 – 713, 2008.

[136] G. Percin, S.T. Lundgren, and T. Butrus. Controlled inkjet printing and deposition of organic polymers and solid particles. *Applied Physics Letters*, 73(16):2375, 1998.

[137] S. Molesa, D. Redinger, D. Huang, and V. Subramanian. High-quality inkjet printed multilevel interconnects and inductive components on plastic for ultra-low cost RFID applications. *Materials Research Society Symposium*, 769:H831 – H836, 2003.

[138] Y. Liu, K. Varahramyan, and T. Cui. Low-voltage all-polymer field-effect transistor fabricated using an inkjet printing technique. *Micromolecular Rapid Communications*, 26:1955 – 1959, 2005.

[139] F. Villani, P. Vacca, G. Nenna, O. Valentino, G. Burrasca, T. Fasolino, C. Minarini, and D. della Sala. Inkjet printed polymer layer on flexible substrate for oled applications. *Journal of Physical Chemistry C*, 113:13398 – 13402, 2009.

[140] D. Soltman and V. Subramanian. Inkjet-printed line morphologies and temperature control of the coffee ring effect. *American Chemical Society*, 24:2224 – 2223, 2008.

[141] R. D. Deegan, O. Bakajin, T. F. Dupont, G. Huber, S. R. Nagel, and T. A. Witten. Capillary flow as the cause of ring stains from dried liquid drops. *Nature*, 389:827–829, 1997.

[142] J.E. Fromm. Numerical calculation of the fluid dynamics of drop-on-demand jets. *IBM Journal of Research and Development*, 28(3):322 – 333, 1984.

[143] A. Blayo and B. Pineaux. Printing processes and their potential for RFID printing. *ACM International Conference Proceeding Series*, 121:27 – 30, 2005.

[144] J. Mei. *Formulation and processing of conductive inks for inkjet printing of electrical components*. PhD thesis, School of Engineering, 2004.

[145] S.F. Wang, J.P. Dougherty, W. Huebner, and J.G. Pepin. Silver-Palladium thick film conductors. *Journal of the American Ceramic Society*, 77(12):3051 – 3072, 1994.

[146] I. Sondi, D.V. Goia, and E. Matijevi. Preparation of highly concentrated stable dispersions of uniform silver nanoparticles. *Journal of Colloid and Interface Science*, 260(1):75 – 81, 2003.

[147] E. Tamjid and B.H. Guenther. Rheology and colloidal structure of silver nanoparticles dispersed in diethylene glycol. *Powder Technology*, 197(1-2):49 – 53, 2010.

[148] O.A. Yeshchenko, I.M. Dmitruk, A.A. Alexeenko, and A.M. Dmytruk. Size-dependent melting of spherical copper nanoparticles embedded in a silica matrix. *Physical Review B*, (8):085434, 2007.

[149] L. Hackspill, J. Besson, and A. Herold. *Chimie minérale II.* Presses universitaires de France, $2^{nd}$ edition, 1968.

[150] C.D. Hodgman, E.C. Weast, and S.M. Selby. *Hanbook of chemistry and physics.* Chemical rubber publishing, $40^{th}$ edition, 1958.

[151] H.N. Naguib and B.K. MacLaurin. Silver migration and the reliability of pd/ag conductors in thick-film dielectric crossover structures. In *IEEE Transactions on Components, Hybrids, and Manufacturing Technology*, volume CHMT-2, page 196 – 206, 1979.

[152] M. Yamamoto, H. Kakiuchi, Y. Kashiwagi, Y. Yoshida, T. Ohno T., and M. Nakamoto. Synthesis of ag-pd alloy nanoparticles suitable as precursors for ionic migration-resistant conductive film. *Bulletin of the Chemical Society of Japan*, 83(11):1386 – 1391, 2010.

[153] K. Vu. Silver migration – The mechanism and effects on thick-film conductors. Technical report, College of Engineering – Chemical and Material Science Engineering Department - San Jose State University, 2003.

[154] M. Pudas, J. Hagberg, and S. Leppävuori. Roller-type gravure offset printing of conductive inks for high-resolution printing on ceramic substrates. *International Journal of Electronics*, 92(5):251 – 269, 2005.

[155] A.R. Rogers, Z. Bao, A. Makhija, and P. Braun. Printing process suitable for reel-to-reel production of high-performance organic transistors and circuits. *Advanced materials*, 11(9):741 – 745, 1999.

[156] Copper applications technology roadmap. International Copper Association, March 2011.

[157] B.C. Sales and M.B. Maple. Oxidation of nickel in the vicinity of its curie temperature. *Physical review letters*, (39):1636 – 1639, 1977.

[158] D. Li, D. Sutton, A. Burgess, D. Graham, and P.D. Calvert. Conductive copper and nickel lines via reactive inkjet printing. *Journal of Materials Chemistry*, 19(22):3719, 2009.

[159] B. Fischer, A. Behrends, D. Freund, D.F. Lupton, and J. Merker. High temperature mechanical properties of the platinum group metals. *Platinum metals review*, 43(1):18 – 28, 1999.

[160] N.R. Bieri, J. Chung, S.E. Haferl, D. Poulikakos, and C.P. Grigoropoulos. Microstructuring by printing and laser curing of nanoparticle solutions. *Applied Physics Letters*, 82(20):3529 – 3531, 2003.

[161] S.K. Tiwari. *Nickel Nanoparticles-Assisted Diffusion Brazing of Stainless Steel 316 for Microfluidic Applications.* PhD thesis, http://hdl.handle.net/1957/14996, 2010.

[162] A. Loiseau, O. Launois, S. Roche, and J.-P. Salvetat. *Understanding carbon nanotubes: from basics to application, Lecture notes in physics.* Springer, 2006.

[163] C.A. Jacobson. *Encyclopaedia of Chemical Reactions*, volume 2. Reinhold Publishing Corporation, 1948.

[164] Z. Nie, C.A. Nijhuis, J. Gong, X. Chen, A. Kumachev, A.W. Martinez, M. Narovlyansky, and G.M. Whitesides. Electrochemical sensing in paper-based microfluidic devices. *Lab on a Chip*, 10(4):477, 2010.

[165] P.W. Bless, R.L. Wahlers, and S.JJ. Stein. Application of glasses in thick film technology. *The American Ceramic Society - Ceramic Transactions*, (20):397 – 417, 1990.

[166] T.T. Hitch. Adhesion, phase morphology, and bondability of reactively-bonded and frit-bonded gold and silver thick-film conductors. *Journal of Electronic Materials*, 3(22):554 – 577, 1974.

[167] Z. Liu and D.D.L. Chung. Comparative study of electrically conductive thick films with and without glasses. *Journal of Electronic Materials*, 33(3):194 – 202, 2004.

[168] J.C. Lin and C.Y. Wang. Effect of surface properties of silver powder on the sintering of its thick film conductor. *Materials Chemistry and Physics*, (45):253 – 261, 1996.

[169] B.Y. Tay and M.J. Edirisinghe. Dispersion and stability of silver inks. *Journal of Material Science*, (37):4653 – 4661, 2002.

[170] J. Bicerano. *Prediction of Polymer Properties.* Marcel Dekker, Inc., $3^{rd}$ edition, 2002.

[171] J.W. Goodwin and R.W. Hughes. *Rheology for Chemists: An Introduction.* Royal Society of Chemistry, 2008.

[172] J. Scher. Rhéologie, texture et texturation des produits alimentaires. *Techniques de l'Ingénieur - F3300V2*, 1998.

[173] N. Midoux. *Mécaniques et Rhéologie des Fluides en Génie Chimique.* ENSIC – Tec and Doc, 1993.

[174] H.A. Barnes, J.F. Hutton, and K. Walters. *An Introduction to Rheology.* Elsevier Science Pub, 1989.

[175] T. Maeder. Introduction aux pâtes/encres de sérigraphie en technologie des couches épaisses. Technical report, Laboratoire de production microtechnique (LPM) – Ecole Polytechnique Fédérale de Lausanne, 2008.

[176] M. Lahti and V. Lantto. Passive RF band-pass filters in an LTCC module made by fine-line thick film pastes. *Journal of the European Ceramic Society*, (21):1997 – 2000, 2001.

[177] S. Jagtap, V. Deshpande, V. Rane, S. Rane, G. Phatak, and D. Amalnerkar. In-house development of co-fireable thick film silver conductor for LTCC applications. *Journal of Materials Science: Materials in Electronics*, 19:522 – 527, 2008.

[178] A. Denneulin, J. Bras, A. Blayo, B. Khelifi, F. Roussel-Dherbey, and C. Neuman. The influence of carbon nanotubes in inkjet printing of conductive polymer suspensions. *Nanotechnology*, 20(38):385701, 2009.

[179] M.M. Voigt, A. Guite, D.-Y. Chung, R.U.A. Khan, A.J. Campbell, D.D.C. Bradley, F. Meng, J.H.G. Steinke, S. Tierney, I. McCulloch, H. Penxten, L. Lutsen, O. Douheret, J. Manca, U. Brokmann, K. Sönnichsen, D. Hülsenberg, W. Bock, C. Barron, N. Blanckaert, S. Springer, J. Grupp, and A. Mosley. Polymer field-effect transistors fabricated by the sequential gravure printing of polythiophene, two insulator layers, and a metal ink gate. *Advanced Functional Materials*, 20:239 – 246, 2010.

[180] P.A. Tipler and G. Mosca. *Electricity and magnetism, light and elementary modern physics.* New York - Freeman, 2004.

[181] T. Neffati. *Electricité Générale – Analyse et Synthèse des Circuits.* Dunod, 2008.

[182] E. Karmazsin. Thermoconductimétrie du solide. Techniques de l'ingénieur - P1300, 2001.

[183] R.C. Jaeger. *Introduction to microelectronic fabrication.* Upper Saddle River, NJ, Prentice Hall, 2002.

[184] L. Solymar and D. Walsh. *Electrical properties of materials.* Oxford University Press, October 2009.

[185] G.L. Ragan, editor. *Microwave Transmission Circuits.* McGraw Gill Book Company, 1948.

[186] C.R. Clayton. *Introduction to Electromagnetic Compatibitily.* Wiley Series in Microwave and Optical Engineering, 1992.

[187] I. Gresham, N. Jain, T. Budka, A. Alexanian, N. Kinayman, B. Ziegner, S. Brown, and P. Staecker. A compact manufacturable 76–77-GHz radar module for commercial ACC applications. In *IEEE Transactions on Microwave Theory and Techniques*, volume 49, pages 44 – 58, 2001.

[188] A. Bolle and A. Nascimbene. Microwave transmission in mobile networks. *Ericsson Review*, 3:124 – 131, 2002.

[189] L. Chai, M. Moroz, A. Shaikh, and V. Stygar. Effect of conductor surface roughness and geometry on microwave loss. Technical report, Ferro Electronic Materials, 2001.

[190] G. Shaker, S. Safavi-Naeini, N. Sangary, and M.M. Tentzeris. Inkjet printing of ultrawideband (UWB) antennas on paper-based substrates. In *IEEE Antennas and Wireless Propagation Letters*, volume 10, pages 111 – 114, 2011.

[191] G.S. Nolas, J. Sharp, and H.J. Goldsmith. *Thermo-electrics Basic Principles and New Materials Development.* Springer, 2001.

[192] G.J. Snyder and E.S. Toberer. Complex thermoelectric materials. *Nature Materials*, 7:105 – 114, 2008.

[193] W. Lee, M.Y. Park, S.H. Cho, J. Lee, C. Kim, G. Jeong, and B.W. Kim. Bidirectional WDM-PON based on gain-saturated reflective semiconductor optical amplifiers. *Photonics Technology Letters, IEEE*, 17(11):2460 – 2462, 2005.

[194] J.C. Bass, N.B. Elsner, and F.A. Leavitt. Performance of the 1 kW thermoelectric generator for diesel engines. In *13th International Conference on Thermoelectrics*, pages 295 – 297, 1994.

[195] J. Yang. Potential applications of thermoelectric waste heat recovery in the automotive industry. In *24th International Conference on Thermoelectrics*, pages 170 – 174, 2005.

[196] W. Shin, M. Matsumiya, N. Izu, and N. Murayama. Hydrogen-selective thermoelectric gas sensor. *Sensors and Actuators B*, 93:304 – 308, 2003.

[197] J. Weber, K. Potje-Kamloth, F. Haase, P. Detemple, F. Völklein, and T. Doll. Coin-size coiled-up polymer foil thermoelectric power generator for wearable electronics. *Sensors and Actuators A*, 132:325 – 330, 2006.

[198] C. Navone, M. Soulier, M. Plissonier, and A.L. Seiler. Development of $(Bi,Sb)_2(Te,Se)_2$-based thermoelectric modules by a screen-printing process. *Journal of Electronic Materials*, 39(9):1755 – 1759, 2006.

[199] The automotive market research store. http://www.just-auto.com/ - accessed on January 2012.

[200] T. Teutsch, R.G. Blankenhorn, and E. Zakel. Lead-free solder bumping process for high temperature automotive application. In *53rd Electronic Components and Technology Conference*, pages 1468 – 1471, 2003.

[201] J. Riegel, H. Neumann, and H.-M. Wiedenmann. Exhaust gas sensors for automotive emission control. *Solid State Ionics*, 152-153:783 – 800, 2002.

[202] A.A. Bergh. Blue laser diode (LD) and light emitting diode (LED) applications. *Physica Status Solidi (a)*, 201(12):2740 – 2754, 2004.

[203] J. Kloeser, K. Heinricht, K. Kutzner, E. Jung, A. Ostmann, and H. Reichl. Fine pitch stencil printing of Sn/Pb and lead free solders for flip chip technology. In *IEEE Transactions on Components, Packaging, and Manufacturing Technology - C*, volume 21, pages 41 – 50, 1998.

[204] E. Billi, J.-P. Viricelle, L. Montanaro, and C. Pijolat. Development of a protected gas sensor for exhaust automotive applications. *IEEE Sensors Journal*, 2(4):342 – 348, 2002.

[205] G. Neri, A. Bonavita, G. Micali, G. Rizzo, E. Callone, and G. Carturan. Resistive CO gas sensors based on $In_2O_2$ and $InSno_x$ nanopowders synthesized via starch aided sol-gel process for automotive applications. *Sensors and Actuators B*, 132:224 – 233, 2008.

[206] J.R. Stetter, W.R. Penrose, and S. Yao. Sensors, chemical sensors, electrochemical sensors, and ECS. *Journal of The Electrochemical Society*, 150(2):S11 – S16, 2003.

[207] Z. Yang, H. Goto, M. Matsumoto, and R. Maeda. Active micromixer for microfluidic systems using lead-zirconate-titanate (PZT)– generated ultrasonic vibration. *Electrophoresis*, (21):116 – 119, 2002.

[208] E.I. Gill, A. Arshak, K. Arshak, and O. Korostynska. Investigation of thick-film polyaniline-based conductimetric ph sensors for medical applications. *IEEE Sensors Journal*, 9(5):555 – 562, 2009.

[209] T. Wang, C. Cook, and B. Derby. Fabrication of a glucose biosensor by piezoelectric inkjet printing. In *Third International Conference on Sensor Technologies and Applications*, pages 82 – 85.

[210] K.W. Jones, Y. Liu, B. Larsen, P. Wang, and M. Zampino. Chemical, structural, and mechanical properties of the LTCC tapes. *The International Journal of Microcircuits and Electronic Packaging*, 23(4):469 – 473, 2000.

[211] B. Raphet. Etats de surface - caractérisation. *Techniques de l'ingénieur - R1230*, 2008.

[212] T. Hu, H. Jantunen, U. Ususmaki, and S. Leppavuori. BST powder sol-gel in tape casting and firing. *Journal of European Ceramic Society*, 24:1111 – 1116, 2004.

[213] V. Vozdecky and A. Roosen. Direct tape casting of nanosized $Al_2o_3$ slurries derived from autogenous nanomilling. *Journal of American Ceramic Society*, 95(5):1313 – 1319, 2010.

[214] D.K. Owens and R.C. Wendt. Estimation of the surface free energy of polymers. *Journal of Applied Polymer Science*, 13(8):1741 – 1747, 1969.

[215] B. Magee. *Screen printing primer.* Graphics Arts Technical Foundation - USA, 1985.

[216] T. Björninen, S. Merilampi, L. Ukkonen, P. Ruuskanen, and L. Sydänheimo. Performance comparison of silver ink and copper conductors for microwave applications. In *Microwaves, Antennas and Propagation, IET (IEEE)*, volume 4, pages 1224 – 1231, 2010.

[217] G. Allen. The future of flexography and lithography in printed electronics. www.nanomarkets.net, 2007 - Accessed on February $6^{th}$ 2012.

[218] D.C. Mulvihill. *Flexography primer.* The Graphic Arts Technical Foundation Series on Printing Processes, 1985.

[219] E. Hrehorova, M. Rebros, A. Pekarovicova, B. Bazuin, A. Ranganathan, S. Garner, G. Merz, J. Tosch, and R. Boudreau. Gravure printing of conductive inks on glass substrates for applications in printed electronics. *Journal of Display Technology*, 7(6):318 – 324, 2011.

[220] T. Mäkelä, S. Jussila, M. Vilkman, H. Kosonen, and R. Korhonen. Roll-to-roll method for producing polyaniline patterns on paper. *Synthetic Metals*, 135-136:41–42, 203.

[221] P. Harrop. Flexo vs gravure. Printed Electronics World - accessed on March $3^{rd}$ 2012, 2006.

[222] L. Hakola. Benefits of inkjet printing for printed electronics. Pira Printed Electronics, 2005.

[223] L. Lavielle. *La mouillabilité*, volume 14. Annales de physique, 1989.

[224] S. Bux, J.-P. Fleurial, R. Blair, P. Gogna, T. Caillat, and R. Kaner. High temperature thermoelectric properties of nano-bulk silicon and silicon germanium. *Materials Research Society*, (1166):1166–N02–04, 2009.

[225] T.C. Harman and J.M. Honig. *Thermoelectric and Thermomagnetic Effects and Applications*. McGraw-Hill, 1967.

[226] H. Obara, S. Higomo, M. Ohta, A. Yamamoto, K. Ueno, and T. Iida. Thermoelectric properties of $Bi_2Te_3$ based thin films with fine grains fabricated by pulsed laser deposition. *Japanese Journal of Applied Physics*, 48(No. 8):085506, 2009.

[227] M. Scheele, N. Oeschlet, K. Meier, A. Kornowski, C. Klinke, and H. Weller. Synthesis and thermoelectric characterization of $Bi_2Te_3$ nanoparticles. *Advanced Functional Materials*, (19):3476 – 3483, 2009.

[228] P. Markowski and A. Dziedzic. Planar and three-dimensional thick-film thermoelectric microgenerators. *Microelectronics Reliability*, (48):890 – 896, 2008.

[229] P. Markowski, L. Straszewski, and A. Dziedzic. Sandwich-type three-dimensional thick-film thermoelectric microgenerators. In *Electronics Technology - ISSE - 31$^{st}$ International Spring Seminar*, pages 404 – 408, 2008.

[230] G. Savelli. *Etude et développement de composants thermoélectriques á base de couches minces*. PhD thesis, Joseph Fourrier University - Grenoble, 2007.

[231] M. Wagner. *Simulation of Thermoelectric Devices*. PhD thesis, Technischen Universitt́ Wien Fakultät für Elektrotechnik und Informationstechnik von, 2007.

[232] B.A. Cook, B.J. Beaudry, J.L. Harringa, and W.J. Barnett. The preparation of SiGe thermoelectric materials by mechanical alloying. In *Energy Conversion Engineering Conference, IECEC-89 Proceedings of the 24th Intersociety*, volume 2, pages 693–700, 1989.

[233] D.-Y. Chung, T. Hogan, P. Brazis, M. Rocci-Lane, C. Kannewurf, M. Bastea, C. Uher, and M.G. Kanatzidis. $CsBi_4Te_6$: A high-performance thermoelectric material for low-temperature applications. *Science*, (287):1024 – 1027, 2000.

[234] M. Strasser, R. Aigner, M. Franosch, and G. Wachutka. Miniaturized thermoelectric generators based on poly-si and poly-sige surface micromachining. *Sensors and Actuators A*, 97 - 98:535 – 542, 2002.

[235] G. Zeng, J.-H. Bahk, J.E. Bowers, H. Lu, A.C. Gossard, S.L. Singer, A. Majumdar, Z. Bian, M. Zebardji, and A. Shakouri. Thermoelectric power generator module of 16 x 16 bi2te3 and 0.6% eras:(ingaas)1-x(inalas)x segmented elements. *Applied physics letters*, (95):083503–1 – 083503–3, 2009.

# Annexes

# Annexe 1 - Substrates properties

## Mechanical properties

### Elastic modulus

When a material is exposed to a force $F$, it lengthens by $\Delta L$. Stress is defined as the ratio of force to section and strain is the ratio of displacement to original length (equations 8.1 and 8.2).

$$\tau = \frac{F}{A} \tag{8.1}$$

$$\epsilon = \frac{\Delta L}{L_0} \cdot 100 \tag{8.2}$$

Where:

- $\tau$ (Pa) is the stress,
- $F$ (N) is the force,
- $A$ ($m^2$) is the material cross-section area,
- $\epsilon$ (%) is the strain,
- $\Delta L$ (m) is the length variation,
- $L_0$ (m) is the material original length.

The elastic or Young modulus, $E$ (Pa), is given by equation 8.3.

$$E = \frac{\tau}{\epsilon} \tag{8.3}$$

Polycrystalline ceramics elastic modulus value ranges from 100 to 800 GPa. Silicate glasses have an elastic modulus ranging from 60 to 80 GPa. Elastic modulus is influenced by the structural density of the material and the atomic bonds density [56]. Fracture stress $\tau_f$ (Pa) is the value of maximum stress that a material can withstand before breaking. For ceramics and silicate glasses this value ranges from 70 to 700 MPa [56].

## Poisson ratio

The Poisson ratio is the ratio of transversal strain to the longitudinal strain .

$$\nu = \frac{\sigma_T}{\sigma_L} \tag{8.4}$$

Where:

- $\nu$ is the Poisson ratio,
- $\sigma_T$ (%) is the transversal strain,
- and $\sigma_L$ (%) is the longitudinal strain.

For many ceramics and glasses, the Poisson ratio ranges from 0.18 to 0.30 [56].

## Elastic constants of some polycrystalline ceramics

Mechanical properties of solids are modified when a second phase is added, for example, the case of dispersed ceramic powders in organic polymers. As a result, sintered tapes have better mechanical properties than green ones. Indeed, added polymers and organic materials decrease the elastic modulus of the bulk powders. Table ii shows the elastic modulus of two green tapes provided by Heraeus and DuPont and tested by *Jones et al., 2000* [210].

| Tape | Composition | Elastic modulus (MPa) |
|---|---|---|
| DP951 and DP943$^{(a)}$ | Barium aluminum silicate | 1.24 – 1.45 |
| CT700 and CT800$^{(b)}$ | Calcium aluminum silicate | 2.59 – 3.17 |

Table ii: Commercial green tapes composition and elastic moduli commercialized by: (a) DuPont (b) Heraeus [210]

Table iii shows elastic modulus and Poisson ratio of some polycrystalline ceramics at 20°C.

| Material | Poisson ratio | Elastic modulus (GPa) |
|---|---|---|
| ZrC | 0.196 | 407 |
| $Al_2O_3$ | 0.233 | 402 |
| $Al_2O_3.MgO$ | 0.268 | 271 |
| MgO | 0.175 | 300 |
| $2MgO.SiO_2$ | 0.239 | 201 |
| SrO | 0.210 | 143 |
| $SrO.TiO_2$ | 0.010 | 538 |
| ZnO | 0.358 | 122 |
| $SiO_2$ | 0.082 | 95 |

Table iii: Poisson ratio and Young's modulus of some polycrystalline ceramics [56]

### Mechanical deformation types

Deformation can be either elastic or permanent. The elastic deformation is due to inter-atomic space solicitation. When the stress is stopped, an elastic material recovers its original form.
Permanent deformations are generated by dislocation and slip. Even after removing the solicitation, the deformation remains and the atoms are displaced from their original positions [55].

## Substrates wettability

Wettability is the tendency of a liquid to spread over a solid substrate. It is characterised by two major parameters:

- the wetting degree determined by contact angle measuring. It depends on the solid/liquid interfacial energies,
- the wetting rate which indicates how fast the liquid spreads over a solid surface.

### Surface energy

Surface properties of solids are characterised by the surface energy, $\gamma_s$. Surface energy is the sum of several terms such as dispersive and polar fractions respectively. Ionic, covalent and metallic interactions also contribute to surface energy [223] (Equation 8.5).

$$\gamma_s = \gamma_s^d + \gamma_s^p + \gamma_s^i + \gamma_s^c + \gamma_s^m \tag{8.5}$$

- $\gamma_s$ (mJ.m$^{-2}$) is the surface energy,
- $\gamma_s^d$ (mJ.m$^{-2}$) is the dispersive component,
- $\gamma_s^p$ (mJ.m$^{-2}$) is the polar component,
- $\gamma_s^i$ (mJ.m$^{-2}$) is the ionic component,
- $\gamma_s^c$ (mJ.m$^{-2}$) is the covalent component,
- and $\gamma_s^m$ (mJ.m$^{-2}$) is the metallic component.

When a solid or a liquid are neither ionic, nor metallic, nor covalent, only Van der Waals forces interfere and the surface energy of the substrate can be given by equation 8.6:

$$\gamma_s = \gamma_s^d + \gamma_s^p \tag{8.6}$$

Substrate wettability by solvent can be studied by calculating the contact angle formed between the fluid and the solid. A liquid can wet a substrate when the adhesion energy between the solid and the liquid is higher or equal to the liquid cohesion energy. A solvent aptitude to wet a solid is expressed by equation 8.7.

$$S_e = W_{sl} + W_{ll} \tag{8.7}$$

Where:

- $S_e$ ($mJ.m^{-2}$) is the spreading coefficient,
- $W_{sl}$ ($mJ.m^{-2}$) is the adhesion energy,
- $W_{ll}$ ($mJ.m^{-2}$) is the cohesion energy.

Dupré expressed $W_{sl}$ and $W_{ll}$ by equations 8.8 and 8.9.

$$W_{sl} = \gamma_s + \gamma_l - \gamma_{sl} \tag{8.8}$$

$$W_{ll} = 2 \cdot \gamma_l \tag{8.9}$$

Where:

- $\gamma_s$ ($mJ.m^{-2}$) is the substrate surface energy,
- $\gamma_l$ ($mN.m^{-1}$) is the liquid surface tension,
- and $\gamma_{sl}$ ($mJ.m^{-2}$) is the interface energy between the substrate and the liquid.

Thus, $S_e$ can be expressed by equation 8.10 [223].

$$S_e = \gamma_s - \gamma_l - \gamma_{sl} \tag{8.10}$$

When $S_e$ is positive, $\gamma_s$ value is high and the liquid is able to wet the substrate. A liquid is able to wet a substrate when its surface tension is lower than the surface energy of the solid [223].

## Contact angle

When liquid spreading reaches the equilibrium, spreading force is equal to 0 and Young's equation is given by equation 8.11:

$$\gamma_s - \gamma_{sl} = \gamma_l \cdot cos\theta \tag{8.11}$$

Where:

- $\gamma_s$ ($mJ.m^{-2}$) is the substrate surface energy,
- $\gamma_{sl}$ ($mJ.m^{-2}$) is the interface energy between the substrate and the liquid,
- $\gamma_l$ ($mN.m^{-1}$) is the liquid surface tension,
- and $\theta$ (degree) is the contact angle formed between the substrate and the liquid.

When the contact angle is equal to 0, the solvent is considered as able to wet the solid completely. At this stage, the critical surface tension ($\gamma_c$) is reached. When the contact angle is higher than 90°, the substrate cannot be wetted by the ink. Figure iii shows different wetting conditions of a surface by a liquid drop.

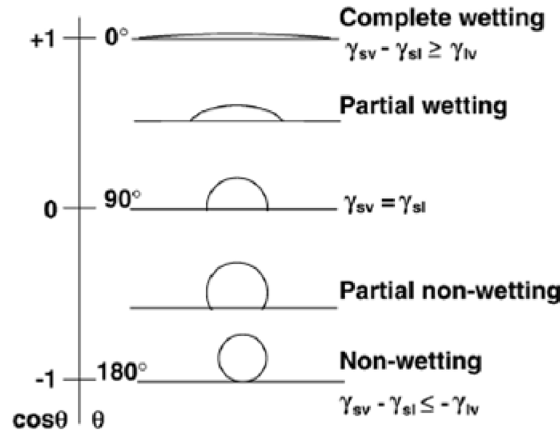


Figure iii: Liquid drop on a solid substrate for different wetting conditions [57]

## Factors affecting contact angle

Wetting and spreading are related to liquid flow properties. Flow can be affected by many properties related to the substrate and/or the fluid [57]:

- surface roughness and heterogeneity: in this case, the apparent contact angle is different from the Young's contact angle predicted only for smooth and homogeneous surfaces. Regarding the substrate homogeneity, in the case of composite substrates, different contact angles can be measured according to Cassie equation (Equation 8.12):

$$cos\theta = f_1 \cdot cos\theta_1 + f_2 \cdot cos\theta_2 \tag{8.12}$$

  Where:

  * $f_1$ and $f_2$ represent the fraction of the surface occupied by the surface type 1 and 2,
  * $\theta_1$ and $\theta_2$ (degree) are the corresponding angles.

- temperature: this factor has a great effect on the fluid viscosity and surface tension. Indeed, when temperature increases, ink viscosity and surface tension decrease. Thus, wetting is facilitated,

- reaction between the solvent and the substrate,

- liquid properties such as viscosity, surface tension and density.

# Annexe 2 - Electrical and thermal properties of materials

Some electrical and thermal characteristics of materials such as conduction, capacitor and dielectric properties, Peltier and Seebeck effects, are presented in this annexe.

## Electrical properties

### Ohm's law

For high conductive metals, diffusion theory is predominant and is expressed by Ohm's law. An electron with a mass equal to $m$ (kg) has a negative electrical charge $e$ =1.60.10$^{-19}$ Coulomb (C). Electrons contribute to the electrical conductivity of metals. The electrical field of a solid is given by equation 8.13.

$$E_{field} = \frac{U}{L} \tag{8.13}$$

Where:

- $E_{field}$ (V.m$^{-1}$) is the electrical field,
- $U$ (V) is the voltage,
- and $L$ (m) is the length.

This electric field causes acceleration $a$ (m.s$^{-2}$) in the solid (equation 8.14):

$$a = \frac{e}{m} \cdot E_{field} \tag{8.14}$$

Therefore, electrons acquire a drift or collision velocity $v_D$ (m.s$^{-1}$) in the same direction as the electrical field. This velocity depends on the average time between two collisions, $t$ (s), also noted free time or relaxation time (equation 8.15).

$$v_D = a \cdot t \tag{8.15}$$

Furthermore, according to equations 8.14 and 8.15, $v_D$ can be expressed by equation 8.16:

$$v_D = (\frac{e \cdot t}{m}) \cdot E_{field} \tag{8.16}$$

The term in parentheses is the electrical mobility $\mu$ (m$^2$.V$^{-1}$.s$^{-1}$). In a typical metal electron mobility is equal to 5.10$^{-3}$ m$^2$.V$^{-1}$.s$^{-1}$.

The electrical current $I$ (A) is the product of the electron density $N_e$, electron charge and drift velocity (equation 8.17).

$$I = N_e \cdot e \cdot v_D \tag{8.17}$$

The relationship between current density and electrical field is given by equation 8.18:

$$I = (\frac{N_e \cdot e^2 \cdot t}{m}) \cdot E_{field} \tag{8.18}$$

Equation 8.18 can be written as shown in equation 8.19 and this represents the Ohm's law.

$$I = c \cdot E_{field} \tag{8.19}$$

$c$ is the electrical conductivity (S.m$^{-1}$ - S for Siemens), and can be written as in equations 8.20 and 8.21.

$$c = \frac{e \cdot t}{m} \cdot N_e \cdot e \tag{8.20}$$

$$c = \mu \cdot N_e \cdot e \tag{8.21}$$

Thus, conductivity is a factor of two products, electron mobility and electron density. According to equation 8.21, electrical conductivity is a constant and it is independent from the electrical field strength [184].

## Capacitors and dielectric constant

A capacitor is a passive component composed of two conductors separated by a dielectric or an insulator material such as paper, mica or air. Capacitor enables electrostatic energy storage. This energy is stocked during a part of the capacitor cycle and generated in the other part. When an electrical current $I$ (A) passes through the capacitor during a time $dt$ (s), the charge ($dq$) is given by equation 8.22.

$$dq = I \cdot dt \tag{8.22}$$

This charge variation leads to a small potential difference $dU$, expressed in equation 8.23:

$$dq = C \cdot dU \tag{8.23}$$

$C$ is called the capacitance of the capacitor and is given in Farad (F). The dielectric constant or dielectric permittivity ($\varepsilon$ - F.m$^{-1}$), given in equation 8.24, relates the material ability to carry alternating current to the vacuum ability to carry alternating current.

$$C = \frac{\varepsilon_r \cdot \varepsilon_0 \cdot A}{L} \tag{8.24}$$

$$\varepsilon_0 = \frac{1}{36 \cdot \pi \cdot 10^9} \tag{8.25}$$

$\varepsilon_0$ is the vacuum permittivity (8.85 x $10^{-12}$ F.m$^{-1}$). $A$ (m$^2$) is the surface of the two conductors of the capacitor and $L$ (m) the dielectric length. Knowing a material relative permittivity ($\varepsilon_r$) is required to properly design instruments such as level controls using radar or capacitance technologies.

Relative permittivity is the ratio of material dielectric constant to vacuum dielectric permittivity. Capacitors can be non polarised such as ceramic, plastic film and polyester capacitors. Electrochemical capacitors are polarised [181]. Dielectric loss is the power loss in a dielectric related to the energy loss when heat is generated by an electrical field.

## Inductance

In electrical circuits, an electrical current $I$ produces a magnetic field and thus, generates a total magnetic flow $M$ acting on the circuit. This magnetic flow tends to oppose changes in the flow by generating a voltage that tends to reduce the current change rate. The ratio of the magnetic flow to the current is called the self-inductance which is usually simply referred to as the inductance of the circuit. The unit of inductance is Henry (H): 1 H = 1 $\text{Wb.A}^{-1}$. Inductance $B$ ($\text{Wb.A}^{-1}$) is given by equation 8.26.

$$B = \frac{N \cdot M}{I} \tag{8.26}$$

Where:

- $B$ ($\text{Wb.A}^{-1}$) is the inductance,
- $N$ is the number of wire turns,
- $M$ is the magnetic flow (in Weber - Wb),
- and $I$ (A) is the current.

Inductance increases linearly with the coil size and the number of turns. it becomes higher when pattern thickness increases. But it decreases when the conductor line width increases. It was also demonstrated that when the ratio of line width to space decreases, the number of turns increases which leads to an increase in the inductance value [21].

## $Q$ factor

In electricity, the $Q$ factor is a dimensionless factor that indicates the overall conservational quality of an electric circuit; it is defined by equation 8.27.

$$Q = \frac{2 \cdot \pi \cdot f \cdot B}{R} = \frac{\sqrt{B \cdot C}}{R \cdot C} \tag{8.27}$$

Where:

- $Q$ is the quality factor,
- $f$ (Hz) is the frequency,
- $B$ ($\text{Wb.A}^{-1}$) is the inductance,
- $R$ (Ohm) is the resistance,
- and $C$ is capacitance (F).

## Electrical properties summary

Table iv summarises the different electrical properties.

| Electrical conductivity - c ($S.m^{-1}$) | $c = \frac{I}{E_{field}}$ | $I \rightarrow$ Current (A); $E_{field} \rightarrow$ Electrical field strength ($V.m^{-1}$) |
|---|---|---|
| Electrical resistivity - $\rho$ (Ohm.m) | $\rho = \frac{R \cdot A}{L} = \frac{E_{field}}{I}$ | $R \rightarrow$ Resistance (Ohm); $A \rightarrow$ Cross sectional area ($m^2$); $L \rightarrow$ Length (m) |
| Resistance - $R$ (Ohm) | $R = \rho \cdot \frac{L}{A} = \rho \cdot \frac{L}{w \cdot th}$ | $w \rightarrow$ Width (m); $th \rightarrow$ Thickness (m) |
| Conductance - $G$ (S) | $G = c \cdot \frac{A}{L}$ | |
| Sheet resistance - $R_s$ (Ohm/square) | $R_s = \frac{\rho}{th} = R \cdot \frac{w}{th}$ | |
| Mobility - $\mu$ ($m^2.V^{-1}.s^{-1}$) | $\mu = \frac{e \cdot t}{m}$ | $e \rightarrow$ Electron charge collision (C); $t \rightarrow$ Collision time (s); $m \rightarrow$ Electron mass (g) |
| Capacitance - $C$ (F) | $C = \frac{\varepsilon_0 \cdot \varepsilon_r \cdot A}{L}$ | $\varepsilon_0 \rightarrow$ Vacuum permittivity ($F.m^{-1}$); $\varepsilon_r \rightarrow$ Relative permittivity ($F.m^{-1}$); $L \rightarrow$ Dielectric distance (m) |
| Inductance - $B$ ($Wb.A^{-1}$) | $B = \frac{N \cdot M}{I}$ | $N \rightarrow$ Number of wire turns; $M \rightarrow$ Magnetic flow (Wb); $I \rightarrow$(Electric current) |

Table iv: Electrical properties summary

# Thermal properties

Materials such as bismuth telluride ($Bi_2Te_3$), silicone germanium ($Si_{1-x}Ge_x$), lead telluride (PbTe) and cobalt triantimonide ($CoSb_3$) exhibit thermoelectric properties. They are used in many applications where heat conversion and heat control or voltage generation are required. Radioisotope thermoelectric generators and waste heat recovery devices are examples of these applications [224][225].

## Thermal conductivity

Thermal conductivity indicates the ability of a material to conduct heat. It predicts the power loss through a material according to equation 8.28:

$$\Delta P = \frac{\kappa \cdot \Delta T \cdot A}{th} \tag{8.28}$$

Where:

- $\kappa$ (W.m$^{-1}$.K$^{-1}$) is the thermal conductivity,
- $\Delta P$ (W) is the power loss,
- $\Delta T$ (K) is the difference in temperature through the material,
- $A$ (m$^2$) is the cross-section area,
- and $th$ (m) is the thickness.

## Thermal conduction

Thermal conductance is analogous to electrical conductance. It is the quantity of heat passing in a 1 m$^2$ cross-section area material when the difference of temperature between the two faces of the material is equal to 1 Kelvin. It is given by equation 8.29.

$$g = \kappa \cdot \frac{A}{th} \tag{8.29}$$

Where:

- $g$ (W.K$^{-1}$) is the thermal conduction,
- $\kappa$ (W.m$^{-1}$.K$^{-1}$) is the thermal conductivity,
- $A$ (m$^2$) is the cross-section area,
- and $th$ (m) is the thickness.

## Heat transfer coefficient

The heat transfer coefficient is the ratio of thermal conductivity to the material thickness. It is given by equation 8.30.

$$HTC = \frac{\kappa}{th} \tag{8.30}$$

Where:

- $HTC$ (W.K$^{-1}$.m$^{-2}$) is the heat transfer coefficient,
- $\kappa$ (W.m$^{-1}$.K$^{-1}$) is the thermal conductivity,
- and $th$ (m) is the thickness.

## Peltier effect

When current flows between two sides, heat is absorbed at one side and diffused at the other side. This is called the Peltier effect. Heat absorbed per second at a junction carrying a current $I$ is given by equation 8.31:

$$H = \Pi_{ab} \cdot I \tag{8.31}$$

Where:

- $H$ (J.s$^{-1}$) is the heat absorbed per second,
- $\Pi_{ab}$ (V) is the Peltier coefficient between two junctions, a and b,
- and $I$ (A) is the current.

The Peltier effect phenomenon is shown on figure iv.

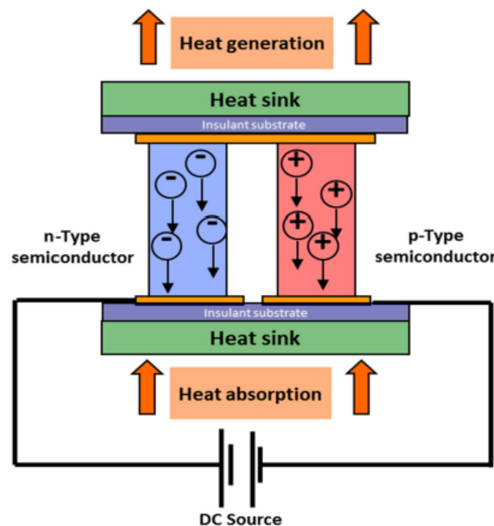


Figure iv: Thermoelectric couple - Peltier effect (Reproduced from Custom Chill Copyright 2005)

The heat sink can be the exchanger used in generators, air conditioning systems or radiators. It is the thermo-module component that transfers the heat generated within a solid material to a fluid medium (air or liquid).

## Seebeck effect

When applying a temperature difference between two junctions of two connected materials, a thermoelectric force ($E_T$ – Volt) is produced and the current flows. This is called the Seebeck effect. A temperature difference between the semiconductors sides is required to generate current [226]. Figure v shows a schematic of a Seebeck thermocouple.

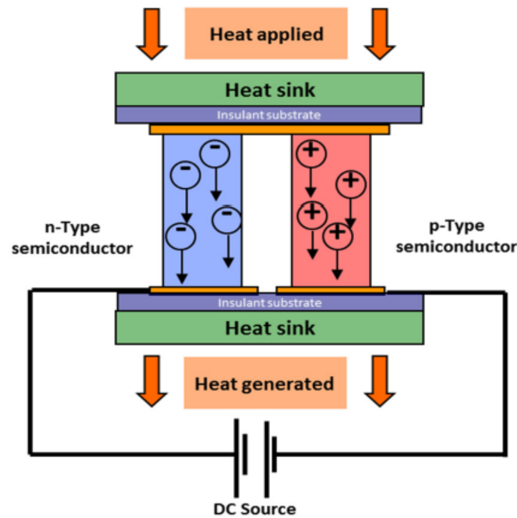


Figure v: Thermocouple schematic - Seebeck effect

## Efficiency of thermoelectric devices

The efficiency of a thermoelectric device is expressed by $Z{\cdot}T$. It is the dimensionless figure of merit of a thermoelectric material, product of a constant coefficient $Z$ and temperature $T$ (equation 8.32).

$$Z \cdot T = \frac{S^2 \cdot T}{\rho \cdot \kappa} \tag{8.32}$$

Where:

- $S$ is the Seebeck coefficient or thermo-power (V.K$^{-1}$),
- $T$ (K) is the temperature,
- $\rho$ (Ohm.m) is the resistivity,
- and $\kappa$ is the device thermal conductivity (W.m$^{-1}$.K$^{-1}$).

To be efficient a thermocouple should have a high Seebeck coefficient and a low resistivity. Thermal conductivity is the sum of lattice thermal conductivity ($\kappa_l$) and electron thermal conductivity ($\kappa_e$) (equation 8.33).

$$\kappa = \kappa_l + \kappa_e \tag{8.33}$$

$Z{\cdot}T$ can be enhanced by reducing electron scattering and thermal conductivity [224][226][227]. The thermoelectric factor can be expressed by equation 8.34 [228].

$$W = S^2 \cdot c = \frac{S^2}{\rho} \tag{8.34}$$

Where:

- $W$ (W.K.m) is the thermoelectric factor,
- $S$ (V.K$^{-1}$) is the Seebeck effect,

- and $c$ (S.m$^{-1}$) is the conductivity.

The thermoelectric force, ($E_T$, Volts - V), of a single thermocouple, is expressed by equation 8.35 [229].

$$E_T = S \cdot \Delta T \tag{8.35}$$

$\Delta T$ is the temperature difference between the hot and the cold sides (K).

The output power ($P_{out}$, Watt - W) is given by equation 8.36 [229]. $R_i$ is the internal electric resistance of the thermocouple (Ohm).

$$P_{out} = \frac{E_T^2}{R_i} = \frac{(S \cdot \Delta T)^2}{R_i} \tag{8.36}$$

Output power should be quickly reached in a thermoelectric material. In order to achieve this, the Seebeck coefficient should be increased and the electrical resistivity decreased.

Another way to enhance the thermoelectric efficiency is by making thermopiles by connecting $n$ thermocouples. Electrical connection is performed in series and thermal connection in parallel. In this case the thermoelectric power is given by equation 8.37 [228]:

$$E_T = n \cdot S \cdot \Delta T \tag{8.37}$$

# Annexe 3 - Thermoelectric components

## Thermoelectric materials

All materials with a high figure of merit $Z \cdot T$ are considered as suitable thermoelectric materials (see equation 8.32). They have high Sebeeck coefficient, high electrical conductivity and low thermal one. Thus, best candidate for thermoelectric component manufacturing are semi-metals and highly doped semiconductors.

### Bismuth and alloys

Bismuth (Bi) is a semiconductor belonging to group V of the periodic table of elements. It has 9.79 g.cm$^{-3}$ density and 271°C melting point. Bismuth resistivity is equal to 160 $\mu$Ohm.cm at 100°C [27]. Bismuth thermal conductivity is very low (5.2 W.m$^{-1}$.K$^{-1}$ at 300 k). For this reason, it is used in thermoelectric applications [230].

When combined to telluride, Bismuth telluride ($Bi_2Te_3$) with lower thermal conductivity, 1.2 W.m$^{-1}$.K$^{-1}$ is obtained. This allows enhancement of $Z \cdot T$ value. Consequently, $Bi_2Te_3$ is largely used in thermoelectric materials manufacturing. Other bismuth alloys can be found such as $Bi_{0.4}Te_3Sb_{1.6}$, $Bi_2Se_3$, etc. [231].

### Germanium and alloys

Germanium is a chemical element from group IVA of the periodic table of elements. It has 5.32 g.cm$^{-3}$ density and melts at 938°C. Its electrical resistivity is equal to 47 $\mu$Ohm.cm. It has high thermal conductivity (58 W.m$^{-1}$.K$^{-1}$) compared to bismuth. In order to perform thermoelectric applications it is usually alloyed to silica. SiGe thermal conductivity is equal to 2.8 W.m$^{-1}$.K$^{-1}$ [27]. Silica and germanium alloys are in the following form $Si_{1-x}Ge_x$.

## Examples of thermoelectric inks applications

Table v shows some thermoelectric materials examples and properties.

| Reference | Thermoelectric | ZT | Thermal conductivity (W. $m^{-1}.K^{-1}$) | Seebeck coefficient ($\mu V.K^{-1}$) | Resistivity (Ohm.m) |
|---|---|---|---|---|---|
| *Cook et al., 1989* [232] | $Si_{0.747}Ge_{0.187}$ doped with $Ga_{0.016}P_{0.050}$ | 0.88 (1273 K) | 2.8 - 3.2 | -175 to 250 | $1.3.10^{-5}$ - $1.7.10^{-5}$ |
| *Chung et al., 2000* [233] | $CsBi4Te_6$ doped with $SbI_3$ | 0.82 (225 K) | 1.48 | 175 (250 K) | $10^{-5}$ |
| *Strasser et al. 2002* [234] | Poly $Si_{70\%}Ge_{30\%}$ | 0.63 - 1.09 | 10.3 | 125 - 147 | $\sim 2.10^{-5}$ |
| *Obara et al., 2009*[226] | p-type $Bi_2Te_3$ | | 0.34 | -200 to -150 (300-500 K) | $10^{-5}$ |
| *Zeng et al., 2009* [235] | ErAs: $(InGaAs)_{0.8}$ $(InAlAs)_{0.2}$ | ~1.2 | 2 (600 K) | 215 (600 K) | 0.18 |

Table v: Thermoelectric materials applications

# Résumé

Depuis son développement dans les années 1950, l'électronique imprimée est un domaine en évolution croissante. Il permet une production à grande échelle de composants électroniques. Les procédés d'impression ont l'avantage d'être des méthodes additives réduisant les pertes et les contraintes écologiques. Ce sont des techniques relativement simples comparées aux méthodes conventionnelles comme la photolithographie et les techniques à faisceaux d'ions focalisés. La table vi compare les techniques conventionnelles aux procédés d'impression dans le domaine de l'électronique imprimée.

| **Méthodes conventionnelles** | **Electronique imprimée** |
|---|---|
| Méthodes bien définies et développées pour la fabrication de composants électroniques | La sérigraphie connue depuis les années 1950 dans la fabrication des circuits imprimés. Les procédés d'impression pour l'électronique sont toujours en phase de développement et d'optimisation. |
| Plusieurs étapes (spin coating, exposition UV, laser, jets moléculaires, faisceaux ioniques, ablation chimiques et mécaniques) | Une seule étape après la fabrication de la forme imprimante |
| Coût élevé | Prix relativement bas |
| Production à grande échelle nécessaire pour être rentable | Possibilité de produire des petites et des grandes quantités |
| Temps de fabrication long | Méthodes rapides |
| Supports rigides (silicium) | Supports rigides et flexibles (céramiques, verres, silice, plastiques, papiers) |
| Limitées par la taille du support | Possibilité d'imprimer des supports de différentes tailles |
| Utilisation de solvants dangereux et perte de certaines parties structurées après ablation | Procédés permettant de déposer les quantités juste nécessaires de matériaux fonctionnels |

Table vi: Comparaison des méthodes conventionnelles à la microélectronique imprimée

# Le projet MULTILAYER

Cette étude s'inscrit dans le projet Européen MULTILAYER dans lequel dix-neuf partenaires sont impliqués. Le projet est divisé en neuf sous-projets qui ont pour but de trouver une solution pour la production de masse de composants électroniques à base de céramique.
Les supports en céramique préparés par coulage ou calandrage sont structurés et/ou imprimés par jet d'encre, sérigraphie, flexographie ou héliogravure. Ensuite, une étape de laminage et de découpage est effectuée afin d'atteindre la forme et la taille souhaitées du conducteur. Cette étape est suivie par le frittage, l'assemblage et l'intégration des composants dans les dispositifs finaux.
La figure vi montre schématiquement la finalité du projet MULTILAYER: la mise en oeuvre, en ligne, les différentes étapes de fabrication.

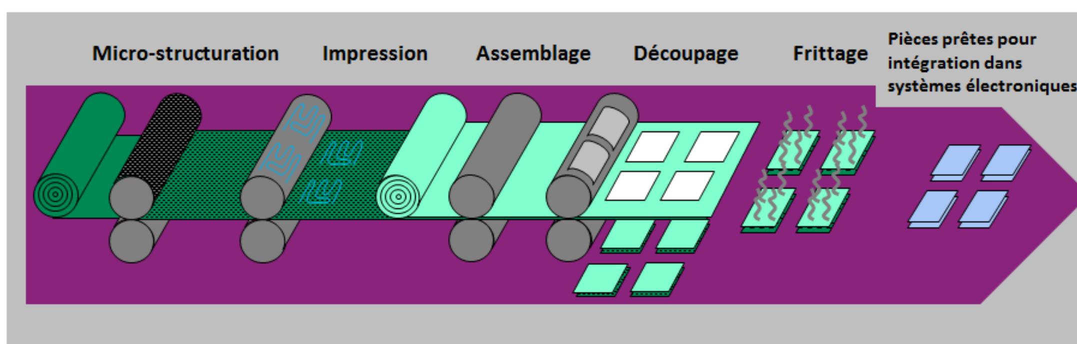


Figure vi: Techniques et procédés des différentes étapes du projet MULTILAYER

Grenoble INP - Pagora et le Laboratoire de Génie de Procédés Papetiers interviennent dans le sous-projet trois, l'impression fonctionnelle. Les quatre procédés d'impression - sérigraphie, flexographie, héliogravure et jet d'encre - sont étudiés afin de déterminer leur potentiel dans l'électronique imprimée et d'évaluer la capacité des systèmes céramiques/métaux imprimés à être intégrés dans les dispositifs suivants:

- Composants permettant la transmission des ondes radio et des micro-ondes : le but de ce démonstrateur est de réduire les risques, le temps de fabrication ainsi que le coût de développement de nouveaux capteurs électriques. Des méthodes pour l'intégration des lignes pouvant transmettre les micro-ondes dans des systèmes céramiques sont développées.

- Appareils thermoélectriques pour des applications domestiques : le but est la production de masse de composants thermoélectriques permettant l'alimentation de capteurs sans fils.

- Structure de refroidissement pour les sytèmes d'éclairage automobile : les diodes électro-luminescentes (LED) sont fabriquées par dépôt de métaux conducteurs sur un support isolant. L'objectif est de réduire les coûts de fabrication et d'utiliser de nouveaux types de supports thermiquement conducteurs.

- Des capteurs mico-fluidiques pour des applications médicales : les procédés d'impression sont optimisés afin de déposer des lignes fines sur des supports LTCC (Low Temperature Co-fired Ceramics) - des céramiques frittées à faibles températures. La sérigraphie est utilisée de manière courante pour réaliser ces applications. Dans ce projet, le jet d'encre, l'héliogravure et la flexographie sont également testées.

La figure vii schématise les différents démonstrateurs dans lesquels seront intégrés les supports céramiques imprimés.

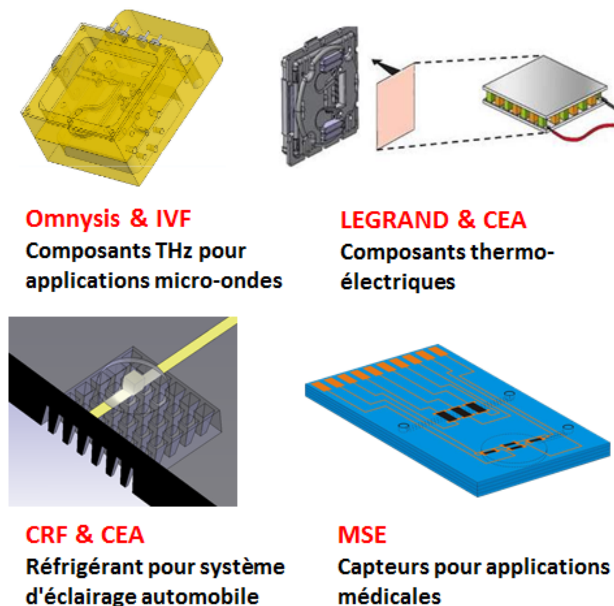


Figure vii: Démonstrateurs fabriqués en intégrant des procédés d'impression

# Le cahier des charges

L'objectif principal de cette étude est l'impression d'encres conductrices sur des supports en céramique. Les lignes imprimées devront supporter des températures supérieures à 800°C adaptées aux systèmes multicouches LTCC.
Les objectifs de cette études sont donc :

- d'étudier différents types de supports (céramiques, verre, silice) afin de choisir les plus adaptés pour l'impression et les systèmes d'encres à base d'eau,
- de formuler de nouvelles encres et optimiser des encres commerciales compatibles avec les supports sélectionnés,
- d'optimiser et formuler des encres adaptées aux procédés d'impression (taille des particules, tension de surface, rhéologie),
- de préparer des encres capables de supporter des températures supérieures à 800°C pendant 10 à 60 minutes,
- de choisir un matériau hautement conducteur, résistant thermiquement et chimiquement et de coût modéré,
- d'imprimer des lignes fines ($< 100\ \mu$m) avec des bords bien définis,
- d'obtenir des lignes avec des résistivités inférieures à $1.10^{-6}$ Ohm.m.

Dans la première partie du manuscrit, une revue bibliographique des travaux antérieurs

sur l'électronique imprimée a été réalisée.
Dans la deuxième partie, les principaux résultats expérimentaux sont présentés sous forme d'un recueil d'articles, numérotés de "Article 1" à "Article 8", et introduits dans leur contexte :

- caractéristiques des supports,
- sérigraphie sur supports frittés en alumine et sur des LTCC (Articles 1, 2 et 3),
- flexographie sur supports LTCC flexibles (Articles 4, 5 et 6),
- héliogravure sur supports LTCC flexibles (Article 7) et jet d'encre sur supports frittés (Article 8).

Finalement, une conclusion générale synthétise les principaux résultats et décrit les travaux futurs dans le cadre de cette étude. La figure viii schématise l'organisation générale du manuscrit et de l'étude.

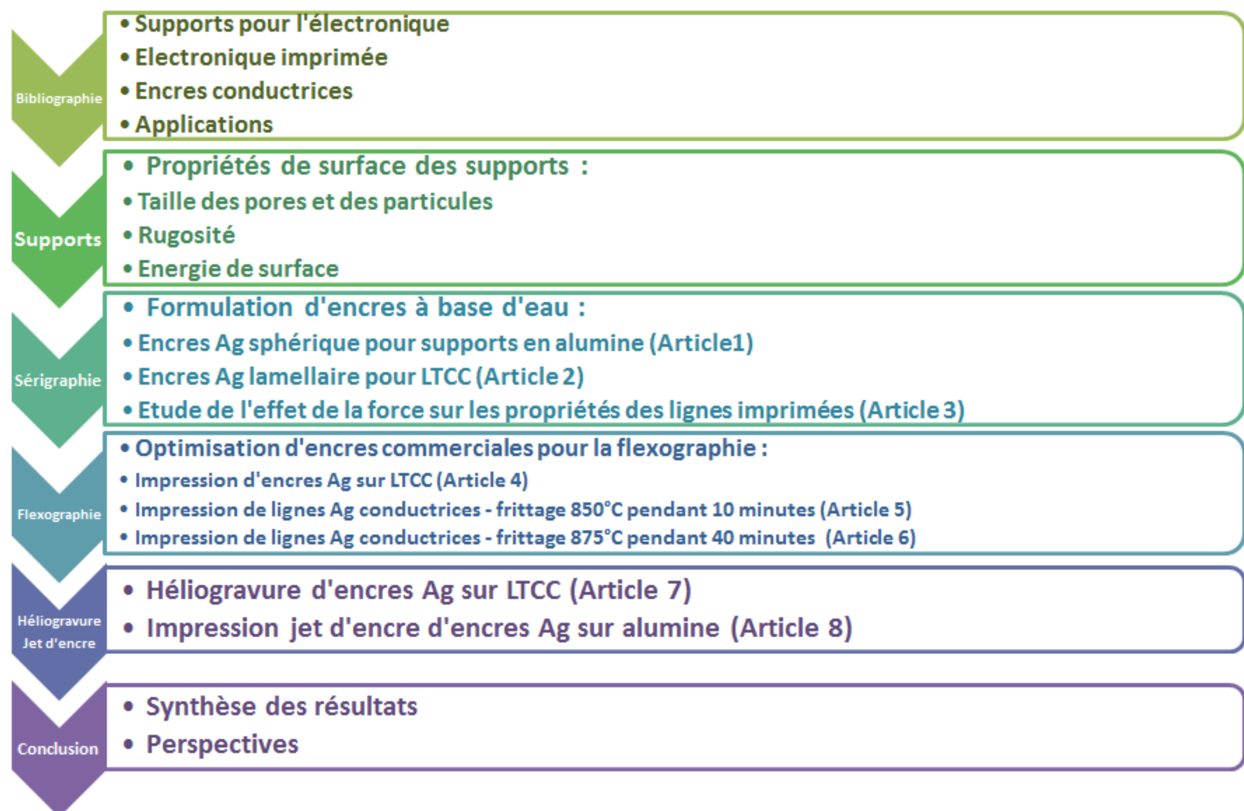


Figure viii: Organisation générale du manuscrit

# Méthodologie

Afin d'aboutir aux objectifs fixés par le cahier des charges, au démarrage de l'étude, une revue bibliographique de l'état de l'art et des travaux antérieurs a été réalisée sur l'électronique imprimée.

Une partie expérimentale basée sur les connaissances acquises dans la revue bibliographique a été ensuite effectuée:

- par analogie à la caractérisation du papier, la surface des supports en céramique a été étudiée. La taille des pores, des particules ainsi que les énergies de surface ont été évaluées. Cela a permis de choisir la taille des particules des encres ainsi que les solvants et les additifs à utiliser pour la formulation de ces encres,
- des encres adaptées aux différents procédés d'impression ont été formulées ou optimisées à partir d'encres commerciales,
- les propriétés rhéologiques et les tensions superficielles des encres ont ensuite été determinées,
- les encres ont été imprimées par sérigraphie, flexographie, héliogravure et jet d'encre,
- les lignes imprimées ont été caractérisées afin de déterminer leur propriétés géométriques (épaisseur, largeur), leur rugosité et étudier leur microstructure,
- certains supports imprimés ont été frittés,
- les lignes frittées ont été caractérisées notamment pour déterminer leur propriétés électriques,
- si les lignes imprimées étaient mal définies ou avaient des propriétés électriques qui ne correspondaient pas au cahier des charges, les formules d'encres, les paramètres d'impression et/ou de frittage ont été optimisés.

La figure ix illustre la méthodologie suivie afin de réaliser les objectifs fixés par le cahier des charges.

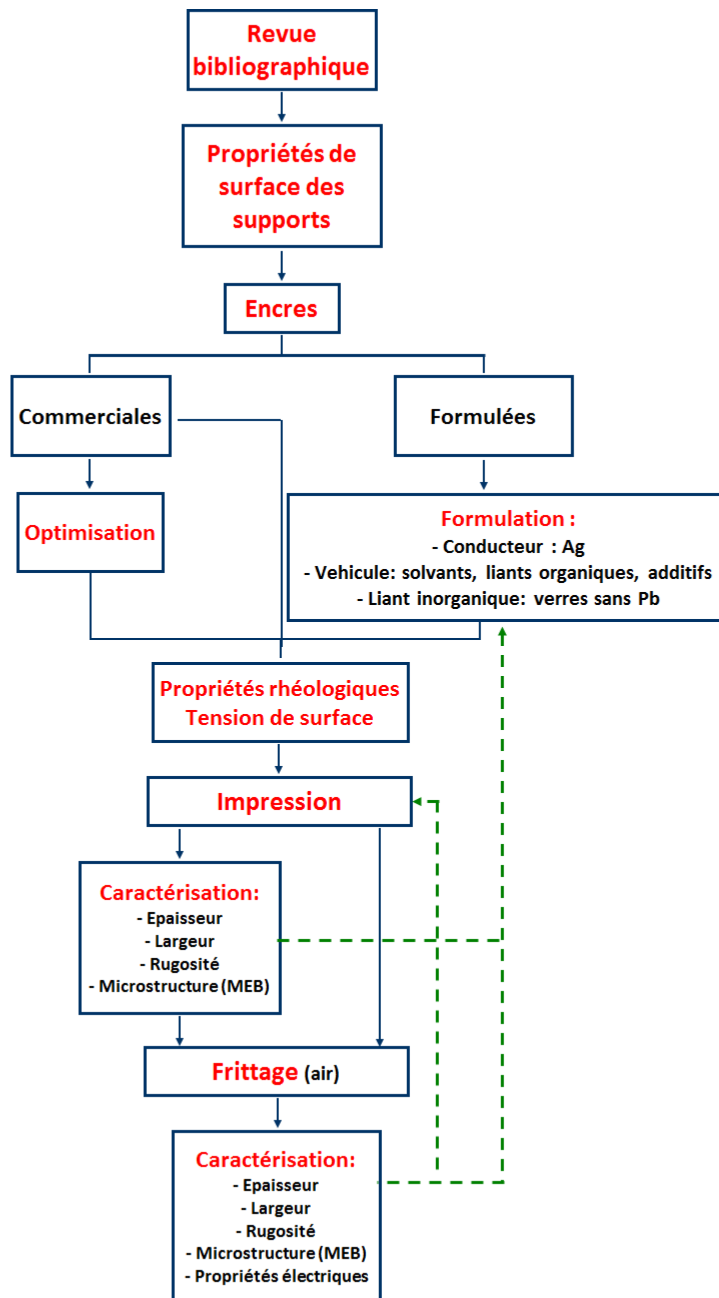


Figure ix: Schéma de la méthodologie de travail

Pour appliquer cette méthodologie, différentes techniques ont été utilisées :

- exploitation des micrographes acquis par Microscopie Electronique à Balayage (MEB) pour étudier la microstructure des supports et des lignes (MEB environnemental Quanta 200),

- topographie de surface pour mesurer les épaisseurs, largeurs et rugosités des supports, des aplats et des lignes (profilomètre 3D Alicona),

- microscopie optique pour observer la définition des lignes (Microscope optique Carl Zeiss),

- mesure des angles de contact pour calculer les énergies de surface (méthode OWRK

- Owens, Wendt, Rabel and Kaelble) et méthode de la goutte pendante pour définir les tensions superficielles (OCA system),

- formulation d'encres conductrices par dispersion mécanique (Dispermat) et broyage tri-cylindre (EXAKT 50),
- études des modèles rhéologiques en cisaillement (Newton, Bingham, Hershel-Bulkley, Casson) et études rhéologiques en oscillation (rhéomètre Anton Paar),
- impression par différents procédés:
  - ∗ sérigraphie : presse sérigraphique automatique DEK Horizon 03i,
  - ∗ flexographie : testeur de laboratoire Flexiproof 100,
  - ∗ héliogravure : testeur de laboratoire IGT 3H,
  - ∗ jet d'encre : imprimante goutte à la demande Fujifilm - Dimatix DMP2831,
- frittage dans un four traditionnel en atmosphère normale (four traditionnel Statop Nagat),
- analyse thermo-gravimétrique (TGA) permettant d'étudier le comportement de l'argent à températures élevées (Perkin Elmer),
- évaluation des propriétés électriques des lignes et films déposées: mesure de la résistace de feuille (4 pointes JANDEL) et calcul de la résistivité (2 pointes JANDEL).

# Revue bibliographique

Dans cette partie, une revue bibliographique concernant les supports utilisés en électronique, les travaux antérieurs réalisés en électronique imprimée, les encres conductrices et les applications potentielles sont traitées. La figure x résume les différents points traités dans cette section du manuscrit.

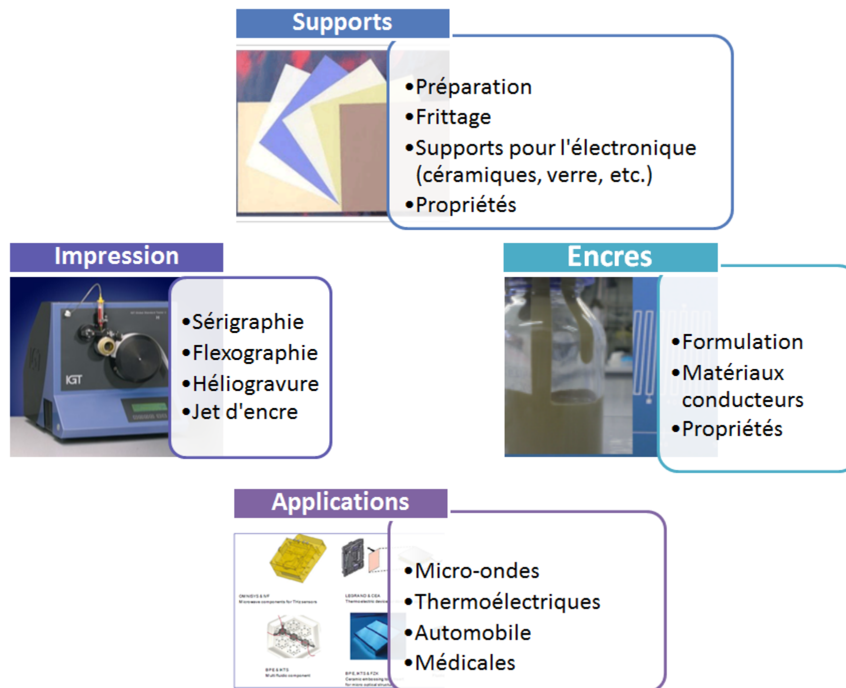


Figure x: Organisation de la recherche bibliographique

Dans le premier chapitre, les supports utilisés en éléctronique - les céramiques frittées à basses et hautes températures, les verres et les silices - sont traités. Les supports peuvent être flexibles ou rigides. Les méthodes de fabrication des supports comme le coulage et le caladrange sont aussi décrites. Les propriétés mécaniques, thermiques et de surface des supports ainsi que leur impact sur le dépôt d'encre et les caractéristiques finales des dispositifs fabriqués sont analysés.
Le frittage des céramiques est aussi traité. Ainsi, les changements observés au niveau de la microstructure des céramiques sont analysés: le rétrécissement, l'augmentation de la taille des particules, la fermeture des pores.

Par la suite, les procédés d'impression (principe, encres, applications, résolution, problèmes correspondants) sont étudiés. La table vii synthétise les différentes propriétés des procédés d'impression.

| **Méthode** | **Résolution** | **Epaisseur moyenne** | **Vicosité** |
|---|---|---|---|
| Offset | 15 $\mu$m | 0,05 - 2,00 $\mu$m | 10 - 100 Pa.s |
| Sérigraphie | 100 $\mu$m | 3,00 - 20,00 $\mu$m | 1 - 120 Pa.s |
| Flexographie | 40 $\mu$m | 0,80 - 2,50 $\mu$m | 50 - 500 mPa.s |
| Héliogravure | 15 $\mu$m | 0,80 - 8,00 $\mu$m | 50 - 200 mPa.s |
| Jet d'encre | 5 $\mu$m | $<$ quelques $\mu$m (encres à base d'eau ou de solvant organique), 10,00 - 20,00 $\mu$m (UV et hot melt) | 1 - 50 mPa.s |

Table vii: Propriétés des procédés d'impression [94][96][108][143]

Dans le troisième chapitre de la partie bibliographique, les principaux matériaux utilisés dans la formulation des encres conductrices sont décrits :

- les matériaux conducteurs : les métaux nobles (argent, or, platine, palladium), les autres métaux (cuivre, nickel), le carbone (noir de carbone, graphite, nanotubes) et les polymères conducteurs (polyaniline, PEDOT:PSS),
- les particules de verre jouant le rôle de matériaux d'adhésion au support après frittage,
- le véhicule essentiellement formé de solvants, de liants organiques et d'additifs. Il confère à l'encre ses propriétés rhéologiques, sa stabilité, assure une bonne dispersion ainsi que la filmification avant frittage.

Dans le dernier chapitre, les applications potentielles en éléctronique imprimée sont décrites:

- les applications dans le domaine des micro-ondes et des fréquences radio,
- les modules thermoélectriques,
- les applications dans le domaine automobile (LED, capteurs),
- les applications médicales (systèmes micro-fluidiques, bio-capteurs, etc.)

La revue bibliographique a permis:

- de choisir l'argent comme matériau conducteur pour sa conductivé élevée ($6.10^7$ $S.m^{-1}$), sa résistance thermique et chimique comparé au cuivre et au nickel et son prix modéré par rapport à l'or,
- d'imprimer les supports en alumine à l'état fritté pour éviter d'exposer l'argent aux températures de frittage de l'alumine ($\sim$ 1600°C),

- d'imprimer les LTCC avant frittage. Le co-frittage céramique/métal est réalisé à des températures de l'ordre de 800 - 900°C.

Cette recherche bibliographique a aussi révélé:

- que les pâtes métalliques de sérigraphie commercialisées sont souvent à base de solvants. Le toluène, le terpinéol, le butyl carbitol sont utilisés pour leur faible taux d'évaporation. Ainsi, le bouchage des mailles de l'écran pourrait être évité. Le défi est alors de formuler des encres à base d'eau imprimables par sérigraphie.

- que le procédé flexographie rotatif n'a pas encore été testé pour l'impression d'encres métalliques sur des supports flexibles en céramique. Le défi est de réussir à déposer des lignes assez épaisses pour supporter les conditions de frittage.

## Principaux résultats obtenus

Afin d'aboutir aux objectifs fixés par le cahier des charges, les supports ont été d'abord caractérisés pour déterminer leurs propriétés (pores, énergie de surface) et choisir la taille des particules et la nature des encres. Ensuite, des encres à base d'eau ont été formulées et adaptées aux différents procédés d'impression. Les imprimés ont été caractérisés (largeur, épaisseur, rugosité et microstructure). Ensuite, une étape de frittage a été conduite. Cette dernière a été suivie par une caractérisation des propriétés géométriques des lignes ainsi que de leurs propriétés électriques (figure xi).

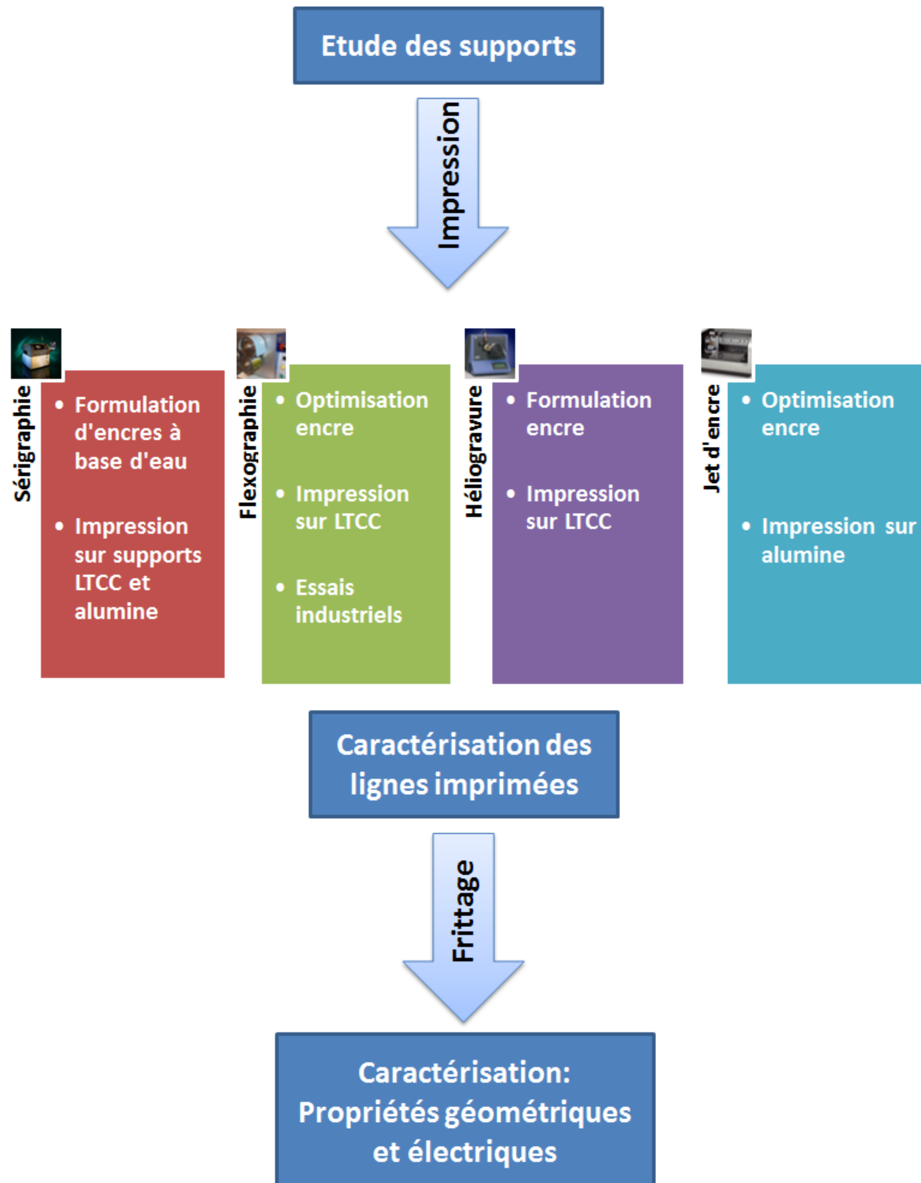


Figure xi: Organisation de la partie expérimentale

## Les supports

Différents types de supports ont été étudiés : alumine, silice, verre et LTCC. Leur microstructure a été analysée avant et après frittage.

La taille des pores, des particules, la rugosité et l'énergie de surface des supports a été déterminées avant et après frittage. Ces propriétés ont orienté la sélection de la taille des particules conductrices et du solvant à utiliser pour formuler les encres.

En se basant sur les caractéristiques des supports, les LTCC non cuits ont été imprimés par des encres contenant des particules de taille comprise entre 1 et 5 $\mu$m. Les supports frittés d'alumine, ne présentant pas de pores en surface, ont été imprimés avec des encres contenant des particules de tailles variables - 0.015 $\mu$m à 3 $\mu$m.

L'énergie de surface des supports a été mesurée entre 30 et 60 mJ.m$^{-2}$. Elle dépendait de leur état (fritté ou non) ainsi que de leur composition initiale. Les énergies de surface les plus élevées ont été enregistrées pour les supports fabriqués à partir de pâtes à base d'eau.
La rugosité des supports a été reliée à la taille des poudres avant coulage. Quand les particules avaient des diamètres supérieurs à 1 $\mu$m, la rugosité mesurée était de l'ordre de 2 à 4 $\mu$m. Alors que, quand la majorité des particules avaient un diamètre inférieur à 1 $\mu$m, la rugosité était plus faible, 0.03 $\mu$m à 0.27 $\mu$m.

Après frittage, l'évaporation des liants et solvants organiques composés de chaînes carbonées hydrophobes a conduit à:

- la diminution de la taille des pores de surface,
- l'élargissement des particules,
- et l'augmentation de l'énergie de surface.

La figure xii montre un support LTCC avant et après frittage.

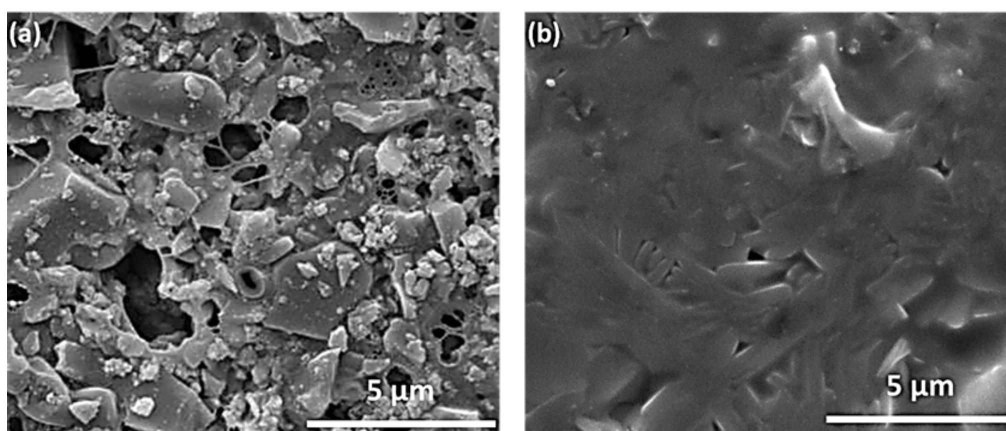


Figure xii: Microstructure d'un support LTCC avant (a) et après (b) frittage - MEB (Microscope Electronique à Balayage)

Les supports d'alumine frittés et les LTCC non frittés ont été sélectionnés pour réaliser les essais d'impression dans la suite de cette étude.

## Sérigraphie sur support en céramique

Des particules d'argent de formes sphérique et lamellaire ont été employées comme matériaux conducteurs. Les particules avaient une taille moyenne de 2 à 3 $\mu$m. La table viii récapitule la composition des pâtes de sérigraphie.

| Matière première | Fonction | Pourcentage massique |
|---|---|---|
| Argent | Conducteur | 45 - 80% |
| Verre | Agent d'adhésion | 1 - 20% |
| Eau<br>Ethylene Glycol<br>Glycerol | Solvant | 1 - 30% |
| Additifs | Stabilité de la dispersion, rhéologie, mouillage | 1 - 3% |
| Polymère acrylique | liant organique | 6 - 30% |

Table viii: Formules pâtes sérigraphiques

Toutes les pâtes avaient un comportement thixotrope rhéofluidifiant. La viscosité diminuait quand le taux de cisaillement augmente. Et les encres revenaient à leur état initial à des taux de cisaillement plus faibles (figure xiii). Les encres de sérigraphie sont des fluides à seuil qui ne coulent pas avant qu'un minimum de force de cisaillement soit atteint : le seuil d'écoulement.

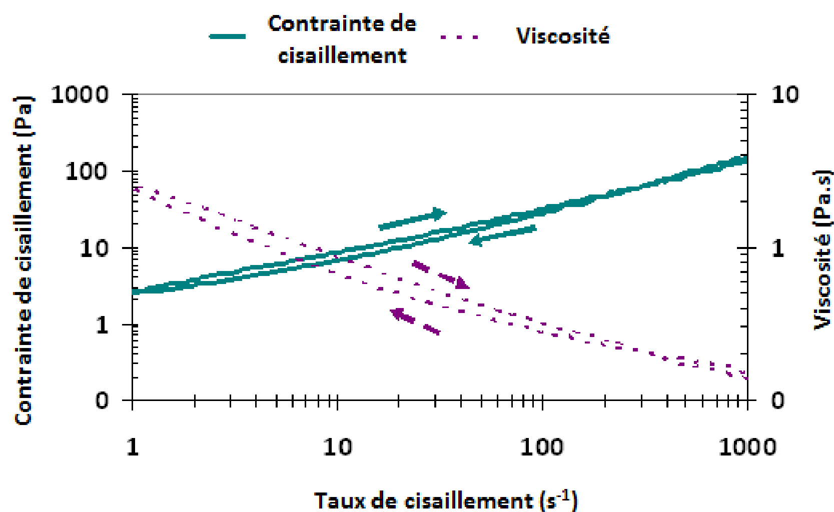


Figure xiii: Comportement rhéologique d'une pâte de sérigraphie contenant 75% d'argent en fonction du taux de cisaillement

La relation entre le comportement rhéologique et la qualité des lignes a été étudiée grâce à la détermination du ratio du module de perte sur le module élastique ($G''/G'$) des encres.

La figure xiv (extraite du ***Paper 2***) montre les résultats obtenus pour des encres contenant 67, 72 et 75% d'argent.

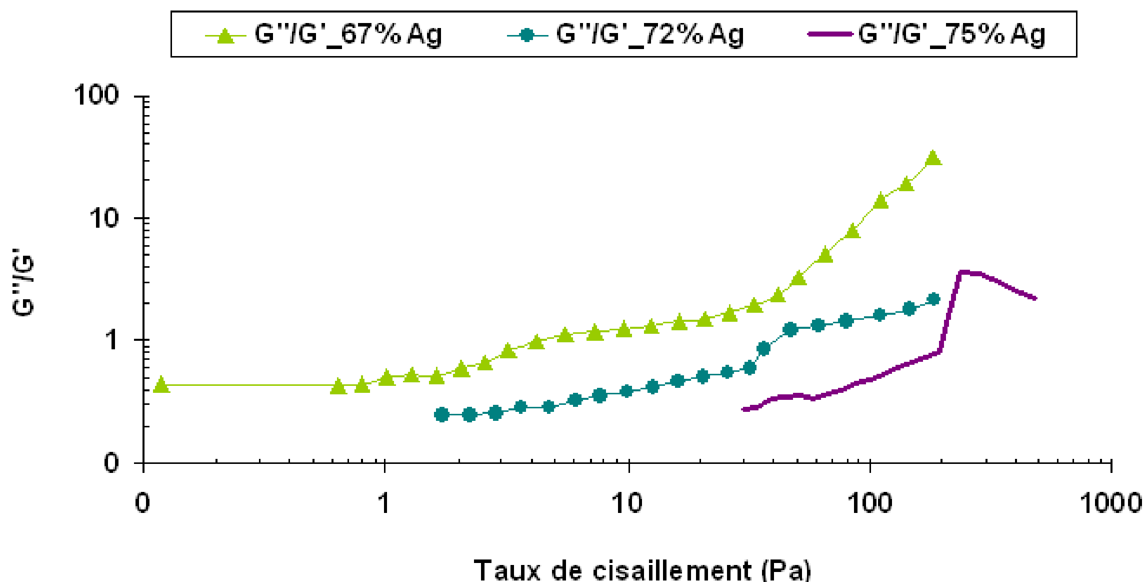


Figure xiv: Evolution de $G''/G'$ en fonction de la force de cisaillement et de la quantité d'argent

Des lignes bien définies ont été déposées avec des encres contenant moins de particules par comparaison aux encres contenant 75% d'argent. En effet, quand la quantité d'argent augmentait, $G''/G'$ diminuait et le caractère élastique de l'encre devenait trop prononcé ce qui perturbait son passage à travers les mailles de l'écran.
Si l'encre était trop fluide ($G''/G'$ élevé), elle se serait étalée facilement sur le support et les lignes imprimées auraient été très larges et mal définies. Ce cas n'a pas été observé sur les encres testées dans cette étude.

L'impression des encres formulées a été réalisée par sérigraphie sur des LTCC non cuits et de l'alumine frittée. Après impression, les lignes d'argent et les supports ont été co-frittés à des températures variant de 500 à 875°C. Le rajout de particules de verre ainsi que l'augmentation du taux d'argent ont permis une meilleure adhésion aux supports déjà frittés. Quand l'impression a été réalisée sur des supports non frittés, les lignes déposées ont adhéré facilement après frittage même sans ajout de poudres de verre.

Avec les particules sphériques, l'effet de la quantité d'argent sur la qualité des lignes a été étudié ***(Paper 1)***. Des lignes moins larges et plus épaisses ont été obtenues avec des encres contenant plus d'argent. Les largeurs des lignes ont diminué de 284 $\mu$m à 234 $\mu$m et leurs épaisseurs augmenté de 7,7 à 9,9 $\mu$m quand le taux d'argent a augmenté de 70 à 77% d'argent. Cela a été attribué à la viscosité des encres. Des lignes avec des résisitivités comprises entre 3,5 et 5,8.$10^{-8}$ Ohm.m ont été obtenues après frittage à 700°C pendant 15 minutes.

Dans cette même étude, l'effet de la température sur les propriétés électriques des encres a été examiné. La résitivité d'une encre contenant 72,5% d'argent a diminué de 7,5 à 2,4.$10^{-8}$ Ohm.m quand la température a augmenté de 700 à 900°C.
Le frittage a permis la formation d'un réseau continu d'argent laissant passer le courant

électrique sur une longueur de ligne de 14 cm. La figure xv montre la microstructure d'une ligne imprimée avant et après frittage à 700°C pendant 15 minutes. Malgré la présence de pores après frittage, la ligne était continue et une résistivité de 3,5.$10^{-8}$ Ohm.m a été mesurée.

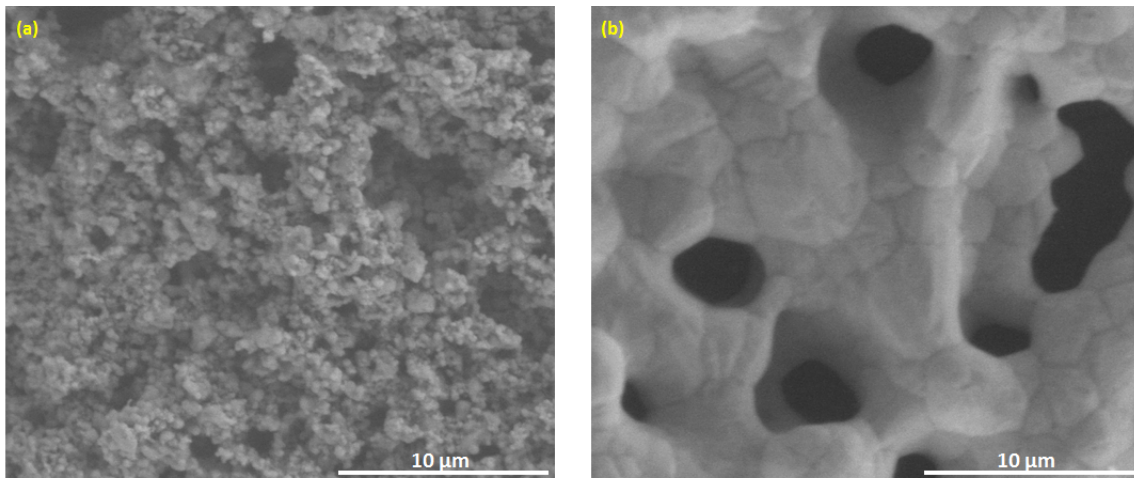


Figure xv: Une encre contenant 72,5% d'argent sérigraphiée sur un support en céramique fritté avant (a) et après (b) frittage (MEB)

Les encres préparées avec un mélange de particules d'argent sphériques et lamellaires ont été imprimées sur des support LTCC non frittés ***(Paper 2)***. Des motifs ayant des bords nets et bien définis ont été obtenus avant et après frittage. Des lignes de largeurs variant de 100 à 600 $\mu$m (figures xvi et xvii) ont été imprimées afin de déterminer la largeur minimale susceptible d'être atteinte par sérigraphie.

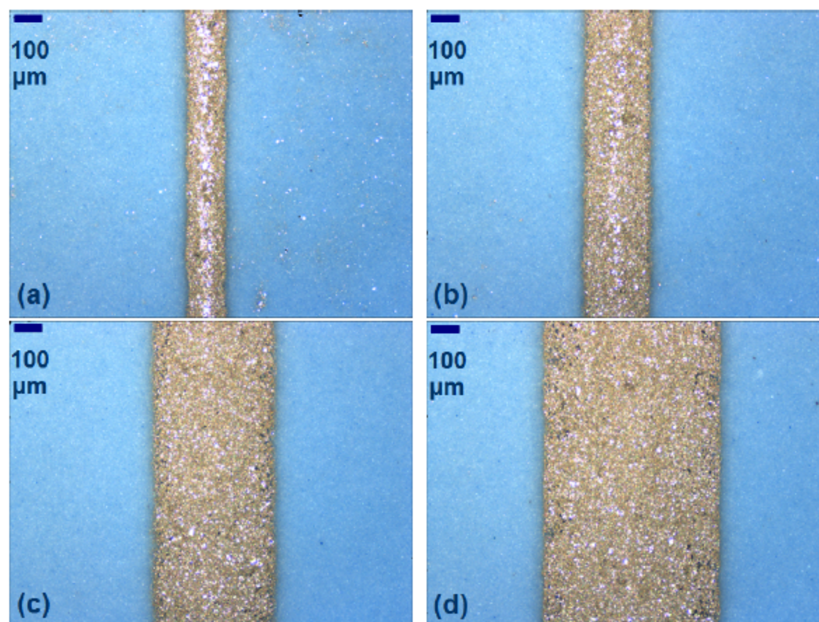


Figure xvi: Lignes d'argent imprimées par sérigraphie sur LTCC avant frittage: (a) 100 $\mu$m; (b) 200 $\mu$m, (c) 400 $\mu$m, (d) 600 $\mu$m (Alicona)

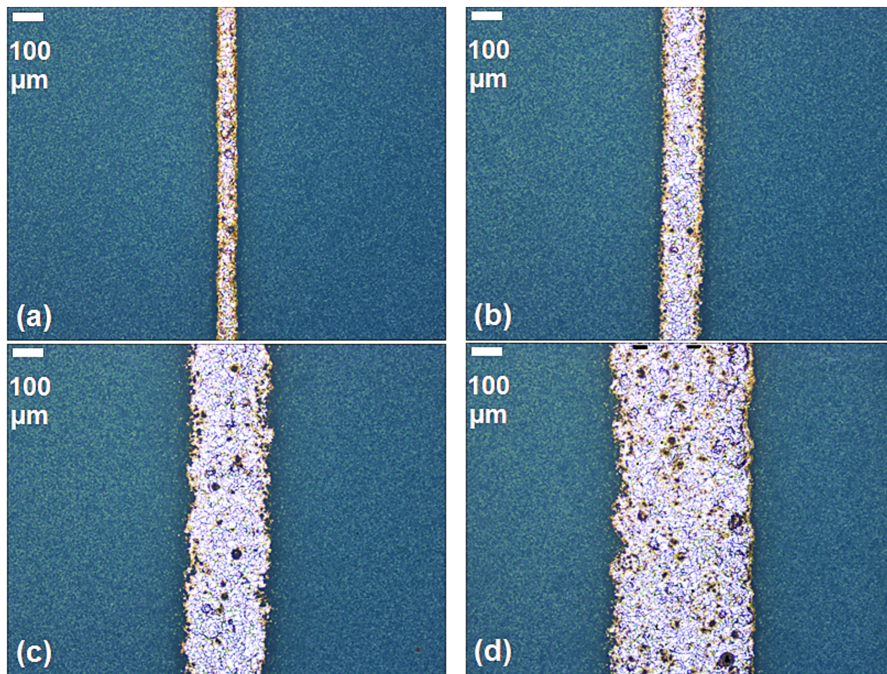


Figure xvii: Lignes d'argent imprimées par sérigraphie sur LTCC après frittage à 875°C pendant 60 minutes: (a) 100 $\mu$m; (b) 200 $\mu$m, (c) 400 $\mu$m, (d) 600 $\mu$m (Alicona)

Une largeur minimum de 130 $\mu$m a été mesurée sur des lignes déposées avec des encres contenant 67 à 72% d'argent. Les épaisseurs déposées ont varié de 9 à 16 $\mu$m.
Après frittage la largeur et l'épaisseur des lignes a diminué à cause du retrait, de la décomposition du liant organique et de l'évaporation du solvant. Une largeur minimum de 42 $\mu$m a été mesurée après frittage. Les épaisseurs après frittage ont varié de 1 à 7 $\mu$m. Elles dépendaient de la largeur des lignes et de la quantité d'argent.
Les lignes et les films imprimés conduisaient le courant même avant frittage. Cela a été attribué à la grande surface de contact entre les particules d'argent lamellaires. Après frittage, la résistivité a diminué considérablement, d'un facteur de $10^3$. Une résistivité de $3.10^{-8}$ Ohm.m a été calculée sur une ligne ayant une largeur de 59 $\mu$m et une épaisseur de 3 $\mu$m après frittage.
Les résistances de feuille ($R_s$ - Ohm/square) ont aussi été déterminées sur des films continus. Elles variaient de 3 à 13 mOhm/square pour des épaisseurs de 3 à 7 $\mu$m après frittage.

Les lignes imprimées avec une encre contenant 75% d'argent n'étaient pas homogènes. Des pores et des discontinuités ont été observés tout au long des lignes après frittage. Pour cette raison, l'effet de la pression d'impression sur la qualité des lignes déposées avec cette encre a été étudié ***(Paper 3)***. Cela a permis de définir une force optimum permettant de déposer des lignes bien définies et épaisses. Les impressions ont été réalisées à des pressions pressions variant de 3 à 12 kg. Une pression optimum de 5 kg a été définie : elle a permis de déposer une ligne avec une épaisseur maximale de 14 $\mu$m et une largeur très proche de la cible fixée à 100 $\mu$m (114 $\mu$m). Cela a été attribué au fait que l'encre en question est une encre à seuil. Une force minimale de 49 N (correspondant à 5 kg) était nécessaire pour permettre le passage d'un maximum de particules à travers les mailles de l'écran. La figure xviii est une topographie qui met en évidence les discontinuités tout au long d'une ligne imprimée à 3 kg.

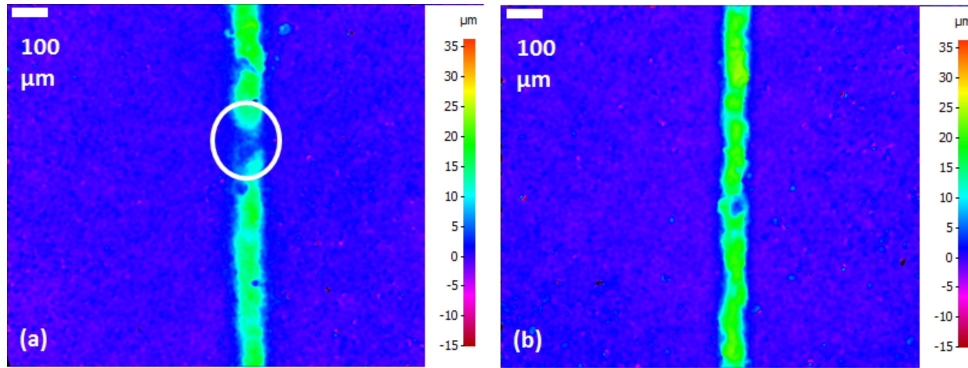


Figure xviii: Topographie des lignes imprimées à 3 kg (a) et 5 kg (b) avant frittage sur alumine frittée (Alicona)

La figure xix est une image acquise au microscope électronique à balayage (MEB). Elle montre que moins de particules d'argent passent à travers l'écran à 3 kg comparé à une impression à 5 kg.

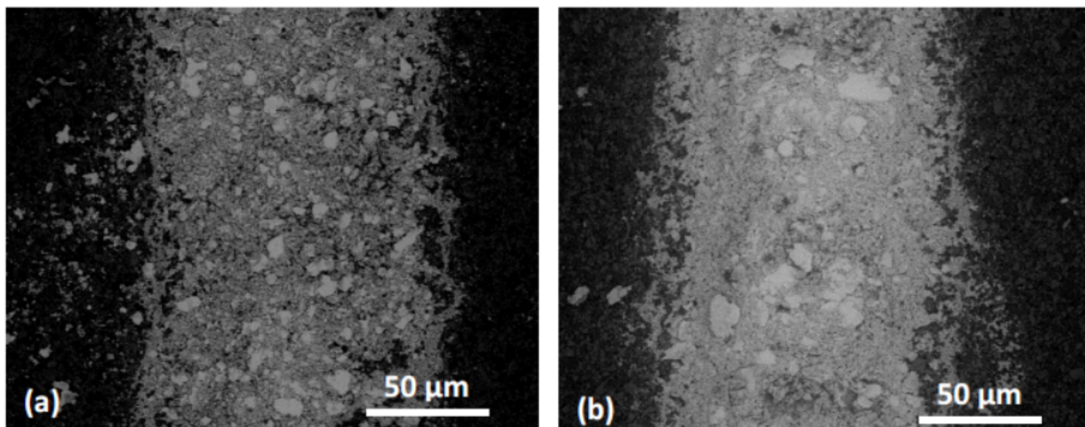


Figure xix: Image MEB des lignes imprimées à 3 kg (a) et 5 kg (b) sur alumine frittée

Ainsi, des forces plus élevées sont nécessaires pour augmenter la quantité de particules transférées. Par contre, à des pressions plus élevées que 7 kg, une légère diminution d'épaisseurs a été observée. La surface des lignes transférées (épaisseur multiplié par la largeur) a été calculée (figure xx) pour toutes les lignes déposées.

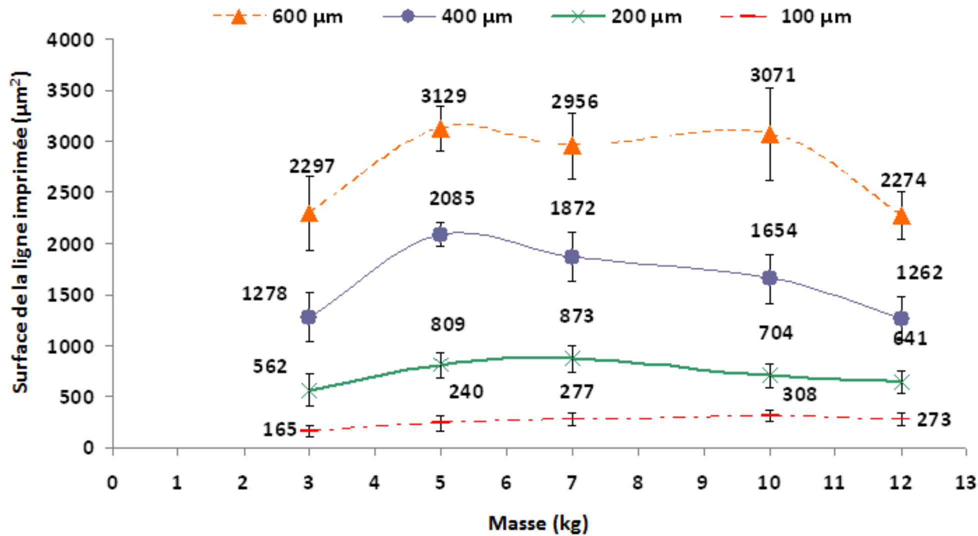


Figure xx: Surface calculée des lignes imprimées après frittage

Une diminution de la quantité de matière transférée (surface) a été détectée à des forces supérieures à 7 kg. Cela a été attribué au comportement visco-élastique de l'encre. En effet, à des taux de cisaillement supérieurs à 150 Pa, $G''/G'$ a légèrement diminué (3,1 à 1,8). Cela montre une légère tendance de l'encre à se restructurer, ce qui pourrait perturber son passage à travers les mailles de l'écran.
Les résistivités électriques des lignes déposées ont varié de 1,8 à $2{,}8.10^{-8}$ Ohm.m. Une ligne de 61 $\mu$m de large et 5 $\mu$m d'épaisseur a permis le passage du courant avec une résistivité de $1{,}8.10^{-8} \pm 0{,}2.10^{-8}$ Ohm.m. Les films déposés avaient des résistances de feuille variant de 4,5 à 5,9 mOhm/square pour des épaisseurs variant de 4 à 7 $\mu$m.

## Flexographie sur LTCC

Le procédé flexographique a été envisagé comme une alternative au procédé sérigraphique du fait de son fort potentiel pour la production de masse. Il offrait notamment l'avantage d'imprimer sur des supports souples en continu (bobine/bobine).
Une encre sérigraphique a ainsi été diluée afin d'obtenir des viscosités adaptées à la flexographie (50 - 500 mPa.s). Les particules de cette encre sont lamellaires avec un diamètre moyen de 0.4 $\mu$m. Cette taille de particules a été choisie pour éviter le bloquage des cellules de l'anilox.
Les encres optimisées contenaient 20, 30 et 40% d'argent. Elles étaient rhéofluidifiantes avec des viscosités augmentant en fonction de la quantité d'argent. La figure xxi montre l'évolution de la viscosité des encres optimisées en fonction du taux de cisaillement et de la quantité d'argent.

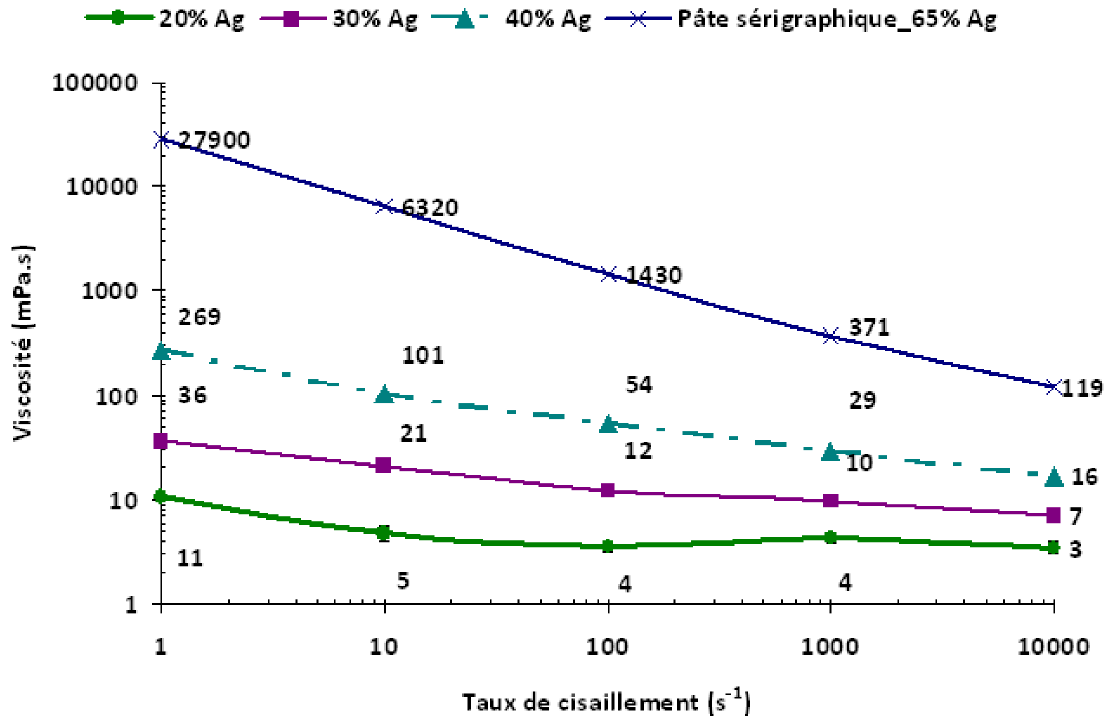


Figure xxi: Comportement rhéologique des encres optimisées (20, 30 et 40% Ag) comparées à l'encre commerciale (65% Ag)

Les encres optimisées ont des tensions superficielles variant de 20 à 22 $mN.m^{-1}$. Une à cinq couches d'encre ont été déposées. Deux types d'anilox avec des linéatures et des volumes de cellules différents ont permis le transfert de l'encre au cliché. Les propriétés des anilox sont données dans la table ix.

| Linéature ($lignes.cm^{-1}$) | 100 | 180 |
|---|---|---|
| Hauteur de cellule ($\mu$m) | 35 $\pm$ 1 | 15 $\pm$ 1 |
| Taille de cellule ($\mu$m) | 91 $\pm$ 4 | 49 $\pm$ 2 |
| Volume de cellule ($cm^3.m^{-2}$) | 10 $\pm$ 3 | 5 $\pm$ 1 |

Table ix: Caractéristiques des anilox mesurées à l'Alicona

L'impression d'encres métalliques sur des supports en céramique non frittés a été réalisée avec succès. La largeur des lignes dépendait de la résolution des anilox. Des lignes de 81 à 92 $\mu$m ont été imprimées avec un anilox ayant une résolution des 180 lignes par cm. Les lignes imprimées avec l'anilox à 100 lignes par cm étaient légèrement plus large, 92 à 105 $\mu$m de largeur.
L'épaisseur des lignes dépend surtout du volume des cellules de l'anilox. Des lignes plus épaisses ($\sim$ 0,70 $\mu$m) ont été déposées avec un anilox à 100 lignes par cm et un volume de cellule de 10 $cm^3.m^{-2}$. L'anilox de 180 lignes par cm ayant un volume de cellule plus faible (5 $cm^3.m^{-2}$) a permis le dépôt de lignes de 0,55 $\mu$m d'épaisseur.

L'impression a été réalisée dans deux directions différentes: (1) pour perpendiculaire au sens d'impression, (2) pour le parallèle à la direction d'impression. Des lignes plus fines ont été déposées dans la direction 2 (81 $\mu$m) comparées aux lignes déposées dans la direction

1 (92 $\mu$m). La figure xxii est une comparaison d'une ligne perpendiculaire à la direction d'impression à une ligne imprimée dans la direction d'impression.

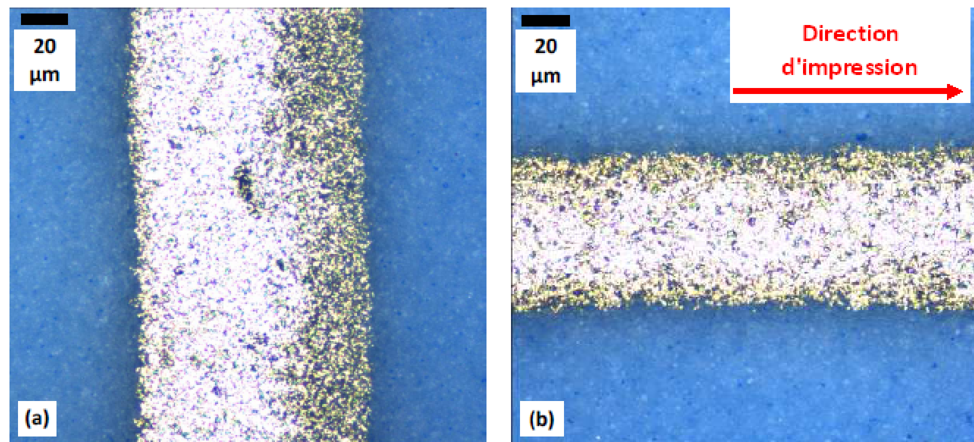


Figure xxii: Encre contenant 30% d'argent imprimée sur un LTCC dans la direction perpendiculaire (a) et la direction parallèle (b) à la direction d'impression

Trois couches ont été nécessaires pour obtenir une épaisseur minimum de 1 $\mu$m ***(Paper 4)***. L'épaisseur des lignes et la quantité d'argent transférée constituait un point critique pour la capacité des lignes déposées à résister au frittage. Les lignes imprimées avec une encre à 20% d'argent n'étaient pas continues après le frittage. Par la suite, elles n'étaient pas capables de conduire le courant.

Deux profils de frittage ont été testés sur une encre contenant 30% d'argent: 875°C pendant 60 minutes et 850°C pendant 10 minutes en atmosphère normale ***(Paper 5)***. Les lignes frittées à 875°C n'ont pas résisté au frittage et l'argent a été décomposé à la fin du cycle. Les lignes frittées à 850°C pendant 10 minutes ont supporté le frittage et elles étaient continues à la fin du cycle (figure xxiii).

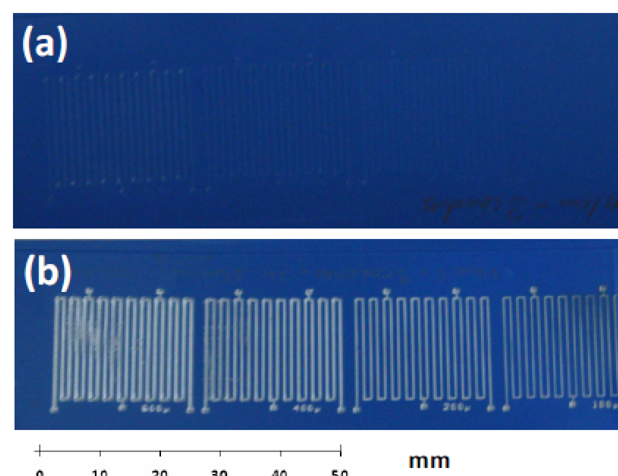


Figure xxiii: 5 couches imprimées avec une encre contenant 30% d'argent sur support LTCC: (a) frittage 60 minutes à 875°C, (b) frittage 10 minutes à 850°C - Frittage réalisé par Micro System Engineering (MSE) partenaire du projet

Les résistivités mesurées sur ces lignes étaient de l'ordre de de 2 à $12.10^{-8}$ Ohm.m après frittage.

Afin de tester le potentiel de la flexographie pour la fabrication de systèmes LTCC multicouches - généralement frittés à 875°C pendant plus de 30 minutes - cinq couches d'encre contenant 40% d'argent ont été superposées. Le frittage a été réalisé en atmosphère normale pendant 40 minutes à 875°C ***(Paper 6)***. Les lignes déposées ont résisté au frittage et des résistivités de l'ordre de 9 à $21.10^{-8}$ Ohm.m ont été calculées sur ces lignes.

Une étude thermogravimétrique (ATG) a été réalisée afin de déterminer l'effet de la température sur des encres contenant des particules d'argent de diamètre moyen égal à 0,4 $\mu$m (figure xxiv).

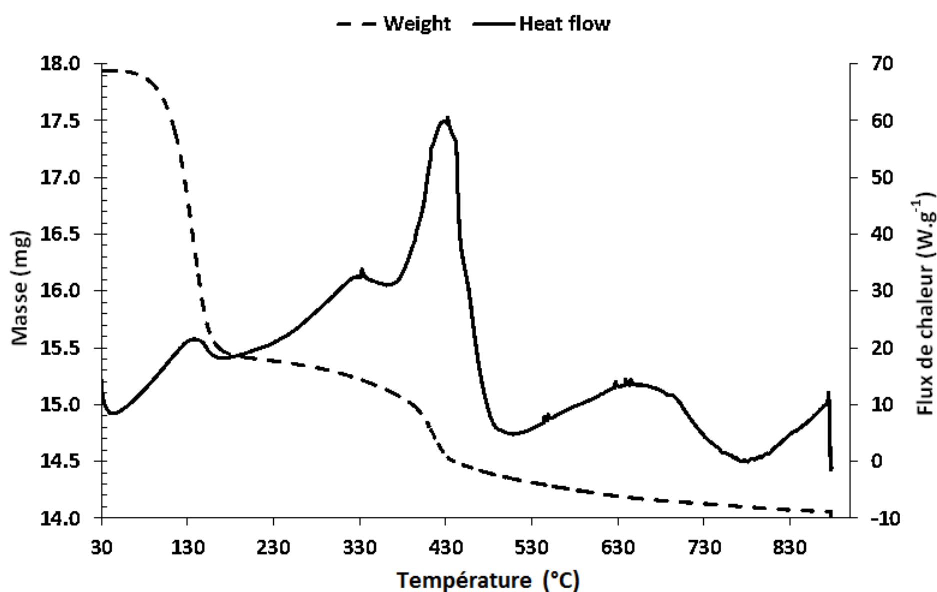


Figure xxiv: ATG d'une encre flexographique contenant 40% d'argent

L'ATG a été réalisée à 875°C pendant une heure. Un pic endothermique accompagné par une perte continue de masse est observé à des températures supérieures à 600°C. Il a été attribuée à une décomposition possible des particules d'argent sub-micrométriques (0,4 $\mu$m).
Il a ainsi été établi qu'une quantité suffisante d'argent devait été transférée au support pour que les particules puissent résister au frittage et ainsi former un réseau conducteur continu.

## Potentiel de l'héliogravure et du jet d'encre pour impression sur céramiques

### Héliogravure sur LTCC flexibles

Des encres contenant 35 à 55% de particules d'argent sphériques de 2 à 3 $\mu$m de diamètre ont été formulées. Ces encres ont ensuité été imprimées sur trois supports LTCC de propriétés différentes (taille des pores, énergie de surface).
Un cylindre gravé en creux avec des rainures de largeurs variables (136, 222, 414 et 605 $\mu$m) et de 45 $\mu$m de profondeur a été gravé pour cette étude afin de déposer des lignes suffisamment épaisses en un seul passage ***(Paper 7)***. De plus, cette profondeur de rainures a permis l'utilisation de particules relativement larges (> 2 $\mu$m). Seules les lignes imprimées avec les chaînes de 136 $\mu$m ont été exploitables. Le transfert de l'encre

au niveau des lignes larges n'était pas complet à cause du ratio élevé de la largeur par rapport à la profondeur des rainures (figure xxv).

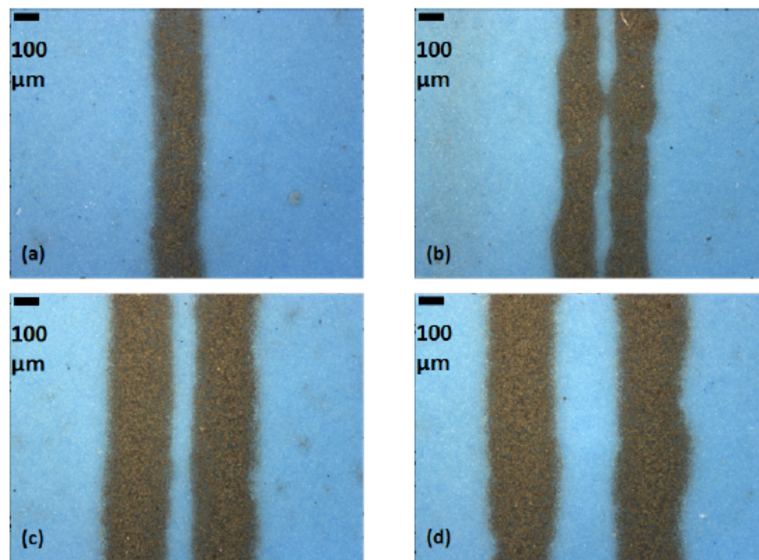


Figure xxv: Encre argent imprimée sur des supports LTCC non frittés: (a) 136 $\mu$m, (b) 222 $\mu$m, (c) 414 $\mu$m, (d) 605 $\mu$m (Alicona)

Les lignes les plus épaisses (5,5 - 5,6 $\mu$m) ont été imprimées avec les encres contenant le plus d'argent (50 et 55%).
Les lignes les plus fines (172 $\mu$m) ont été imprimées sur le support ayant la plus faible composante dispersive par rapport à l'énergie de surface totale ($\gamma_s^d/\gamma_s = 0{,}38$). En effet, les encres formulées étaient plutôt hydrophobes à tendance dispersive. Un agent de mouillage siliconé a été rajouté en cours de formulation ce qui a conduit à la diminution de la tension superficielle de l'eau (le solvant). Des tensions superficielle variant de 16 à 12 mN.m$^{-1}$ en fonction de la quantité d'argent ont été mesurées. Par la suite, par manque de compatibilité entre les encres formulées et les supports à faible caractère dispersif, l'étalement de l'encre était limité et des lignes fines ont été définies.

Les lignes imprimées ont ensuite été frittées à 800°C pendant 10 minutes. La quantité d'argent transférée n'était pas suffisante pour former un réseau conducteur continu (figure xxvi).

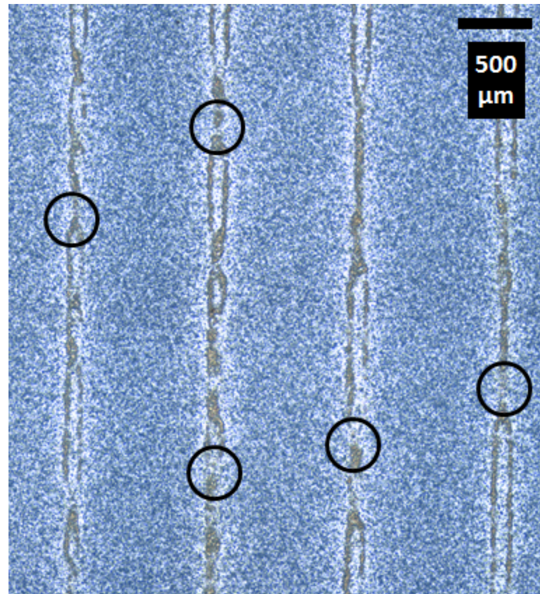


Figure xxvi: Lignes argent imprimées sur LTCC par héliogravure après frittage à 800°C pendant 10 minutes en atmosphère normale (Alicona)

Pendant le frittage, aucune décomposition des particules de taille supérieure à 2 $\mu$m n'a été détectée (ATG - figure xxvii). Une faible quantité d'argent a été transférée aux supports. L'élargissement des particules d'argent suite à leur fusion n'était pas suffisant pour former un réseau continu.

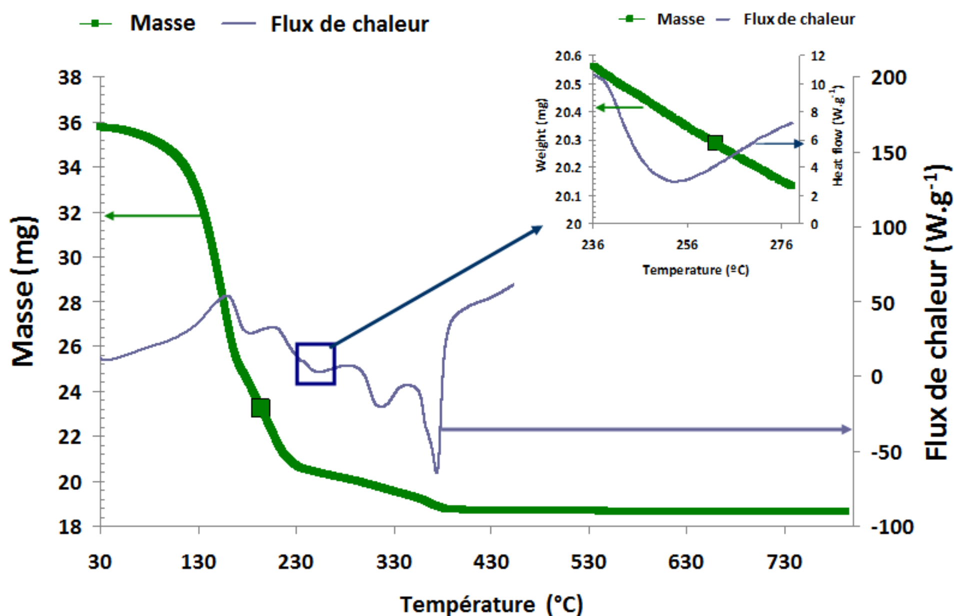


Figure xxvii: ATG d'une encre contenant 50% de particules d'argent sphérique de diamètre moyen de 2 à 3 $\mu$m

De manière à améliorer le transfert de l'encre et ainsi déposer des lignes plus épaisses, un nouveau cylindre a éta conçu. Des alvéoles plus profondes (100 $\mu$m) et une trame hélicoïdale devraient permettre de mieux transférer l'encre.

### Jet d'encre sur céramiques frittées

Une nano-suspension commerciale conçue pour impression jet d'encre sur supports en alumine frittés et contenant 42% d'argent a été optimisée afin de diminuer sa viscosité (12 mPa.s) et permettre son éjection à travers un orifice de 20 $\mu$m de diamètre ***(Paper 8)***. Les particules d'argent avaient un diamètre moyen de 15 nm. La nano-suspension commerciale contenait aussi un agent d'adhésion à base de silicone et de potassium de taille égale à 100 nm.
L'encre modifiée contenait 21% d'argent et avait une viscosité de 4 mPa.s. Sa tension de surface était égale à 51 mN.m$^{-1}$. L'impression a été réalisée sur de l'alumine frittée ayant une énergie de surface de 56 mJ.m$^{-2}$. L'impression d'une seule couche a conduit au dépôt de gouttes espacées. Pour cette raison, trois couches ont été imprimées (figure xxviii).

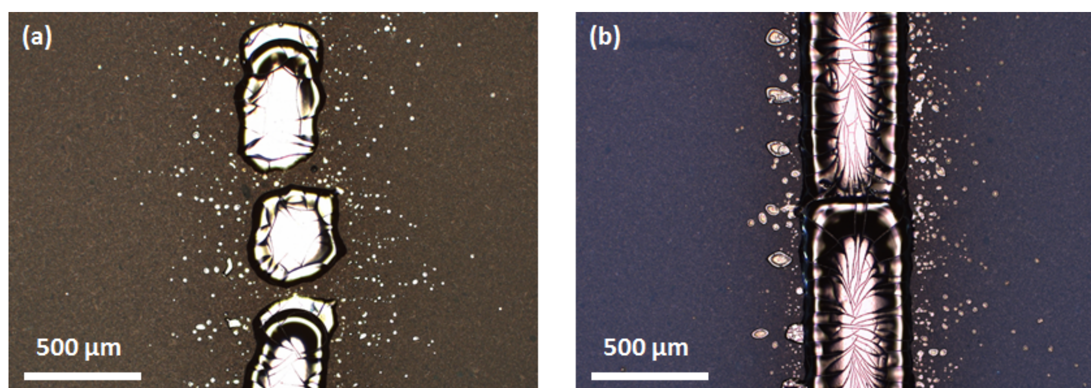


Figure xxviii: Encre argent imprimée par procédé jet d'encre sur support alumine fritté: (a) une couche, (b) trois couches (microscope optique)

L'effet de la température sur les propriétés électriques et géométriques des lignes a été déterminé. Les supports imprimés ont été frittés à 500, 700, 800 et 900°C pendant 15 minutes. Une température optimale de 700°C a permis la fusion des particules d'argent ainsi que de l'agent d'adhésion. La figure xxix montre la micro-structure des lignes frittées à 500 et à 700°C. Elle met en évidence la fusion de l'agent d'adhésion à 700°C.

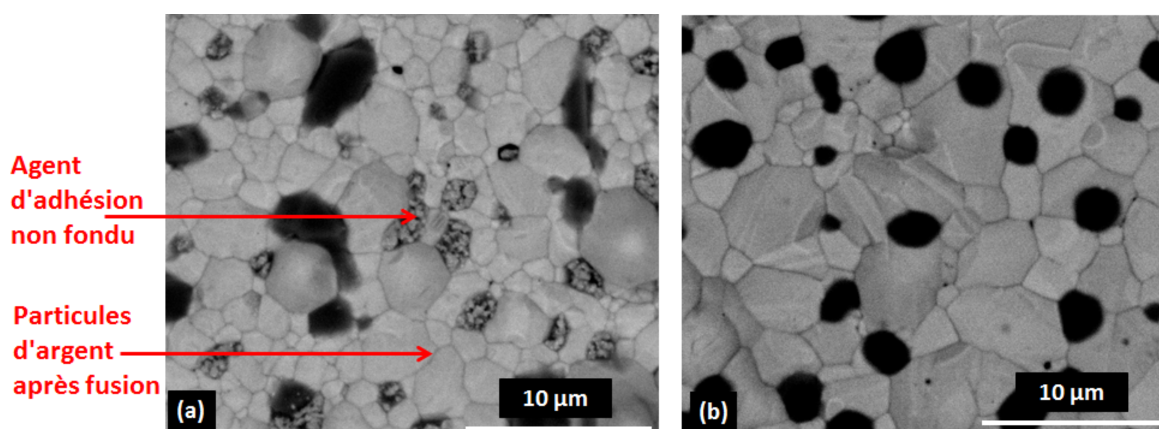


Figure xxix: Argent déposé sur support en alumine et fritté à 500°C (a) et 700°C (b) (MEB)

Par la suite, les lignes les plus lisses ($R_a$ = 0,54 $\mu$m) avec la plus faible résistivité (1,7.10$^{-8}$ Ohm.m) ont été obtenues à cette température. La décomposition de l'argent a débuté à des températures supérieures à 700°C. Cela a été traduit par une augmentation de la résistivité à 800°C (11.10$^{-8}$ Ohm.m) et une discontinuité des lignes imprimées à 900°C.

Afin d'obtenir des lignes continues et conductrices par impression d'une seule couche, la viscosité de l'encre ainsi que sa tension superficielle peuvent être diminuées afin de faciliter son étalement sur l'alumine.

# Conclusions and perspectives

Le potentiel des procédés d'impression dans les applications électroniques sur des supports en céramique a été démontré dans cette étude.

La sérigraphie est un procédé déjà développé pour l'électronique imprimée. La nouveauté de ce travail est la formulation de pâtes sérigraphiques écologiques à base d'eau. Ces encres peuvent remplacer les pâtes commerciales à base de solvants souvent irritants et nocifs. Des résistivités de l'ordre de 2 à $6.10^{-8}$ Ohm.m ont été calculées sur les lignes et aplats déposés.
Les formules préparées pourront être optimisées en utilisant un broyeur tri-cylindre afin de mieux les homogénéiser et de déposer des lignes continues sans pores.
Dans la suite de ce travail, des encres thermo-électriques préparées au sein du Commissariat à l'Énergie Atomique et aux Énergies Alternatives (CEA), seront déposées par sérigraphie afin de remplir des trous de 300 $\mu$m de hauteur et 500 $\mu$m de diamètre. Ainsi des composants thermo-électriques permettant la transformation de la chaleur thermique en électricité peuvent être préparés.
De plus, des lignes imprimées pouvant transmettre les ondes radios sont en cours d'analyse. Cette partie de l'étude se déroule en partenariat avec Swerea IVF et Omnysis (Suède).

La flexographie est un procédé permettant la production de masse de pièces électroniques. Le potentiel de la flexographie a été démontré dans des études antérieures pour des supports polymères ou papiers.
Dans cette étude, des encres métalliques ont été imprimées pour la première fois par flexographie sur des supports en céramique. Les lignes déposées ont été capables de supporter les conditions de frittage des systèmes multicouches LTCC (875°C pendant 40 minutes). Des résistivités proches de celles de l'argent pur ont été calculées, 2 à $12.10^{-8}$ Ohm.m.
Dans la suite de ce travail, l'étude de la flexographie d'encre argent sur des supports en céramique sera réalisée à l'échelle industrielle en partenariat avec le CEA et KMS (Allemagne).

Les lignes d'argent déposées par héliogravure n'étaient pas capables de supporter les conditions de frittage des céramiques. Afin d'optimiser ce procédé, un nouveau cylindre avec des alvéoles de 100 $\mu$m de profondeur et des largeurs variant de 80 à 600 $\mu$m a été gravé. Ce cylindre permettra d'imprimer des encres plus visqueuses que celles déjà testées. De plus, des particules lamellaires ayant une plus grande surface de contact pourraient être testées.

Concernant le procédé jet d'encre, des lignes d'argent de résistivité égale à $1{,}7.10^{-8}$ Ohm.m ont été imprimées. Trois couches ont été requises afin de permettre le contact entre les gouttes déposées. La formulation des encres (viscosité, tension superficielle) et les paramètres d'impression (espace entre les gouttes, fréquence, voltage, vitesse) pourraient être optimisés afin de déposer des lignes continues par l'impression d'une unique couche sur l'alumine.

Cette étude a ainsi mis en évidence le potentiel des procédés d'impression dans la fabrication de pièces électroniques sur des supports en céramique. Ce travail ouvre des perspectives pour l'industrialisation et la production de masse de composants électroniques hautement conducteurs.